

Structure-Function Studies of Nicotinic Acetylcholine Receptors Using Unnatural Amino Acids and Synthetic Agonist Analogs

Thesis by
Angela Patricia Blum

In Partial Fulfillment of the
Requirements for the Degree of
Doctor of Philosophy



California Institute of Technology
Pasadena, CA
2012
(Defended September 8, 2011)

© 2012

Angela Patricia Blum

All Rights Reserved

To my beloved furry companions:

Cyrano and Burrito

ACKNOWLEDGEMENTS

I owe much gratitude to many people for their help and support during my tenure at Caltech. It's hard to believe that I've been associated with Caltech for nearly eight years. I started as a Summer Undergraduate Research Fellow (SURF) in the Grubbs lab. At the time, the lab was packed with amazing scientists like Jacob Berlin, Andy Hejl, Anna Wenzel, and Tim Funk who rekindled my love for science. When it came time to pick a graduate school and later a research lab, the choice was quite easy for me; I couldn't imagine working in any other lab. After rejoining the lab, it took me six months and a lot of soul-searching to realize that I wanted to become a chemical biologist and not an organometallic chemist. Bob was incredibly supportive of this decision and has continued to serve as a great mentor over the years.

Although it was difficult to leave the Grubbs lab behind, it was easy to transition into the Dougherty group. Dennis has a hands-off management style that works well for my personality. He enabled me to take intellectual ownership over my research and gave me a great deal of scientific freedom, while also making sure that I never lost sight of the overall goal of a given project. Dennis is never too busy for his students and always makes us feel like we are his priority. I have learned a great deal about how to be a good teacher from Dennis, and I am confident that the critical thinking skill set I honed in his lab will equip me to tackle any problem in chemical biology or life in general.

Henry Lester is a longtime collaborator of the Dougherty lab and a great source of biology and electrophysiology wisdom. He provided much insight for many of the projects presented in this thesis. I am also indebted to the other members of my

committee, Prof. Peter Dervan and Prof. Jacqueline Barton, for their many words of advice and encouragement throughout my graduate career.

I've been very fortunate to have had three incredible mentors in science, Prof. Louis Kuo, Tobias Ritter, and Tim Funk. Prof. Kuo was my favorite professor in college and the reason I decided to pursue a career in academia. Tim Funk was my mentor during my summer as a SURF. He is a great example of how to be successful scientist and a good person. I owe my work ethic and confidence at the chemistry bench to Tobias Ritter, a former Grubbs lab postdoctoral scholar. He is a source of endless knowledge and is a truly creative scientist. I also thank the other members of "Church 130" in the Grubbs lab for serving as my big brothers and sisters in chemistry.

All of the members of the Dougherty lab have been essential for my success at Caltech. Many of the older students were helpful in my transition into chemical biology. I especially thank Ariele Hanek for her insight, support, and friendship.

My fellow sixth-year Dougherty lab members, Jai Shanata, Sean Kedrowski, and Kay Limapichat, have been particularly important components of my graduate experience. Sean and I were both refugees from synthetic chemistry labs. As such, we've shared a lot of common experiences, and I'm thankful to have had someone to commiserate with in the lab. Sean has great critical thinking skills and always has a clever take on confusing experimental results. He's decided to return to synthetic chemistry for his postdoctoral work, and I'm confident that he will be a great asset to the Jacobsen lab at Harvard. Jai and I are guaranteed to be on opposite sides of any argument, which is funny because we are probably more similar than we are different. I wish him much luck in his new career as a professor at Loyola College in New Orleans,

and I look forward to seeking his advice in a few years when I apply for similar positions. I actually considered dedicating this thesis to Kay. She certainly deserves a great deal of credit for sitting behind me and listening to all of my grumblings over the years. We have a very deep understanding of one another, probably because our philosophies in life and personalities are pretty similar despite our very different upbringings. She's always had my back, especially when it mattered most, and I consider her one of my dearest friends.

Nyssa Puskar is the lone representative of the fifth-year class in the Dougherty lab and is a longtime friend and confidant. Her sweeter-than-sugar personality and positive outlook are the perfect counterparts to my cynicism, and I am often inspired by her patience, strong work ethic, humility, and unwavering faith.

Noah Duffy and Darren Nakamura were next to join the group. Noah is the MacGyver of the lab, and I am convinced that he can fix *anything*. I will never forget the day he removed the broken lock from my bike by wailing on it with a hammer (and some other interesting tools); I cherished every weird look we got that day. Darren has a great sense of humor and great humility. I consider myself lucky to have gotten the chance to know him (and his alter-ego "Dexter") during his short time at Caltech.

The third year class is composed of an interesting cast of characters. It has been a pleasure to get to know Kristina McCleary. She's very bright and has a lot of biology knowledge that has been quite useful to me recently. I find her practical approach to problems very refreshing. I am envious of Ethan Van Arnam's adventurous spirit and his frequent world travels. We share a similar life philosophy and love of nature, and so I hope that we stay in touch after my departure from Caltech. Ximena Da Silva is another

great friend and fellow animal lover. I've enjoyed listening to all of the crazy stories from her childhood and am absolutely convinced that she should sell her life story to the Lifetime Movie Network. I am inspired by Maggie Thompson's bravery. She's chosen to start over in a different graduate program, a decision that took much self-reflection and great courage. I'm very proud of her and am confident that she will make an extraordinary physician. Erin Lamb has an off-beat humor that is endearing. Her everyday behavior is incredibly entertaining, and I'm sure that her quirky way of looking at the world will afford her many great adventures in life. Clint Regan is new to the Dougherty lab, but I am already intrigued by his sense of humor. I suspect he'll be a very amusing addition to the lab culture. I'm also delighted that another round of former synthetic chemists (Erin and Clint) will be able to pick up where Sean and I left off.

I've enjoyed getting to know the first and second year classes of the Dougherty lab. Fan Liu has been a great addition to the lab. His modeling studies will likely provide useful insight into many projects. Chris Marrota is my "BFF" in the boot camp gym class, and I am happy to have met someone that is *almost* as competitive as I am. In the lab, he has a strong work ethic and a great eagerness to learn. Oliver Shafaat and Tim Miles can already "talk the talk" of science. They seem well equipped to be very successful in the lab. Fan, Chris, Oliver, and Tim all share a palpable passion for science, and I am confident that the legacy of the Dougherty lab will be safe in their hands.

Wesley Yu and Laurel German were brave enough to endure a few summers in the lab with me. Wesley is an incredibly gifted Caltech undergrad who always seems to have a crazy idea that could (A) cure a disease, (B) make lots of money, or (C) impress a girl. I first met Laurel when she was fifteen (a sophomore at Polytechnic School), and I

was amazed at the speed with which she acclimated to the lab. She's truly a very capable person and a real Renaissance teenager; active and proficient in a wide range of after-school activities and other hobbies. This fall, Wesley will enter medical school at UCSF and Laurel will be a freshman at Yale. There are simply no words to express how proud I am of them.

My family also deserves a great deal of gratitude. My mother has been a good role model, having strong conviction and *infallible* personal integrity. She's made many personal sacrifices for her children, for which I am very grateful. I still consider my older brother to be the smartest person I've ever met. He has a Ph.D. in a field that requires a lot of math, and he somehow figured out how to put up with a really annoying little sister. My sister-in-law is an incredibly kind and unassuming person whom I am blessed to have in my life. My nearly two-year-old niece, Katherine Elizabeth Blum, is an adorable little girl whom I hope to one day know very well and eventually spoil rotten.

Justin "Bieber" Wong is a very patient and understanding person whom I have truly under-appreciated. I consider myself very lucky that he finally (after much campaigning) agreed to date me four years ago. He's an exceptionally responsible and stable person who has been a very good influence in my life. He's helped me figure out what I want to do "when I grow up," and I look forward to helping him do the same.

One of the perks of dating Justin is that he comes with a large extended family. His parents are both former scientists, and as such we formed an instant kinship. Justin's older sister Courtney is pursuing a Ph.D. in organizational communication at UCSB. She's an over-achiever like me, and I've enjoyed commiserating with her over the years about life as a graduate student. Justin's younger brother Adam has an infectious laugh

and a warm spirit that is comforting to be around. “The aunts” are an incredibly kind, friendly, and beautiful group of women. They’ve made me feel welcome and accepted from the start. I also absolutely adore the entire Toy family. Amanda Toy and Kristin Toy (Justin’s cousins) are like sisters to me, and I feel so very fortunate to have them in my life.

Those that know me well won’t be surprised that I chose to dedicate this thesis to my two pets. I’ve always felt more comfortable with animals than I do people. It’s possible that I am inspired by their unassuming and forgiving nature. My cat Burrito is possibly the sweetest and most gentle creature in the entire world. She’s been my companion for 14 years, and I’m hoping her kidneys will hold out for many more. Cyrano is a mischievous Boston Terrier (with a bit of a Napoleon complex) who truly brings joy to every day. I’ve heard people say that dogs are a reflection of their owners. I’d say that’s pretty accurate in our case.

ABSTRACT

This dissertation primarily describes structure-function studies of the prototypical Cys-loop ligand-gated ion channel, the nicotinic acetylcholine receptors (nAChRs).

Agonists that bind nAChRs, including acetylcholine, nicotine, and the smoking cessation drug varenicline, share one of the longest-known, best-studied pharmacophores, consisting of a cationic N and a hydrogen bond acceptor. A major theme of this thesis is concerned with defining the nAChR residues that bind the nicotinic pharmacophore. Chapters 2 and 3 establish that a hydrogen bond links the pharmacophore's hydrogen bond acceptor to a backbone NH in the protein. The establishment of this interaction, and the disproval of other predicted interactions, represents the completion of the nicotinic pharmacophore binding model. Chapter 4 uses this model to characterize how the nAChR differentiates between stereoisomers of an agonist.

Chapter 5 describes functional studies of a vicinal disulfide that has played a pivotal role in a number of pioneering studies of nAChRs. Despite its historical importance, the functional role of this disulfide has not been defined. We identify a speculative role for the vicinal disulfide that involves the formation of a functionally important network of hydrogen bonds.

Chapter 6 outlines three strategies for the photochemical cleavage of protein and peptide backbones using unnatural amino acids. One of these strategies is based on a selenide-mediated cleavage of a backbone ester moiety. Model studies establish the viability of this chemistry and suggest that it could be a useful tool for protein structure-function studies.

Chapter 7 concerns preliminary work from a collaboration with laboratories from USC and Caltech that is aimed at developing small-molecule treatments for vision loss associated with photoreceptor degeneration. The initial goal of this project is to develop a photosensitive small molecule that can activate a voltage-gated potassium channel.

The final chapter discusses work that was done in the Grubbs lab at Caltech in which a strategy for preparing *N*-heterocyclic carbene-containing metal complexes was developed.

TABLE OF CONTENTS

LIST OF FIGURES.....	xvii
LIST OF TABLES.....	xx
LIST OF SCHEMES.....	xxii

CHAPTER 1: Introduction.....1

1.1 Chemical Signaling in the Brain	1
1.2 Nicotinic Acetylcholine Receptors (nAChRs): The Prototype of the Cys-Loop Superfamily of Ligand-Gated Ion Channels	2
1.3 Using Physical Organic Chemistry to Study Ion Channels: The Power of Unnatural Amino Acids	7
1.4 Incorporation of Unnatural Amino Acids Through Nonsense or Frameshift Suppression Methodology	11
1.5 Electrophysiology as an Assay of Receptor Function	15
1.6 Mutant Cycle Analysis	16
1.7 The Nicotinic Pharmacophore	18
1.8 Summary of Dissertation Work	20
1.9 References	22

CHAPTER 2: The Nicotinic Pharmacophore: The Pyridine N of Nicotine and Carbonyl of ACh Hydrogen Bond Across a Subunit Interface to a Backbone NH.....27

2.1 Abstract	27
2.2 Introduction	28
2.3 Results	32
2.3.1 General Strategy	32
2.3.2 Optimization of nonsense suppression experiments	33
2.3.3 Amide-to-Ester backbone mutation at β 2L119 impacts receptor function in A2B3	35

2.3.4 <i>Mutant cycle analyses indicate strong receptor-agonist interactions at β2L119 in A2B3</i>	38
2.3.5 <i>Studies in the A3B2 subunit stoichiometry give similar results</i>	40
2.3.6 <i>Studies with smoking cessation drugs at both subunit stoichiometries</i>	42
2.4 Discussion	43
2.5 Experimental Section	52
2.6 Acknowledgements	55
2.7 References	56
 CHAPTER 3: Residues that Contribute to Binding of the Nicotinic Pharmacophore in the Muscle-Type Nicotinic Receptor	60
3.1 Abstract	60
3.2 Introduction	61
3.3 Results	64
3.3.1 <i>General Strategy</i>	64
3.3.2 <i>Mutagenesis studies of γL119/δL121</i>	68
3.3.3 <i>Mutagenesis studies of the backbone CO of γN107/δN109</i>	70
3.3.4 <i>Impact of the α1G153K mutation</i>	71
3.4 Discussion	72
3.5 Experimental Section	76
3.6 Acknowledgements	78
3.7 References	79

CHAPTER 4: Stereochemical Preferences of the Nicotinic Receptor: Pharmacophore Binding Interactions of Epibatidine Enantiomers	82
4.1 Abstract	82
4.2 Introduction	82
4.3 Results	87
<i>4.3.1 General Strategy</i>	87
<i>4.3.2 EC₅₀ values at the $\alpha 4(L9'A)\beta 2$ receptor</i>	89
<i>4.3.3 Cation-π interaction to Trp B</i>	91
<i>4.3.4 Hydrogen bond to the backbone CO of Trp B</i>	92
<i>4.3.5 Hydrogen bond to $\beta 2L119$</i>	93
<i>4.3.6 A hydrogen bond to TyrA?</i>	93
4.4 Discussion	95
4.5 Experimental Section	99
4.6 Acknowledgements	102
4.7 References	103
 CHAPTER 5: Evidence for an Extended Hydrogen Bond Network in the Binding Site of the Nicotinic Receptor: Concerning the Role of the Vicinal Disulfide of the $\alpha 1$ Subunit.....	 107
5.1 Abstract	107
5.2 Introduction	107
5.3 Results	110
<i>5.3.1 Conformational Analysis and Experimental Design</i>	110
<i>5.3.2 Mutagenesis Studies</i>	112
5.4 Discussion	121
5.5 Experimental Section	125

5.6 Acknowledgements	131
5.7 References	132
CHAPTER 6: New Approaches to Photochemical Cleavage of Peptide and Protein Backbones.....	137
6.1 Abstract	137
6.2 Introduction	137
6.3 Results	139
6.3.1 Caged selenide strategy	139
6.3.1.1 Chemical biology studies of proteolysis by 1 and 2	144
6.3.1.2 In vitro studies of proteolysis by 1 and 2	144
6.3.1.3 Nonsense suppression experiments with 1 and 2 in <i>Xenopus oocytes</i>	146
6.3.2 Strategies based on a photocaged aniline and the chemistry of the NPE protecting group	148
6.3.2.1 Nonsense suppression experiments with 7 and 17 in <i>Xenopus oocytes</i>	150
6.4 Discussion	153
6.5 Experimental Section	154
6.6 Acknowledgements	170
6.7 References	171
CHAPTER 7. Progress Toward Small-Molecule Activators of Voltage-Gated Ion Channels for Treatment of Visual Impairment Resulting from Photoreceptor Loss.....	174
7.1 Abstract	174
7.2 Introduction	174
7.3 Progress	177
7.4 Future Directions	183
7.5 Experimental Section	183

7.6 Acknowledgements	184
7.7 References	185
CHAPTER 8. Synthesis of <i>N</i>-Heterocyclic Carbene-Containing Metal Complexes from 2-(Pentafluorophenyl)Imidazolidines.....	186
8.1 Abstract	186
8.2 Introduction	186
8.3 Results	188
8.4 Discussion	191
8.5 Experimental Section	192
8.6 Acknowledgements	208
8.7 References	209
APPENDIX 1: Characterizing the Pharmacophore Binding Interactions of Cytisine in the ($\alpha 4$)₂($\beta 2$)₃ Receptor.....	211
A1.1 Results and Discussion	211
A1.2 Experimental Section	215
A1.3 References	216
APPENDIX 2: Full Collection of Data for the Backbone Ester Mutation at L119 in the $\alpha 4\beta 2$ and Muscle-Type Nicotinic Acetylcholine Receptors (nAChRs).....	217
APPENDIX 3: Synthetic Routes Considered for the Preparation of the Key Aryl Selenide α-Hydroxy Acid in Chapter 6.....	220
A3.1 Results and Discussion	220
A3.2 Experimental Section	231
A3.3 References	239

LIST OF FIGURES

Figure 1.1	Topology of a Cys-loop receptor subunit	2
Figure 1.2	Stoichiometries of several nAChRs	3
Figure 1.3	nAChR structure	5
Figure 1.4	Fluorinated Trp side chains (indole rings) and calculated cation- π binding energies	9
Figure 1.5	An example fluorination plot giving a linear trend indicative of a cation- π interaction	9
Figure 1.6	Amide-to-ester mutation	10
Figure 1.7	An overview of the nonsense and frameshift suppression methodologies used to incorporate unnatural amino acids (UAAs)	12
Figure 1.8	Schematic of the production of amino-acylated tRNA	13
Figure 1.9	Implementation of the nonsense or frameshift suppression methodology for incorporating unnatural amino acids into ion channels expressed in <i>Xenopus</i> oocytes	14
Figure 1.10	The electrophysiology assay	16
Figure 1.11	Structures and electrostatic potential maps of agonists of the nAChR	19
Figure 2.1	Key structures considered in the present work	29
Figure 2.2	Key interactions seen in the crystal structure of nicotine bound to AChBP (pdb: 1UW6)	31
Figure 2.3	Representative current waveforms and dose-response relations for <i>S</i> -Nicotine and <i>S</i> -MPP at the A2B3 receptor	35
Figure 2.4	Double mutant cycle analysis for <i>S</i> -Nic and <i>S</i> -MPP on wild-type A2B3 and ($\alpha 4$) ₂ ($\beta 2$ L119Lah) ₃	39
Figure 2.5	Depiction of the two stoichiometries of the $\alpha 4\beta 2$ receptor	40
Figure 2.6	“Internitrogen distances” and electrostatic potential maps (as calculated in Spartan) for (A) <i>S</i> -nicotine, (B) (–)-cytisine and (C) varenicline	48

Figure 2.7	Additional interactions seen in the crystal structure of nicotine bound to AChBP (pdb: 1UW6)	51
Figure 3.1	Depiction of binding interactions of the nicotinic pharmacophore as predicted by AChBP structures	62
Figure 3.2	Agonists and unnatural amino acids used in this study	65
Figure 3.3	Double mutant cycle analysis for ACh and choline on wild-type and $\alpha 1\beta 1(L9'S)\gamma(L119Lah)/\delta(L121Lah)$ mutant receptors	70
Figure 4.1	The binding interactions of the nicotinic pharmacophore shown for (+)-epibatidine	85
Figure 4.2	Agonists and unnatural amino acids used in this study	86
Figure 4.3	Fluorination plots of epibatidine compounds	91
Figure 5.1	Vicinal disulfide structure	108
Figure 5.2	The β turn found in AChBP structures	116
Figure 5.3	Double mutant cycle analyses	118
Figure 5.4	Three-dimensional mutant cycle analysis with the triple mutant, $\alpha 1C193A/\alpha 1S191Aah/(\gamma D174N/\delta D180N)$	120
Figure 6.1	Npg and the second-generation SNIPP unnatural α -hydroxy acids, 1 and 2	139
Figure 6.2	Depiction of the topology of the Shaker B K ⁺ channel and the location of sites used to incorporate Npg	147
Figure 6.3	Proposed photochemical cleavage strategy using caged aniline 17	149
Figure 6.4	Proposed photochemical cleavage strategy using α -hydroxy acid 7	149
Figure 7.1	Depiction of experimental design for studies with [Ru] 1, 2, and 3	179
Figure 7.2	Structure of Ru ²⁺ (bpy) ₃ complexes with alkyl chains ([Ru] 1, 2, and 3)	179
Figure 7.3	Depiction of experimental design for studies with [Ru] 4	181
Figure 7.4	Structure of [Ru] 4	181
Figure 7.5	Current-voltage relationships of wild-type (WT) ShIR and ShIR mutants	182

Figure A1.1	Unnatural amino acids used in this study	212
Figure A1.2	Fluorination plot for (-)-cytisine	214
Figure A3.1	Original retro-synthetic pathway proposed by Eastwood	221
Figure A3.2	Second retro-synthetic pathway	223
Figure A3.3	Third retro-synthetic pathway	227

LIST OF TABLES

Table 2.1	EC ₅₀ values, Hill coefficients, and relative efficacies for mutations to β 2L119 in the A2B3 stoichiometry	36
Table 2.2	EC ₅₀ values, Hill coefficients, and relative efficacies for mutations to β 2A108 in the A2B3 stoichiometry	37
Table 2.3	Coupling parameters (Ω) and $\Delta\Delta G^\circ$ values for mutant cycle analyses for A2B3	38
Table 2.4	EC ₅₀ values, Hill coefficients, and relative efficacies for mutations to β 2L119 in the A3B2 stoichiometry	41
Table 2.5	Coupling parameters (Ω) and $\Delta\Delta G^\circ$ values for mutant cycle analyses in A3B2	42
Table 2.6	EC ₅₀ values, Hill coefficients, and relative efficacies for (-)-cytisine and varenicline at both subunit stoichiometries	43
Table 3.1	EC ₅₀ and Hill coefficient (\pm standard error of the mean) values for mutations made to α 1 ₂ β 1 γ δ	68
Table 3.2	Comparison of coupling coefficients (Ω) and coupling energies ($\Delta\Delta G^\circ$) for double mutant cycles	69
Table 4.1	EC ₅₀ and Hill coefficient values (\pm standard error of the mean) for epibatidine and <i>N</i> -methyl derivatives	90
Table 4.2	EC ₅₀ fold-shifts and fluorination plot slopes for the epibatidine (Epi) compounds and also for ACh and nicotine (Nic)	92
Table 4.3	Relative efficacy values and EC ₅₀ fold-shifts resulting from mutation of TyrA (Y98) for the epibatidine (Epi) compounds, ACh and nicotine (Nic)	94
Table 5.1	EC ₅₀ , Hill coefficient (\pm standard error of the mean) and ΔG° values for mutations made to α 1 ₂ β 1 γ δ	113
Table 5.2	EC ₅₀ , Hill coefficient (\pm standard error of the mean) and ΔG° values for each mutation made to the vicinal disulfide in neuronal receptors, α 4 β 4, α 7 and α 4 β 2	113
Table 5.3	EC ₅₀ , Hill coefficient (\pm standard error of the mean) and $\Delta\Delta G^\circ$ values for double mutations made to α 1 ₂ β 1 γ δ	117
Table 5.4	Coupling energies for each face of the three-dimensional mutant cycle	120

Table 6.1	Current (I_{\max}) obtained for control studies of Pro64 and Lys65 in ShB using different codon combinations	151
Table 6.2	Current (I_{\max}) obtained for studies with 7 and 17 at Pro64 in ShB	152
Table 8.1	Comparison of the pyrolysis of 2-(pentafluorophenyl)imidazolidines to >95% in benzene or toluene	189
Table 8.2	Comparison of percent conversion to pentafluorobenzene in different solvents in the thermolysis of 1 after one hour at 45 °C	190
Table 8.3	<i>N</i> -heterocyclic carbene complexes prepared from 2-(pentafluorophenyl)imidazolidines	191
Table A1.1	EC ₅₀ values and Hill coefficients for (–)-cytisine at the A2B3 stoichiometry	214
Table A1.2	EC ₅₀ fold-shifts for Trp-F ₃ and Trp-F ₄ at TrpB, fluorination plot slopes and EC ₅₀ fold-shifts for Tah at Thr155 for all agonists that have been studied at A2B3	215
Table A2.1	EC ₅₀ values, Hill coefficients, and relative efficacies for the muscle-type receptor	218
Table A2.2	EC ₅₀ values, Hill coefficients, and relative efficacies for the α4β2 receptor	219

LIST OF SCHEMES

Scheme 6.1	Synthesis of selenide α -hydroxy acid 1	141
Scheme 6.2	Synthesis of selenide α -hydroxy acid 2	141
Scheme 6.3	Synthesis of depsipeptides 12 and 14	142
Scheme 6.4	Depsipeptide cleavage reactions	143
Scheme 6.5	Synthesis of the <i>N</i> -pent-4-enoyl (4PO) derivative of 17	150
Scheme 8.1	Preparation of 3 from the thermolysis of 1,3-bis (2,4,6-trimethylphenyl)-2-(pentafluorophenyl)imidazolidine 1	188
Scheme 8.2	Preparation of 3 from the thermolysis of 1,3-bis (2,4,6-trimethylphenyl)-2-(trichloromethyl)imidazolidine 4	188
Scheme A3.1	Synthesis of TBS-protected aryl bromide 3	222
Scheme A3.2	Failed synthesis of the desired α -hydroxy acid, 1	222
Scheme A3.3	Failed synthesis of benzyl alcohol 7 by <i>ortho</i> -lithiation of benzyl alcohol	224
Scheme A3.4	Synthesis of benzyl bromide 6 from benzyl alcohol 7	225
Scheme A3.5	Another failed synthesis of the desired α -hydroxy acid, 1	225
Scheme A3.6	Model enolate reactions	226
Scheme A3.7	Model reactions providing precedent for key steps in route 3	227
Scheme A3.8	Model reaction that condense the two steps of Scheme A3.7 into one	228
Scheme A3.9	Literature procedure for the enantio-enriched synthesis of 11 from 2-nitrophenylpyruvic acid	228
Scheme A3.10	Racemic reduction of 2-nitrophenylpyruvic acid and attempted reduction of α -hydroxy acid 11	229
Scheme A3.11	Successful racemic preparation of the desired α -hydroxy acid, 1	230

CHAPTER 1: Introduction

1.1 Chemical Signaling in the Brain

The adult human brain uses an intricate process to communicate between its more than one-hundred billion (10^{11}) neurons. This process begins when an electrical signal, called an action potential, is generated in one neuron termed the presynaptic nerve cell. The action potential travels down the axon of the presynaptic neuron until it reaches the synaptic cleft (the space between two nerve cells). This triggers the mobilization of vesicles that contain small-molecule neurotransmitters. These vesicles ultimately fuse to the terminal of the presynaptic nerve cell, releasing their neurotransmitter contents into the synaptic cleft. Neurotransmitters diffuse across the synaptic cleft and bind a special class of integral membrane proteins, called ligand-gated ion channels, on a postsynaptic neuron. Upon binding the neurotransmitter, the ligand-gated ion channel undergoes a conformational change that opens an ion-conducting pore. This event enables ions to diffuse across the otherwise impermeable membrane of the postsynaptic nerve cell, thereby generating a new electrical signal to propagate the message that originated in the presynaptic cell. This process is called synaptic transmission, and its regulation is central to many important processes including memory, thought, sensory perception, and awareness.

Our lab is interested in using physical organic chemistry to understand the chemical component of synaptic transmission— the activation of a ligand-gated ion channel by a small molecule.

1.2 Nicotinic Acetylcholine Receptors (nAChRs): The Prototype of the Cys-Loop Superfamily of Ligand-Gated Ion Channels

The Cys-loop (or pentameric receptor) superfamily is a large and important class of neurotransmitter-gated ion channels. Among this superfamily are receptors for the neurotransmitters acetylcholine (nicotinic acetylcholine receptors), γ -aminobutyric acid (GABA_A and GABA_C), glycine (GlyR), and serotonin (5-HT₃).¹ The family is essential for proper brain function and is also implicated in an assortment of neurological disorders including Alzheimer's disease, Parkinson's disease, schizophrenia, and depression.^{2, 3}

The Cys-loop receptors are pentamers composed of five subunits arranged around a central ion-conducting pore. Subunits share a common structure consisting of a large, N-terminal extracellular domain that contains the agonist binding site and also the signature disulfide loop, four transmembrane α -helices (M1-M4) that line the ion pore, and a short extracellular C-terminus (**Figure 1.1**). Nicotinic acetylcholine receptors (nAChRs) are arguably the best-characterized members of the family and are therefore generally considered the prototypical Cys-loop receptor.¹⁻³

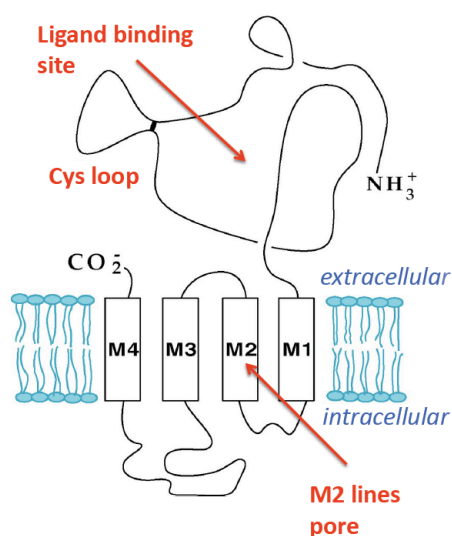


Figure 1.1. Topology of a Cys-loop receptor subunit.

The nAChRs mediate rapid synaptic transmission in the central and peripheral nervous systems.^{1, 4, 5} They are activated endogenously by the neurotransmitter acetylcholine and also, coincidentally, by nicotine. There are 16 mammalian genes that code for 16 nAChR subunits, termed $\alpha 1$ - $\alpha 7$, $\alpha 9$, $\alpha 10$, $\beta 1$ - $\beta 4$, γ , δ , ϵ . These subunits arrange as pentamers to form more than 20 active and pharmacologically distinct nAChR subtypes in humans. Of these subtypes, $\alpha 1_2\beta 1\gamma\delta$ is the best studied owing to its precise subunit stoichiometry (**Figure 1.2**) and its abundance in the electric organs of eels and rays.^{1, 4, 5} In humans, the $\alpha 1_2\beta 1\gamma\delta$ subtype, often called the “muscle-type” receptor, is expressed postsynaptically at neuromuscular junctions in the peripheral nervous system. Many other nAChR subtypes are expressed in the central nervous system at nerve synapses. The most abundant of these are likely the $\alpha 4\beta 2$ and $\alpha 7$ subtypes.^{2, 6} The $\alpha 4\beta 2$ subtype is the neuroreceptor most associated with nicotine addiction^{2, 6} and also the intended target of Pfizer’s smoking cessation drug Chantix® (varenicline).⁷⁻⁹ This subtype assembles into two viable stoichiometries, $\alpha 4_2\beta 2_3$ and $\alpha 4_3\beta 2_2$ (**Figure 1.2**), but the $\alpha 4_2\beta 2_3$ stoichiometry is more sensitive to nicotine and is upregulated during chronic nicotine exposure.¹⁰ The $\alpha 7$ subtype is a homopentamer that is often linked to schizophrenia and Alzheimer’s disease.³

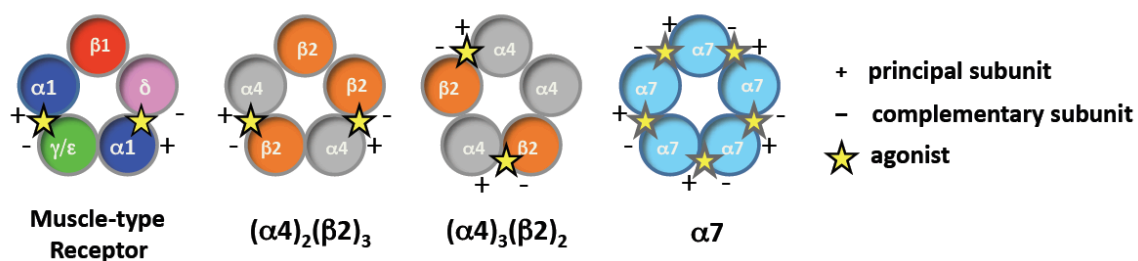


Figure 1.2. Stoichiometries of several nAChRs.

Much of our understanding of the structure of the nAChR comes from early mutagenesis studies,^{11, 12} and affinity labeling studies,^{1,13-16} which provided information about the location of the agonist-binding site and the residues involved.^{1, 4, 5} No high-resolution structure of a nAChR exists, but a great deal of relevant structural information has become available within the last 20 years. A major advance came in the early 2000s with the identification and structural characterization of a family of snail acetylcholine binding proteins (AChBPs).¹⁷⁻²² The AChBPs are soluble, pentameric proteins that share 20–25% sequence identity with the extracellular ligand-binding domain of the nAChRs. As such, their X-ray crystallography structures have served as structural templates for many of our studies of the residues involved in agonist binding in the nAChRs. Note, however, that the AChBPs are not neurotransmitter-gated ion channels; they are simply soluble proteins that evolved to contain a binding site. As such, they offer little information about the activation/gating pathway of the nAChRs. There is also a cryo-electron microscopy (EM) structure of the *Torpedo californica* ray nAChR.^{23, 24} This structure is of lower resolution than the AChBP structures (many amino acid side chains cannot be resolved), but it does provide a general picture of the overall secondary structural layout of a full-length nAChR (**Figure 1.3A**). Another major breakthrough in Cys-loop receptor research has come very recently with the publication of X-ray crystallography images of GluCl, an anion-selective invertebrate Cys-loop receptor that binds inhibitory neurotransmitters.²⁵ This protein does not bind ACh or other nicotinic agonists, and so it is almost certain that there will be interesting differences in its agonist binding site and also in its channel pore owing to its preference for anions (where nAChRs prefer cations). A key goal of research in the Dougherty lab is to test the

relevance of these model structures to the nAChRs and to try to use these static images to infer information about the conformational changes responsible for receptor activation and channel gating. The studies presented in this thesis primarily focus on residues in the agonist binding site, and so the AChBP structures have heavily guided this research.

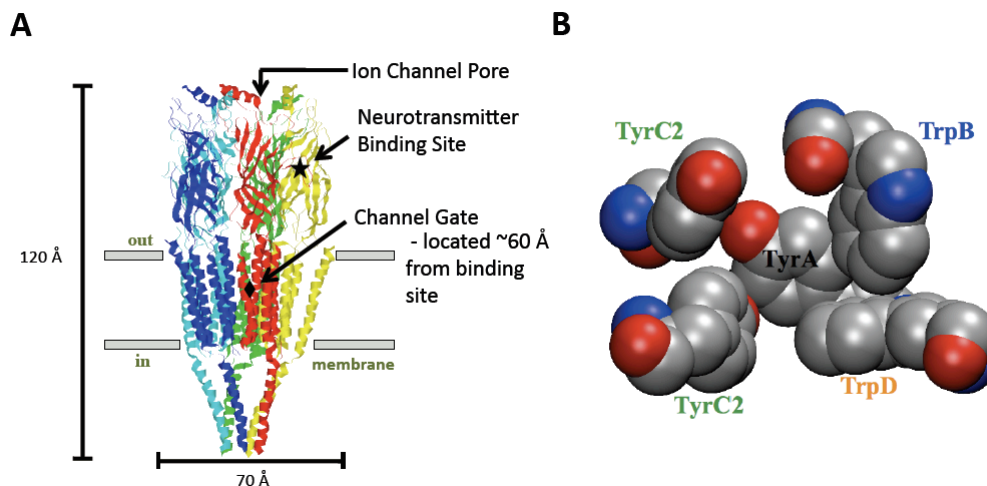


Figure 1.3. nAChR structure. (A) Structure of the nAChR based on cryo-EM structure of the *Torpedo* receptor (pdb: 2BG9). (B) Enlargement of aromatic box from AChBP (pdb: 119B).

Agonists bind at the interface of adjacent subunits in the nAChR pentamer.^{1, 4, 5}

The agonist binding site is a compact pocket comprised of amino acids from several noncontiguous regions from the “principal” (always an α subunit) and “complementary” (e.g., γ or δ in $\alpha_1\beta_1\gamma\delta$ or β_2 in $\alpha_4\beta_2$) subunits. These regions are referred to as loops A, B, and C from the principal subunit and loops D, E, and F from the complementary subunit. The α subunits are defined by a universally conserved vicinal disulfide between C192 and C193 (using $\alpha_1\beta_1\gamma\delta$ numbering). This disulfide has played a pivotal role in a number of pioneering studies in nAChR research,^{13, 14, 26-31} but its functional role in native receptors remains uncertain. Five conserved aromatic residues – α 1Y93 (loop A), α 1W149 (loop B), α 1Y190 (loop C), α 1Y198 (loop C), and γ W55/ δ W57 (loop D) – form

what is known as the aromatic binding box. For simplicity, these residues are often referred to as TrpA, TrpB, TyrC1, TyrC2 and TrpD representing the loop in which they reside (**Figure 1.3B**). Several aromatic box residues (particularly TrpB) have been shown to play roles in agonist binding to the nAChRs³²⁻³⁴ while others are predicted to play a role in shaping the agonist binding site or relaying conformational changes that are initiated upon agonist binding.

The ion channel pore is lined by the M2 helix from each subunit of the pentamer (**Figures 1.1 and 1.3A**). Each M2 helix contributes several highly conserved hydrophobic residues that constitute the channel gate. Of these, the L9' residue (where 9' represents the ninth residue from the cytoplasmic end of the transmembrane helix) comprises the narrowest constriction point in the *Torpedo* cryo-EM structure and sits at the approximate midpoint of the M2 helix.^{24, 34} This residue has been shown to play a critical role in channel gating, and when mutated to a more polar amino acid, the pore is stabilized in an open, ion-conducting conformation.^{35, 36} Given the 60 Å distance separating the L9' residue and the agonist binding site, it has been a bit of a mystery in nAChR research as to how structural changes that occur upon agonist binding are communicated to the channel gate. It has been suggested that a 'conformational wave' is responsible for transmitting conformational changes that initiate at the agonist binding site to the L9' residue.³⁷ Movements of the C loop, which contains the vicinal disulfide and two of the five aromatic box residues, have been strongly implicated³⁸⁻⁴⁰ in the gating process and are likely to be involved in the proposed conformational wave. Chapter 5 discusses a potential role for the vicinal disulfide and other residues of loop C in communicating conformational changes of the receptor.

1.3 Using Physical Organic Chemistry to Study Ion Channels: The Power of Unnatural Amino Acids

The overarching goal of the Dougherty lab is to obtain “chemical-scale” information – on a distance scale that is interesting to a physical organic chemist – on the structure and function of these receptors. By this we mean information about the functional groups, noncovalent interactions or conformational changes that are important for the activation and gating of these complex integral membrane proteins.

To obtain such an understanding, we could take a classical pharmacological approach and mutate the small molecule agonists of the receptor. This is certainly a viable strategy that we have used in several chapters of this thesis, but to obtain an understanding of the residues affected by mutation of the agonist, we must also mutate the receptor. A total chemical synthesis or even semisynthesis of a multisubunit, many kDA protein like the nAChR would certainly be quite a feat, made even more difficult if multiple variations in receptor structure are needed. But even if they were synthetically accessible, the proteins would need to be reconstituted into their native conformation and embedded into an appropriate membrane. An appropriate solution is to use conventional mutagenesis combined with heterologous expression of the protein. However, the extent of structural perturbations that can be performed by this methodology is limited by the structures of the side chains of the 20 naturally occurring amino acids.

As an illustration of these limitations, consider a study of a cation- π interaction in a protein. A cation- π interaction is a stabilizing, noncovalent (primarily electrostatic) interaction between a π system and a cation.⁴¹⁻⁴⁴ Nearly all neurotransmitters and ligands that bind to receptors and ion channels contain a positive charge,⁴⁵ and nature has equipped proteins with suitable π systems to bind these charges in the form of the

aromatic amino acids Phe, Tyr and Trp. In the Protein Data Bank, there is one cation- π interaction for every 77 amino acids, and approximately 26% of all Trp residues are involved in cation- π interactions.⁴²

To probe a cation- π interaction by conventional mutagenesis, the aromatic side chain of interest could be completely ablated by incorporation of an Ala residue, but this is a fairly dramatic mutation that doesn't directly probe the electrostatic component of the interaction and could affect the structure/function of the protein in a number of ways. Alternatively, the residue could be modified to one of the other two aromatic residues. However, although there are differences in cation- π binding energies between the aromatic amino acids, there are also many substantial structural differences that could also impact the protein's structure/function.

The use of an amino acid that is not found in nature – an unnatural amino acid – could provide a more productive probe of the cation- π interaction. For example, a Trp residue can be replaced with Trp derivatives bearing progressively fluorinated side chains. Due to the electronegativity of the atom, each fluorine added to an aromatic side chain diminishes the cation- π binding ability of the ring in an additive fashion. Moreover, the innate cation binding ability of the mutant side chain (**Figure 1.4**) can be plotted versus a functional measure of the protein (discussed below) to produce a “fluorination plot” (**Figure 1.5**). A linear trend in the fluorination plot is the signature of a cation- π interaction. The structural change incurred from replacing a hydrogen with a fluorine should also be quite subtle, certainly more subtle than the structural perturbations available in conventional mutagenesis. This thesis uses the fluorination strategy to probe cation- π interactions in the nAChR.

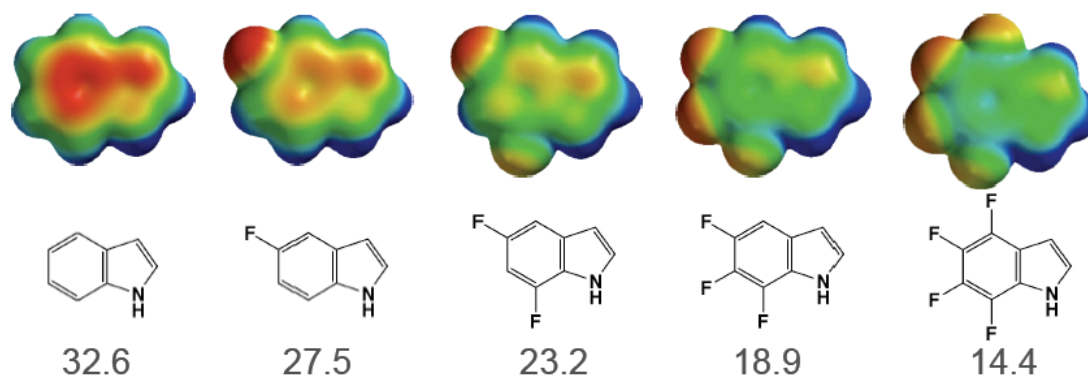


Figure 1.4. Fluorinated Trp side chains (indole rings) and calculated cation- π binding energies. Binding energies (kcal/mol) are from gas-phase *ab initio* calculations of the interaction between an indole side chain and a Na^+ ion.³³ Electrostatic potential maps show negative potentials (regions that a positive charge is likely to bind) in red and positive potentials in blue.

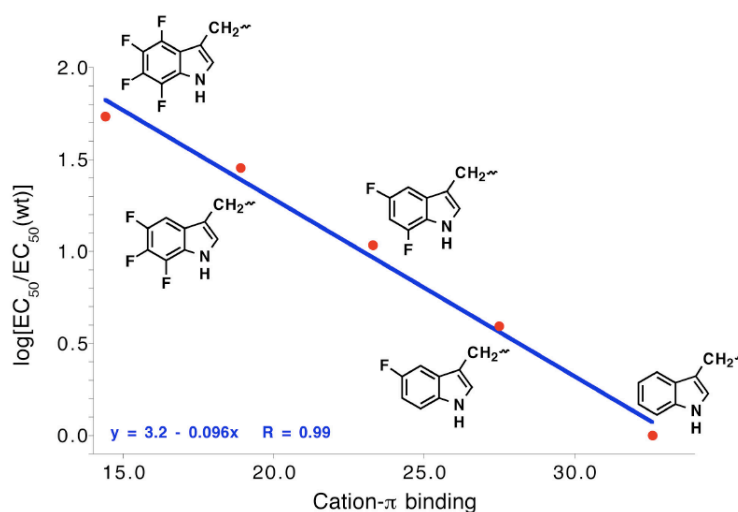


Figure 1.5. An example fluorination plot giving a linear trend indicative of a cation- π interaction. This plot was used to establish the cation- π interaction between an agonist and the $\alpha_1\beta_1\gamma\delta$ receptor.³³

Another testament of the usefulness of unnatural amino acids is seen in the study of hydrogen bonding interactions to the backbone amide bond of a protein. Since conventional mutagenesis is limited to side chain modification, it is difficult (if not impossible) to directly probe the importance of an amide bond by this methodology.

Backbone amide bonding can be probed using an unnatural amino acid strategy by replacing the residue that contributes the backbone NH with its α -hydroxy acid analog (**Figure 1.6**).⁴⁶⁻⁴⁹ This mutation converts the amide bond to an ester with two major effects on backbone hydrogen bonding. The backbone NH is replaced with an O and can therefore no longer serve as a hydrogen bond donor. This mutation also attenuates the hydrogen bonding ability of the *i-1* CO by converting it to an ester CO, which is well-established to be a poorer hydrogen bond acceptor than an amide CO. Thus, incorporation of an α -hydroxy acid can probe the hydrogen bonding ability of the associated amide NH and amide CO. This mutation can also potentially introduce an unfavorable electrostatic interaction by the introduction of an electronegative O, but this effect has been shown to be quite small in model studies, with an estimated 0.3–0.4 kcal/mol energetic consequence.^{50, 51} Overall, the amide-to-ester mutation results in a relatively subtle change in protein structure that maintains the original side chain properties and backbone conformational preferences (*e.g.*, bond lengths, bond angles and *cis-trans* conformational preferences) of the parent amide backbone.

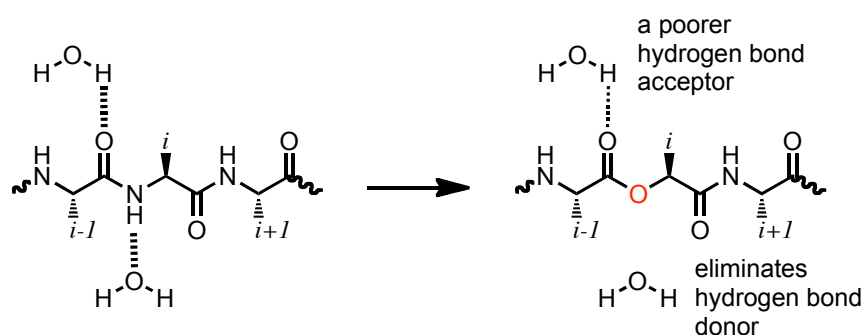


Figure 1.6. Amide-to-ester mutation.

Thus, unnatural amino acids enable subtle probes of protein structure and function that are not limited by the chemical diversity of conventional amino acid side chains.

Instead these studies are limited only by the boundaries of chemical synthesis and also by the diversity of structures that can be incorporated into proteins by a cellular ribosome via the nonsense or frameshift suppression methodology described below.

1.4 Incorporation of Unnatural Amino Acids Through Nonsense or Frameshift Suppression Methodology

Nonsense suppression methodology was developed in the late 1980s for the site-specific incorporation of unnatural amino acids into proteins.⁵²⁻⁵⁴ In normal protein synthesis, mRNA is decoded by a ribosome and matched by its three nucleotide codon to its cognate tRNA. The nonsense suppression method employs a stop codon (UAG, UGA or UAA), which does not code for any natural tRNAs and is instead used to signify a stop (termination) in protein synthesis. The unnatural amino acid is appended to an “orthogonal” suppressor tRNA with the corresponding anticodon. An orthogonal tRNA is one that is not recognized by any of the endogenous aminoacyl-tRNA synthetases, the enzymes that append natural amino acids onto their cognate tRNAs. During protein synthesis, the ribosome incorporates the unnatural amino acid into the polypeptide sequence at the site of interest (the location of the stop codon) (**Figure 1.7**).

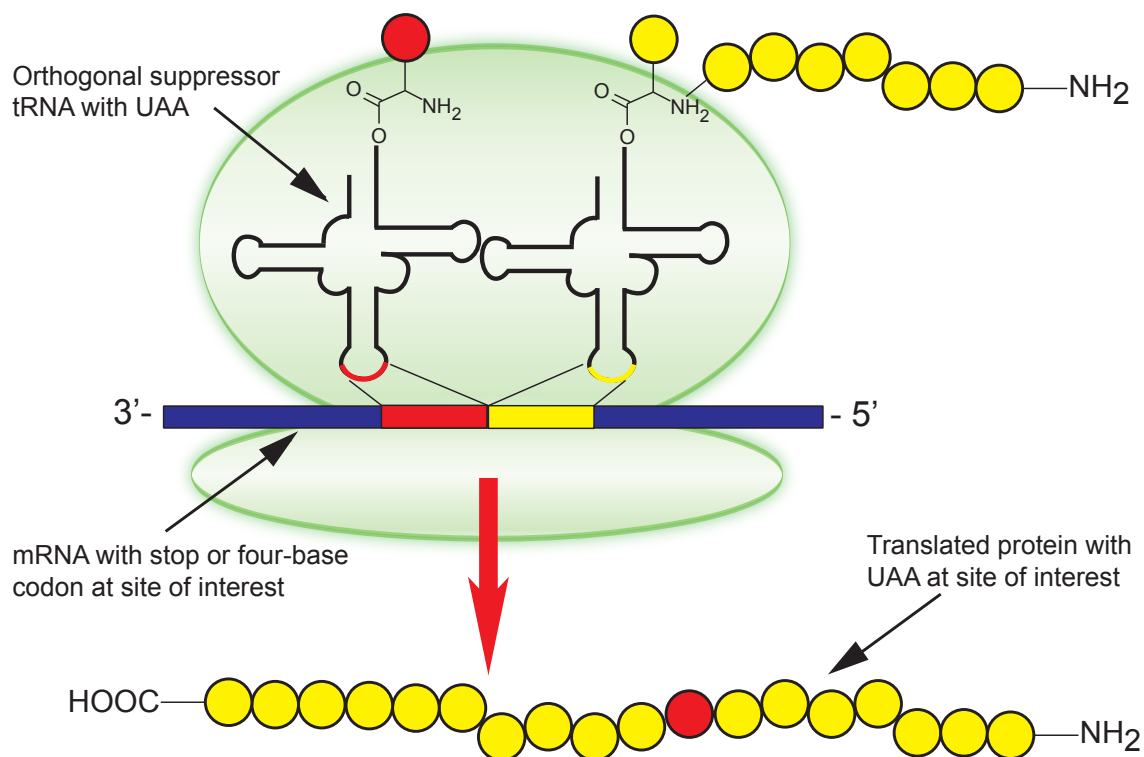


Figure 1.7. An overview of the nonsense and frameshift suppression methodologies used to incorporate unnatural amino acids (UAAs).

An alternative method for incorporating unnatural amino acids is frameshift suppression, which uses a four-base codon (GGGT) instead of a stop codon.^{55, 56} This method employs a suppressor tRNA with the corresponding four-base anticodon to incorporate the unnatural amino acid and, as a result, suppresses the reading frame shift that would normally occur when the ribosome encounters a four-base codon. By using combinations of stop (TAG or TGA) and four-base (GGGT) codons, multiple unnatural amino acids can be incorporated into a single protein.⁵⁷

Both methodologies require a combination of techniques in chemical synthesis and molecular biology.^{45, 58, 59} Standard mutagenesis protocols are used to mutate a stop codon (or four base codon) into the gene of the protein being studied at the site of

interest. The suppressor tRNA is transcribed without the last two nucleotides of the acceptor stem (C and A). The deoxy-C and A (dCA) dinucleotide is then chemically synthesized and used as an adapter to append an unnatural amino acid to truncated suppressor tRNA (**Figure 1.8**). Unnatural amino acids are chemically synthesized and their α -amino groups are protected by a photo- or I_2 - labile protecting group (α -hydroxy acids are not protected). The free carboxylate of the amino acid is then activated as a cyanomethyl ester to facilitate acylation onto the dCA dinucleotide. This complex is then enzymatically ligated onto the acceptor stem of the truncated suppressor tRNA to yield amino-acylated tRNA.

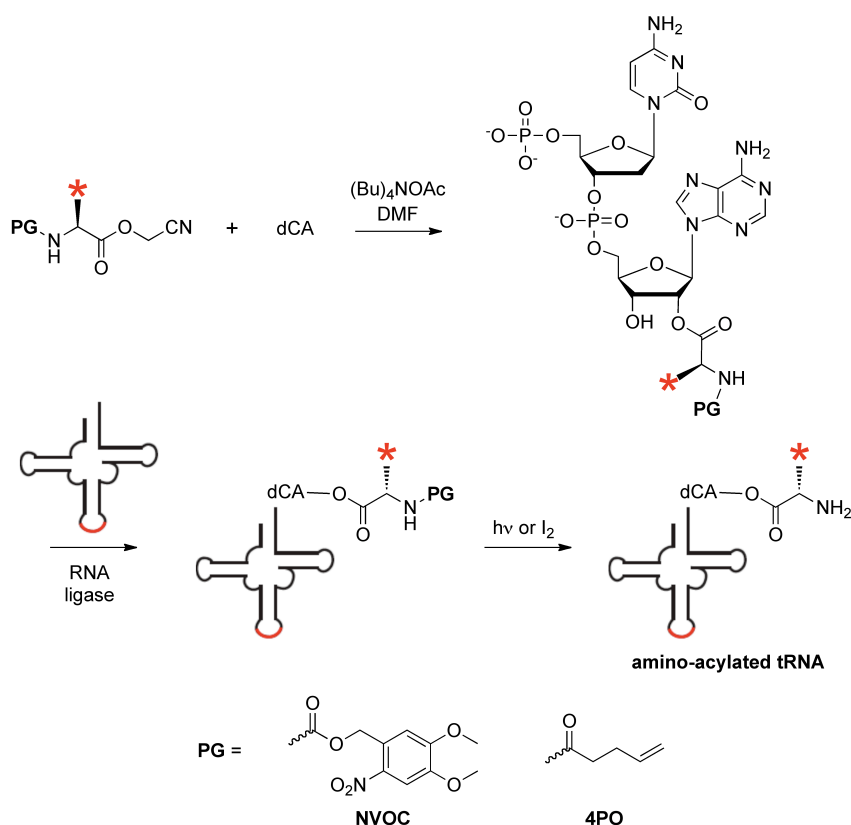


Figure 1.8. Schematic of the production of amino-acylated tRNA. The nitroveratryloxycarbonyl (NVOC) protecting group is photolabile and the 4-PO protecting group is removable by treatment with I_2 .

With the mRNA bearing the stop codon and the amino-acylated tRNA in hand, we use heterologous expression to express the proteins in a native-like membrane environment (**Figure 1.9**). In our studies, we use *Xenopus* oocytes, egg cell precursors from an African frog, as our heterologous expression system. Upon injection of mRNA and amino-acylated tRNA, the oocyte synthesizes, folds, assembles, and transports the protein to the surface of the cell membrane. When expressed in a *Xenopus* oocyte, the pharmacology and physiology of the proteins are indistinguishable from those found in native environments.⁴⁵

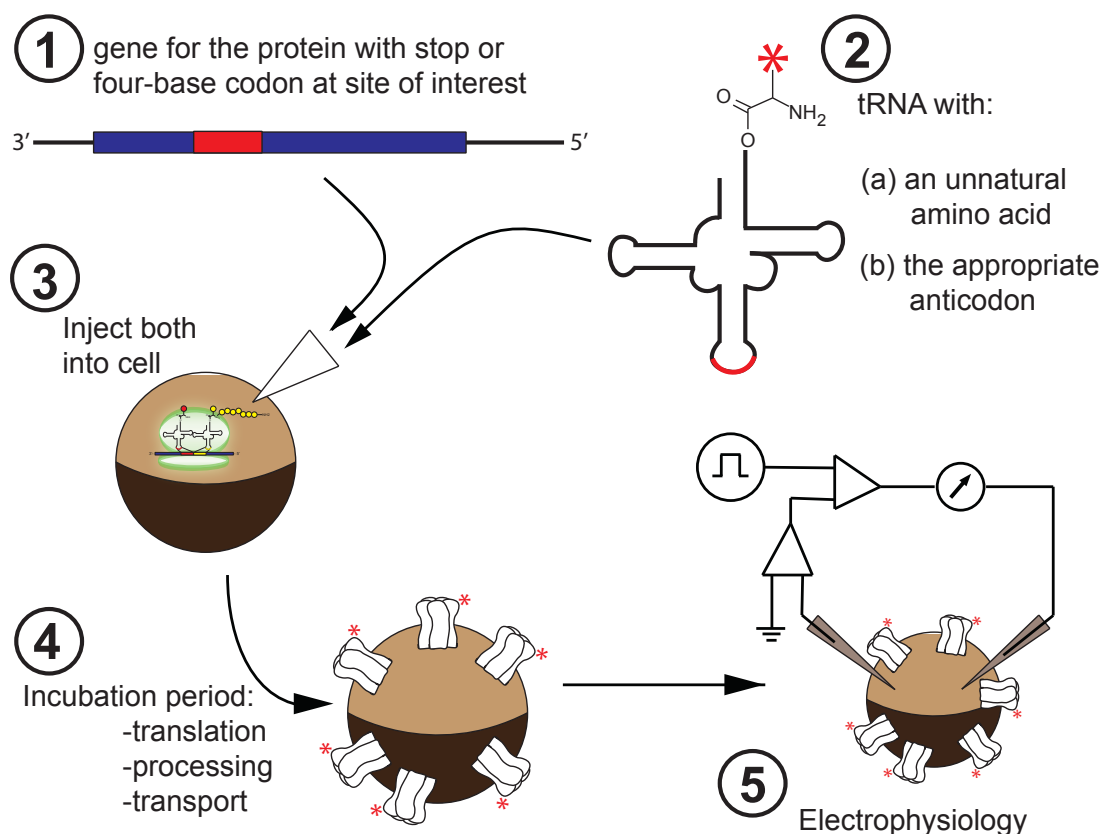


Figure 1.9. Implementation of the nonsense or frameshift suppression methodology for incorporating unnatural amino acids into ion channels expressed in *Xenopus* oocytes.

1.5 Electrophysiology as an Assay of Receptor Function

The suppressor tRNA used in these applications is a stoichiometric reagent. After incorporation of the unnatural amino acid into the protein, the tRNA cannot be aminoacylated with more unnatural amino acid within the cell. As such, protein yields cannot exceed the amount of injected tRNA. A sensitive assay is therefore needed to assess the function of mutant proteins. Because we are studying ligand-gated ion channel proteins that enable the flow of ions across the cell membrane, we can use the highly sensitive assay of two-electrode voltage clamp electrophysiology to monitor the impact of each mutation on protein function by measuring changes in agonist-induced current (**Figure 1.10**). In these assays, increasing concentrations of agonist are applied to the cell, which in turn, induce increasing currents (**Figure 1.10B**). From this, a dose-response relationship is generated, which is fit to the Hill equation (**equation 1**) to yield the EC_{50} —the concentration of the agonist that induces a half-maximal current or the midpoint of a dose-response curve (**Figure 1.10C**). We use EC_{50} as a convenient metric to compare ion channel function. Mutations that disrupt the function of a protein (loss-of-function mutations) will result in an increase in EC_{50} , because higher concentrations of agonist are required to evoke the same response. In contrast, a mutation that improves the function of the protein (a gain-of-function mutation) will require lower concentrations of agonist to achieve the same response and will therefore result in a lower EC_{50} value.

$$I_{Response} = \frac{I_{Max\ Response}}{1 + \left(\frac{EC_{50}}{[Agonist]}\right)^n} \quad (1)$$

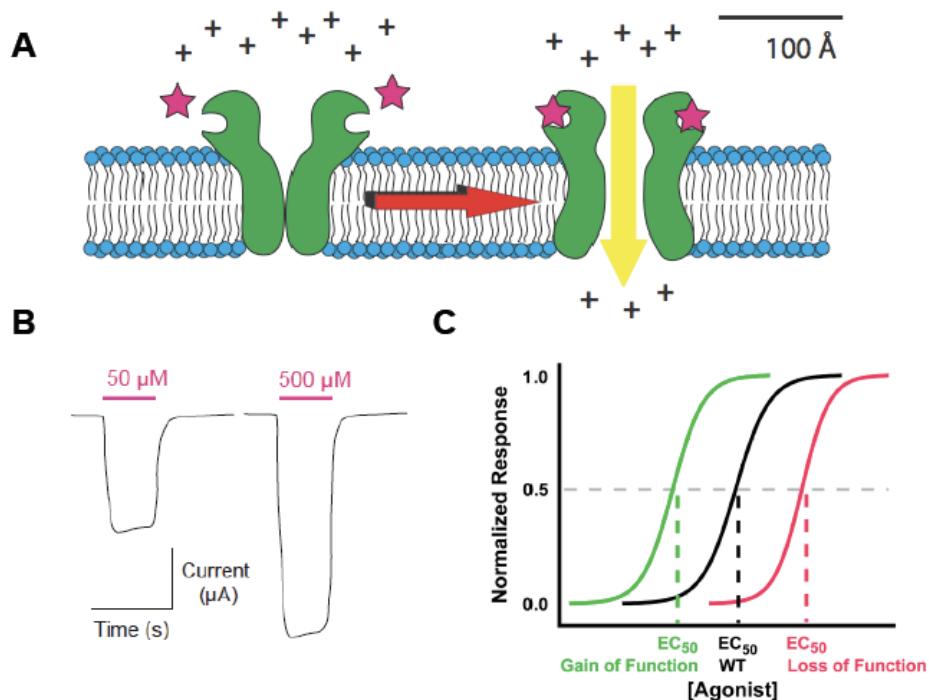


Figure 1.10. The electrophysiology assay. (A) Agonists bind to the ligand-gated ion channel and induce a conformational change in the protein that opens the ion channel pore. This facilitates the passage of ions across the membrane, producing a current that can be measured by electrophysiology. (B) Depiction of an agonist induced current measurement at varying concentrations. (C) Dose-response curves: The black curve represents the dose-response relation for the wild-type protein. The pink and green curves show the dose-response relation for a loss-of-function or gain-of-function mutation, respectively.

EC₅₀ is a composite measure of an agonist's potency, which is influenced by the agonist's affinity for the receptor and also its ability to induce opening of the ion channel (efficacy). As such, we use EC₅₀ as a metric to evaluate mutations that affect agonist binding or channel gating. Mutations that occur at the agonist binding site (60 Å away from the channel gate) are assumed to mainly affect binding while those farther away are expected to primarily affect gating, although there are exceptions.

1.6 Mutant Cycle Analysis

A common theme in many chapters of this thesis is to use mutant cycle analysis to understand the energetic coupling of a noncovalent interaction. Mutant cycle analysis is

the standard method used to measure the strength of intramolecular or intermolecular interactions in proteins or in protein-ligand complexes.⁶⁰ EC₅₀-based mutant cycle analyses have been employed by our lab⁶¹⁻⁶⁴ and others⁶⁵⁻⁶⁷ to investigate many interactions in Cys-loop receptors. In this thesis, mutant cycle analysis is used to study protein-protein interactions between amino acid residues (Chapter 5) and also to study protein-agonist interactions (Chapters 2 and 3). The latter requires mutation of an amino acid of the protein and also “mutation” of the agonist by classical pharmacological strategies.

In the case of two non-interacting residues (or residue and agonist pair), mutation of one site should have no energetic impact on the second site, and so the effect of simultaneous mutation of both sites should be multiplicative.⁶⁰ In a double mutant cycle analysis, this is seen in a coupling coefficient (Ω) of 1 (unity), where $\Omega = [EC_{50}(WT) * EC_{50}(\text{double mutant})] / [EC_{50}(\text{mutant 1}) * EC_{50}(\text{mutant 2})]$. If, on the other hand, the two residues (or residue/agonist pair) do interact, then the effect of simultaneous mutation will be greater or less than the product of the individual effects. In our studies, we generally define a significant interaction as having an Ω of <0.2 or >5 .

It is also standard practice to convert the coupling coefficient (Ω) into a free energy by the equation $\Delta\Delta G^\circ = -RT\ln(\Omega)$.⁶⁰ This is a convenient metric that we consider to be approximately equivalent to the strength of the interaction being studied. A coupling energy of >1 kcal/mol is typically considered indicative of a strong noncovalent interaction.

Mutant cycle analysis can also take on multi-dimensional forms when studying the interaction of three residues in a protein or other higher levels of cooperativity. In

Chapter 5, a three-dimensional mutant cycle analysis is used to characterize the interaction of three amino acids that we believe are important for channel gating.

1.7 The Nicotinic Pharmacophore

The nAChR has the longest known, best-studied pharmacophore of any neuroreceptor. A pharmacophore is an abstract description of the essential chemical features (*e.g.*, functional groups) of a group of structurally related ligands that are required for molecular recognition by a biological receptor. The nicotinic pharmacophore was first discussed in a 1970 publication by Beers and Reich in which two essential components – a cationic nitrogen (N^+) and a hydrogen bond acceptor – were identified in the structures of ACh and nicotine.⁶⁸ In later years, this model was revisited by several researchers, notably Barlow and Johnson⁶⁹ and Sheridan and co-workers,⁷⁰ and from these studies it was suggested that there is an optimal distance that separates the two components called the ‘internitrogen’ distance (because most nicotinic agonists have a pyridine N and a cationic N). Many of these studies converge around an optimal distance of 4.8 Å by comparing the structures of several agonists, but this number has been a topic of much debate, especially given that many high affinity agonists like epibatidine have larger internitrogen distances.⁷¹ A comparison of the structures and electrostatic potential maps of nicotinic agonists is shown in **Figure 1.11**.

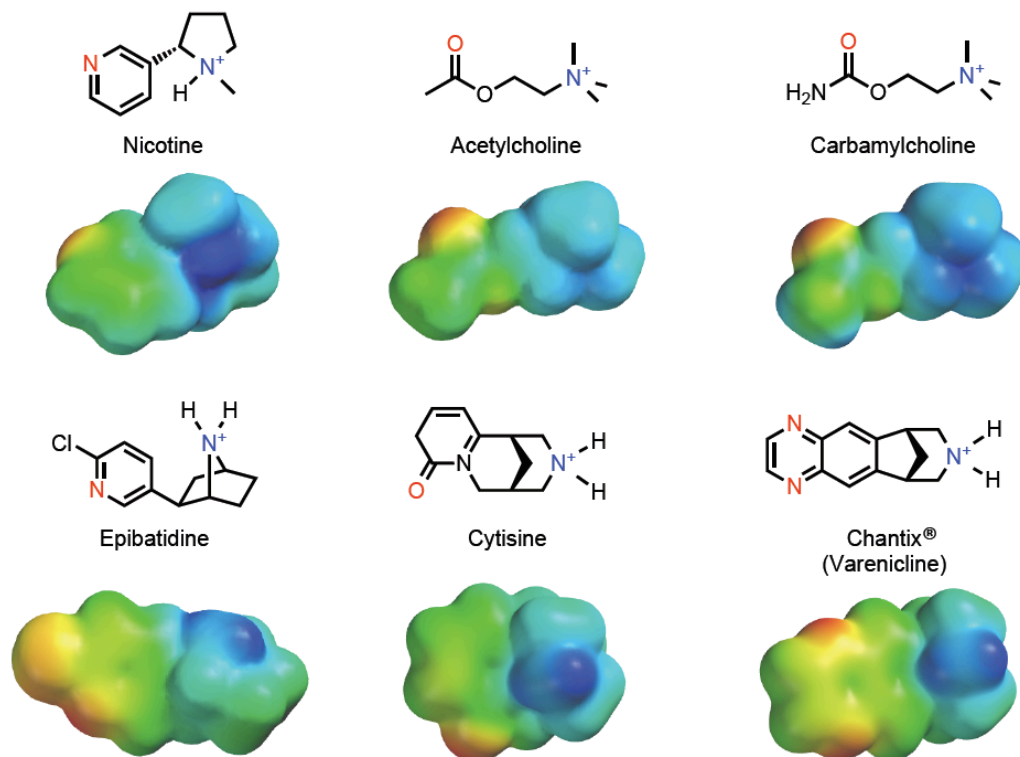


Figure 1.11. Structures and electrostatic potential maps of agonists of the nAChR. All structures contain the essential two-point pharmacophore – a cationic N (blue) and a hydrogen bond acceptor (red). Note that (+)-cytisine is shown in this figure, but (–)-cytisine is the natural isomer and is typically used in studies involving nAChRs.

In 1990, we suggested that the cationic N of acetylcholine could bind to an aromatic residue in the nAChR via a cation- π interaction.⁷² Subsequent studies involving incorporation of fluorinated amino acid derivatives (as described above; also see **Figure 1.5**) validated this model in several nAChRs, showing that ACh, nicotine and other agonists make a cation- π interaction to TrpB of the aromatic box (**Figure 1.3B**).^{33, 34, 73} AChBP structures with ligands bound confirmed this cation- π interaction and also suggested a second interaction to agonists with protonatable nitrogens (like the N⁺ of nicotine) – a hydrogen bond to the backbone CO of TrpB.^{18, 21} This interaction was subsequently validated by backbone ester mutagenesis in full-length receptors.^{34, 73} The AChBP structures also suggested a hydrogen bonding interaction involving the hydrogen

bond accepting group of the pharmacophore,^{18, 74} and this interaction is the focus of Chapters 2 and 3 of this thesis.

1.8 Summary of Dissertation Work

This dissertation primarily describes structure-function studies of the nAChR using a combination of unnatural amino acid mutagenesis, electrophysiology, mutant cycle analysis, and synthetic agonist analogs.

Chapters 2 and 3 describe studies aimed at probing binding interactions of the nicotinic pharmacophore using backbone ester mutagenesis and mutant cycle analyses with a synthetic analog of nicotine. These studies established a hydrogen bond between the pharmacophore's hydrogen bond acceptor, the pyridine N of nicotine or the acetyl CO of ACh, and a backbone NH of a residue in the complementary subunit. This interaction was shown to be important for binding of several agonists in the muscle-type receptor and also in both stoichiometries of $\alpha 4\beta 2$. The only agonist that violates this binding model is Pfizer's smoking cessation drug, varenicline.

Chapter 4 is an application of the pharmacophore binding model that seeks to understand the stereoselectivity of agonist binding by the nAChRs. Given that the nAChR is a chiral molecule, it is surprising that the two epibatidine enantiomers are equipotent. It is known that methylation of the NH of epibatidine negatively impacts the potency of one of the enantiomers at the $\alpha 4\beta 2$ receptor. In an attempt to understand these observations, we characterized the pharmacophore binding interactions of the epibatidine enantiomers and their *N*-methyl derivatives.

Chapter 5 describes studies concerning the vicinal disulfide, a conserved structural unit that defines the nAChR α subunits. We uncovered a hydrogen bond

network that was shown, by mutant cycle analysis, to link the peptide NH of the vicinal disulfide to another amide bond via a β turn and also to a functionally important residue in the complementary subunit. From this we propose that the role of the vicinal disulfide is to distort the β turn and thereby properly position a backbone NH that enables formation of the intersubunit hydrogen bond.

Strategies for the photochemical cleavage of protein and peptide backbones are described in Chapter 6. The first strategy is based on a selenide-mediated cleavage of a backbone ester moiety and utilizes an α -hydroxy acid whose side chain is a *o*-nitrobenzyl caged aryl selenide nucleophile. Studies with a model tripeptide establish the viability of the chemistry, but *in vivo* and *in vitro* studies of this methodology have been challenging. Also described are alternative backbone cleavage strategies based on aniline-mediated intramolecular cyclization and the photochemistry of the (2-nitrophenyl)ethyl (NPE) protecting group.

In Chapter 7, initial studies of a multi-institution collaboration are described. The preliminary studies presented herein seek to develop a small molecule strategy for photo-activation of a voltage-gated potassium channel. The ultimate goal of this collaboration is to develop a small molecule that can restore vision to patients whose retinal photoreceptors are compromised by disease.

Chapter 8 describes work that was completed prior to candidacy in the laboratory of Prof. Robert H. Grubbs in which a strategy was devised to prepare NHC-containing organometallic complexes from the thermolysis of 2-(pentafluorophenyl)imidazolidines. This is a simple, base-free method that could offer access to NHC complexes with functionality that is incompatible with other methods.

1.9 REFERENCES

1. Corringer, P. J.; Le Novère, N.; Changeux, J. P., Nicotinic receptors at the amino acid level. *Annu. Rev. Pharmacol. Toxicol.* **2000**, 40, 431-58.
2. Romanelli, M. N.; Gratterer, P.; Guandalini, L.; Martini, E.; Bonaccini, C.; Gualtieri, F., Central nicotinic receptors: structure, function, ligands, and therapeutic potential. *ChemMedChem* **2007**, 2, (6), 746-67.
3. Jensen, A. A.; Frolund, B.; Liljefors, T.; Krogsgaard-Larsen, P., Neuronal nicotinic acetylcholine receptors: structural revelations, target identifications, and therapeutic inspirations. *J. Med. Chem.* **2005**, 48, (15), 4705-45.
4. Grutter, T.; Changeux, J. P., Nicotinic receptors in wonderland. *Trends Biochem. Sci.* **2001**, 26, (8), 459-63.
5. Karlin, A., Emerging structure of the nicotinic acetylcholine receptors. *Nat. Rev. Neurosci.* **2002**, 3, (2), 102-14.
6. Gotti, C.; Zoli, M.; Clementi, F., Brain nicotinic acetylcholine receptors: native subtypes and their relevance. *Trends Pharmacol. Sci.* **2006**, 27, (9), 482-91.
7. Coe, J. W.; Brooks, P. R.; Vetelino, M. G.; Wirtz, M. C.; Arnold, E. P.; Huang, J.; Sands, S. B.; Davis, T. I.; Lebel, L. A.; Fox, C. B.; Shrikhande, A.; Heym, J. H.; Schaeffer, E.; Rollema, H.; Lu, Y.; Mansbach, R. S.; Chambers, L. K.; Rovetti, C. C.; Schulz, D. W.; Tingley, F. D.; O'Neill, B. T., Varenicline: an alpha4beta2 nicotinic receptor partial agonist for smoking cessation. *J. Med. Chem.* **2005**, 48, (10), 3474-3477.
8. Gonzales, D.; Rennard, S. I.; Nides, M.; Oncken, C.; Azoulay, S.; Billing, C. B.; Watsky, E. J.; Gong, J.; Williams, K. E.; Reeves, K. R., Varenicline, an alpha4beta2 nicotinic acetylcholine receptor partial agonist, vs. sustained-release bupropion and placebo for smoking cessation. *J. Am. Med. Assoc.* **2006**, 296, (1), 47-55.
9. Mihalak, K. B.; Carroll, F. I.; Luetje, C. W., Varenicline is a partial agonist at alpha4beta2 and a full agonist at alpha7 neuronal nicotinic receptors. *Mol. Pharmacol.* **2006**, 70, (3), 801-805.
10. Moroni, M.; Zwart, R.; Sher, E.; Cassels, B. K.; Bermudez, I., Alpha4Beta2 nicotinic receptors with high and low acetylcholine sensitivity: pharmacology, stoichiometry, and sensitivity to long-term exposure to nicotine. *Mol. Pharmacol.* **2006**, 70, (2), 755-68.
11. Czajkowski, C.; Kaufmann, C.; Karlin, A., Negatively charged amino acid residues in the nicotinic receptor delta subunit that contribute to the binding of acetylcholine. *Proc. Natl. Acad. Sci. USA* **1993**, 90, (13), 6285-9.
12. Dennis, M.; Giraudat, J.; Kotzby-Hibert, F.; Goeldner, M.; Hirth, C.; Chang, J. Y.; Lazure, C.; Chretien, M.; Changeux, J. P., Amino acids of the *Torpedo marmorata* acetylcholine receptor alpha subunit labeled by a photoaffinity ligand for the acetylcholine binding site. *Biochemistry* **1988**, 27, (7), 2346-2357.
13. Chabala, L. D.; Lester, H. A., Activation of acetylcholine receptor channels by covalently bound agonists in cultured rat myoballs. *J. Physiol.* **1986**, 379, 83-108.
14. Karlin, A., Chemical modification of the active site of the acetylcholine receptor. *J. Gen. Physiol.* **1969**, 54, (1), 245-64.

15. Silman, I.; Karlin, A., Acetylcholine receptor: covalent attachment of depolarizing groups at the active site. *Science* **1969**, 164, (3886), 1420-1421.
16. Kao, P. N.; Dwork, A. J.; Kaldany, R. R.; Silver, M. L.; Wideman, J.; Stein, S.; Karlin, A., Identification of the alpha subunit half-cystine specifically labeled by an affinity reagent for the acetylcholine receptor binding site. *J. Biol. Chem.* **1984**, 259, (19), 11662-5.
17. Brejc, K.; van Dijk, W. J.; Klaassen, R. V.; Schuurmans, M.; van Der Oost, J.; Smit, A. B.; Sixma, T. K., Crystal structure of an ACh-binding protein reveals the ligand-binding domain of nicotinic receptors. *Nature* **2001**, 411, (6835), 269-76.
18. Celie, P.; van Rossum-Fikkert, S.; Van Dyke, W.; Brejc, K.; Smit, A.; Sixma, T., Nicotine and carbamylcholine binding to nicotinic acetylcholine receptors as studied in AChBP crystal structures. *Neuron* **2004**, 41, 907-914.
19. Rucktooa, P.; Smit, A. B.; Sixma, T. K., Insight in nAChR subtype selectivity from AChBP crystal structures. *Biochem. Pharmacol.* **2009**, 78, (7), 777-87.
20. Hansen, S. B.; Sulzenbacher, G.; Huxford, T.; Marchot, P.; Bourne, Y.; Taylor, P., Structural characterization of agonist and antagonist-bound acetylcholine-binding protein from *Aplysia californica*. *J. Mol. Neurosci.* **2006**, 30, (1-2), 101-2.
21. Hansen, S. B.; Sulzenbacher, G.; Huxford, T.; Marchot, P.; Taylor, P.; Bourne, Y., Structures of *Aplysia* AChBP complexes with nicotinic agonists and antagonists reveal distinctive binding interfaces and conformations. *EMBO J.* **2005**, 24, (20), 3635-46.
22. Taylor, P.; Talley, T. T.; Radic, Z.; Hansen, S. B.; Hibbs, R. E.; Shi, J., Structure-guided drug design: conferring selectivity among neuronal nicotinic receptor and acetylcholine-binding protein subtypes. *Biochem. Pharmacol.* **2007**, 74, (8), 1164-71.
23. Miyazawa, A.; Fujiyoshi, Y.; Stowell, M.; Unwin, N., Nicotinic acetylcholine receptor at 4.6 Å resolution: transverse tunnels in the channel wall. *J. Mol. Biol.* **1999**, 288, (4), 765-86.
24. Unwin, N., Refined structure of the nicotinic acetylcholine receptor at 4 Å resolution. *J. Mol. Biol.* **2005**, 346, (4), 967-89.
25. Hibbs, R. E.; Gouaux, E., Principles of activation and permeation in an anion-selective Cys-loop receptor. *Nature* **2011**, 474, (7349), 54-60.
26. Karlin, A.; Bartels, E., Effects of blocking sulfhydryl groups and of reducing disulfide bonds on the acetylcholine-activated permeability system of the electroplax. *Biochim. Biophys. Acta* **1966**, 126, (3), 525-35.
27. Damle, V. N.; Karlin, A., Effects of agonists and antagonists on the reactivity of the binding site disulfide in acetylcholine receptor from *Torpedo californica*. *Biochemistry* **1980**, 19, (17), 3924-32.
28. Czajkowski, C.; Karlin, A., Agonist binding site of Torpedo electric tissue nicotinic acetylcholine receptor. A negatively charged region of the delta subunit within 0.9 nm of the alpha subunit binding site disulfide. *J. Biol. Chem.* **1991**, 266, (33), 22603-22612.
29. Czajkowski, C.; Karlin, A., Structure of the nicotinic receptor acetylcholine-binding site. *J. Biol. Chem.* **1995**, 270, (7), 3160-3164.

30. Martin, M.; Czajkowski, C.; Karlin, A., The contributions of aspartyl residues in the acetylcholine receptor gamma and delta subunits to the binding of agonists and competitive antagonists. *J. Biol. Chem.* **1996**, 271, (23), 13497-503.
31. Walker, J. W.; Lukas, R. J.; McNamee, M. G., Effects of thio-group modifications on the ion permeability control and ligand binding properties of *Torpedo californica* acetylcholine receptor. *Biochemistry* **1981**, 20, (8), 2191-9.
32. Puskar, N. L.; Xiu, X.; Lester, H. A.; Dougherty, D. A., Two neuronal nicotinic acetylcholine receptors, alpha4beta4 and alpha7, show differential agonist binding modes. *J. Biol. Chem.* **2011**, 286, (16), 14618-27.
33. Zhong, W.; Gallivan, J. P.; Zhang, Y.; Li, L.; Lester, H. A.; Dougherty, D. A., From *ab initio* quantum mechanics to molecular neurobiology: a cation- π binding site in the nicotinic receptor. *Proc. Natl. Acad. Sci. USA* **1998**, 95, (21), 12088-93.
34. Xiu, X.; Puskar, N. L.; Shanata, J. A.; Lester, H. A.; Dougherty, D. A., Nicotine binding to brain receptors requires a strong cation- π interaction. *Nature* **2009**, 458, (7237), 534-7.
35. Filatov, G. N.; White, M. M., The role of conserved leucines in the M2 domain of the acetylcholine receptor in channel gating. *Mol. Pharmacol.* **1995**, 48, (3), 379-84.
36. Labarca, C.; Nowak, M. W.; Zhang, H.; Tang, L.; Deshpande, P.; Lester, H. A., Channel gating governed symmetrically by conserved leucine residues in the M2 domain of nicotinic receptors. *Nature* **1995**, 376, (6540), 514-6.
37. Grosman, C.; Zhou, M.; Auerbach, A., Mapping the conformational wave of acetylcholine receptor channel gating. *Nature* **2000**, 403, (6771), 773-776.
38. Shi, J.; Koeppe, J. R.; Komives, E. A.; Taylor, P., Ligand-induced conformational changes in the acetylcholine-binding protein analyzed by hydrogen-deuterium exchange mass spectrometry. *J. Biol. Chem.* **2006**, 281, (17), 12170-7.
39. Sixma, T. K.; Smit, A. B., Acetylcholine binding protein (AChBP): a secreted glial protein that provides a high-resolution model for the extracellular domain of pentameric ligand-gated ion channels. *Annu. Rev. Biophys. Biomol. Struct.* **2003**, 32, 311-34.
40. Gao, F.; Mer, G.; Tonelli, M.; Hansen, S. B.; Burghardt, T. P.; Taylor, P.; Sine, S. M., Solution NMR of acetylcholine binding protein reveals agonist-mediated conformational change of the C-loop. *Mol. Pharmacol.* **2006**, 70, (4), 1230-5.
41. Dougherty, D. A., Cation- π interactions in chemistry and biology: a new view of benzene, Phe, Tyr, and Trp. *Science* **1996**, 271, (5246), 163-8.
42. Gallivan, J. P.; Dougherty, D. A., Cation- π interactions in structural biology. *Proc. Natl. Acad. Sci. USA* **1999**, 96, (17), 9459-64.
43. Ma, J. C.; Dougherty, D. A., The cation- π interaction. *Chem. Rev.* **1997**, 97, (5), 1303-1324.
44. Zacharias, N.; Dougherty, D. A., Cation- π interactions in ligand recognition and catalysis. *Trends Pharmacol. Sci.* **2002**, 23, (6), 281-7.
45. Dougherty, D. A., Physical organic chemistry on the brain. *J. Org. Chem.* **2008**, 73, (10), 3667-3673.
46. Koh, J. T.; Cornish, V. W.; Schultz, P. G., An experimental approach to evaluating the role of backbone interactions in proteins using unnatural amino acid mutagenesis. *Biochemistry* **1997**, 36, 11314-11322.

47. Deechongkit, S.; Nguyen, H.; Powers, E. T.; Dawson, P. E.; Gruebele, M.; Kelly, J. W., Context-dependent contributions of backbone hydrogen bonding to beta-sheet folding energetics. *Nature* **2004**, 430, (6995), 101-5.
48. Deechongkit, S.; Dawson, P. E.; Kelly, J. W., Toward assessing the position-dependent contributions of backbone hydrogen bonding to beta-sheet folding thermodynamics employing amide-to-ester perturbations. *J. Am. Chem. Soc.* **2004**, 126, (51), 16762-71.
49. England, P. M.; Zhang, Y. N.; Dougherty, D. A.; Lester, H. A., Backbone mutations in transmembrane domains of a ligand-gated ion channel: Implications for the mechanism of gating. *Cell* **1999**, 96, (1), 89-98.
50. Fu, Y.; Gao, J.; Bieschke, J.; Dendle, M. A.; Kelly, J. W., Amide-to-*E*-olefin *versus* amide-to-ester backbone H-bond perturbations: evaluating the O-O repulsion for extracting H-bond energies. *J. Am. Chem. Soc.* **2006**, 128, (50), 15948-15949.
51. Gao, J.; Kelly, J. W., Toward quantification of protein backbone-backbone hydrogen bonding energies: An energetic analysis of an amide-to-ester mutation in an alpha-helix within a protein. *Protein Sci.* **2008**, 17, (6), 1096-101.
52. Bain, J. D.; Wacker, D. A.; Kuo, E. E.; Chamberlin, R. A., Site-specific incorporation of non-natural residues into peptides: effect of residue structure on suppression and translation efficiencies. *Tetrahedron* **1991**, 47, 2389-2400.
53. Ellman, J. A.; Mendel, D.; Schultz, P. G., Site-specific incorporation of novel backbone structures into proteins. *Science* **1992**, 255, (5041), 197-200.
54. Noren, C. J.; Anthony-Cahill, S. J.; Griffith, M. C.; Schultz, P. G., A general-method for site-specific incorporation of unnatural amino-acids into proteins. *Science* **1989**, 244, 182-188.
55. Rodriguez, E. A.; Lester, H. A.; Dougherty, D. A., Improved amber and opal suppressor tRNAs for incorporation of unnatural amino acids *in vivo*. Part 1: minimizing misacylation. *RNA* **2007**, 13, (10), 1703-14.
56. Rodriguez, E. A.; Lester, H. A.; Dougherty, D. A., Improved amber and opal suppressor tRNAs for incorporation of unnatural amino acids *in vivo*. Part 2: evaluating suppression efficiency. *RNA* **2007**, 13, (10), 1715-22.
57. Rodriguez, E. A.; Lester, H. A.; Dougherty, D. A., In vivo incorporation of multiple unnatural amino acids through nonsense and frameshift suppression. *Proc. Natl. Acad. Sci. USA* **2006**, 103, (23), 8650-5.
58. Nowak, M. W.; Gallivan, J. P.; Silverman, S. K.; Labarca, C. G.; Dougherty, D. A.; Lester, H. A., *In vivo* incorporation of unnatural amino acids into ion channels in a *Xenopus* oocyte expression system. *Methods Enzymol.* **1998**, 293, 504-529.
59. Nowak, M. W.; Kearney, P. C.; Sampson, J. R.; Saks, M. E.; Labarca, C. G.; Silverman, S. K.; Zhong, W.; Thorson, J.; Abelson, J. N.; Davidson, N.; et al., Nicotinic receptor binding site probed with unnatural amino acid incorporation in intact cells. *Science* **1995**, 268, (5209), 439-42.
60. Horovitz, A., Double-mutant cycles: a powerful tool for analyzing protein structure and function. *Fold Des.* **1996**, 1, (6), R121-6.
61. Blum, A. P.; Gleitsman, K. R.; Lester, H. A.; Dougherty, D. A., Evidence for an extended hydrogen bond network in the binding site of the nicotinic receptor:

- concerning the role of the vicinal disulfide of the $\alpha 1$ subunit. *J. Biol. Chem.* **2011**.
62. Blum, A. P.; Lester, H. A.; Dougherty, D. A., Nicotinic pharmacophore: the pyridine N of nicotine and carbonyl of acetylcholine hydrogen bond across a subunit interface to a backbone NH. *Proc. Natl. Acad. Sci. USA* **2010**, 107, (30), 13206-11.
 63. Gleitsman, K. R.; Kedrowski, S. M. A.; Lester, H. A.; Dougherty, D. A., An intersubunit hydrogen bond in the nicotinic acetylcholine receptor that contributes to channel gating. *J. Biol. Chem.* **2008**, 283, (51), 35638-35643.
 64. Kedrowski, S. M.; Bower, K. S.; Dougherty, D. A., 1-Oxo-5-hydroxytryptamine: a surprisingly potent agonist of the 5-HT₃ (serotonin) receptor. *Org. Lett.* **2007**, 9, (17), 3205-7.
 65. Kash, T. L.; Jenkins, A.; Kelley, J. C.; Trudell, J. R.; Harrison, N. L., Coupling of agonist binding to channel gating in the GABA(A) receptor. *Nature* **2003**, 421, (6920), 272-5.
 66. Price, K. L.; Millen, K. S.; Lummis, S. C., Transducing agonist binding to channel gating involves different interactions in 5-HT₃ and GABA_C receptors. *J. Biol. Chem.* **2007**, 282, (35), 25623-30.
 67. Venkatachalan, S. P.; Czajkowski, C., A conserved salt bridge critical for GABA_A receptor function and loop C dynamics. *Proc. Natl. Acad. Sci. USA* **2008**, 105, (36), 13604-9.
 68. Beers, W. H.; Reich, E., Structure and activity of acetylcholine. *Nature* **1970**, 228, (5275), 917-22.
 69. Barlow, R. B.; Johnson, O., Relations between structure and nicotine-like activity: X-ray crystal structure analysis of (–)-cytisine and (–)-lobeline hydrochloride and a comparison with (–)-nicotine and other nicotine-like compounds. *Br. J. Pharmacol.* **1989**, 98, (3), 799-808.
 70. Sheridan, R. P.; Nilakantan, R.; Dixon, J. S.; Venkataraghavan, R., The ensemble approach to distance geometry: application to the nicotinic pharmacophore. *J. Med. Chem.* **1986**, 29, (6), 899-906.
 71. Glennon, R. A.; Dukat, M.; Liao, L., Musings on $\alpha 4\beta 2$ nicotinic acetylcholine (nACh) receptor pharmacophore models. *Curr. Top. Med. Chem.* **2004**, 4, (6), 631-44.
 72. Dougherty, D. A.; Stauffer, D. A., Acetylcholine binding by a synthetic receptor. Implications for biological recognition. *Science* **1990**, 250, 1558-1560.
 73. Cashin, A. L.; Petersson, E. J.; Lester, H. A.; Dougherty, D. A., Using physical chemistry to differentiate nicotinic from cholinergic agonists at the nicotinic acetylcholine receptor. *J. Am. Chem. Soc.* **2005**, 127, (1), 350-356.
 74. Gao, F.; Bren, N.; Burghardt, T. P.; Hansen, S.; Henchman, R. H.; Taylor, P.; McCammon, J. A.; Sine, S. M., Agonist-mediated conformational changes in acetylcholine-binding protein revealed by simulation and intrinsic tryptophan fluorescence. *J. Biol. Chem.* **2005**, 280, (9), 8443-51.

CHAPTER 2: The Nicotinic Pharmacophore: The Pyridine N of Nicotine and Carbonyl of ACh Hydrogen Bond Across a Subunit Interface to a Backbone NH*

2.1 ABSTRACT

Pharmacophore models for nicotinic agonists have been proposed for four decades. Central to these models is the presence of a cationic nitrogen and a hydrogen bond acceptor. It is now well-established that the cationic center makes an important cation- π interaction to a conserved tryptophan, but the donor to the proposed hydrogen bond acceptor has been more challenging to identify. A structure of nicotine bound to the acetylcholine binding protein (AChBP) predicted that the binding partner of the pharmacophore's second component was a water molecule, which also hydrogen bonds to the backbone of the complementary subunit of the receptors. Here we use unnatural amino acid mutagenesis coupled with agonist analogs to examine whether such a hydrogen bond is functionally significant in the $\alpha 4\beta 2$ neuronal nAChR, the receptor most associated with nicotine addiction. We find evidence for the hydrogen bond with the agonists nicotine, acetylcholine, carbamylcholine, epibatidine, and cytisine, but do not find evidence for the hydrogen bond with varenicline. These data represent a completed nicotinic pharmacophore for most nicotinic agonists and offer insight into the design of new therapeutic agents that selectively target these receptors.

* *This chapter is adapted from:* Blum, A. P.; Lester, H. A.; Dougherty, D. A., Nicotinic pharmacophore: The pyridine N of nicotine and carbonyl of acetylcholine hydrogen bond across a subunit interface to a backbone NH. *Proceedings of the National Academy of Sciences of the USA* **2010**, 107, (30), 13206-11. Copyright 2010 by the National Academy of Sciences. *The work described in this chapter concerning cytisine, varenicline and the A3B2 receptor was done in collaboration with Nyssa L. Puskar, Darren T. Nakamura, Ximena Da Silva Tavarres Bongoll, and Dr. Jai A. P. Shanata.*

2.2 INTRODUCTION

The nicotinic acetylcholine receptor (nAChR) is a pentameric, ligand-gated ion channel activated by the neurotransmitter acetylcholine (ACh), and also by nicotine and structurally related agonists.¹⁻³ Nicotinic receptors mediate fast synaptic transmission at the neuromuscular junction of the peripheral nervous system. In addition, a family of paralogous nAChRs termed the neuronal receptors function in the central nervous system and certain autonomic ganglia, and the addictive and cognitive properties of nicotine are associated with these neuronal receptors.^{4, 5} Neuronal receptors comprised of $\alpha 4$ and $\beta 2$ subunits are most strongly associated with nicotine addiction.⁶⁻⁹ They are upregulated during chronic nicotine exposure and are implicated in various disorders, including Alzheimer's disease and schizophrenia, and in protection against Parkinson's disease. Interest in the development of molecules that selectively target $\alpha 4\beta 2$ receptors has been growing, highlighted by the development of the smoking cessation drug, varenicline.⁶

Many have undertaken the task of dissecting nicotinic agonists into a core pharmacophore, since the first publication on the topic in 1970.¹⁰ While the details are debated, two aspects are clear. Nicotinic agonists contain a cationic nitrogen and a hydrogen bond acceptor (**Figure 2.1A**).^{11, 12} In 1990, we proposed that binding of the cationic nitrogen of acetylcholine would be mediated through a cation- π interaction with an aromatic residue of the nAChRs.¹³ We subsequently validated this model with the identification of a cation- π interaction to a conserved tryptophan residue for both acetylcholine and nicotine.^{14, 15} In fact, the cation- π interaction has been shown to be a general contributor to agonist affinity across the entire family of Cys-loop (pentameric) neurotransmitter-gated ion channels.¹⁶

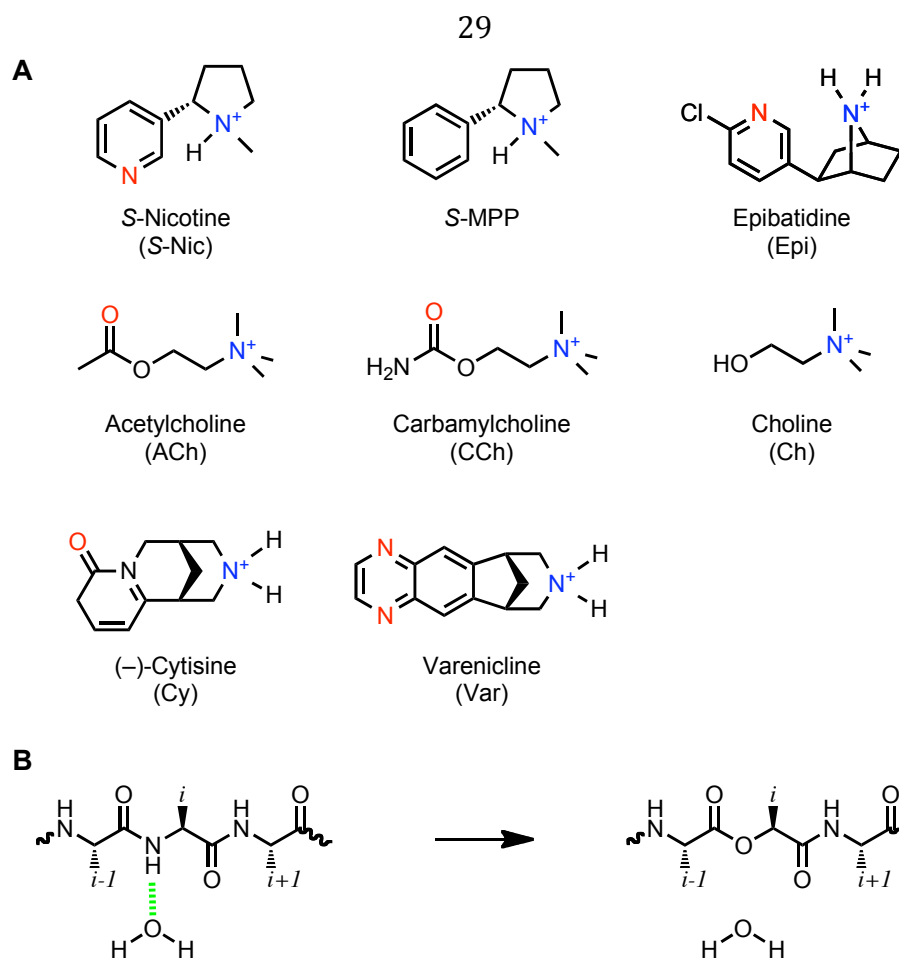


Figure 2.1. Key structures considered in the present work. (A) Structures of agonists used. Hydrogen bond acceptor moieties are red and cationic nitrogens are blue. Cytisine and varenicline are smoking cessation drugs. (B) Backbone amide-to-ester mutation strategy for perturbing a hydrogen bond.

In the nAChRs, ligand binding occurs at the interface between adjacent principal ($\alpha 4$ in $\alpha 4\beta 2$) and complementary ($\beta 2$) subunits. Three segments from the $\alpha 4$ subunit (historically referred to as the A, B and C “loops”) form the principal face of the ligand binding domain, which contains the cation- π binding site, and three segments from the $\beta 2$ subunit (D, E and F) form the complementary face. A major advance in the study of nAChRs was the discovery of the water-soluble acetylcholine binding proteins (AChBP).¹⁷⁻²² AChBP serves as a structural template for the extracellular, N-terminal, ligand binding domain of the nAChRs, sharing 20–24% sequence identity with the

ligand-binding domain of the much larger ion channel proteins. Several AChBP structures with ligands bound have been published, including structures of AChBP in complex with the ACh analog carbamylcholine (CCh) and with nicotine¹⁸ and the nicotine analog epibatidine.²¹ Drugs that target the nAChR, such as nicotine and epibatidine, typically contain a protonatable amine rather than the quaternary ammonium seen in ACh. Along with the cation- π interaction, the crystallography indicated a hydrogen bond between the N⁺H and the backbone carbonyl of the tryptophan that also forms the cation- π interaction, and functional studies on intact receptors confirmed the hydrogen bonding interaction.^{14, 23}

Concerning the second component of the pharmacophore, the hydrogen bond acceptor, the AChBP structure produced intriguing results. With nicotine bound, the pyridine nitrogen makes a hydrogen bond to a water molecule that is positioned by hydrogen bonds to the main chains of two residues, the CO of N107 and the NH of L119, both in the complementary subunit (α 4 β 2 numbering; residues are in the β 2 sequence FYSNAVVS^YDGSIFWL^PPA) (**Figure 2.2**).¹⁸ In other structures, including those with CCh or epibatidine bound, the overall binding site structure is preserved, although the key water molecule is not always evident, especially in lower-resolution structures.

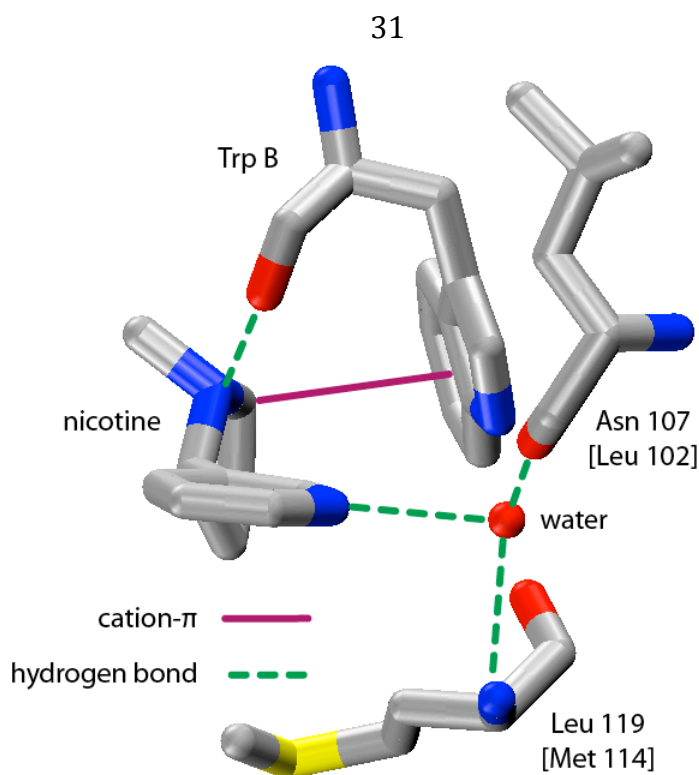


Figure 2.2. Key interactions seen in the crystal structure of nicotine bound to AChBP (pdb: 1UW6). Residue numbering is for the $\alpha 4\beta 2$ receptor, with AChBP homologs in brackets.

A key question, then, is the extent to which predictions based on the AChBPs, which evolved to bind a target molecule, relate to the nAChRs, which evolved to undergo a global structural change (to gate) on binding ACh. Here we describe a novel approach to probe with high precision a specific structural interaction in a complex receptor protein. Using unnatural amino acid mutagenesis and agonist analogs, we find that nicotine, acetylcholine, epibatidine, carbamylcholine and the smoking cessation drug cytisine (the lead compound for the development of varenicline) make the same hydrogen bond to backbone NH of $\beta 2L119$ in both stoichiometries of the $\alpha 4\beta 2$ receptor, supporting a common pharmacophore for these agonists. Varenicline does not make this interaction and therefore violates the nicotinic pharmacophore.

2.3 RESULTS

2.3.1 General Strategy

A well-established strategy for probing potential backbone hydrogen bonds is to replace the residue that contributes the hydrogen bond donor with its α -hydroxy analog (**Figure 2.1B**).²⁴⁻²⁸ This mutation converts a backbone amide to a backbone ester, a subtle change that impacts backbone hydrogen bonding in two ways. The backbone NH that can donate a hydrogen bond is removed, and the carbonyl oxygen, by virtue of being part of an ester rather than an amide, is a weaker hydrogen bond acceptor.

In the present context, simply seeing a change in receptor function in response to appropriate backbone ester substitutions would not prove the presence of the proposed interaction. Backbone mutation is certainly subtle, but when installed in an important region of the receptor it could affect function in a number of ways. As such, we sought a way to provide a direct connection between any consequences of backbone mutation and the proposed hydrogen bond. To do this, we considered the molecule, *S*-*N*-methyl-2-phenylpyrrolidine (*S*-MPP, **Figure 2.1A**). In this structure a phenyl ring replaces the pyridyl group of nicotine, obliterating the possibility of forming the proposed hydrogen bond. This would allow a novel “double mutant cycle” analysis that links the backbone NH to the pyridine N. If the mutant cycle analysis shows that the effects of the two changes – the backbone mutation and the modification of the drug – are substantially non-additive, this would provide compelling evidence for the proposed interaction.

The metric used to evaluate receptors is EC₅₀, the effective concentration of agonist required to achieve half-maximal response. This is a functional measure that can be influenced by changes to drug binding and/or efficacy of activation of the receptor.

Previously we have shown that subtle mutations to TrpB of the binding site primarily, if not exclusively, affect agonist binding,¹⁴ but we cannot assume the same for Leu119. Since the goal here is to map the pharmacophore for a collection of agonists, we are interested in factors that influence receptor activation. We consider EC₅₀ to be an appropriately useful guide for understanding agonism and designing new agonists, but more detailed studies of the mutations considered here would be valuable.

2.3.2 Optimization of nonsense suppression experiments

The $\alpha 4\beta 2$ receptor is a pentamer with two possible stoichiometries, $(\alpha 4)_2(\beta 2)_3$ and $(\alpha 4)_3(\beta 2)_2$ termed A2B3 and A3B2, respectively. Our initial studies will focus on the A2B3 receptor, which shows the higher sensitivity to nicotine and is thought to be upregulated during chronic nicotine exposure.²⁹ Later studies will compare the findings for this receptor with those of A3B2. Subunit stoichiometry can be managed by controlling mRNA injection ratios. Exclusive expression of A2B3 or A3B2 can be verified by monitoring I-V relationships of agonist-induced currents, as described previously.¹⁴

This study represents the first report of unnatural amino acid mutagenesis in the $\beta 2$ subunit of $\alpha 4\beta 2$. Since nonsense suppression often produces low protein yields of the subunit where the suppression occurs, it was critical to ensure that a receptor with excess $\beta 2$ subunit, *i.e.*, the A2B3 stoichiometry, was exclusively produced in nonsense suppression experiments. To that end, mRNA ratios substantially favoring the $\beta 2$ subunit were explored. We found that an injected mRNA ratio of 1:20 of $\alpha 4:\beta 2$ (with $\beta 2$ containing the nonsense suppression site) gave I-V relationships indicative of A2B3,¹⁴ while still providing enough current to conduct meaningful dose-response experiments. A

10:1 mRNA injection ratio of $\alpha 4$: $\beta 2$ was sufficient for studies with A3B2. The $\alpha 4$ subunit also contained a known mutation in the M2 transmembrane helix (L9'A), which improves receptor expression and lowers whole-cell EC_{50} values, but does not influence the binding trends of the receptor.³⁰

One challenge in incorporating a hydroxy acid at $\beta 2$ L119 was to limit the amount of current observed from oocytes injected with full length tRNA that was not synthetically appended to an amino or α -hydroxy acid. Such current would indicate that the suppressor tRNA was aminoacylated by an endogenous aminoacyl-tRNA synthetase and delivered a natural amino acid at the mutation site. We observed significant background currents attributable to such infidelity when using the suppressor tRNA THG73, which has been the workhorse of our unnatural amino acid mutagenesis experiments³¹. Employing the recently developed opal suppressor tRNA TQOpS',^{32, 33} significantly reduced this background current at $\beta 2$ L119. Aminoacylation from TQOpS' was assessed for each agonist by injection of unacylated TQOpS', and full dose-response relations were generated for agonists displaying >20 nA of current. Suppression experiments typically produced ≥ 1 μ A of current and yielded Hill and EC_{50} values that were markedly different from unacylated TQOpS' control experiments, and so the small background currents are not expected to distort the reported EC_{50} values. With these conditions, characterization of mutant receptors was straightforward (**Figure 2.3**).

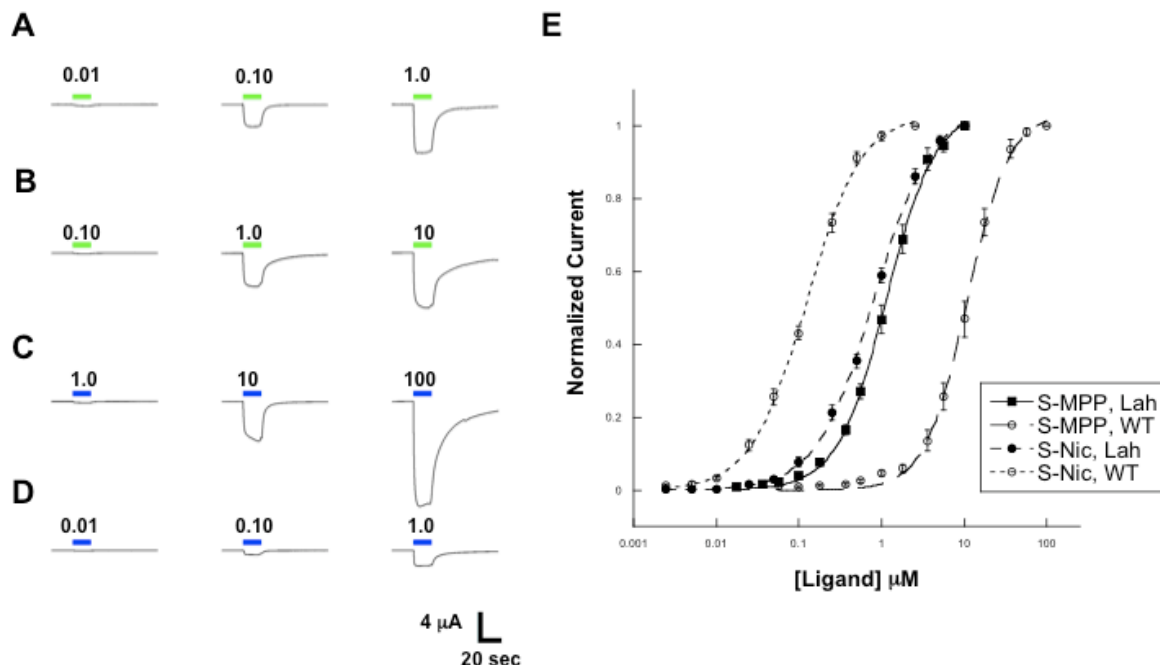


Figure 2.3. Representative current waveforms and dose-response relations for *S*-Nicotine and *S*-MPP at the A2B3 receptor. Agonist-induced current waveforms for (A) *S*-Nicotine on wild-type A2B3. (B) *S*-Nicotine on $(\alpha 4)_2(\beta 2\text{L119Lah})_3$. (C) *S*-MPP on wild-type A2B3. (D) *S*-MPP on $(\alpha 4)_2(\beta 2\text{L119Lah})_3$. Concentrations are in μM . (E) Dose-response relations for *S*-Nicotine and *S*-MPP on wild-type A2B3 or $(\alpha 4)_2(\beta 2\text{L119Lah})_3$.

2.3.3 Amide-to-Ester backbone mutation at $\beta 2\text{L119}$ impacts receptor function in A2B3

To probe the hydrogen bond suggested by the AChBP structures, $\beta 2\text{L119}$ (of A2B3) was replaced with its α -hydroxy analog (leucine, α -hydroxy; Lah). Meaningful increases in EC_{50} for the backbone amide-to-ester mutation were seen for the conventional agonists nicotine, ACh, CCh, and epibatidine, suggesting a significant functional role for the backbone NH (Table 2.1, Figure 2.3). In contrast, no shift was seen for the very weak agonist choline.

Table 2.1. EC₅₀ values, Hill coefficients, and relative efficacies for mutations to β 2L119 in the A2B3 stoichiometry. All studies gave current values at +70 mV (normalized to -110 mV) of ≤ 0.08 , confirming the A2B3 stoichiometry. Errors are standard error of the mean. (\pm)-Epi is racemic epibatidine. Mutations identified as “Leu” represent recovery of the wild-type receptor by nonsense suppression. The relative efficacy is the ratio of the I_{\max} of a saturating concentration of agonist / I_{\max} of a saturating concentration of ACh. By definition, the relative efficacy of ACh is 1.

Agonist	Mutation	EC ₅₀ (nM)	Hill (n _H)	Relative Efficacy
S-Nic	WT	120 \pm 5	1.3 \pm 0.1	0.27 \pm 0.01
	Leu	120 \pm 3	1.5 \pm 0.1	
	Lah	800 \pm 30	1.3 \pm 0.1	
S-MPP	WT	11000 \pm 400	1.7 \pm 0.1	0.23 \pm 0.01
	Leu	14000 \pm 900	1.5 \pm 0.1	
	Lah	1100 \pm 40	1.5 \pm 0.1	
ACh	WT	360 \pm 20	1.3 \pm 0.1	[1]
	Leu	440 \pm 20	1.3 \pm 0.1	
	Lah	3000 \pm 100	1.2 \pm 0.1	
CCh	WT	7200 \pm 80	1.3 \pm 0.1	0.50 \pm 0.1
	Leu	7900 \pm 200	1.2 \pm 0.1	
	Lah	29000 \pm 800	1.2 \pm 0.1	
Ch	WT	140000 \pm 4000	1.6 \pm 0.1	0.060 \pm 0.01
	Leu	140000 \pm 20000	1.2 \pm 0.1	
	Lah	150000 \pm 5000	1.4 \pm 0.1	
(\pm)-Epi	WT	0.79 \pm 0.04	1.4 \pm 0.1	0.47 \pm 0.03
	Leu	0.58 \pm 0.05	1.5 \pm 0.1	
	Lah	2.9 \pm 0.1	1.3 \pm 0.1	

As noted above, we considered *S*-MPP as a potentially informative structure for probing the pyridine hydrogen bond. As such, we adapted existing synthetic protocols³⁴ to prepare *N*-methyl-2-phenylpyrroline (MPP). Recrystallization of the dibenzoyl tartrate salt (at the phenylpyrrolidine stage) gave the *S* enantiomer.

As expected, *S*-MPP is a much poorer agonist than nicotine, showing a ~120-fold higher EC₅₀ with the wild-type A2B3 receptor. For nicotine, the *S* enantiomer is the higher affinity enantiomer and the one traditionally used in studies of nicotinic receptors. We find that *S*-MPP has a two-fold lower EC₅₀ than racemic MPP, indicating that the higher affinity enantiomer is being used.

Incorporation of a backbone ester at β 2L119 leads to a remarkable change in relative agonist potencies. Instead of the increase in EC₅₀ seen with nicotine, *S*-MPP

actually shows a *decrease* in EC₅₀; *S*-MPP is a more potent agonist when the backbone ester is present than when the natural backbone amide is present. In fact, when the backbone ester is present, nicotine and *S*-MPP display comparable potency (**Figure 2.3E**).

The AChBP structure also predicts that a second residue in the complementary subunit positions the water molecule in proximity to the pyridine N of nicotine. The backbone carbonyl of β 2N107 is expected to make a hydrogen bond to the water molecule in conjunction with the first hydrogen bond made by β 2L119 (**Figure 2.2**). As noted above, an established strategy for attenuating the hydrogen bonding ability of a backbone carbonyl is to mutate the (*i*+1) residue to its α -hydroxy acid (**Figure 2.1B**). However, nonsense suppression experiments at the β 2A108 site gave inconsistent results that suggested we could not reliably control the stoichiometry of the mutant receptor (**Table 2.2**). As such, we have been unable to successfully probe this interaction.

Table 2.2. EC₅₀ values, Hill coefficients, and relative efficacies for mutations to β 2A108 in the A2B3 stoichiometry. To confirm stoichiometry, current values at +70 mV (normalized to –110 mV) were determined. In previous studies,¹⁴ we found that a value of ≥ 0.2 was indicative of the A3B2 stoichiometry and a value of ≤ 0.08 was indicative of the A2B3 stoichiometry. Note that the current values at +70 mV for “Aah” and “Vah” at this site were consistent with the A3B2 stoichiometry (not the A2B3 stoichiometry we had intended to study) despite the fact that we injected an excess of β 2 (up to 100 fold-more than α 4). Errors are standard error of the mean. Mutations identified as “Ala” represent recovery of the wild-type receptor by nonsense suppression.

Agonist	Mutation	EC ₅₀ (nM)	Hill (n _H)	I _{norm} (+70mV)
<i>S</i> -Nic	α 4(L9'A) β 2	120 \pm 10	1.3 \pm 0.1	0.05 \pm 0.01
	α 4(L9'A) β 2(A108Ala)	140 \pm 10	1.5 \pm 0.1	0.07 \pm 0.01
	α 4(L9'A) β 2(A108Aah)	20 \pm 10	1.4 \pm 0.1	0.40 \pm 0.02
	α 4(L9'A) β 2(A108Val)	50 \pm 10	1.1 \pm 0.1	0.09 \pm 0.06
	α 4(L9'A) β 2(A108Vah)	50 \pm 10	1.1 \pm 0.1	0.23 \pm 0.03
<i>S</i> -MPP	α 4(L9'A) β 2	11000 \pm 400	1.7 \pm 0.1	0.08 \pm 0.01
	α 4(L9'A) β 2(A108Aah)	10000 \pm 600	2.0 \pm 0.1	0.3 \pm 0.03
ACh	α 4(L9'A) β 2	360 \pm 20	1.3 \pm 0.1	0.04 \pm 0.01
	α 4(L9'A) β 2(A108Ala)	640 \pm 20	1.1 \pm 0.1	0.070 \pm 0.01
	α 4(L9'A) β 2(A108Aah)	130 \pm 10	1.2 \pm 0.1	0.40 \pm 0.02
	α 4(L9'A) β 2(A108Val)	400 \pm 10	1.0 \pm 0.1	0.090 \pm 0.03
	α 4(L9'A) β 2(A108Vah)	600 \pm 50	0.72 \pm 0.1	0.2 \pm 0.06

2.3.4 Mutant cycle analyses indicate strong receptor-agonist interactions at $\beta 2L119$ in A2B3

As noted above, a mutant cycle analysis is the standard way to determine whether pairs of mutations are independent or are coupled. EC₅₀-based mutant cycle analyses have been performed by our lab and others to investigate multiple interactions in Cys-loop receptors and related structures^{28, 35-37}. For several different agonist pairs, coupling coefficients (Ω) and coupling energies ($\Delta\Delta G^\circ$) were calculated (**Table 2.3**).

Table 2.3. Coupling parameters (Ω) and $\Delta\Delta G^\circ$ values for mutant cycle analyses for A2B3.

Agonist	Ω	$\Delta\Delta G^\circ$ (kcal/mol)
ACh/Ch	0.16	1.1
CCh/ Ch	0.3	0.71
S-Nic/ S-MPP	0.012	2.6

Mutant cycle analysis for the *S*-nicotine/*S*-MPP pair and the $\beta 2L119/\beta 2L119Lah$ pair predicts a substantial coupling energy of 2.6 kcal/mol (**Figure 2.4**). This is a relatively large energy for a putative hydrogen bond, and it provides strong evidence for a hydrogen bonding interaction between the pyridine N of nicotine and the backbone NH of $\beta 2L119$ in the A2B3 receptor.

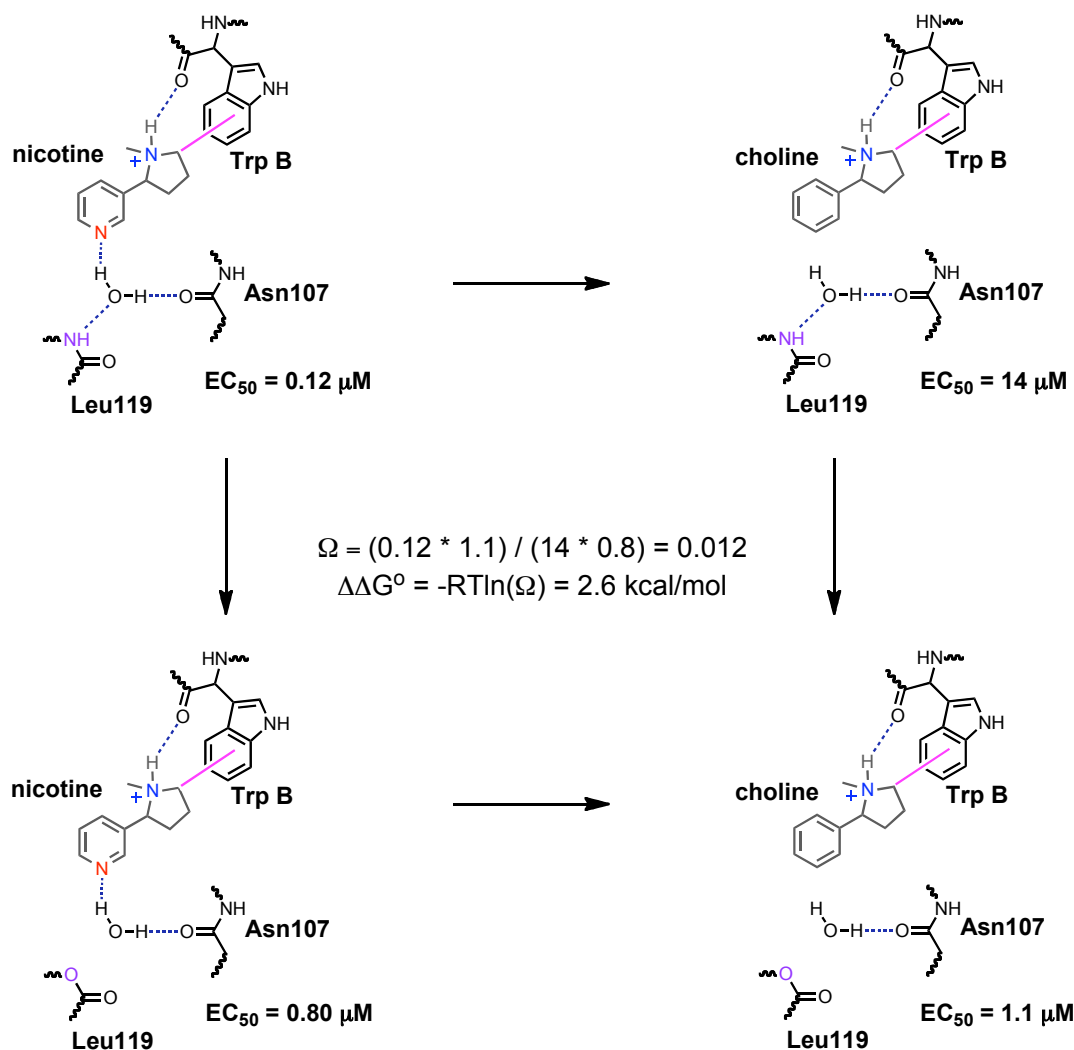


Figure 2.4. Double mutant cycle analysis for *S*-Nic and *S*-MPP on wild-type A2B3 and $(\alpha 4)_2(\beta 2\text{L119Lah})_3$.

We also considered double mutant cycle analyses for the agonists ACh and CCh using choline as the reference compound, as it lacks the key hydrogen bond acceptor. This is a much less subtle probe than the *S*-nicotine/*S*-MPP pair, but it still could produce relevant results. Indeed, we find that for both the ACh/Ch and CCh/Ch pairs, smaller, but still meaningful, coupling energies are seen in the A2B3 receptor (**Table 2.3**).

2.3.5 Studies in the A3B2 subunit stoichiometry give similar results

Recall that the $\alpha 4\beta 2$ receptor can assemble into two different pentameric stoichiometries A2B3 ($((\alpha 4)_2(\beta 2)_3)$) and A3B2 ($((\alpha 4)_3(\beta 2)_2)$). Even though both forms have two agonist binding sites (at appropriate subunit interfaces, shown in **Figure 2.5**), and are both composed of identical $\alpha 4$ and $\beta 2$ subunits, agonists are generally more potent at the A2B3 stoichiometry (*i.e.*, they give lower EC_{50} values) and this stoichiometry alone is thought to be upregulated during chronic nicotine exposure.²⁹ We sought to determine whether differences in the pharmacophore binding interactions of the two stoichiometries could account for the differences in receptor pharmacology by evaluating the impact of backbone mutation at $\beta 2L119$ in A3B2 for ACh and nicotine.

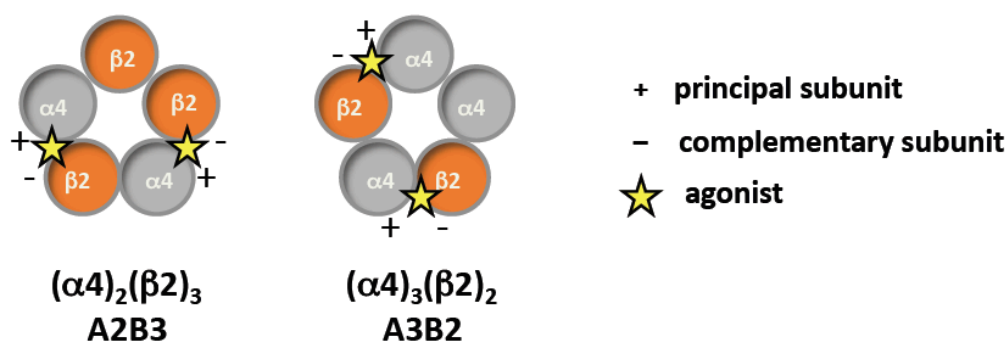


Figure 2.5. Depiction of the two stoichiometries of the $\alpha 4\beta 2$ receptor. Agonist binding sites are depicted at appropriate subunit interfaces.

Note that in all of our studies of the $\alpha 4\beta 2$ receptor (both stoichiometries), we introduce the L9'A mutation³⁰ to improve receptor expression. Mutations of this type generically increase receptor sensitivity to agonists, and they do so in an additive manner.^{38, 39} Thus, in the present study the A3B2 receptors have three L9'A mutations and therefore generally show greater potency than A2B3 receptors, which have two L9'A

mutations, even though the A2B3 stoichiometry is the high affinity form in true wild-type receptors.

For ACh and nicotine, the fold-shifts in EC_{50} in response to the backbone ester mutation at $\beta 2L119$ in the A3B2 stoichiometry (**Table 2.4**) are comparable to what was seen for the A2B3 stoichiometry (**Table 2.1**). Likewise, agonists lacking a hydrogen bond acceptor displayed similar behavior in the two stoichiometries – no shift in EC_{50} was seen for choline and a large gain of function was seen for *S*-MPP, even larger than the one seen in A2B3.

Table 2.4. EC_{50} values, Hill coefficients, and relative efficacies for mutations to $\beta 2L119$ in the A3B2 stoichiometry. All studies gave current values at +70 mV (normalized to –110 mV) of ≥ 0.20 , confirming the A3B2 stoichiometry. Errors are standard error of the mean. (\pm)-Epi is racemic epibatidine. Mutations identified as “Leu” represent recovery of the wild-type receptor by nonsense suppression. The relative efficacy is the ratio of the I_{max} of a saturating concentration of agonist / I_{max} of a saturating concentration of ACh. By definition, the relative efficacy of ACh is 1.

Agonist	Mutation	EC_{50} (nM)	Hill (n_H)	Relative Efficacy
<i>S</i> -Nic	WT	12 \pm 0.1	1.6 \pm 0.1	0.56 \pm 0.04
	Leu	12 \pm 0.1	1.6 \pm 0.1	
	Lah	67 \pm 3	1.4 \pm 0.1	
<i>S</i> -MPP	WT	4500 \pm 100	1.1 \pm 0.1	0.39 \pm 0.03
	Leu	4200 \pm 300	1.6 \pm 0.1	
	Lah	130 \pm 10	1.2 \pm 0.1	
ACh	WT	26 \pm 1	1.1 \pm 0.1	[1]
	Leu	26 \pm 1	1.6 \pm 0.1	
	Lah	220 \pm 10	1.2 \pm 0.1	
Ch	WT	90000 \pm 2000	1.4 \pm 0.1	0.70 \pm 0.06
	Leu	76000 \pm 200	1.4 \pm 0.1	
	Lah	74000 \pm 2000	1.5 \pm 0.1	

Mutant cycle analyses of the ACh/Ch and *S*-Nic/*S*-MPP pairs gave strong energetic couplings of 1.3 and 3.1 kcal/mol, respectively (**Table 2.5**). These values are comparable to what was seen in the A2B3 stoichiometry, suggesting that the hydrogen bond to $\beta 2L119$ does not differentiate the two subunit stoichiometries.

Table 2.5. Coupling parameters (Ω) and $\Delta\Delta G^\circ$ values for mutant cycle analyses in A3B2.

Agonist	Ω	$\Delta\Delta G^\circ$ (kcal/mol)
ACh/Ch	0.12	1.3
S-Nic/S-MPP	0.0055	3.1

2.3.6 Studies with smoking cessation drugs at both subunit stoichiometries

We also evaluated whether two established smoking cessation compounds (**Figure 2.1A**) are sensitive to the amide-to-ester mutation at β 2L119. Varenicline (marketed by Pfizer as Chantix® in the U.S.) was designed to target α 4 β 2 receptors, and was approved for use as a smoking cessation aid in 2006.⁶ Cytisine is a naturally occurring alkaloid that served as a lead compound for the development of varenicline. It is marketed for smoking cessation in Eastern Europe as Tabex®, although compelling clinical trials that establish its effectiveness have not been published.⁴⁰

Our results for varenicline are surprising (**Table 2.6**). With only a 2-fold shift in A2B3 and no meaningful shift in A3B2, it would appear that there is no hydrogen bond between a quinoxaline N of varenicline and the backbone NH of β 2L119 in the α 4 β 2 receptor. With the exception of choline (which does not contain the hydrogen bond acceptor), this is the only agonist that we have found to be insensitive to this mutation.

Table 2.6. EC₅₀ values, Hill coefficients, and relative efficacies for (–)-cytisine and varenicline at both subunit stoichiometries. All studies gave current values at +70 mV (normalized to –110 mV) of ≤ 0.08 or ≥ 0.20 , confirming the A2B3 and A3B2 stoichiometries, respectively. Errors are standard error of the mean. Cy is (–)-cytisine and Var is varenicline. Mutations identified as “Leu” represent recovery of the wild-type receptor by nonsense suppression. The relative efficacy is the ratio of the I_{\max} of a saturating concentration of agonist / I_{\max} of a saturating concentration of ACh.

Agonist	Mutation	EC ₅₀ (nM)	Hill (n _H)	Relative Efficacy
A2B3 Stoichiometry				
Cy	WT	6.9 ± 0.3	1.4 ± 0.1	0.030 ± 0.01
	Leu	8.7 ± 0.4	1.2 ± 0.1	
	Lah	540 ± 30	0.98 ± 0.1	
Var	WT	3.1 ± 0.1	1.4 ± 0.1	0.12 ± 0.02
	Leu	2.6 ± 0.2	1.3 ± 0.1	
	Lah	4.7 ± 0.2	1.3 ± 0.1	
A3B2 Stoichiometry				
Cy	WT	3.1 ± 0.1	1.9 ± 0.1	0.54 ± 0.05
	Leu	3.6 ± 0.1	1.9 ± 0.1	
	Lah	51 ± 2	1.4 ± 0.1	
Var	WT	0.95 ± 0.02	1.7 ± 0.1	0.33 ± 0.01
	Leu	1.0 ± 0.1	1.5 ± 0.1	
	Lah	1.1 ± 0.1	1.2 ± 0.1	

Cytisine also produces intriguing results. A remarkable 62-fold shift is seen for this subtle backbone ester mutation in the A2B3 receptor. This is among the strongest effects we have ever seen for a backbone ester mutation in any protein. A much smaller effect is seen in the A3B2 receptor, although it is still larger than what is seen for any other drug/receptor combination for mutation at $\beta 2L119$.

2.4 DISCUSSION

The nicotinic receptor has produced one of the longest-known, best-studied pharmacophores. The original study of Beers and Reich¹⁰ proposed that two points, a cationic nitrogen and a hydrogen bond acceptor, were required for successful interaction with biological receptors. Later discussion debated the optimal distance between the two points (deemed the “internitrogen distance”), and more recent models have alluded to pharmacophore binding partners within the biological receptors. Despite 40 years of interest in the nicotinic pharmacophore, the binding partners of the essential two point

pharmacophore have only recently been identified. Pioneering mutagenesis and affinity labeling studies of the receptor from *Torpedo* rays identified a number of aromatic amino acids near the binding site.^{1, 3} Early unnatural amino acid mutagenesis studies showed that one of these aromatics, now termed TrpB, makes a cation- π interaction with ACh in the muscle-type nAChR,¹⁵ and more recent studies established a comparable interaction to both ACh and nicotine in the $\alpha 4\beta 2$ receptor.¹⁴

The search for the presumed hydrogen bond donor to the acetyl group of ACh and the pyridine N of nicotine was much more challenging. A breakthrough came with the discovery of the AChBPs, and in 2004 a structure of nicotine bound to AChBP was reported.¹⁸ As shown in **Figure 2.2**, that AChBP structure confirmed the cation- π interaction to TrpB. It also implicated a hydrogen bond between the pyrrolidine N⁺H and the backbone carbonyl of TrpB, an interaction that was subsequently confirmed by unnatural amino acid mutagenesis.^{14, 23}

Importantly, the AChBP structure also suggested the binding partner for the second element of the pharmacophore. In AChBP, the pyridine N of nicotine makes a water-mediated hydrogen bond to a backbone NH and to a backbone carbonyl (**Figure 2.2**). This elegant arrangement emphasizes the interfacial nature of the agonist binding site, as the pyridine N interacts with residues that are on the complementary subunit, while TrpB, which makes the cation- π interaction and the hydrogen bond to the pyrrolidine N⁺H, lies in the principal subunit. The value of AChBP in guiding nAChR research is undeniably large, especially in the present context. It would have been very challenging to guess the hydrogen bond partner(s) to agonists such as ACh and nicotine before the structure of AChBP with nicotine bound. Nevertheless, AChBP is not a

nAChR. AChBP evolved to bind ligands, not to gate an ion channel in response to ACh binding. As such, tests of predictions from AChBP structures in real receptors are always essential.

Here we employ a novel strategy to test the water-mediated hydrogen bonding model of **Figure 2.2** in the neuronal, $\alpha 4\beta 2$ nAChR. The $\alpha 4\beta 2$ receptor shows high affinity for nicotine, and it is generally accepted to be the dominant receptor subtype that contributes to nicotine addiction. Our studies of $\alpha 4\beta 2$ are made possible by recent advances¹⁴ that allow us to express significant quantities of $\alpha 4\beta 2$ in *Xenopus* oocytes, to control subunit stoichiometry, and to efficiently incorporate unnatural amino acids into the receptor. Recently, we have shown that the cation- π interaction and the hydrogen bond to TrpB are strong in the A2B3 receptor.¹⁴

To probe the second hydrogen bond suggested by AChBP, we mutated $\beta 2L119$ to its α -hydroxy analog. This removes the critical NH, and, indeed, the agonists nicotine, ACh, CCh, and epibatidine all show 5–7-fold increases in EC_{50} in response to the mutation in the A2B3 stoichiometry. While consistent with the hydrogen bonding model, these observations certainly do not prove it. It could be that the backbone mutation is simply generically disruptive to receptor function.

To make an explicit connection between the pyridine N of nicotine and the backbone NH of $\beta 2L119$, we combined backbone mutagenesis with a modification of the agonist, removing the pyridine N to create *S*-MPP. Of course, *S*-MPP would never be the target of a medicinal chemistry study; it can be anticipated to be a terrible drug at the nAChR. Here it is used as a chemical probe, to evaluate a key binding interaction of the potent drug nicotine.

Studies with *S*-MPP produced remarkable results. As expected, it is a very poor agonist at the wild-type receptor. However, completely opposite to what is seen with nicotine, ACh, or epibatidine, introduction of the backbone ester at β 2L119 *lowers* EC_{50} for *S*-MPP in the A2B3 stoichiometry. In fact, *S*-MPP and nicotine are comparably potent at the mutant receptor (**Figure 2.3E**). Clearly the backbone mutation has had dramatically different effects on the two agonists. The effect can be quantified by a mutant cycle analysis, which reveals a coupling energy of 2.6 kcal/mol between the backbone mutation and the agonist “mutation.” This is a quite substantial energy, especially when one considers that these chemical changes – both in the protein and in the ligand – are more structurally subtle than those typically employed in mutant cycle analysis studies using conventional mutagenesis.

The results with *S*-MPP provide strong support for the nicotine binding model based on the AChBP structure. As noted above, however, AChBP structures with CCh or epibatidine bound do not include the key water molecule, although other components of the hydrogen bonding network are comparably positioned. We find that ACh, CCh, and epibatidine all respond to the backbone ester mutation in a way that is comparable to that seen for nicotine. In addition, choline, a weak agonist that lacks the hydrogen bond acceptor of ACh and CCh, is not influenced by the backbone mutation. We thus conclude that all the drugs studied here (with the exception of varenicline as discussed below) make a hydrogen bonding interaction with the backbone NH of β 2L119; the nicotinic pharmacophore has thus been completed by interactions with the complementary subunit. Note that these studies do not establish that the interaction between the hydrogen bond acceptor component of the agonists and the backbone NH of

β 2L119 is mediated by a water molecule; a direct interaction would be just as compatible with our data. At present, we feel the water-mediated interaction is the most reasonable interpretation, but further experiments to address this point would be valuable.

Nearly identical responses to the amide-to-ester mutation at β 2L119 were seen in the A3B2 stoichiometry for ACh, nicotine, choline, and *S*-MPP, suggesting that this hydrogen bonding interaction is present in both receptor stoichiometries. Other studies in our lab have shown that ACh and nicotine are also equivalently sensitive to perturbations of the other binding interaction of the pharmacophore – the cation- π interaction to TrpB and the hydrogen bond to the backbone CO of TrpB. As such, it is still a mystery as to why the two stoichiometries have vastly different agonist affinities given that they both have two agonist binding sites composed of identical subunits. It is possible that the accessory subunit – the fifth subunit that does not participate in a binding interface, an α 4 in A3B2 and β 2 in A2B3 – makes the difference.

The two smoking cessation compounds, varenicline and cytisine, show interesting variations with regard to the backbone ester mutation. Varenicline is qualitatively different from all the other compounds considered here. With a minimal (<2-fold) effect at the A2B3 stoichiometry and no meaningful effect at the A3B2 stoichiometry, we conclude that varenicline violates the nicotinic pharmacophore and does not make a hydrogen bond to the backbone NH of L119 in the β 2 subunit. **Figure 2.6** provides a rationalization. By visual inspection, and from the distances shown, it is clear that the quinoxaline nitrogens of varenicline are not well aligned with the hydrogen bond acceptor moieties of nicotine and varenicline, and so they cannot hydrogen bond to L119. While medicinal chemists and pharmacologists familiar with this system may have

anticipated this result, experimental confirmation of expectations from modeling is always valuable.

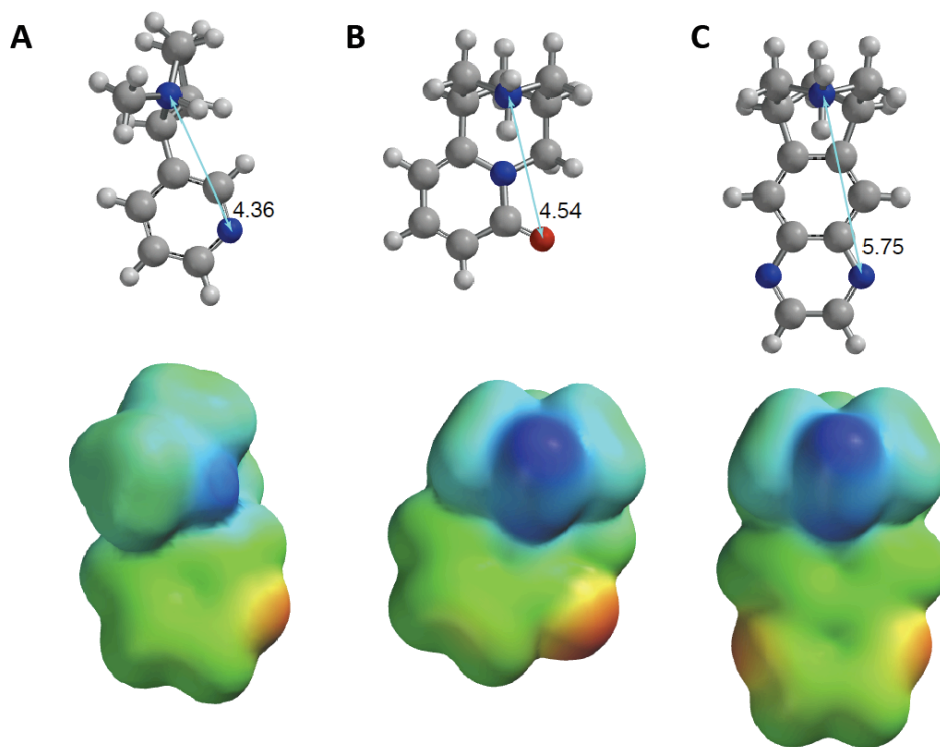


Figure 2.6. “Internitrogen distances” and electrostatic potential maps (as calculated in Spartan) for (A) *S*-nicotine, (B) (–)-cytisine and (C) varenicline. Geometries were optimized at RHF-3-21G*. The electrostatic potential map range is –20 to +700. The molecule ranges are: nicotine = +27 to +658; cytisine –18 to +701; and varenicline +35 to +691.

Cytisine shows an intriguing hydrogen bonding pattern, distinct from the other agonists considered here. More so than the other drugs, cytisine shows a strong stoichiometry selectivity in the $\alpha 4\beta 2$ receptor, having a much greater efficacy at the A3B2 stoichiometry than at the A2B3. Interestingly, cytisine also shows the greatest stoichiometry differences for the amide-to-ester mutation. The A2B3 stoichiometry shows a remarkable 62-fold rise in EC_{50} , much larger than anything we have seen previously. The A3B2 stoichiometry shows a much smaller effect.

Despite these differences, cytosine shows the strongest sensitivity to backbone ester mutation of any of the agonists tested at both stoichiometries. We can rationalize this general effect with reference to the electrostatic potential plots of **Figure 2.6**. Visually, the carbonyl oxygen of cytosine presents a much stronger negative electrostatic potential than the corresponding nitrogen of nicotine. Quantitative evaluation of the electrostatic potentials at these atoms confirms the visual. Thus, the oxygen of cytosine should be a better hydrogen bond acceptor than the nitrogen of nicotine, completely consistent with expectation for an amide carbonyl *vs.* a pyridine nitrogen.

We have now used chemical-scale investigations of functional receptors to establish a three-point interaction between nicotine and the $\alpha 4\beta 2$ neuronal nAChR, the receptor most strongly associated with nicotine addiction. A cation- π interaction to TrpB has been established by progressive fluorination of the key tryptophan. Backbone mutagenesis has been used to establish two key hydrogen bonds: the pyrrolidine N^+H hydrogen bonds to the backbone carbonyl of TrpB, and the pyridine N of nicotine hydrogen bonds to the backbone NH of $\beta 2L119$. Studies of these two hydrogen bonds were inspired by the AChBP structures, emphasizing the substantial impact of AChBP on nAChR research.

At the same time, AChBP is not a neurotransmitter-gated ion channel; it evolved to serve a different function than a nAChR. As such, we should anticipate some differences between the two structures. Indeed, two features of the nicotine-AChBP structure have been shown to be not functionally significant in studies of nAChRs. The AChBP structure clearly shows a cation- π interaction between the CH_3 of nicotine and a tyrosine at the agonist binding site termed TyrC2 (**Figure 2.7**).¹⁸ This methyl group –

which carries a charge comparable to a CH₃ attached to the N⁺ of ACh, points directly at the center of the aromatic ring of TyrC2 and essentially makes van der Waals contact with the ring, unquestionably a cation- π interaction. However, we find no experimental support for this cation- π interaction in either the muscle-type or the $\alpha 4\beta 2$ nAChR. In each system, inserting 4-CN-Phe at TyrC2 gives essentially wild-type receptor function.^{14, 15} A CN group is very strongly deactivating in a cation- π interaction, and so this result is in conflict with the AChBP structure. Note that in a different Cys-loop receptor, the residue at position C2 does make a functionally significant cation- π interaction to the natural agonist serotonin.⁴¹ Also, in the neuronal $\alpha 7$ receptor, epibatidine (but not ACh) has been recently shown to make a cation- π interaction with the C2 tyrosine.⁴²

In addition, all AChBP structures – the nicotine, CCh, and epibatidine bound structures considered here as well as the “apo” structure – contain a strong hydrogen bond between the indole NH of TrpB and the backbone carbonyl of the residue that corresponds to $\beta 2L119$ (**Figure 2.7**). N...O distances range from 2.7 to 3.0 Å. However, earlier studies of the muscle-type receptor found no evidence for an important interaction of this kind. In particular, TrpB can be substituted by unnatural amino acids in which the indole ring is replaced by a naphthalene or an *N*-methylindole with very little impact on EC₅₀.¹⁵ All of these analogs lack the critical hydrogen bond-donating NH of the Trp indole ring.

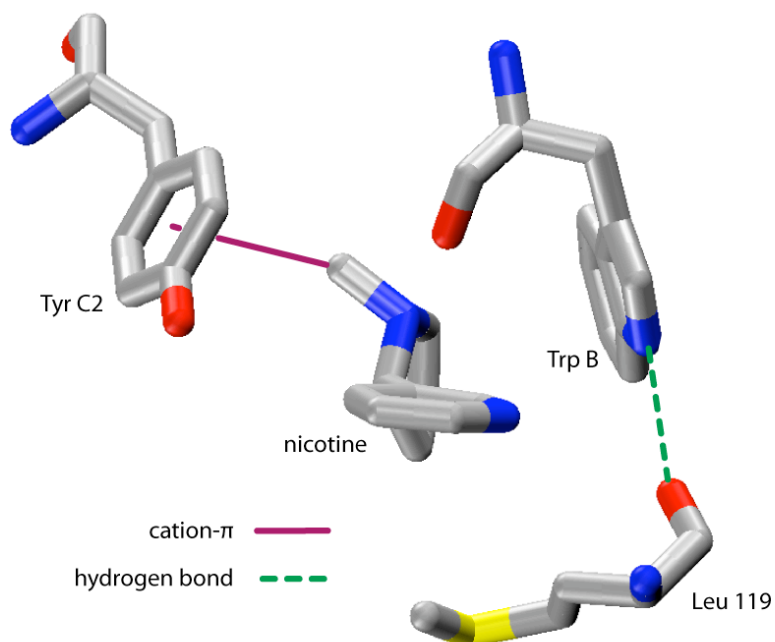


Figure 2.7. Additional interactions seen in the crystal structure of nicotine bound to AChBP (pdb: 1UW6). Residue numbering is for the $\alpha 4\beta 2$ receptor.

In summary, we have used a combination of unnatural amino acid mutagenesis and chemical synthesis to provide strong evidence for a functionally important hydrogen bond between the pyridine N of nicotine and the backbone NH of $\beta 2$ L119 in the nicotine-sensitive $\alpha 4\beta 2$ receptor at both subunit stoichiometries. A similar interaction contributes to the binding of ACh, CCh, epibatidine, and cytosine, but not to the binding of the popular smoking cessation drug, varenicline. We have now used unnatural amino acid mutagenesis to establish three strong contact points between this critical receptor and nicotine: the cation- π interaction to the side chain of TrpB; the hydrogen bond between the pyrrolidine N^+H and the backbone carbonyl of TrpB; and the hydrogen bond between the pyridine N and the backbone NH of $\beta 2$ L119. There is much interest in the pharmaceutical industry in developing subtype-selective agonists of neuronal nAChRs, and it seems likely that the complementary subunit will play the dominant role in

discriminating among subtypes. As such, these studies of a key binding interaction involving the complementary binding site suggest a general strategy for developing insights that could lead to subtype-specific pharmaceuticals.

2.5 EXPERIMENTAL SECTION

Rat $\alpha 4$ and $\beta 2$ cDNA in the pAMV vector was linearized with the restriction enzyme Not 1. mRNA was prepared by *in vitro* transcription using the mMessage Machine T7 kit (Ambion). Unnatural mutations were introduced by the standard Stratagene QuickChange protocol, using a TGA mutation at the site of interest. The $\alpha 4$ subunit contained a known mutation in the M2 transmembrane helix (L9'A) that improves receptor expression and lowers whole-cell EC₅₀ values, but does not influence the ligand-binding trends of the receptor.³⁰ Stage V-VI *Xenopus laevis* oocytes were injected with mRNA in $\alpha 4$ L9'A: $\beta 2$ ratio of 1:1 for wild-type experiments, 1:20 for suppression in A2B3 and 10:1 for suppression in A3B2. Hydroxy or amino acids were appended to the dinucleotide dCA and enzymatically ligated to the truncated 74-nucleotide TQOpS' tRNA as previously described.³¹ Each cell was injected with 75 nL of a 1:1 mixture of mRNA (20-25 ng of total mRNA): tRNA (20-30 ng), with oocytes injected with Leu ligated to TQOpS' receiving an additional 75 nL after 24 hrs of incubation at 18 °C. Wild-type recovery experiments (injection of tRNA appended to the natural amino acid) were performed to evaluate the fidelity of the unnatural suppression experiments. Additional controls, mRNA only and 74-mer TQOpS' ligated to dCA (TQOpS'-dCA), were also examined. While small currents (typically less than 200 nA) were seen for TQOpS'-dCA control experiments, EC₅₀ and Hill values were substantially different from suppression values.

Electrophysiology experiments were performed 24-48 hrs after injection using the OpusXpress 6000A instrument (Axon Instruments) in two-electrode voltage clamp mode at a holding potential of -60 mV. The running buffer was Ca^{2+} free ND96 solution (96 mM NaCl, 2 mM KCl, 1 mM MgCl_2 , and 5 mM HEPES, pH 7.5). During typical recordings, agonists were applied for 15 s followed by a 116 s wash with the running buffer. For recordings with epibatidine, cytisine and varenicline, the first 8 drug concentrations were applied for 90 s with a 116 s wash with running buffer, while the remaining concentrations were applied for 15 s with a 116 s wash. Dose-response data were obtained for ≥ 8 agonist concentrations on ≥ 6 cells. All EC_{50} and Hill coefficient values were obtained by fitting dose-response relations to the Hill equation and are reported as averages \pm standard error of the fit. A detailed error analysis of nonsense suppression experiments reveals data are reproducible to $\pm 50\%$ in EC_{50} .^{43, 44} Voltage jump experiments were conducted to verify stoichiometry as described previously.¹⁴

Double mutant cycle analyses were performed with EC_{50} values to calculate coupling coefficients (Ω) using the equation: $\Omega = (\text{EC}_{50}^{\text{Leu, ligand}} * \text{EC}_{50}^{\text{Lah, ligand analog}}) / (\text{EC}_{50}^{\text{Leu, ligand analog}} * \text{EC}_{50}^{\text{Lah, ligand}})$, where [Leu, ligand] and [Leu, ligand analog] represent the EC_{50} of the wild-type receptor with either ligand and [Lah, ligand] and [Lah, ligand analog] represent the EC_{50} of the ester mutation with either ligand. Coupling energies, $\Delta\Delta G^{\circ}_{\text{int}}$, were calculated from the equation $\Delta\Delta G^{\circ}_{\text{int}} = -RT\ln\Omega$.

Synthesis of *N*-methyl-2-phenylpyrrolidine hydrochloride. 2-phenylpyrrolidine (5.0 g, 34 mmol), prepared according to a published protocol,³⁴ was mixed with dibenzoyl-*L*-tartaric acid (6.1 g, 17 mmol) in a 100 mL round-bottom flask equipped with a reflux condenser. To this was added 35% ethanol in ethylacetate (30 mL). The solution was

heated to boiling for 10 minutes and then cooled to room temperature overnight. The white crystals were collected, rinsed with cold ethylacetate and then submitted to five sequential recrystallizations. Yield (10%, 2.2 g). ^1H NMR (CDCl_3 , 300 MHz) δ 8.20 (4H, m), 7.61-7.32 (16H, m), 5.92 (2H, s), 5.03 (4H, b), 4.54 (2H, dd, $J = 9.1, 6.7$ Hz), 3.38 (4H, m), 2.27–2.00 (8H, m); ^{13}C NMR (CDCl_3 , 75 MHz) δ 172.58, 166.45, 134.91, 132.73, 130.54, 129.70, 128.83, 128.76, 128.03, 127.37, 75.60, 62.74, 44.80, 30.42, 23.37. HRMS (FAB+) m/z calc'd for $\text{C}_{10}\text{H}_{14}\text{N}$ [M^+]: 148.1126, found 148.1081. To obtain enantioenriched 2-phenylpyrrolidine, the product was vigorously stirred in a 1:1 mixture of 2 M NaOH: CH_2Cl_2 . The organic layer was then extracted with additional CH_2Cl_2 (3 \times), washed with brine, dried over Na_2SO_4 , and concentrated to yield enantioenriched 2-phenylpyrrolidine as a yellow oil (Yield: 95%). NMR spectra are consistent with previously reported data. HRMS (FAB+) m/z calc'd for $\text{C}_{10}\text{H}_{14}\text{N}$ [$\text{M}+\text{H}$]: 148.1126, found 148.1134. To establish enantiomeric excess, the product was converted to ethyl 2-phenylpyrrolidine-1-carboxylate via a previously described procedure,⁴⁵ and this material was evaluated by analytical chiral HPLC analysis using a Chiralcel OD-H column (4.6 mm \times 25 cm) from Daicel Chemical Industries, Ltd. with 2% isopropyl alcohol in hexanes, giving an enantiomeric excess of 96%. ^1H NMR of ethyl 2-phenylpyrrolidine-1-carboxylate (CH_3OD , 300 MHz) δ 7.32-7.15 (5H, m), 4.92 (1H, m), 4.08 (1H, m), 3.92 (1H, m), 3.59 (2H, q, $J = 7.7$ Hz), 2.34 (1H, m), 1.95–1.86 (4H, m), 1.26 (1H, t, $J = 7.0$ Hz), 0.94 (1H, t, $J = 7\text{Hz}$); ^{13}C NMR of ethyl 2-phenylpyrrolidine-1-carboxylate (CDCl_3 , 75 MHz) δ 155.40, 144.32, 128.22, 126.59, 125.44, 60.85, 47.34, 47.03, 35.71, 23.58, 14.79. HRMS of ethyl 2-phenylpyrrolidine-1-carboxylate (FAB+) m/z calc'd for $\text{C}_{13}\text{H}_{18}\text{O}_2\text{N}$ [$\text{M}+\text{H}$]: 220.1338, found 220.1336.

Enantioenriched 2-phenylpyrrolidine from above, (0.13 g, 0.86 mmol) was added to a two-neck, 25 mL round-bottom flask equipped with a reflux condenser. To this was added 4 mL of formic acid and 2 mL of 37 wt% formaldehyde (in H₂O). The mixture was stirred and heated to reflux at 80 °C for 3 hrs. The solution was cooled to room temperature and made basic (pH 12) by the addition of 2M NaOH. The organics were extracted with CH₂Cl₂, washed with brine, dried over Na₂SO₄ and concentrated. The resulting yellow oil was placed into a 25 mL round-bottom flask and dissolved in 5 mL of cold ether. HCl (g) was generated and passed into the solution by slow addition of HCl (aq, 12 M) into H₂SO₄ (aq). The resulting white crystals were collected by filtration and dried. Yield: 83%, 140 mg. $[\alpha]_D^{24} = -110^\circ$ (c = 1, CHCl₃); ¹H NMR (CDCl₃, 300 MHz) δ 7.66 (2H, m), 7.32 (3H, m), 4.14 (1H, m), 3.95 (1H, b), 3.05 (2H, m), 2.60 (3H, d, *J* = 4.7 Hz), 2.29 (4H, m); ¹³C NMR (CDCl₃, 75 MHz) δ 131.99, 129.89, 129.31, 128.76, 73.05, 44.43, 37.67, 31.94, 20.95; HRMS (FAB+) *m/z* calc'd for C₁₁H₁₆N [M⁺]: 162.1283, found 162.1325.

2.6 ACKNOWLEDGEMENTS

We thank Ariele P. Hanek and Sean M. A. Kedrowski for helpful discussions. This work was supported by the NIH (NS 34407; NS 11756) and the California Tobacco-Related Disease Research Program of the University of California, grant number 16RT-0160. Varenicline tartrate was a generous gift from Targacept.

2.7 REFERENCES

1. Corringer, P. J.; Le Novère, N.; Changeux, J. P., Nicotinic receptors at the amino acid level. *Annu. Rev. Pharmacol. Toxicol.* **2000**, 40, 431-58.
2. Grutter, T.; Changeux, J. P., Nicotinic receptors in wonderland. *Trends Biochem. Sci.* **2001**, 26, (8), 459-63.
3. Karlin, A., Emerging structure of the nicotinic acetylcholine receptors. *Nat. Rev. Neurosci.* **2002**, 3, (2), 102-14.
4. Gotti, C.; Zoli, M.; Clementi, F., Brain nicotinic acetylcholine receptors: native subtypes and their relevance. *Trends Pharmacol. Sci.* **2006**, 27, (9), 482-91.
5. Romanelli, M. N.; Gratterer, P.; Guandalini, L.; Martini, E.; Bonaccini, C.; Gualtieri, F., Central nicotinic receptors: structure, function, ligands, and therapeutic potential. *ChemMedChem* **2007**, 2, (6), 746-67.
6. Coe, J. W.; Brooks, P. R.; Vetelino, M. G.; Wirtz, M. C.; Arnold, E. P.; Huang, J.; Sands, S. B.; Davis, T. I.; Lebel, L. A.; Fox, C. B.; Shrikhande, A.; Heym, J. H.; Schaeffer, E.; Rollema, H.; Lu, Y.; Mansbach, R. S.; Chambers, L. K.; Rovetti, C. C.; Schulz, D. W.; Tingley, F. D., 3rd; O'Neill, B. T., Varenicline: an $\alpha 4\beta 2$ nicotinic receptor partial agonist for smoking cessation. *J. Med. Chem.* **2005**, 48, (10), 3474-7.
7. Mansvelder, H. D.; Keath, J. R.; McGehee, D. S., Synaptic mechanisms underlie nicotine-induced excitability of brain reward areas. *Neuron* **2002**, 33, (6), 905-19.
8. Nashmi, R.; Xiao, C.; Deshpande, P.; McKinney, S.; Grady, S. R.; Whiteaker, P.; Huang, Q.; McClure-Begley, T.; Lindstrom, J. M.; Labarca, C.; Collins, A. C.; Marks, M. J.; Lester, H. A., Chronic nicotine cell specifically upregulates functional $\alpha 4$ nicotinic receptors: basis for both tolerance in midbrain and enhanced long-term potentiation in perforant path. *J. Neurosci.* **2007**, 27, (31), 8202-18.
9. Tapper, A.; McKinney, S.; Nashmi, R.; Schwarz, J.; Deshpande, P.; Labarca, C.; Whiteaker, P.; Collins, A.; Lester, H., Nicotine activation of $\alpha 4$ receptors: sufficient for reward, tolerance and sensitization. *Science* **2004**, 306, 1029-1032.
10. Beers, W. H.; Reich, E., Structure and activity of acetylcholine. *Nature* **1970**, 228, (5275), 917-22.
11. Glennon, R. A.; Dukat, M., Central nicotinic receptor ligands and pharmacophores. *Pharm. Acta. Helv.* **2000**, 74, (2-3), 103-14.
12. Glennon, R. A.; Dukat, M.; Liao, L., Musings on $\alpha 4\beta 2$ nicotinic acetylcholine (nACh) receptor pharmacophore models. *Curr. Top. Med. Chem.* **2004**, 4, (6), 631-44.
13. Dougherty, D. A.; Stauffer, D. A., Acetylcholine binding by a synthetic receptor. Implications for biological recognition. *Science* **1990**, 250, 1558-1560.
14. Xiu, X.; Puskar, N. L.; Shanata, J. A.; Lester, H. A.; Dougherty, D. A., Nicotine binding to brain receptors requires a strong cation- π interaction. *Nature* **2009**, 458, (7237), 534-7.
15. Zhong, W.; Gallivan, J.; Zhang, Y.; Li, L.; Lester, H.; Dougherty, D., From *ab initio* quantum mechanics to molecular neurobiology: A cation- π binding site in the nicotinic receptor. *Proc. Natl. Acad. Sci. USA* **1998**, 95, 12088-12093.

16. Dougherty, D. A., Cys-loop neuroreceptors: Structure to the rescue? *Chem. Rev.* **2008**, 108, (5), 1642-1653.
17. Brejc, K.; van Dijk, W. J.; Klaassen, R. V.; Schuurmans, M.; van Der Oost, J.; Smit, A. B.; Sixma, T. K., Crystal structure of an ACh-binding protein reveals the ligand-binding domain of nicotinic receptors. *Nature* **2001**, 411, (6835), 269-76.
18. Celie, P.; van Rossum-Fikkert, S.; Van Dyke, W.; Brejc, K.; Smit, A.; Sixma, T., Nicotine and carbamylcholine binding to nicotinic acetylcholine receptors as studied in AChBP crystal structures. *Neuron* **2004**, 41, 907-914.
19. Rucktooa, P.; Smit, A. B.; Sixma, T. K., Insight in nAChR subtype selectivity from AChBP crystal structures. *Biochem. Pharmacol.* **2009**, 78, (7), 777-87.
20. Hansen, S. B.; Sulzenbacher, G.; Huxford, T.; Marchot, P.; Bourne, Y.; Taylor, P., Structural characterization of agonist and antagonist-bound acetylcholine-binding protein from *Aplysia californica*. *J. Mol. Neurosci.* **2006**, 30, (1-2), 101-2.
21. Hansen, S. B.; Sulzenbacher, G.; Huxford, T.; Marchot, P.; Taylor, P.; Bourne, Y., Structures of *Aplysia* AChBP complexes with nicotinic agonists and antagonists reveal distinctive binding interfaces and conformations. *EMBO J.* **2005**, 24, (20), 3635-46.
22. Taylor, P.; Talley, T. T.; Radic, Z.; Hansen, S. B.; Hibbs, R. E.; Shi, J., Structure-guided drug design: conferring selectivity among neuronal nicotinic receptor and acetylcholine-binding protein subtypes. *Biochem. Pharmacol.* **2007**, 74, (8), 1164-71.
23. Cashin, A. L.; Petersson, E. J.; Lester, H. A.; Dougherty, D. A., Using physical chemistry to differentiate nicotinic from cholinergic agonists at the nicotinic acetylcholine receptor. *J. Am. Chem. Soc.* **2005**, 127, (1), 350-356.
24. Koh, J. T.; Cornish, V. W.; Schultz, P. G., An experimental approach to evaluating the role of backbone interactions in proteins using unnatural amino acid mutagenesis. *Biochemistry* **1997**, 36, 11314-11322.
25. England, P. M.; Zhang, Y. N.; Dougherty, D. A.; Lester, H. A., Backbone mutations in transmembrane domains of a ligand-gated ion channel: Implications for the mechanism of gating. *Cell* **1999**, 96, (1), 89-98.
26. Deechongkit, S.; Dawson, P. E.; Kelly, J. W., Toward assessing the position-dependent contributions of backbone hydrogen bonding to beta-sheet folding thermodynamics employing amide-to-ester perturbations. *J. Am. Chem. Soc.* **2004**, 126, (51), 16762-71.
27. Deechongkit, S.; Nguyen, H.; Powers, E. T.; Dawson, P. E.; Gruebele, M.; Kelly, J. W., Context-dependent contributions of backbone hydrogen bonding to beta-sheet folding energetics. *Nature* **2004**, 430, (6995), 101-5.
28. Gleitsman, K. R.; Kedrowski, S. M. A.; Lester, H. A.; Dougherty, D. A., An intersubunit hydrogen bond in the nicotinic acetylcholine receptor that contributes to channel gating. *J. Biol. Chem.* **2008**, 283, (51), 35638-35643.
29. Moroni, M.; Zwart, R.; Sher, E.; Cassels, B. K.; Bermudez, I., Alpha4Beta2 nicotinic receptors with high and low acetylcholine sensitivity: pharmacology, stoichiometry, and sensitivity to long-term exposure to nicotine. *Mol. Pharmacol.* **2006**, 70, (2), 755-68.
30. Fonck, C.; Cohen, B. N.; Nashmi, R.; Whiteaker, P.; Wagenaar, D. A.; Rodrigues-Pinguet, N.; Deshpande, P.; McKinney, S.; Kwoh, S.; Munoz, J.; Labarca, C.;

- Collins, A. C.; Marks, M. J.; Lester, H. A., Novel seizure phenotype and sleep disruptions in knock-in mice with hypersensitive alpha4 nicotinic receptors. *J. Neurosci.* **2005**, 25, (49), 11396-411.
31. Nowak, M. W.; Gallivan, J. P.; Silverman, S. K.; Labarca, C. G.; Dougherty, D. A.; Lester, H. A., *In vivo* incorporation of unnatural amino acids into ion channels in a *Xenopus* oocyte expression system. *Methods Enzymol.* **1998**, 293, 504-529.
 32. Rodriguez, E. A.; Lester, H. A.; Dougherty, D. A., Improved amber and opal suppressor tRNAs for incorporation of unnatural amino acids *in vivo*. Part 1: Minimizing misacylation. *RNA* **2007**, 13, (10), 1703-1714.
 33. Rodriguez, E. A.; Lester, H. A.; Dougherty, D. A., Improved amber and opal suppressor tRNAs for incorporation of unnatural amino acids *in vivo*. Part 2: Evaluating suppression efficiency. *RNA* **2007**, 13, (10), 1715-1722.
 34. Dunsmore, C. J.; Carr, R.; Fleming, T.; Turner, N. J., A chemo-enzymatic route to enantiomerically pure cyclic tertiary amines. *J. Am. Chem. Soc.* **2006**, 128, (7), 2224-5.
 35. Kash, T. L.; Jenkins, A.; Kelley, J. C.; Trudell, J. R.; Harrison, N. L., Coupling of agonist binding to channel gating in the GABA_A receptor. *Nature* **2003**, 421, (6920), 272-5.
 36. Price, K. L.; Millen, K. S.; Lummis, S. C., Transducing agonist binding to channel gating involves different interactions in 5-HT₃ and GABA_C receptors. *J. Biol. Chem.* **2007**, 282, (35), 25623-30.
 37. Venkatachalan, S. P.; Czajkowski, C., A conserved salt bridge critical for GABA_A receptor function and loop C dynamics. *Proc. Natl. Acad. Sci. USA* **2008**, 105, (36), 13604-9.
 38. Filatov, G. N.; White, M. M., The role of conserved leucines in the M2 domain of the acetylcholine receptor in channel gating. *Mol. Pharmacol.* **1995**, 48, (3), 379-84.
 39. Labarca, C.; Nowak, M. W.; Zhang, H.; Tang, L.; Deshpande, P.; Lester, H. A., Channel gating governed symmetrically by conserved leucine residues in the M2 domain of nicotinic receptors. *Nature* **1995**, 376, 514-516.
 40. Etter, J.-F., Cytisine for Smoking Cessation: A literature review and a meta-analysis. *Arch. Intern. Med.* **2006**, 166, (15), 1553-1559.
 41. Mu, T. W.; Lester, H. A.; Dougherty, D. A., Different binding orientations for the same agonist at homologous receptors: A lock and key or a simple wedge? *J. Am. Chem. Soc.* **2003**, 125, (23), 6850-6851.
 42. Puskar, N. L.; Xiu, X.; Lester, H. A.; Dougherty, D. A., Two neuronal nicotinic acetylcholine receptors, alpha4beta4 and alpha7, show differential agonist binding modes. *J. Biol. Chem.* **2011**, 286, (16), 14618-27.
 43. Torrice, M. M., Chemical-scale studies of the nicotinic and muscarinic acetylcholine receptors. Ph.D. Thesis. California Institute of Technology, Pasadena, CA, **2009**.
 44. Torrice, M. M.; Bower, K. S.; Lester, H. A.; Dougherty, D. A., Probing the role of the cation- π interaction in the binding sites of GPCRs using unnatural amino acids. *Proc. Natl. Acad. Sci. USA* **2009**, 106, (29), 11919-24.

45. Felpin; Girard, S.; Vo-Thanh, G.; Robins, R. J.; Villieras, J.; Lebreton, J., Efficient enantiomeric synthesis of pyrrolidine and piperidine alkaloids from tobacco. *J. Org. Chem.* **2001**, 66, (19), 6305-6312.

CHAPTER 3: Residues that Contribute to Binding of the Nicotinic Pharmacophore in the Muscle-Type Nicotinic Receptor*

3.1 ABSTRACT

The agonist binding site of nicotinic acetylcholine receptors (nAChRs) spans an interface between two subunits of the pentameric receptor. The principal component is contributed by an α subunit, and it binds the cationic moiety of the nicotinic pharmacophore. The other part of the pharmacophore – a hydrogen bond acceptor – has recently been shown to bind to the complementary, non- α , subunit. Studies of the neuronal (CNS) receptor $\alpha 4\beta 2$ show that the backbone NH of Leu119 is the donor to the acceptor on the agonist, an interaction presaged by studies of the structurally homologous acetylcholine binding proteins (AChBP). The AChBP structures further suggested that the hydrogen bond to Leu119 was mediated by a water molecule, and that a second hydrogen bonding interaction occurs to the backbone CO of Asn107, also on the complementary subunit. Here we provide new insights into the nature of the interactions between the hydrogen bond acceptor of nicotinic agonists and the backbone features of the complementary subunit. We find that, like the neuronal receptor, the nAChR of the neuromuscular junction (muscle-type) shows a strong interaction with Leu119 (γ L119/ δ L121 in muscle-type receptor numbering) for both ACh and nicotine. However, we find no evidence for a functionally significant interaction with Asn107 (γ N107/ δ N109). Surprisingly, the potent nicotine analog epibatidine does not make a functionally important hydrogen bond to

* This work was done in collaboration with Laurel A. German, a high school student from Polytechnic School.

either γ L119/ δ L121 nor γ N107/ δ N109. In addition, a mutation that has been shown to profoundly affect interactions to the principal component of the agonist binding site of the muscle-type receptor, Gly153Lys, has no impact on interactions involving the complementary subunit.

3.2 INTRODUCTION

Nicotinic acetylcholine receptors (nAChRs) are ligand-gated ion channels that propagate neurotransmission in the central and peripheral nervous systems and are activated by the neurotransmitter acetylcholine and also by nicotine.¹⁻³ The nAChRs are members of a superfamily of ligand-gated ion channels called the Cys-loop (or pentameric) receptors, which also includes receptors for the neurotransmitters γ -aminobutyric acid (GABA_A and GABA_C), glycine (GlyR) and serotonin (5-HT₃). The family is implicated in an assortment of neurological disorders including Alzheimer's disease, Parkinson's disease, schizophrenia, and depression, and are also essential for learning, memory and sensory perception.^{4, 5}

nAChRs are pentamers, composed of five subunits arranged symmetrically around a central ion-conducting pore.¹⁻³ There are 16 mammalian genes that encode 16 homologous but functionally distinct nAChR subunits (α 1- α 7, α 9, α 10, β 1- β 4, γ , δ , ϵ). From various combinations of these subunits, >20 active nAChR subtypes have been established. Of the various nAChR subtypes, the heteropentameric α 1 β 1 γ δ is the most studied, owing to its precise subunit stoichiometry and abundance in the electric organ of eels and rays, which facilitated many early studies of nAChRs.¹ In humans, this subtype is expressed post-synaptically at neuromuscular junctions of the peripheral nervous system and is therefore referred to as the 'muscle-type' receptor. Other nAChRs mediate

synaptic transmission between nerve cells in the central nervous system and autonomic ganglia and are collectively referred to as “neuronal” subtypes. These include $\alpha 4\beta 2$, which is strongly implicated in nicotine addiction⁶⁻⁹ and is the target of the recently developed smoking cessation drug Chantix® (varenicline).⁶

The nicotinic pharmacophore is one of the longest-known, best-studied pharmacophores, and it is comprised of a cationic nitrogen and a hydrogen bond acceptor.^{10, 11} Agonists bind at subunit interfaces,¹⁻³ and a combination of structure-function studies¹²⁻¹⁶ and structural studies of the acetylcholine binding proteins (AChBP),¹⁷⁻²² which share considerable sequence homology with the ligand binding domain of the nAChR, have mapped binding interactions of the pharmacophore onto these interfaces. The α subunits contribute the principal component of the agonist binding site, which binds to the cationic end of agonists. This binding site is well-characterized (**Figure 3.1**), consisting of a cation- π interaction to one of several conserved aromatic residues and a hydrogen bond from the N⁺H of the drug to a backbone carbonyl (except in the case of ACh, which cannot serve as a hydrogen bond donor).¹³⁻¹⁶

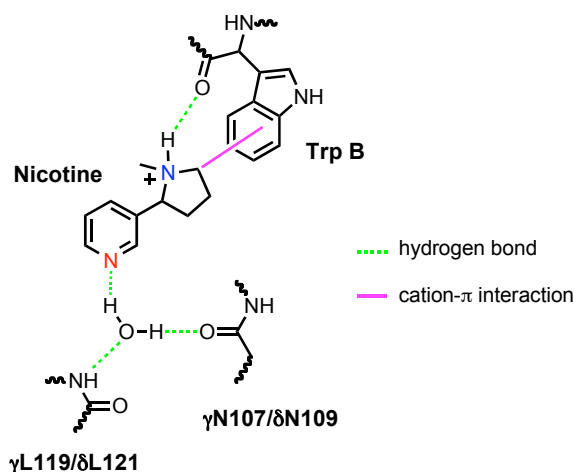


Figure 3.1. Depiction of binding interactions of the nicotinic pharmacophore as predicted by AChBP structures.^{18, 20} Residue numbering is for the muscle-type receptor. TrpB is from the principal subunit ($\alpha 1$).

The complementary component of the agonist binding site is formed by non- α subunits, and recent work has shown that it makes a hydrogen bonding interaction to the hydrogen bond acceptor of agonists. Crystal structures of AChBPs with several drugs bound produced a model in which two backbone residues – the NH of Leu119 and the CO of Asn107 – coordinate a water molecule, which in turn hydrogen bonds to the hydrogen bond acceptor of agonists (**Figure 1.3**).^{18, 20} Recent studies of the neuronal $\alpha 4\beta 2$ receptor confirmed that the NH of Leu119 of the $\beta 2$ subunit does hydrogen bond to the pyridine N of nicotine and to the carbonyl O of ACh.¹²

Note that the pharmacology of the muscle-type receptor is quite distinct from neuronal receptors such as $\alpha 4\beta 2$, most importantly in the fact that nicotine is quite potent at the neuronal receptor¹⁵ but not at the receptors of the neuromuscular junction.¹³ This distinction allows smokers to become addicted to nicotine without adverse peripheral effects.¹⁵ We have shown that binding interactions in the principal component of the agonist binding site strongly differentiate the interaction of nicotine with the two receptor subtypes. ACh, nicotine¹⁵ and epibatidine (See Chapter 4) each form strong cation- π interactions in $\alpha 4\beta 2$, but only ACh and epibatidine make the cation- π interaction in the muscle-type receptor.¹³ Similarly, the hydrogen bond to the backbone CO of the principal subunit is less sensitive to mutation in the muscle-type receptor than in the $\alpha 4\beta 2$ subtype.^{13, 15}

The present work focuses on the complementary component of the agonist binding site of the muscle-type nAChR. We wished to know whether the hydrogen bond to the NH of Leu119 was important for agonist binding in the muscle-type receptor, as it is in $\alpha 4\beta 2$. We also sought to determine a role for the backbone CO of Asn107. An

important residue in distinguishing the pharmacology of the muscle-type from $\alpha 4\beta 2$ is at site 153 of the α subunit, where the $\alpha 1G153K$ mutation in the muscle-type substantially alters interactions in the principal component of the agonist binding site, thereby greatly increasing nicotine affinity.^{15, 23} We wished to determine whether this mutation also impacts the agonist binding interactions to the complementary component of the agonist binding site.

Using unnatural amino acid mutagenesis and mutant cycle analysis we find that the hydrogen bond to Leu119 ($\gamma L119/\delta L121$ in muscle-type receptor numbering) is active in the muscle-type receptor as seen previously in the neuronal $\alpha 4\beta 2$ subtype. However, we find no interaction with the backbone CO of N107 ($\gamma N107/\delta N109$). Interestingly, the close nicotine homologue epibatidine shows no hydrogen bonding interaction to either residue in the complementary subunit. Finally, we find that the $\alpha 1G153K$ mutation that profoundly affects binding interactions in the principal subunit has no effect on binding interactions involving the complementary subunit.

3.3 RESULTS

3.3.1 General Strategy

Potential hydrogen bonds to a protein backbone can be probed by replacing the residue that contributes the backbone NH with its α -hydroxy acid analog.²⁴⁻²⁷ This mutation eliminates a hydrogen bond donor by replacing the backbone NH with an O (**Figure 3.2B**). In addition, the α -hydroxy substitution attenuates the hydrogen bonding ability of the *i-1* carbonyl by converting it to an ester carbonyl. It is well-established that carbonyls of esters are much poorer hydrogen bond acceptors than those of amides. Interestingly, in many studies, both quantitative and qualitative, it has been shown that the two effects

associated with backbone ester incorporation – removal of the NH hydrogen bond donor and attenuation of the CO hydrogen bond acceptor – can have similar energetic consequences.^{12, 24-31} Thus, incorporation of an α -hydroxy acid can probe the hydrogen bonding ability of the associated amide NH and amide carbonyl and, if either are important for agonist binding, the appropriate backbone ester mutation should have an impact on agonist potency. Backbone ester mutations can be efficiently incorporated site-specifically into nAChRs expressed in *Xenopus* oocytes by nonsense suppression methodology.^{12, 28, 30, 31}

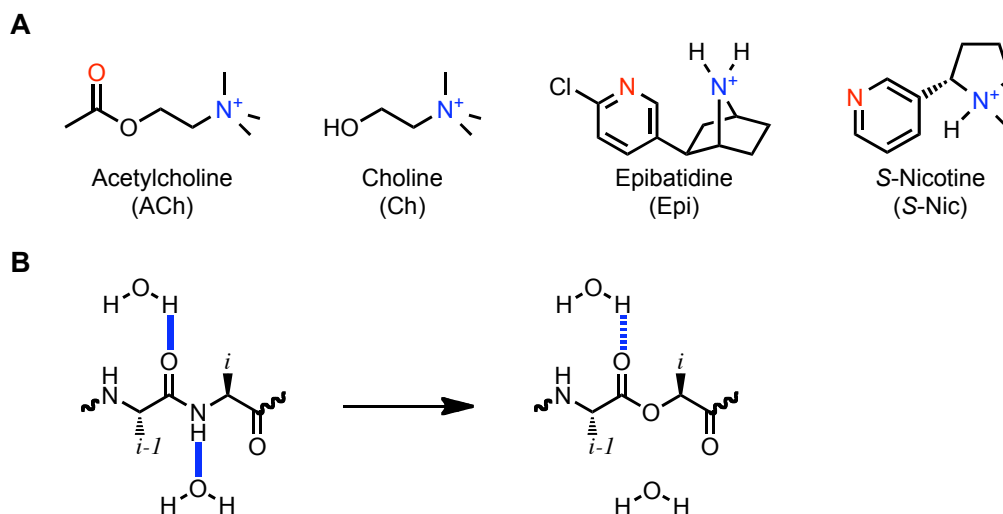


Figure 3.2. Agonists and unnatural amino acids used in this study. (A) Agonists used in this study with pharmacophore highlighted: the positively charged nitrogen is shown in blue and the hydrogen bond acceptor is shown in red. (B) Illustration of amide-to-ester mutation. Introduction of an α -hydroxy acid in place of an amino acid eliminates the hydrogen bond donor (backbone NH) of the i residue and attenuates the hydrogen bond accepting ability of the $i-1$ carbonyl.

These studies use EC_{50} , the effective agonist concentration needed to reach a half-maximal response, as a readout of the functional impact of each mutation. EC_{50} is a composite measure that is influenced by agonist binding and also by channel gating (pore

opening). We do not distinguish these mechanisms here, but we feel that for studies of comparative pharmacology, EC_{50} is an acceptable metric.

In the $\alpha 4\beta 2$ receptor, removal of the backbone NH of the residue analogous to $\gamma L119/\delta L121$ had a measurable impact on receptor function, but that alone does not establish a hydrogen bond to the agonist. As such, we used double mutant cycle analysis to verify the interaction between ACh and the backbone NH of the analogous $\gamma L119/\delta L121$ residue.¹² Mutant cycle analysis is the standard method to determine whether two mutations are energetically coupled.³² EC_{50} -based mutant cycle analysis has been used to probe interactions in Cys-loop receptors by many labs, including our own.^{12, 28, 30, 31, 33-35} It is also standard practice to convert the coupling coefficient (Ω) obtained from a mutant cycle analysis into a free energy by the equation $\Delta\Delta G^\circ = -RT\ln(\Omega)$, where $\Omega = [EC_{50}(WT) * EC_{50}(\text{double mutant})] / [EC_{50}(\text{mutant 1}) * EC_{50}(\text{mutant 2})]$.³² In these experiments, we are using the backbone ester mutation as the first mutation and choline (an analog of ACh that lacks the hydrogen bond accepting acetyl) as the second, thus removing or attenuating both the hydrogen bond donor and acceptor of the presumed interaction. A coupling energy of greater than 1 kcal/mol is generally regarded as compelling evidence in support of the interaction being probed.

In our previous experiments with the $\alpha 4\beta 2$ subtype, we also performed a mutant cycle analysis with the nicotine analog *S-N*-methyl-2-phenylpyrrolidine (*S*-MPP).¹² In this structure, the pyridyl ring of nicotine is replaced with a phenyl ring, thus removing the hydrogen bond-accepting pyridine N. This is certainly a much more subtle probe than the ACh/Ch comparison. However, given the low potency of nicotine at the muscle-type

receptor, it is not surprising that *S*-MPP is a very poor agonist that cannot be studied due to channel block at the concentrations needed to observe dose-response relationships.

These studies use the known L9'S mutation in the M2 transmembrane region of the $\beta 1$ subunit (where 9' is ninth amino acid from the cytoplasmic end of the M2 transmembrane α -helix).^{36, 37} This mutation is introduced to generically increase the sensitivity of the protein to agonists, and it results in a systematic ~ 40 -fold decrease in EC_{50} . Given that the 9' position is ~ 60 Å away from the agonist binding site, this mutation is expected to primarily effect gating and not agonist binding. The backbone ester mutation was performed at γ L119/ δ L121 in the absence and presence of the L9'S background mutation and gave similar shifts in EC_{50} for ACh (**Table 3.1**), suggesting that the L9'S mutation does not have a substantial influence on agonist binding to this residue. The agonist concentrations that were required to obtain a dose-response relation for epibatidine, nicotine and choline in the absence of the L9'S mutation were in the range of channel block, so all comparisons are done using this mutation. An analogous mutation was also used in the studies with $\alpha 4\beta 2$.¹²

Table 3.1. EC₅₀ and Hill coefficient (\pm standard error of the mean) values for mutations made to $\alpha 1_2\beta 1\gamma\delta$. The fold-shift is the ratio of the nonsense suppression EC₅₀ values of the ester mutant over the natural amino acid. Fold-shifts previously reported for experiments¹² with $\alpha 4\beta 2$ are given in parentheses. Mutations identified as “Leu” and “Val” represent recovery of the wild-type receptor by nonsense suppression.

Agonist	Mutation	EC ₅₀ nM	Fold-Shift	Hill
ACh	$\alpha 1\beta 1\gamma\delta$	16000 \pm 300		1.3 \pm 0.1
	$\alpha 1\beta 1\gamma(L119Leu)\delta(L121Leu)$	16000 \pm 500		1.5 \pm 0.1
	$\alpha 1\beta 1\gamma(L119Lah)\delta(L121Lah)$	230000 \pm 6000	14	1.5 \pm 0.1
ACh	$\alpha 1\beta 1(L9'S)\gamma\delta$	610 \pm 40		1.4 \pm 0.1
	$\alpha 1\beta 1(L9'S)\gamma(L119Leu)\delta(L121Leu)$	310 \pm 20		1.5 \pm 0.1
	$\alpha 1\beta 1(L9'S)\gamma(L119Lah)\delta(L121Lah)$	9100 \pm 700	29 (7)	1.6 \pm 0.2
Ch	$\alpha 1\beta 1(L9'S)\gamma\delta$	840000 \pm 20000		1.6 \pm 0.1
	$\alpha 1\beta 1(L9'S)\gamma(L119Leu)\delta(L121Leu)$	780000 \pm 30000		1.7 \pm 0.1
	$\alpha 1\beta 1(L9'S)\gamma(L119Lah)\delta(L121Lah)$	1000000 \pm 50	1.3 (1)	1.8 \pm 0.1
\pm -Epi	$\alpha 1\beta 1(L9'S)\gamma\delta$	320 \pm 20		1.5 \pm 0.1
	$\alpha 1\beta 1(L9'S)\gamma(L119Leu)\delta(L121Leu)$	400 \pm 20		1.5 \pm 0.1
	$\alpha 1\beta 1(L9'S)\gamma(L119Lah)\delta(L121Lah)$	520 \pm 30	1.3 (5)	1.6 \pm 0.1
S-Nic	$\alpha 1\beta 1(L9'S)\gamma\delta$	22000 \pm 800		1.6 \pm 0.1
	$\alpha 1\beta 1(L9'S)\gamma(L119Leu)\delta(L121Leu)$	23000 \pm 700		1.7 \pm 0.1
	$\alpha 1\beta 1(L9'S)\gamma(L119Lah)\delta(L121Lah)$	230000 \pm 30000	10 (7)	2.2 \pm 0.5
ACh	$\alpha 1\beta 1(L9'S)\gamma(V108Val)\delta(V110Val)$	290 \pm 10		1.3 \pm 0.1
	$\alpha 1\beta 1(L9'S)\gamma(V108Vah)\delta(V110Vah)$	410 \pm 50	1.4	1.2 \pm 0.2
	$\alpha 1\beta 1(L9'S)\gamma(V108Val)\delta(V110Val)$	620000 \pm 20000		1.4 \pm 0.1
Ch	$\alpha 1\beta 1(L9'S)\gamma(V108Val)\delta(V110Val)$	790000 \pm 60000	1.3	1.4 \pm 0.1
	$\alpha 1\beta 1(L9'S)\gamma(V108Vah)\delta(V110Vah)$	230 \pm 6		1.4 \pm 0.1
	$\alpha 1\beta 1(L9'S)\gamma(V108Val)\delta(V110Val)$	240 \pm 6	1.0	1.5 \pm 0.1
\pm -Epi	$\alpha 1\beta 1(L9'S)\gamma(V108Vah)\delta(V110Vah)$	15000 \pm 1000		1.2 \pm 0.1
	$\alpha 1\beta 1(L9'S)\gamma(V108Val)\delta(V110Val)$	33000 \pm 2000	2.2	1.6 \pm 0.1
	$\alpha 1\beta 1(L9'S)\gamma(V108Vah)\delta(V110Vah)$			
S-Nic	$\alpha 1\beta 1(L9'S)\gamma(V108Val)\delta(V110Val)$			
	$\alpha 1\beta 1(L9'S)\gamma(V108Vah)\delta(V110Vah)$			
	$\alpha 1\beta 1(L9'S)\gamma(V108Vah)\delta(V110Vah)$			
ACh	$\alpha 1(G153K)\beta 1(L9'S)\gamma\delta$	7.2 \pm 0.7		1.3 \pm 0.1
	$\alpha 1(G153K)\beta 1(L9'S)\gamma(L119Leu)\delta(L121Leu)$	7.6 \pm 0.7		1.8 \pm 0.3
	$\alpha 1(G153K)\beta 1(L9'S)\gamma(L119Lah)\delta(L121Lah)$	180 \pm 20	24	1.3 \pm 0.1
Ch	$\alpha 1(G153K)\beta 1(L9'S)\gamma\delta$	30000 \pm 2000		1.0 \pm 0.1
	$\alpha 1(G153K)\beta 1(L9'S)\gamma(L119Leu)\delta(L121Leu)$	27000 \pm 2000		1.1 \pm 0.1
	$\alpha 1(G153K)\beta 1(L9'S)\gamma(L119Lah)\delta(L121Lah)$	68000 \pm 3000	3	1.3 \pm 0.1
\pm -Epi	$\alpha 1(G153K)\beta 1(L9'S)\gamma\delta$	4.3 \pm 0.5		0.77 \pm 0.5
	$\alpha 1(G153K)\beta 1(L9'S)\gamma(L119Leu)\delta(L121Leu)$	2.3 \pm 0.4		0.74 \pm 0.1
	$\alpha 1(G153K)\beta 1(L9'S)\gamma(L119Lah)\delta(L121Lah)$	9.6 \pm 0.4	4	1.1 \pm 0.1
S-Nic	$\alpha 1(G153K)\beta 1(L9'S)\gamma\delta$	320 \pm 30		1.4 \pm 0.2
	$\alpha 1(G153K)\beta 1(L9'S)\gamma(L119Leu)\delta(L121Leu)$	360 \pm 40		0.95 \pm 0.1
	$\alpha 1(G153K)\beta 1(L9'S)\gamma(L119Lah)\delta(L121Lah)$	6500 \pm 500	18	1.3 \pm 0.1

3.3.2 Mutagenesis studies of $\gamma L119/\delta L121$

To probe for the presumed hydrogen bond to the backbone NH of $\gamma L119/\delta L121$ in the muscle-type nAChR, the leucine was replaced with its α -hydroxy acid analog (leucine, α -hydroxy; Lah). ACh and nicotine showed substantial increases in EC₅₀, confirming that the backbone NH is important for receptor activation by these agonists (Table 3.1). We have performed similar backbone mutations at locations throughout the nAChRs to probe for various hydrogen bonds and typically see informative, but modest increases in EC₅₀

of ~5–20-fold.^{12, 28, 31} The 29-fold increase in EC₅₀ seen for ACh is among the largest responses we have seen for a backbone ester mutation. It is also much larger than the 7-fold increase that was seen for the equivalent mutation in the $\alpha 4\beta 2$ receptor. The responsiveness of nicotine to the backbone ester mutation was also interesting, given its lack of participation in the cation- π interaction in the muscle-type receptor.¹³ The agonist epibatidine, however, was unresponsive to backbone ester mutation, in contrast to the 5-fold increase in EC₅₀ seen in the $\alpha 4\beta 2$ receptor for the analogous mutation.

As expected, choline was unresponsive to the backbone mutation, giving no shift in EC₅₀ upon incorporation of the α -hydroxy acid. Mutant cycle analysis between γ L119Lah/ δ L121Lah and ACh/choline gave a large energetic coupling of 1.9 kcal/mol (Table 3.2 and Figure 3.3), which is nearly double the value seen for analogous mutations in the $\alpha 4\beta 2$ receptor.

Table 3.2. Comparison of coupling coefficients (Ω) and coupling energies ($\Delta\Delta G^\circ$) for double mutant cycles. Corresponding values obtained from experiments with $\alpha 4\beta 2$ ¹² are given in parentheses.

Agonist	Mutant	Ω	$\Delta\Delta G^\circ$ (kcal/mol)
ACh/Ch	$\alpha 1\beta 1(L9'S)\gamma(L119Lah)\delta(L121Lah)$	0.044 (0.16)	1.9 (1.1)
ACh/Ch	$\alpha 1\beta 1(L9'S)\gamma(V108Vah)\delta(V110Vah)$	0.90	0.061
ACh/Ch	$\alpha 1(G153K)\beta 1(L9'S)\gamma(L119Lah)\delta(L121Lah)$	0.11	1.3

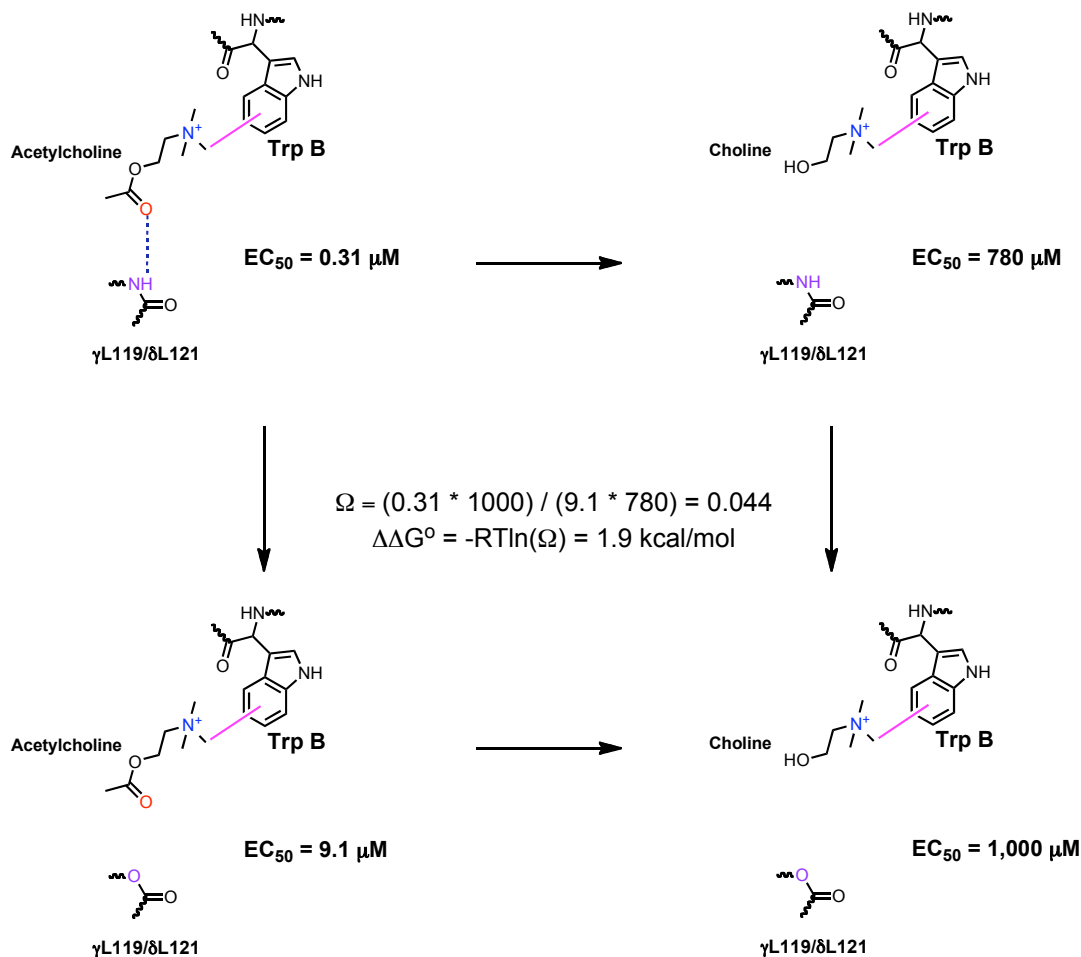


Figure 3.3. Double mutant cycle analysis for ACh and choline on wild-type and $\alpha 1\beta 1(L9'S)\gamma(L119Lah)/\delta(L121Lah)$ mutant receptors.

3.3.3 Mutagenesis studies of the backbone CO of $\gamma N107/\delta N109$

The second hydrogen bond predicted by the AChBP structures is to the backbone CO of $\gamma N107/\delta N109$. Like $\gamma L119/\delta L121$, this residue is thought to coordinate the water molecule that hydrogen bonds to the pyridine nitrogen of nicotine. To probe for a hydrogen bond to this backbone CO, the *i+1* residue, $\gamma V108/\delta V110$, is replaced with its α -hydroxy acid analog (valine, α -hydroxy; Vah). As discussed above, this converts a backbone amide to a backbone ester and in doing so places an electron-withdrawing O

next to the backbone CO in question, thereby attenuating the hydrogen bond accepting ability of this moiety (**Figure 3.2B**).

Early efforts to probe the CO of the residue analogous to γ N107/ δ N109 in the $\alpha 4\beta 2$ receptor gave inconsistent results that led us to question whether we could reliably control the stoichiometry of the mutant receptor (See Chapter 2). Since the muscle-type receptor has just one possible stoichiometry ($\alpha 1_2\beta 1\gamma\delta$), we anticipated that comparable experiments would experience fewer complications, and, indeed, nonsense suppression studies at γ V108/ δ V110 gave functional mutant receptors. However, ACh, nicotine, epibatidine and choline were all unresponsive to the backbone ester mutation (**Table 3.1**). A mutant cycle analysis between γ V108Vah/ δ V110Vah and ACh/choline gives simple additivity ($\Omega = 0.90$), indicating no energetic coupling ($\Delta\Delta G^\circ = 0.061$ kcal/mol) (**Table 3.2**). These data are inconsistent with the second hydrogen bond predicted by the AChBP structures and strongly suggest that γ N107/ δ N109 does not play a significant functional role in the nAChRs.

3.3.4 Impact of the $\alpha 1$ G153K mutation

We have shown previously that introduction of a single mutation in the $\alpha 1$ subunit of the muscle-type receptor, $\alpha 1$ G153K, has dramatic effects on the EC_{50} for nicotine, and that the increased potency of nicotine is, at least in part, a consequence of an enhanced cation- π interaction to nicotine in the mutant muscle-type receptor.¹⁵ The $\alpha 1$ G153 residue is located just four residues from the cation- π binding residue, TrpB, and is a Lys in the high affinity $\alpha 4\beta 2$ subtype, but a Gly in the muscle-type receptor and also in other low affinity subtypes like the $\alpha 7$ homopentamer. It is proposed that when a Lys (or any residue other than Gly) is present at this position, a backbone hydrogen bond is formed

between the protein segment containing α 1G153 “loop B” and another protein segment “loop C,” which, in turn, shapes the agonist binding site in such a way that favors formation of the cation- π interaction to nicotine.²³ Molecular dynamics simulations suggest that this interaction is discouraged when a Gly is present at this position.²³

In the present study we find that the α 1G153K mutation generically increases agonist affinity for the muscle-type receptor by 30–100-fold (**Table 3.1**). However, this mutation had little effect on the magnitudes of EC₅₀ fold-shifts seen for ACh or choline in response to backbone mutation at γ L119/ δ L121. Similarly, mutant cycle analysis of γ L119Lah/ δ L121Lah and ACh/choline with the α 1G153K mutation gave a coupling energy that was comparable to the value seen in the absence of the mutation (**Table 3.2**). A small increase in the fold-shift in EC₅₀ was seen for nicotine and epibatidine, suggesting that the α 1G153K mutation may have moderate effects on agonist binding to the γ L119/ δ L121 residue for these agonists.

3.4 DISCUSSION

In recent years, the well-studied nicotinic pharmacophore has been mapped onto specific binding interactions in the nAChR. The cationic N binds to the principal component of the agonist binding site in the α subunit, and the hydrogen bond acceptor binds to the complementary, non- α subunit. Guided by structures of AChBP,^{18, 20} backbone mutagenesis and mutant cycle analysis studies established a hydrogen bond between the pharmacophore acceptor (pyridine N of nicotine; carbonyl O of ACh) and the backbone NH of β 2Leu119 in the α 4 β 2 neuronal nAChR (analogous to the γ L119/ δ L121 residue in the muscle-type receptor).¹² In the present work, we evaluate binding interactions to the

hydrogen bond acceptor of the pharmacophore in the pharmacologically distinct muscle-type nAChR.

The AChBP structures actually predict that the hydrogen bond to the hydrogen bond acceptor is mediated by a water molecule that hydrogen bonds to both the backbone NH of γ L119/ δ L121 and the backbone CO of another residue in the complementary subunit, γ N107/ δ N109. The backbone ester strategy employed here allows us to probe both components of the hydrogen bond system.

ACh and nicotine both show a strong hydrogen bonding interaction with the backbone NH of γ L119/ δ L121 in the muscle-type receptor. Nicotine shows very poor potency at the wild-type muscle receptor, and so we were surprised to find that nicotine is very sensitive to the backbone ester mutation at γ L119/ δ L121, more sensitive than it is to mutation of the corresponding residue in α 4 β 2, where nicotine is a very potent agonist. Backbone mutation at γ L119/ δ L121 also impacted ACh potency much more in the muscle-type receptor than in the α 4 β 2 receptor. This may suggest that this hydrogen bond is stronger in the muscle-type receptor, and it is possible that ACh and nicotine sit more closely to this residue in the muscle-type receptor than they do in the α 4 β 2 subtype. For nicotine, this is consistent with the fact that it does not make a cation- π interaction to TrpB in the muscle-type receptor,¹³ but does in α 4 β 2.¹⁵

Given the strong interaction between nicotine and γ L119/ δ L121, it is quite surprising that epibatidine is unresponsive to mutation at this site in the muscle-type receptor. Also unlike nicotine, epibatidine *does* make the cation- π interaction to TrpB in this receptor.¹³ This suggests that perhaps epibatidine binds closer to TrpB than nicotine, and thus further from γ L119/ δ L121. Despite the fact that they are very similar

structurally, it is clear that epibatidine and nicotine display differential binding preferences in the muscle-type nAChR.

We find that all agonists tested were unaffected by backbone mutation at γ V108/ δ V110 in the muscle-type receptor, ruling out a functional role for a hydrogen bond to the backbone CO of γ N107/ δ N109. Note that efforts to study this mutation in $\alpha 4\beta 2$ were not successful for technical reasons, and so this is the first evaluation of this potential binding interaction. As noted above, many studies have shown that this type of backbone mutation can strongly impact the strength of a hydrogen bond to a backbone carbonyl. For example, when using this strategy to probe the hydrogen bond from the N^+H of agonists to the CO of TrpB in $\alpha 4\beta 2$, the ester mutation caused increases in EC_{50} from 9-fold to 27-fold. Also, similar mutations have been shown to have significant impacts on the stabilities of both α -helices and β -sheets.^{31, 38, 39} As such, our current data strongly suggest that γ N107/ δ N109 does not play a significant role in agonist binding.

Our results thus find support for one, but not the other, of the two water-mediated hydrogen bonds predicted by the AChBP structures. Note that for either backbone ester mutation, the proposed water molecule could remain after mutation (coordinated by the backbone component that is not mutated), and so it was possible that neither mutation would have a large effect. However, this is not the case, as the 29-fold shift with ACh seen for the γ L119Lah/ δ L121Lah mutation is quite large for this type of perturbation. Furthermore, there is a fundamental distinction between the two hydrogen bond interactions seen in AChBP. The backbone NH of γ L119/ δ L121 can hydrogen bond *directly* to the hydrogen bond acceptor of agonists; the backbone CO of γ N107/ δ N109 can only do so through an intermediary water. Perhaps this distinction rationalizes the

differing ways the two putative hydrogen bonds respond to our probes, including the possibility that the key water molecule seen in AChBP is not present in the nAChR. The backbone NH of γ L119/ δ L121 would then interact directly with the hydrogen bond acceptor of agonists.

Earlier studies have shown that the identity of the residue at position 153 of the α subunit strongly impacts receptor function.²³ An α 1G153K in the muscle-type receptor greatly increases nicotine potency, and it does so by facilitating a strong cation- π interaction to TrpB that is absent in the wild-type receptor.¹⁵ We have now found that the α 1G153K mutation does not have a substantial impact on the γ L119/ δ L121 interaction. This is perhaps not surprising, given that the α 1G153 residue is located in the principal component of the agonist binding site, while γ L119/ δ L121 lies across the subunit interface in the complementary component of the binding site.

In summary, we have shown that ACh and nicotine both engage in a hydrogen bond to the complementary subunit residue γ L119/ δ L121 in the muscle-type nAChR, but the nicotine analog epibatidine does not. In the α 4 β 2 receptor all three agonists engage in this interaction, but the sensitivity of ACh and nicotine to backbone ester mutation at this residue is less than what is seen in the muscle-type receptor. We have also shown that the backbone CO of γ N107/ δ N109, which is predicted by AChBP structures to participate in a water-mediated hydrogen bond with γ L119/ δ L121, is not important for agonist-mediated activation of the muscle-type receptor. Introduction of the α 1G153K mutation has only marginal effects on the γ L119/ δ L121 hydrogen bond. Taken together, these data provide a clearer picture of the agonist binding mechanisms of the muscle-type nAChR

and highlight subtle variations in the mechanisms used by different receptor subtypes, which could offer new insight into the design of subtype-selective therapies.

3.5 EXPERIMENTAL SECTION

Mutagenesis. Nonsense suppression was performed using techniques described previously⁴⁰ on mouse muscle embryonic nAChR ($\alpha_1\beta_1\gamma\delta$) cDNA in the pAMV vector. For nonsense suppression experiments, a TAG (for mutation at γ V108/ δ V110) or TGA stop codon (for mutation at γ L119/ δ L121) was introduced at the site of interest by the standard Stratagene QuickChange protocol and verified through sequencing. The β_1 subunit contains a background mutation in the transmembrane M2 helix (β_1 L9'S) that is known to lower whole-cell EC_{50} values.^{36, 37} The α_1 subunit contains a hemagglutinin epitope in the M3-M4 cytoplasmic loop that does not alter EC_{50} values in control experiments. cDNA was linearized with the restriction enzyme NotI and mRNA was prepared by *in vitro* transcription using the mMessage Machine T7 kit (Ambion).

Stage V-VI *Xenopus laevis* oocytes were injected with mRNA in a 10:1:1:1 or 1:1:5:5 ratio of α_1 : β_1 : γ : δ for wild-type/conventional or nonsense suppression experiments, respectively. α -Hydroxy acids and amino acids were appended to the dinucleotide dCA and enzymatically ligated to the truncated 74-nucleotide amber suppressor tRNA THG73 or opal suppressor tRNA TQOpS' as previously described.⁴⁰ For wild-type or conventional experiments, 1-2 ng of mRNA was injected per oocyte in a single 75 nL injection. For nonsense suppression experiments, each cell was injected with 75 nL of a 1:1 mixture of mRNA (20-25 ng of total mRNA) and tRNA (10-25 ng). Amino acids bearing a 6-nitroveratryloxycarbonyl protecting group were deprotected prior to injection

via irradiation with a 500 W Hg/Xe arc lamp, filtered with WG-334 and UG-11 filters prior to injection. Oocytes were incubated at 18 °C for 16-20 or 24-48 hrs after injection for the wild-type/conventional or nonsense suppression experiments, respectively. Wild-type recovery control experiments (injection of tRNA appended to the natural amino acid) were performed to evaluate the fidelity of the nonsense suppression experiments. Additional controls, injections of mRNA only and mRNA with 76-mer THG73, were also performed and gave minimal currents in electrophysiology experiments (~100 nA or less for controls compared to >>2 μ A for nonsense suppression experiments).

Electrophysiology. Two-electrode voltage clamp electrophysiology was used to measure the functional effects of each mutation. Electrophysiology recordings were performed after injection and incubation as described above using the OpusXpress 6000A instrument (Axon Instruments) at a holding potential of -60 mV. The running buffer was a Ca^{2+} free ND96 solution (96 mM NaCl, 2 mM KCl, 1 mM MgCl_2 , and 5 mM HEPES, pH 7.5). Agonist doses in Ca^{2+} -free ND96 were applied for 15 s followed by a 116 s wash with the running buffer. Dose-response data were obtained for ≥ 8 agonist concentrations on ≥ 8 cells. Dose response relations were fit to the Hill equation to obtain EC_{50} and Hill coefficient values, which are reported as averages \pm standard error of the fit. A detailed error analysis of nonsense suppression experiments shows that data are reproducible to $\pm 50\%$ in EC_{50} .⁴¹

3.6 ACKNOWLEDGEMENTS

This work was supported by the NIH (NS 34407; NS 11756) and the California Tobacco-Related Disease Research Program of the University of California, grant number 16RT-0160.

3.7 REFERENCES

1. Corringer, P. J.; Le Novère, N.; Changeux, J. P., Nicotinic receptors at the amino acid level. *Annu. Rev. Pharmacol. Toxicol.* **2000**, 40, 431-58.
2. Karlin, A., Emerging structure of the nicotinic acetylcholine receptors. *Nat. Rev. Neurosci.* **2002**, 3, (2), 102-14.
3. Grutter, T.; Changeux, J. P., Nicotinic receptors in wonderland. *Trends Biochem. Sci.* **2001**, 26, (8), 459-63.
4. Jensen, A. A.; Frolund, B.; Liljefors, T.; Krogsgaard-Larsen, P., Neuronal nicotinic acetylcholine receptors: structural revelations, target identifications, and therapeutic inspirations. *J. Med. Chem.* **2005**, 48, (15), 4705-45.
5. Romanelli, M. N.; Gratterer, P.; Guandalini, L.; Martini, E.; Bonaccini, C.; Gualtieri, F., Central nicotinic receptors: structure, function, ligands, and therapeutic potential. *ChemMedChem* **2007**, 2, (6), 746-67.
6. Coe, J. W.; Brooks, P. R.; Vetelino, M. G.; Wirtz, M. C.; Arnold, E. P.; Huang, J.; Sands, S. B.; Davis, T. I.; Lebel, L. A.; Fox, C. B.; Shrikhande, A.; Heym, J. H.; Schaeffer, E.; Rollema, H.; Lu, Y.; Mansbach, R. S.; Chambers, L. K.; Rovetti, C. C.; Schulz, D. W.; Tingley, F. D., 3rd; O'Neill, B. T., Varenicline: an alpha4beta2 nicotinic receptor partial agonist for smoking cessation. *J. Med. Chem.* **2005**, 48, (10), 3474-7.
7. Mansvelder, H. D.; Keath, J. R.; McGehee, D. S., Synaptic mechanisms underlie nicotine-induced excitability of brain reward areas. *Neuron* **2002**, 33, (6), 905-19.
8. Nashmi, R.; Xiao, C.; Deshpande, P.; McKinney, S.; Grady, S. R.; Whiteaker, P.; Huang, Q.; McClure-Begley, T.; Lindstrom, J. M.; Labarca, C.; Collins, A. C.; Marks, M. J.; Lester, H. A., Chronic nicotine cell specifically upregulates functional alpha4 nicotinic receptors: basis for both tolerance in midbrain and enhanced long-term potentiation in perforant path. *J. Neurosci.* **2007**, 27, (31), 8202-18.
9. Tapper, A.; McKinney, S.; Nashmi, R.; Schwarz, J.; Deshpande, P.; Labarca, C.; Whiteaker, P.; Collins, A.; Lester, H., Nicotine activation of alpha4 receptors: sufficient for reward, tolerance and sensitization. *Science* **2004**, 306, 1029-1032.
10. Beers, W. H.; Reich, E., Structure and activity of acetylcholine. *Nature* **1970**, 228, (5275), 917-22.
11. Glennon, R. A.; Dukat, M.; Liao, L., Musings on alpha4beta2 nicotinic acetylcholine (nACh) receptor pharmacophore models. *Curr. Top. Med. Chem.* **2004**, 4, (6), 631-44.
12. Blum, A. P.; Lester, H. A.; Dougherty, D. A., Nicotinic pharmacophore: the pyridine N of nicotine and carbonyl of acetylcholine hydrogen bond across a subunit interface to a backbone NH. *Proc. Natl. Acad. Sci. USA* **2010**, 107, (30), 13206-11.
13. Cashin, A. L.; Petersson, E. J.; Lester, H. A.; Dougherty, D. A., Using physical chemistry to differentiate nicotinic from cholinergic agonists at the nicotinic acetylcholine receptor. *J. Am. Chem. Soc.* **2005**, 127, (1), 350-356.
14. Puskar, N. L.; Xiu, X.; Lester, H. A.; Dougherty, D. A., two neuronal nicotinic acetylcholine receptors, alpha4beta4 and alpha7, show differential agonist binding modes. *J. Biol. Chem.* **2011**, 286, (16), 14618-27.

15. Xiu, X.; Puskar, N. L.; Shanata, J. A.; Lester, H. A.; Dougherty, D. A., Nicotine binding to brain receptors requires a strong cation- π interaction. *Nature* **2009**, 458, (7237), 534-7.
16. Zhong, W.; Gallivan, J.; Zhang, Y.; Li, L.; Lester, H.; Dougherty, D., From *ab initio* quantum mechanics to molecular neurobiology: A cation- π binding site in the nicotinic receptor. *Proc. Natl. Acad. Sci. USA* **1998**, 95, 12088-12093.
17. Brejc, K.; van Dijk, W. J.; Klaassen, R. V.; Schuurmans, M.; van Der Oost, J.; Smit, A. B.; Sixma, T. K., Crystal structure of an ACh-binding protein reveals the ligand-binding domain of nicotinic receptors. *Nature* **2001**, 411, (6835), 269-76.
18. Celie, P.; van Rossum-Fikkert, S.; Van Dyke, W.; Brejc, K.; Smit, A.; Sixma, T., Nicotine and carbamylcholine binding to nicotinic acetylcholine receptors as studied in AChBP crystal structures. *Neuron* **2004**, 41, 907-914.
19. Hansen, S. B.; Sulzenbacher, G.; Huxford, T.; Marchot, P.; Bourne, Y.; Taylor, P., Structural characterization of agonist and antagonist-bound acetylcholine-binding protein from *Aplysia californica*. *J. Mol. Neurosci.* **2006**, 30, (1-2), 101-2.
20. Hansen, S. B.; Sulzenbacher, G.; Huxford, T.; Marchot, P.; Taylor, P.; Bourne, Y., Structures of *Aplysia* AChBP complexes with nicotinic agonists and antagonists reveal distinctive binding interfaces and conformations. *EMBO J.* **2005**, 24, (20), 3635-46.
21. Rucktooa, P.; Smit, A. B.; Sixma, T. K., Insight in nAChR subtype selectivity from AChBP crystal structures. *Biochem. Pharmacol.* **2009**, 78, (7), 777-87.
22. Taylor, P.; Talley, T. T.; Radic, Z.; Hansen, S. B.; Hibbs, R. E.; Shi, J., Structure-guided drug design: conferring selectivity among neuronal nicotinic receptor and acetylcholine-binding protein subtypes. *Biochem. Pharmacol.* **2007**, 74, (8), 1164-71.
23. Grutter, T.; Prado de Carvalho, L.; Le Novere, N.; Corringer, P. J.; Edelstein, S.; Changeux, J. P., An H-bond between two residues from different loops of the acetylcholine binding site contributes to the activation mechanism of nicotinic receptors. *Embo J.* **2003**, 22, (9), 1990-2003.
24. Deechongkit, S.; Dawson, P. E.; Kelly, J. W., Toward assessing the position-dependent contributions of backbone hydrogen bonding to beta-sheet folding thermodynamics employing amide-to-ester perturbations. *J. Am. Chem. Soc.* **2004**, 126, (51), 16762-71.
25. Deechongkit, S.; Nguyen, H.; Powers, E. T.; Dawson, P. E.; Gruebele, M.; Kelly, J. W., Context-dependent contributions of backbone hydrogen bonding to beta-sheet folding energetics. *Nature* **2004**, 430, (6995), 101-5.
26. England, P. M.; Zhang, Y. N.; Dougherty, D. A.; Lester, H. A., Backbone mutations in transmembrane domains of a ligand-gated ion channel: Implications for the mechanism of gating. *Cell* **1999**, 96, (1), 89-98.
27. Koh, J. T.; Cornish, V. W.; Schultz, P. G., An experimental approach to evaluating the role of backbone interactions in proteins using unnatural amino acid mutagenesis. *Biochemistry* **1997**, 36, 11314-11322.
28. Blum, A. P.; Gleitsman, K. R.; Lester, H. A.; Dougherty, D. A., Evidence for an extended hydrogen bond network in the binding site of the nicotinic receptor: concerning the role of the vicinal disulfide of the α 1 subunit. *J. Biol. Chem.* **2011**.

29. England, P. M.; Lester, H. A.; Dougherty, D. A., Mapping disulfide connectivity using backbone ester hydrolysis. *Biochemistry* **1999**, 38, (43), 14409-14415.
30. Gleitsman, K. R.; Kedrowski, S. M. A.; Lester, H. A.; Dougherty, D. A., An Intersubunit hydrogen bond in the nicotinic acetylcholine receptor that contributes to channel gating. *J. Biol. Chem.* **2008**, 283, (51), 35638-35643.
31. Gleitsman, K. R.; Lester, H. A.; Dougherty, D. A., Probing the role of backbone hydrogen bonding in a critical beta sheet of the extracellular domain of a cys-loop receptor. *Chembiochem* **2009**, 10, (8), 1385-91.
32. Horovitz, A., Double-mutant cycles: a powerful tool for analyzing protein structure and function. *Fold Des.* **1996**, 1, (6), R121-6.
33. Kash, T. L.; Jenkins, A.; Kelley, J. C.; Trudell, J. R.; Harrison, N. L., Coupling of agonist binding to channel gating in the GABA_A receptor. *Nature* **2003**, 421, (6920), 272-5.
34. Price, K. L.; Millen, K. S.; Lummis, S. C., Transducing agonist binding to channel gating involves different interactions in 5-HT₃ and GABA_C receptors. *J. Biol. Chem.* **2007**, 282, (35), 25623-30.
35. Venkatachalan, S. P.; Czajkowski, C., A conserved salt bridge critical for GABA_A receptor function and loop C dynamics. *Proc. Natl. Acad. Sci. USA* **2008**, 105, (36), 13604-9.
36. Filatov, G. N.; White, M. M., The role of conserved leucines in the M2 domain of the acetylcholine receptor in channel gating. *Mol. Pharmacol.* **1995**, 48, (3), 379-84.
37. Labarca, C.; Nowak, M. W.; Zhang, H.; Tang, L.; Deshpande, P.; Lester, H. A., Channel gating governed symmetrically by conserved leucine residues in the M2 domain of nicotinic receptors. *Nature* **1995**, 376, (6540), 514-6.
38. Deechongkit, S.; Nguyen, H.; Jager, M.; Powers, E. T.; Gruebele, M.; Kelly, J. W., Beta-sheet folding mechanisms from perturbation energetics. *Curr. Opin. Struct. Biol.* **2006**, 16, (1), 94-101.
39. Jager, M.; Deechongkit, S.; Koepf, E. K.; Nguyen, H.; Gao, J.; Powers, E. T.; Gruebele, M.; Kelly, J. W., Understanding the mechanism of beta-sheet folding from a chemical and biological perspective. *Biopolymers* **2008**, 90, (6), 751-8.
40. Nowak, M. W.; Gallivan, J. P.; Silverman, S. K.; Labarca, C. G.; Dougherty, D. A.; Lester, H. A., *In vivo* incorporation of unnatural amino acids into ion channels in a *Xenopus* oocyte expression system. *Methods Enzymol.* **1998**, 293, 504-529.
41. Torrice, M. M., Chemical-scale studies of the nicotinic and muscarinic acetylcholine receptors. Ph.D. Thesis. California Institute of Technology, Pasadena, CA, 2009.

CHAPTER 4: Stereochemical Preferences of the Nicotinic Receptor: Pharmacophore Binding Interactions of Epibatidine Enantiomers*

4.1 ABSTRACT

The nicotinic acetylcholine receptor is responsive to a number of small alkaloids, and not surprisingly, the prototype nicotine shows a strong bias for one drug enantiomer over the other. However, for the closely related and highly potent epibatidine, the two enantiomers are equipotent at the neuronal $\alpha 4\beta 2$ receptor. Moreover, *N*-methylation of epibatidine negatively impacts the potency of just one enantiomer. To understand these observations, we sought to characterize the ligand binding mechanisms of the two enantiomers of epibatidine and their *N*-methyl derivatives. Using unnatural amino acid mutagenesis, we find that despite their equipotency, the enantiomers of epibatidine display striking differences in sensitivities to perturbations of key binding interactions, while their *N*-methyl derivatives are nearly identically sensitive to these perturbations. These data suggest that other non-covalent interactions may be important for defining epibatidine potency or that a combination of effects arising from agonist binding and receptor gating give rise to the observed potencies.

4.2 INTRODUCTION

Synaptic transmission in the central and peripheral nervous systems is mediated by nicotinic acetylcholine receptors (nAChRs).¹⁻³ nAChRs are ligand-gated ion channels that are activated by the neurotransmitter acetylcholine and also by nicotine and other

* This work was done in collaboration with Wesley Yu, a Caltech undergraduate student.

agonists that adhere to the nicotinic pharmacophore. They are implicated in essential processes including learning, memory, and antinociception and are also therapeutic targets for many disorders and conditions including Alzheimer's disease, Parkinson's disease, schizophrenia, and nicotine addiction.^{4, 5}

nAChRs are the prototype of a superfamily of structurally and functionally related neurotransmitter-gated ion channels called the Cys-loop (or pentameric) receptors. This group contains several other families of receptors, including the 5-HT₃ serotonin receptors; the GABA_A and GABA_C receptors; and glycine receptors. Each family member is a pentamer, composed of five subunits arranged around a central, ion-conducting pore. Individual subunits consist of a four-helix transmembrane domain that contains the ion channel gate, an N-terminal extracellular ligand-binding domain and a short extracellular C-terminus. There are 16 known mammalian nAChR subunits that give rise to >20 active nAChR subtypes in humans.^{4, 6} nAChR subtypes are expressed in the peripheral nervous system at neuromuscular junctions (muscle-type receptors) and also in neurons of the central nervous system (neuronal receptors). The $\alpha 4\beta 2$ receptor is the most abundant neuronal nAChR and the subtype most associated with nicotine addiction.⁷⁻¹⁰ It is also the intended target of Chantix®, an established smoking cessation drug.⁷

In the $\alpha 4\beta 2$ subtype, agonist binding occurs at the interface of adjacent principal ($\alpha 4$) and complementary ($\beta 2$) subunits. Each subunit contributes several 'loop' segments that constitute the agonist binding site. The $\alpha 4$ subunit provides loops A, B and C, while the $\beta 2$ subunit supplies loops D, E and F. Loops A, B, C and D contribute five highly conserved aromatic residues collectively referred to as the 'aromatic box' that are

important for agonist binding. Nicotinic agonists share a common pharmacophore, comprised of two essential components – a cationic N and a hydrogen bond acceptor (the CO of ACh or the pyridine N of nicotine) separated by an appropriate ‘internitrogen’ distance.^{11, 12} The binding partners of the nicotinic pharmacophore have been identified by unnatural amino acid mutagenesis studies¹³⁻¹⁶ and also by the structural characterization of the acetylcholine binding proteins (AChBPs),¹⁷⁻²² which share ~25% sequence homology to the extracellular ligand binding domain of the nAChRs. The binding interactions of the pharmacophore are summarized in **Figure 4.1** using epibatidine, a structural analog of nicotine, as the model compound. In this model, the cationic center of the pharmacophore engages in a cation- π interaction to the aromatic box residue, TrpB. Agonists with protonatable nitrogens like nicotine and epibatidine (but not ACh) can also participate in a hydrogen bond to the backbone CO of TrpB. The second component of the pharmacophore, the hydrogen bond acceptor, makes a hydrogen bond to the backbone NH of L119 of the complementary β 2 subunit. In the AChBP structure with nicotine bound,¹⁷ this interaction is depicted as a water-mediated hydrogen bond, but the key structural water is not present in structures with carbamylcholine bound¹⁷ or (+)-epibatidine bound.^{18, 20} The overall binding model shown in **Figure 4.1** has been verified for several agonists including ACh, nicotine and (\pm)-epibatidine by mutagenesis studies in the α 4 β 2 receptor.¹⁴⁻¹⁶

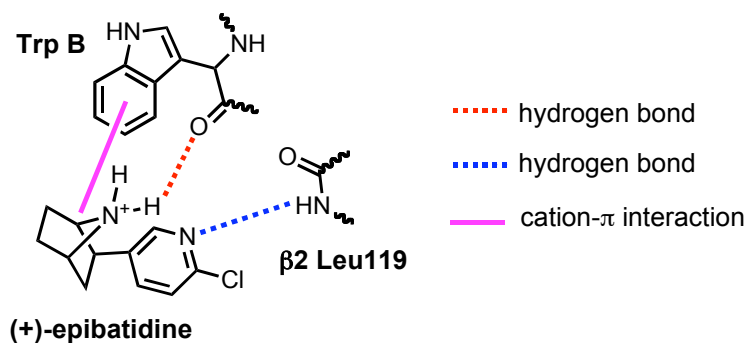


Figure 4.1. The binding interactions of the nicotinic pharmacophore shown for (+)-epibatidine. Note that the nicotine-bound AChBP crystal structure¹⁷ also predicts a second hydrogen bond to the pharmacophore's hydrogen bond acceptor involving another residue in the complementary subunit ($\beta 2N107$), however, this residue was shown to be unimportant for agonist binding in the muscle-type receptor as discussed in Chapter 3 of this thesis.

One puzzling aspect of nAChR pharmacology is that the two enantiomers of epibatidine (**Figure 4.2A**) are equipotent.²³ This is surprising given that the nAChR is a chiral molecule that ought to engage in some degree of chiral recognition. Indeed, this is the case for nicotine– the naturally occurring stereoisomer, *S*-(-)-nicotine, has a higher affinity for the nAChR and is also 10–100-fold more potent than its enantiomer.²⁴⁻²⁶ Moreover, the molecular structures of epibatidine and nicotine are strikingly similar. Both adhere to the nicotinic pharmacophore with a pyridine N as the hydrogen bond acceptor and a cationic N that is part of a five-membered ring (epibatidine's five-membered ring is part of its azabicycloheptane structure), and so it is curious that the stereoisomers of the two agonists are received differently by the nAChRs.

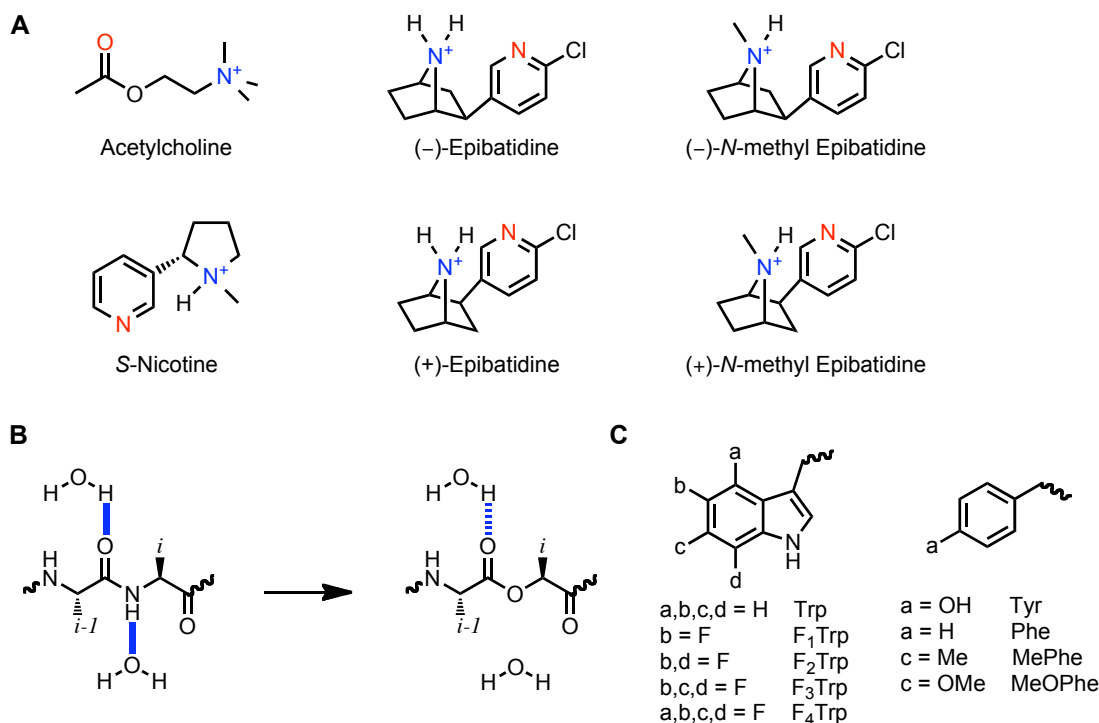


Figure 4.2. Agonists and unnatural amino acids used in this study. (A) Agonist structures. (B) Unnatural amino acids used to probe interactions to TrpB and TyrA. (C) The backbone ester strategy for probing hydrogen bonds to a protein backbone.

N-Methylation of the epibatidine enantiomers produces stereoisomers with different EC₅₀ values (a measure of potency) at the $\alpha 4\beta 2$ receptor.^{23, 27} While the EC₅₀ of (-)-*N*-methyl epibatidine is equivalent to the values seen for both enantiomers of the parent compound, the EC₅₀ of (+)-*N*-methyl is ten-fold higher. We wondered whether this difference in EC₅₀ was the result of a disruption to a hydrogen bond, possibly the hydrogen bond to the backbone CO of TrpB, that results from *N*-methylation of the (+)-epibatidine, but not its enantiomer.

Here, we use unnatural amino acid mutagenesis to characterize the strength of the pharmacophore binding interactions of epibatidine enantiomers and their *N*-methyl derivatives to determine whether established agonist binding mechanisms account for the observed similarities and differences in agonist potency. Surprisingly, we find that the

two enantiomers of epibatidine respond differently to mutagenesis studies of these interactions despite their equipotency, and the *N*-methyl enantiomers respond similarly to these mutations even though there is a ten-fold discrepancy in their potency at the wild-type $\alpha 4\beta 2$ receptor. These data suggest that other factors could contribute to the observed potencies, which could include alternative binding interactions or gating effects.

4.3 RESULTS

4.3.1 General Strategy

These studies use nonsense suppression methodology to study the binding interactions of the pharmacophore for each enantiomer of epibatidine and *N*-methyl epibatidine in the $\alpha 4\beta 2$ receptor expressed in *Xenopus* oocytes. The $\alpha 4\beta 2$ subtype assembles into two viable pentameric stoichiometries, $(\alpha 4)_2(\beta 2)_3$ and $(\alpha 4)_3(\beta 2)_2$. This work focuses on the $(\alpha 4)_2(\beta 2)_3$ stoichiometry, which is more sensitive to nicotine⁷⁻¹⁰ and is upregulated during chronic nicotine exposure.²⁸ In these studies, EC_{50} , the agonist concentration that elicits a half-maximal response (the midpoint of a dose-response curve), is used as a functional measure of agonist potency. EC_{50} is influenced by agonist binding and also by receptor gating (ion pore opening). Given the 60 Å distance between the agonist binding site and the channel gate, it is anticipated that mutations made to the residues studied here primarily affect agonist binding and not channel gating. This assumption is, in part, supported by single-channel studies of $\alpha 4\beta 2$ that showed that mutations to TrpB had little impact on P_{open} (the probability that the channel is open),¹⁴ suggesting that changes in EC_{50} that result from mutation of this residue are likely to primarily result from disruptions to agonist binding.

Each interaction to the nicotinic pharmacophore depicted in **Figure 4.1** can be readily probed by nonsense suppression methodology. Hydrogen bonds to protein backbones can be probed by replacing the residue that contributes the backbone NH with the analogous α -hydroxy acid (**Figure 4.2B**).²⁹⁻³² This converts the backbone amide to an ester and in doing so eliminates a hydrogen bond donor by replacing the backbone NH with an O. As such, we probe the hydrogen bond to the backbone NH of L119 by replacing this residue with the corresponding α -hydroxy acid (Lah; leucine, α -hydroxy). It is also well-established that the CO of an ester is a much poorer hydrogen bond acceptor than the CO associated with an amide, and so the hydrogen bond-accepting ability of the backbone CO (of the *i-1* residue) is also attenuated by backbone ester mutations. Therefore, we probe the hydrogen bond to the backbone CO of TrpB by replacing the *i+1* residue, Thr155, with its α -hydroxy analog. We consider the fold-shift in EC₅₀ for a backbone ester mutation to be an indication of the strength of the hydrogen bond interaction being probed. We feel this is appropriate given the subtlety of these mutations (which convert a single backbone NH to an O) and the structural similarity of the agonists used in these studies.

To probe for the cation- π interaction, a series of fluorinated Trp analogs is incorporated at TrpB (**Figure 4.2C**).³³⁻³⁵ Fluorination attenuates the cation binding ability of the Trp side chain in an additive fashion. A linear correlation between the EC₅₀ and the cation- π binding ability of the side chain is indicative of cation- π interaction. In these studies we will be using the relative slope of these linear correlations (or ‘fluorination plots’) as an indication of the relative strength of a cation- π interaction. As

an alternative measure, the EC₅₀ fold-shifts for each fluorinated mutant will also be compared.

4.3.2 EC₅₀ values at the $\alpha 4(L9'A)\beta 2$ receptor

Consistent with what has been reported for the wild-type $\alpha 4\beta 2$ receptor,²⁷ we find that both enantiomers of epibatidine and (–)-*N*-methyl epibatidine are equipotent and the EC₅₀ of (+)-*N*-methyl epibatidine is ~ten-fold higher than the other three compounds at the $\alpha 4(L9'A)\beta 2$ receptor (**Table 4.1**). Mutagenesis studies of the three interactions of the pharmacophore are discussed below.

Table 4.1. EC₅₀ and Hill coefficient values (\pm standard error of the mean) for epibatidine and *N*-methyl derivatives. Mutations identified as “Leu,” “Thr,” “Trp,” and “Tyr” represent recovery of the wild type receptor by nonsense suppression.

Mutation	Agonist	EC ₅₀ (nM)	Hill
$\alpha 4(\text{L9'A})\beta 2$	(+)-Epi	0.87 \pm 0.03	1.5 \pm 0.1
	(-)-Epi	1.1 \pm 0.04	1.6 \pm 0.1
	(+)-Epi-Me	8.6 \pm 0.5	1.7 \pm 0.2
	(-)-Epi-Me	0.42 \pm 0.04	1.5 \pm 0.1
$\alpha 4(\text{L9'A})\beta 2(\text{L119Leu})$	(+)-Epi	0.58 \pm 0.04	1.3 \pm 0.1
	(-)-Epi	0.73 \pm 0.03	1.4 \pm 0.1
	(+)-Epi-Me	8.9 \pm 0.7	1.3 \pm 0.1
	(-)-Epi-Me	0.42 \pm 0.04	1.6 \pm 0.1
$\alpha 4(\text{L9'A})\beta 2(\text{L119Lah})$	(+)-Epi	2.7 \pm 0.1	1.3 \pm 0.1
	(-)-Epi	3.8 \pm 0.2	1.1 \pm 0.1
	(+)-Epi-Me	30 \pm 2	1.4 \pm 0.1
	(-)-Epi-Me	0.91 \pm 0.06	1.9 \pm 0.2
$\alpha 4(\text{L9'A/T155Thr})\beta 2$	(+)-Epi	0.89 \pm 0.09	1.2 \pm 0.1
	(-)-Epi	1.8 \pm 0.07	1.5 \pm 0.1
	(+)-Epi-Me	6.2 \pm 0.4	1.4 \pm 0.1
	(-)-Epi-Me	0.35 \pm 0.02	1.6 \pm 0.2
$\alpha 4(\text{L9'A/T155Tah})\beta 2$	(+)-Epi	4 \pm 0.3	1.3 \pm 0.1
	(-)-Epi	17 \pm 0.6	1.4 \pm 0.1
	(+)-Epi-Me	93 \pm 7	1.5 \pm 0.1
	(-)-Epi-Me	4.1 \pm 0.3	1.3 \pm 0.1
$\alpha 4(\text{L9'A/W154Trp})\beta 2$	(+)-Epi	0.92 \pm 0.04	1.5 \pm 0.1
	(-)-Epi	1.2 \pm 0.04	1.7 \pm 0.1
	(+)-Epi-Me	7.6 \pm 0.5	1.3 \pm 0.1
	(-)-Epi-Me	0.65 \pm 0.08	1.5 \pm 0.2
$\alpha 4(\text{L9'A/W154F}_1\text{Trp})/\beta 2$	(+)-Epi	1.8 \pm 0.1	1.3 \pm 0.1
	(-)-Epi	9.2 \pm 0.4	1.5 \pm 0.1
	(+)-Epi-Me	35 \pm 2	1.3 \pm 0.1
	(-)-Epi-Me	3.5 \pm 0.3	1.3 \pm 0.1
$\alpha 4(\text{L9'A/W154F}_2\text{Trp})/\beta 2$	(+)-Epi	2.3 \pm 0.1	1.3 \pm 0.1
	(-)-Epi	15 \pm 0.6	1.3 \pm 0.1
	(+)-Epi-Me	44 \pm 3	1.2 \pm 0.1
	(-)-Epi-Me	5.7 \pm 0.7	1.2 \pm 0.1
$\alpha 4(\text{L9'A/W154F}_3\text{Trp})/\beta 2$	(+)-Epi	16 \pm 1	1.2 \pm 0.1
	(-)-Epi	76 \pm 1	1.3 \pm 0.1
	(+)-Epi-Me	190 \pm 10	1.6 \pm 0.1
	(-)-Epi-Me	33 \pm 2	1.4 \pm 0.1
$\alpha 4(\text{L9'A/W154F}_4\text{Trp})/\beta 2$	(+)-Epi	20 \pm 2	1.0 \pm 0.1
	(-)-Epi	210 \pm 7	1.3 \pm 0.1
	(+)-Epi-Me	400 \pm 20	1.2 \pm 0.1
	(-)-Epi-Me	35 \pm 3	1.2 \pm 0.1
$\alpha 4(\text{L9'A/Y98Tyr})\beta 2$	(+)-Epi	0.64 \pm 0.04	1.5 \pm 0.1
	(-)-Epi	0.8 \pm 0.05	1.4 \pm 0.1
	(+)-Epi-Me	6.4 \pm 0.2	1.3 \pm 0.1
	(-)-Epi-Me	0.77 \pm 0.2	1.0 \pm 0.1
$\alpha 4(\text{L9'A/Y98MeOPhe})\beta 2$	(+)-Epi	9.2 \pm 0.6	1.3 \pm 0.1
	(-)-Epi	9.2 \pm 0.5	1.5 \pm 0.1
	(+)-Epi-Me	45 \pm 2	1.4 \pm 0.1
	(-)-Epi-Me	0.8 \pm 0.1	1.9 \pm 0.1
$\alpha 4(\text{L9'A/Y98MePhe})\beta 2$	(+)-Epi	42 \pm 3	1.5 \pm 0.1
	(-)-Epi	16 \pm 1	1.3 \pm 0.1
	(+)-Epi-Me	34 \pm 2	1.3 \pm 0.1
	(-)-Epi-Me	0.89 \pm 0.09	2.0 \pm 0.3
$\alpha 4(\text{L9'A/Y98Phe})\beta 2$	(+)-Epi	1.5 \pm 0.1	1.4 \pm 0.1
	(-)-Epi	40 \pm 2	1.3 \pm 0.1
	(+)-Epi-Me	66 \pm 4	1.1 \pm 0.1
	(-)-Epi-Me	0.82 \pm 0.08	1.6 \pm 0.1

4.3.3 Cation- π interaction to Trp B

All epibatidine isomers and derivatives were highly sensitive to fluorination of the TrpB side chain, but differences were seen in the magnitude of their sensitivities and in the slopes of their fluorination plots (**Figure 4.3** and **Table 4.2**). (+)-Epibatidine gave the smallest fluorination plot slope of any of the four epibatidine compounds. This slope was also smaller than the slopes seen for ACh and nicotine in previous studies.¹⁴ In contrast, its enantiomer, (–)-epibatidine, gave the largest slope we have ever seen at the $(\alpha 4)_2(\beta 2)_3$ stoichiometry. This difference was not seen in the *N*-methyl enantiomers, which gave equivalent fluorination slopes.

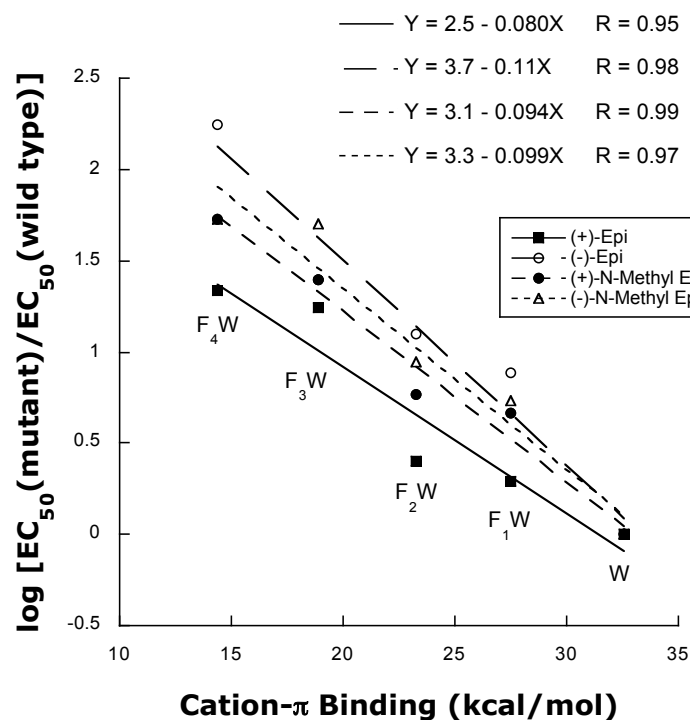


Figure 4.3. Fluorination plots of epibatidine compounds.

Table 4.2. EC₅₀ fold-shifts and fluorination plot slopes for the epibatidine (Epi) compounds and also for ACh and nicotine (Nic). The data for ACh and nicotine are from previously published studies.^{14, 15}

Mutation	(+)-Epi	(-)-Epi	(+)- <i>N</i> -methyl Epi	(-)- <i>N</i> -methyl Epi	ACh*	Nic*
EC ₅₀ Fold-Shift						
$\alpha 4(\text{L9'A/W154F}_1\text{Trp})\beta 2$	2.0	7.7	4.6	5.4	4.3	2.9
$\alpha 4(\text{L9'A/W154F}_2\text{Trp})\beta 2$	2.5	13	5.8	8.8	4.5	3.6
$\alpha 4(\text{L9'A/W154F}_3\text{Trp})\beta 2$	17	63	25	51	30	13
$\alpha 4(\text{L9'A/W154F}_4\text{Trp})\beta 2$	22	180	53	54	65	47
$\alpha 4(\text{L9'A/T155Tah})\beta 2$	4.5	9.4	15	12	1.0	21
$\alpha 4(\text{L9'A})\beta 2(\text{L119Lah})$	4.7	5.2	3.4	2.2	7.0	7.0
Fluorination Plot Slope						
	0.080	0.11	0.094	0.099	0.10	0.089

Comparison of the magnitudes of the EC₅₀ fold-shifts suggests a similar trend. The EC₅₀ fold-shifts for (+)-epibatidine were significantly smaller than those seen for (–)-epibatidine, highlighted by the 22- vs. 180-fold-shift seen for F₄Trp. In contrast, the shifts for the *N*-methyl derivatives were relatively similar despite the ten-fold difference in wild-type EC₅₀ for these enantiomers.

4.3.4 Hydrogen bond to the backbone CO of Trp B

The epibatidine compounds were also affected by backbone ester mutation of $\alpha 4\text{T155}$ (Table 4.2), suggesting that they each make a hydrogen bond to the backbone CO of TrpB. In general, the epibatidine compounds are less sensitive to this mutation than nicotine.¹⁴ The EC₅₀ fold-shift seen for (–)-epibatidine was double the shift seen for its enantiomer, which is surprising given that (–)-epibatidine was also more sensitive to fluorination at TrpB.

In general, the *N*-methyl derivatives were more sensitive to backbone ester mutation than the parent molecules. Similar to the trend seen in studies of the cation- π interaction, the *N*-methyl derivatives showed nearly identical shifts in EC₅₀ in response to

backbone mutation despite the order-of-magnitude difference in their wild-type EC₅₀ values.

4.3.5 Hydrogen bond to β 2L119

The EC₅₀ of each epibatidine compound was impacted by incorporation of an α -hydroxy acid at β 2L119 (**Table 4.2**), although the magnitudes of the fold-shifts were smaller than what is seen for ACh and nicotine.¹⁵ This suggests that the hydrogen bond to the backbone NH of this residue does not play a major role in binding epibatidine.

4.3.6 A hydrogen bond to TyrA?

A closer examination of the AChBP structure with (+)-epibatidine bound suggested that a second hydrogen bond might link the N⁺H of epibatidine to the receptor.^{18, 20} This hydrogen bond is to the phenol OH of the aromatic box residue TyrA. In the AChBP structure, (+)-epibatidine comes within 4 Å of this side chain.

It should be noted that we were skeptical as to whether we could obtain meaningful information from mutagenesis studies of TyrA, as this residue has been suggested to play a role in channel gating, although there is disagreement on this subject.^{36, 37} The potency of ACh has been shown to be impacted by mutation of this residue to a Phe in *Torpedo*,^{37, 38} muscle-type,³⁶ α 7,³⁹ and α 4 β 2¹⁴ nAChRs. This is surprising given that the cationic N of ACh cannot serve as a hydrogen bond donor and therefore cannot participate in the hydrogen bond predicted for epibatidine by the AChBP structure. A single-channel study of the muscle-type receptor found that the predominant effect of the TyrA to Phe mutation is to alter the affinity of the agonist binding site, although a small, yet statistically significant, effect on P_{open} was seen.⁴⁰ Mutation of TyrA

to MePhe and MeOPhe in $\alpha 4\beta 2$ also impacts the EC_{50} of ACh and nicotine, but to a lesser extent (**Table 4.3**).¹⁴ It could be that mutation of the 4-position of the TyrA side chain generically impacts receptor function, possibly owing to its involvement in interactions with other residues of the protein that are important for protein structure/function or that, indeed, channel gating is effected by mutation of this residue. Given this history, it was anticipated that it would be difficult to tease out information about the predicted interaction to TyrA using EC_{50} comparisons. Nevertheless, we attempted to probe this interaction.

With respect to EC_{50} fold-shifts, one of the more surprising results from our studies of TyrA is that (–)-*N*-methyl epibatidine is completely insensitive to any of the mutations we tested (**Table 4.3**). This is particularly remarkable because it is the more potent enantiomer of the *N*-methyl derivatives and so might have been considered to be more likely to participate in the predicted hydrogen bond than its enantiomer (which *is* sensitive to mutation of TyrA). Importantly, these data also suggest that mutation of this residue does not generically impact receptor function. To our knowledge, (–)-*N*-methyl epibatidine is the only agonist that has been shown to be insensitive to mutation of TyrA.

Table 4.3. Relative efficacy values and EC_{50} fold-shifts resulting from mutation of TyrA (Y98) for the epibatidine (Epi) compounds, ACh and nicotine (Nic). The data for ACh and nicotine are from previously published studies.¹⁴ The relative efficacy of an agonist is defined as the ratio: I_{\max} of agonist at a saturating concentration / I_{\max} of acetylcholine at a saturating concentration. By definition, the relative efficacy of ACh is 1.

Mutation	(+)-Epi	(–)-Epi	(+)- <i>N</i> -methyl Epi	(–)- <i>N</i> -methyl Epi	ACh*	Nic*
	EC_{50} Fold-Shift					
$\alpha 4(L9'A/Y98MeOPhe)\beta 2$	14	12	7.0	1.0	7.4	5.0
$\alpha 4(L9'A/Y98MePhe)\beta 2$	66	20	5.3	1.2	8.7	3.5
$\alpha 4(L9'A/Y98Phe)\beta 2$	2.3	50	10	1.1	27	10
Relative Efficacy WT	0.3	0.7	0.5	0.6	[1]	0.3
Relative Efficacy Y98F	7	0.7	2	4	[1]	0.2

The EC₅₀ values of the other three epibatidine compounds were sensitive to TyrA mutations. While the magnitude of the impact on EC₅₀ varies between these compounds, no obvious trends are seen. (+)-Epibatidine is more sensitive to the MeOPhe and MePhe mutations than to the Tyr to Phe mutation; (–)-Epibatidine is most sensitive to the Tyr to Phe mutation; and (+)-Epibatidine is generically sensitive to mutation of this side chain.

A comparison of the relative efficacy of each agonist at the $\alpha 4(\text{L9'A})\beta 2$ receptor with and without the TyrA to Phe mutation shows dramatic differences for three of the epibatidine compounds, but no major difference for nicotine or (–)-epibatidine (**Table 4.3**). It is again interesting that the efficacies of the *N*-methyl derivative enantiomers are similarly affected by mutation, but the parent enantiomers display striking differences.

Efficacy is a measure of the agonist's ability to gate the channel, and so it is quite possible that the observed effects on efficacy and EC₅₀ are primarily or partially the result of effects on channel gating. As such, it would be valuable to perform detailed single-channel studies to determine whether the observed impacts on agonist potency and efficacy are the result of alterations in channel gating, agonist binding or both.

4.4 DISCUSSION

Epibatidine was first isolated in 1974 by Daly and co-workers from the skin of the Ecuadorian 'poison dart' frog *Epipedobates tricolor*, which secretes the compound as a poison in the skin on their backs for protection from predators.⁴¹ Daly demonstrated that epibatidine is a powerful analgesic, ~200 times more potent than morphine, but does not target opioid receptors. The latter finding generated excitement, because it meant that epibatidine was less likely to be addictive, but formidable toxic side effects have prevented its use as a therapeutic.²³ Instead, epibatidine is often used as a structural

starting point for the development of new pharmaceuticals.²³ Due to its high uptake and slow clearance from mouse brains, epibatidine has also been used as a parent structure for the development of radiotracers for *in vivo* labeling of nAChRs.^{42, 43}

The analgesic properties of epibatidine were shown to be mediated by the nAChR.²³ Indeed, epibatidine is a potent agonist of the nAChR, activating the receptors at lower concentrations than nicotine (~100-fold lower EC₅₀ than nicotine). Although the two molecules share a common pharmacophore and a remarkably similar structural layout, striking differences are seen in the potencies of their enantiomers at the nAChRs. *R*-(+)-nicotine has a 10–100-fold higher EC₅₀ than its enantiomer at nAChRs,²⁴⁻²⁶ but the enantiomers of epibatidine are equipotent. The equipotency of the epibatidine enantiomers is puzzling, given that the nAChR is a chiral molecule that should preferentially bind to one enantiomer of a substrate.

We sought to probe the pharmacophore binding interactions of the two enantiomers of epibatidine in $\alpha 4\beta 2$ in the hope of gaining a better understanding of the origin of their equipotency. We anticipated that (+)-epibatidine and (–)-epibatidine would behave in a similar fashion to perturbation of the three pharmacophore interactions, or that a compensatory relationship would be active. Consistent with expectation, we found that both enantiomers behaved identically to perturbation of the hydrogen bond to the complementary subunit, but this interaction does not appear to be very important for epibatidine binding in general. We also found that (–)-epibatidine is much more sensitive to perturbation of both TrpB interactions than its enantiomer– a surprising result given the equipotency of the two agonists.

N-Methylation of epibatidine has been shown to have a relatively dramatic effect on the potency of one of the epibatidine enantiomers. While (–)-*N*-methyl epibatidine shares the same potency as the parent compounds, its enantiomer has a ten-fold higher EC₅₀. To explain this discrepancy in EC₅₀, we wondered whether one of the interactions of the pharmacophore was disrupted by methylation of one enantiomer, but not the other. Surprisingly, we found that both enantiomers of the *N*-methyl derivative are nearly identically sensitive to perturbation of the three interactions. Thus, our data concerning the interactions of the pharmacophore do not account for the equipotency of epibatidine enantiomers or the discrepancy in EC₅₀ seen for the *N*-methyl derivatives, but rather suggests that an alternative explanation is viable.

It could be that additional noncovalent interactions compensate for the stronger cation- π and hydrogen bond interactions seen for (–)-epibatidine and that disruption of these same or other interactions are responsible for the discrepancy in *N*-methyl derivative EC₅₀ values. The AChBP structure with (+)-epibatidine bound suggests several possible interactions, including polar contacts between the pyridine ring Cl and residues in the complementary subunit of the protein as well as a second hydrogen bond to the N⁺H of the pharmacophore.^{18, 20} We anticipate that the predicted interactions with the Cl are unlikely to account for the large discrepancies in sensitivities we observe, because an epibatidine derivative lacking the Cl ((±)-norchloroepibatidine) has only minimally perturbed affinity and potency relative to the parent agonist.⁴⁴ The second predicted hydrogen bond involving the N⁺H of the pharmacophore is to TyrA, one of the five aromatic box residues that are conserved across the Cys-loop family. This residue has played a complicated role in nAChR research.^{36, 37, 40} ACh cannot serve as a hydrogen

bond donor and therefore cannot participate in the proposed interaction to TyrA, yet its EC₅₀ is still very sensitive to mutation of this residue. Furthermore, single molecule studies suggest that mutation of this residue primarily effects agonist binding and not channel gating although small effects to P_{open} are seen for ACh.⁴⁰

Our studies of this residue in the present context did not lead to any clear explanations for the potency of epibatidine and its derivatives, but they did show that the potency of (–)-*N*-methyl epibatidine is completely insensitive to mutation of TyrA, suggesting that mutations at this site do not generically affect agonist potency. While no measureable impact on the EC₅₀ of (–)-*N*-methyl epibatidine was observed, the relative efficacy of this agonist was impacted by the TyrA to Phe mutation as were the relative efficacies of (+)-epibatidine and (+)-*N*-methyl epibatidine. Note that we are reporting *relative* efficacy values that are referenced to the I_{max} elicited by ACh. It is possible that the efficacy of ACh is also affected by the TyrA to Phe mutation, but this is probably not the case as the relative efficacies of (–)-epibatidine and nicotine are not affected by this mutation. Since efficacy is a measure of the ability of the agonist to induce channel opening, it is likely that mutations to TyrA may affect channel gating for some, if not all, agonists. As such, a single-channel kinetic study could be useful in understanding the effects of mutations to TyrA.

An alternative explanation for the observed agonist potencies is that a collection of hydrophobic interactions account for the observed similarities and differences in agonist potencies and sensitivities to mutations of the pharmacophore binding residues. Recall that the structure of epibatidine includes an azabicycloheptane structure, which could present a large hydrophobic surface area to the nAChR that might be more

accessible in the (+) enantiomer (which makes a weaker interactions with TrpB). The discrepancy in EC_{50} of the *N*-methyl derivatives could also be the consequence of steric effects that are introduced by methylation of one enantiomer but not the other. Given that EC_{50} is influenced by agonist binding and receptor gating, it is also possible that a combination of gating and binding effects coincidentally give rise to equipotency in one scenario and differences in potency in the other and also to the observed differences in sensitivities to perturbation of the pharmacophore interactions.

In summary, we have used nonsense suppression to evaluate the pharmacophore binding interactions of the enantiomers of epibatidine and *N*-methyl epibatidine to account for similarities and differences seen in their EC_{50} values at the neuronal $\alpha 4\beta 2$ receptor. We find that all agonists participate in the pharmacophore interactions – a cation- π interaction to Trp B, a hydrogen bond to the backbone CO of TrpB, and a hydrogen bond to the backbone NH of L119 of the complementary subunit. However, we see surprising differences and similarities in their sensitivities to perturbations of these interactions that do not account for their respective EC_{50} values. Future work will seek to identify additional noncovalent interactions that could be responsible for the observed potencies of the four epibatidine compounds. It is also likely that a detailed kinetic analysis of the mutations used to probe these interactions would be valuable in uncovering this mystery.

4.5 EXPERIMENTAL SECTION

Nonsense suppression methodology was used to introduce unnatural amino acids and α -hydroxy acids site specifically in the $\alpha 4\beta 2$ receptor.⁴⁵ Unnatural mutations were introduced to rat $\alpha 4$ and $\beta 2$ cDNA in the pAMV vector by the standard Stratagene

QuickChange protocol, using a TAG codon for mutations to the $\alpha 4$ subunit and a TGA codon for mutations to $\beta 2$. Mutations were verified by sequencing. cDNA was linearized with the restriction enzyme Not 1 and mRNA was prepared by *in vitro* transcription using the mMessage Machine T7 kit (Ambion). The $\alpha 4$ subunit contained the L9'A background mutation, which is known to increase receptor expression and sensitivity to agonists without affecting other aspects of receptor pharmacology.⁴⁶ The same mutation was used in our previous studies of the pharmacophore binding interactions in the $\alpha 4\beta 2$ receptor.^{14, 15}

Stage V-VI *Xenopus laevis* oocytes were injected with mRNA in a 1:1, 3:1 or 1:20 ratio of $\alpha 4$ L9'A: $\beta 2$ for wild-type experiments, nonsense suppression experiments in $\alpha 4$ or nonsense suppression experiments in $\beta 2$, respectively. α -Hydroxy or amino acids were chemically acylated to the dinucleotide dCA and enzymatically ligated to the truncated 74-nucleotide THG73 or TQOpS' tRNA as previously described⁴⁵ for nonsense suppression experiments in $\alpha 4$ or $\beta 2$, respectively. For nonsense suppression experiments, each cell was injected with 75 nL of a 1:1 mixture of mRNA (20-25 ng of total mRNA): tRNA (20-30 ng) while a 75 nL injection of 10 ng of mRNA was used for wild-type experiments. Injected oocytes were incubated for 24-48 hrs at 18 °C before electrophysiology recordings. Several control experiments were conducted to evaluate the fidelity of the nonsense suppression experiments, which included wild-type recovery experiments (injection of tRNA appended to the natural amino acid) and also injection of mRNA only or mRNA with unacylated suppressor tRNA. Negligible currents were seen for these controls.

Electrophysiology experiments were performed 24-48 hrs after injection using the OpusXpress 6000A instrument (Axon Instruments) in two-electrode voltage clamp mode with a holding potential of -60 mV. Ca^{2+} free ND96 solution was used as the running buffer (96 mM NaCl, 2 mM KCl, 1 mM MgCl_2 , and 5 mM HEPES, pH 7.5). During electrophysiology recordings, the first 8 agonist doses (lowest concentrations) were applied for 90 seconds with a 116 s wash with running buffer, while the remaining doses were applied for 15 s with a 116 s wash. Dose-response data were obtained for ≥ 8 agonist concentrations on ≥ 6 cells. All EC_{50} and Hill coefficient values were obtained by fitting dose-response relations to the Hill equation and are reported as averages \pm standard error of the fit. A detailed error analysis of nonsense suppression experiments reveals data are reproducible in EC_{50} to $\pm 50\%$.⁴⁷ The stoichiometry of each mutant was verified by voltage jump experiments as described previously.¹⁴

Preparation of epibatidine and *N*-methyl enantiomers. 40 mg of (\pm)-epibatidine (Tocris) was separated by chiral HPLC using an Astec ChirobioticT column analytical column (Sigma Aldrich) with a 1.5 mL flow rate and 0.6% TEA and 0.4% AcOH in methanol as the mobile phase. Two fractions were collected with enantiomeric excess values of $>99\%$. The fractions were concentrated to a 10 mL volume and 15 mL of 2M NaOH was added. The organic layer was extracted with CH_2Cl_2 (4 \times) and concentrated to afford pale yellow powders. Fraction 1 ((+)-epibatidine): $[\alpha]_{\text{D}}^{20} = +7.0^\circ$ ($c = 1$, CHCl_3). Fraction 2 ((-)-epibatidine): $[\alpha]_{\text{D}}^{20} = -6.5^\circ$ ($c = 1$, CHCl_3). NMR spectra before and after separation were identical and are consistent with previously reported data.⁴⁸

To prepare the *N*-methyl derivatives, 10 mg of each enantiomer (0.048 mmol) was added to a separate two-neck, 25 mL round-bottom flask equipped with a reflux

condenser. To this was added 3 mL of formic acid and 1.5 mL of 37 wt% formaldehyde (in H₂O). The mixture was stirred and heated to reflux at 80 °C for 7 hrs. The solution was cooled to room temperature and made basic (pH 12) by the addition of 2M NaOH. The organics were extracted with CH₂Cl₂ (3×), washed with brine, dried over Na₂SO₄ and concentrated. The resulting oil was purified by flash column chromatography on silica gel (7% methanol in CH₂Cl₂). $R_f = 0.34$. NMR spectra are consistent with previously reported data.⁴² Yield of (+)-*N*-methyl epibatidine: >90%, 10 mg. $[\alpha]_D^{20} = +120^\circ$ (c = 1, CHCl₃). Yield of (–)-*N*-methyl epibatidine: >90%, 10 mg. $[\alpha]_D^{20} = -120^\circ$ (c = 1, CHCl₃).

4.6 ACKNOWLEDGEMENTS

We thank Dr. Scott Virgil for his assistance in the HPLC separation of epibatidine enantiomers.

4.7 REFERENCES

1. Karlin, A., Emerging structure of the nicotinic acetylcholine receptors. *Nat. Rev. Neurosci.* **2002**, 3, (2), 102-14.
2. Grutter, T.; Changeux, J. P., Nicotinic receptors in wonderland. *Trends Biochem. Sci.* **2001**, 26, (8), 459-63.
3. Corringer, P. J.; Le Novere, N.; Changeux, J. P., Nicotinic receptors at the amino acid level. *Annu. Rev. Pharmacol. Toxicol.* **2000**, 40, 431-58.
4. Jensen, A. A.; Frolund, B.; Liljefors, T.; Krogsgaard-Larsen, P., Neuronal nicotinic acetylcholine receptors: structural revelations, target identifications, and therapeutic inspirations. *J. Med. Chem.* **2005**, 48, (15), 4705-45.
5. Romanelli, M. N.; Gratterer, P.; Guandalini, L.; Martini, E.; Bonaccini, C.; Gualtieri, F., Central nicotinic receptors: structure, function, ligands, and therapeutic potential. *ChemMedChem* **2007**, 2, (6), 746-67.
6. Gotti, C.; Zoli, M.; Clementi, F., Brain nicotinic acetylcholine receptors: native subtypes and their relevance. *Trends Pharmacol. Sci.* **2006**, 27, (9), 482-91.
7. Coe, J. W.; Brooks, P. R.; Vetelino, M. G.; Wirtz, M. C.; Arnold, E. P.; Huang, J.; Sands, S. B.; Davis, T. I.; Lebel, L. A.; Fox, C. B.; Shrikhande, A.; Heym, J. H.; Schaeffer, E.; Rollema, H.; Lu, Y.; Mansbach, R. S.; Chambers, L. K.; Rovetti, C. C.; Schulz, D. W.; Tingley, F. D.; O'Neill, B. T., Varenicline: An $\alpha 4 \beta 2$ nicotinic receptor partial agonist for smoking cessation. *J. Med. Chem.* **2005**, 48, (10), 3474-3477.
8. Mansvelder, H. D.; Keath, J. R.; McGehee, D. S., Synaptic mechanisms underlie nicotine-induced excitability of brain reward areas. *Neuron* **2002**, 33, (6), 905-19.
9. Nashmi, R.; Xiao, C.; Deshpande, P.; McKinney, S.; Grady, S. R.; Whiteaker, P.; Huang, Q.; McClure-Begley, T.; Lindstrom, J. M.; Labarca, C.; Collins, A. C.; Marks, M. J.; Lester, H. A., Chronic nicotine cell specifically upregulates functional $\alpha 4$ nicotinic receptors: basis for both tolerance in midbrain and enhanced long-term potentiation in perforant path. *J. Neurosci.* **2007**, 27, (31), 8202-18.
10. Tapper, A.; McKinney, S.; Nashmi, R.; Schwarz, J.; Deshpande, P.; Labarca, C.; Whiteaker, P.; Collins, A.; Lester, H., Nicotine activation of $\alpha 4$ receptors: sufficient for reward, tolerance and sensitization. *Science* **2004**, 306, 1029-1032.
11. Beers, W. H.; Reich, E., Structure and activity of acetylcholine. *Nature* **1970**, 228, (5275), 917-22.
12. Glennon, R. A.; Dukat, M.; Liao, L., Musings on $\alpha 4 \beta 2$ nicotinic acetylcholine (nACh) receptor pharmacophore models. *Curr. Top. Med. Chem.* **2004**, 4, (6), 631-44.
13. Zhong, W.; Gallivan, J. P.; Zhang, Y.; Li, L.; Lester, H. A.; Dougherty, D. A., From *ab initio* quantum mechanics to molecular neurobiology: a cation- π binding site in the nicotinic receptor. *Proc. Natl. Acad. Sci. USA* **1998**, 95, (21), 12088-93.
14. Xiu, X.; Puskar, N. L.; Shanata, J. A.; Lester, H. A.; Dougherty, D. A., Nicotine binding to brain receptors requires a strong cation- π interaction. *Nature* **2009**, 458, (7237), 534-7.
15. Blum, A. P.; Gleitsman, K. R.; Lester, H. A.; Dougherty, D. A., Evidence for an extended hydrogen bond network in the binding site of the nicotinic receptor:

- concerning the role of the vicinal disulfide of the $\alpha 1$ subunit. *J. Biol. Chem.* **2011**. *In press*.
16. Cashin, A. L.; Petersson, E. J.; Lester, H. A.; Dougherty, D. A., Using physical chemistry to differentiate nicotinic from cholinergic agonists at the nicotinic acetylcholine receptor. *J. Am. Chem. Soc.* **2005**, 127, (1), 350-356.
 17. Celie, P.; van Rossum-Fikkert, S.; Van Dyke, W.; Brejc, K.; Smit, A.; Sixma, T., Nicotine and carbamylcholine binding to nicotinic acetylcholine receptors as studied in AChBP crystal structures. *Neuron* **2004**, 41, 907-914.
 18. Hansen, S. B.; Sulzenbacher, G.; Huxford, T.; Marchot, P.; Bourne, Y.; Taylor, P., Structural characterization of agonist and antagonist-bound acetylcholine-binding protein from *Aplysia californica*. *J. Mol. Neurosci.* **2006**, 30, (1-2), 101-2.
 19. Brejc, K.; van Dijk, W. J.; Klaassen, R. V.; Schuurmans, M.; van Der Oost, J.; Smit, A. B.; Sixma, T. K., Crystal structure of an ACh-binding protein reveals the ligand-binding domain of nicotinic receptors. *Nature* **2001**, 411, (6835), 269-76.
 20. Hansen, S. B.; Sulzenbacher, G.; Huxford, T.; Marchot, P.; Taylor, P.; Bourne, Y., Structures of *Aplysia* AChBP complexes with nicotinic agonists and antagonists reveal distinctive binding interfaces and conformations. *EMBO J.* **2005**, 24, (20), 3635-46.
 21. Rucktooa, P.; Smit, A. B.; Sixma, T. K., Insight in nAChR subtype selectivity from AChBP crystal structures. *Biochem. Pharmacol.* **2009**, 78, (7), 777-87.
 22. Taylor, P.; Talley, T. T.; Radic, Z.; Hansen, S. B.; Hibbs, R. E.; Shi, J., Structure-guided drug design: conferring selectivity among neuronal nicotinic receptor and acetylcholine-binding protein subtypes. *Biochem. Pharmacol.* **2007**, 74, (8), 1164-71.
 23. Daly, J. W., Nicotinic agonists, antagonists, and modulators from natural sources. *Cell. Mol. Neurobiol.* **2005**, 25, (3-4), 513-52.
 24. Glennon, R. A.; Dukat, M., Nicotine receptor ligands. *Med. Chem. Res.* **1996**, 6, (7-8), 465-486.
 25. Holladay, M. W.; Lebold, S. A.; Lin, N.-H., Structure – activity relationships of nicotinic acetylcholine receptor agonists as potential treatments for dementia. *Drug Dev. Res.* **1995**, 35, (4), 191-213.
 26. Tønder, J. E.; Olesen, P. H.; Hansen, J. B.; Begtrup, M.; Pettersson, I., An improved nicotinic pharmacophore and a stereoselective CoMFA-model for nicotinic agonists acting at the central nicotinic acetylcholine receptors labelled by [3H]-N-methylcarbamylcholine. *Journal of Computer-Aided Molecular Design* **2001**, 15, (3), 247-258.
 27. Bertrand, S.; Patt, J. T.; Spang, J. E.; Westera, G.; Schubiger, P. A.; Bertrand, D., Neuronal nAChR stereoselectivity to non-natural epibatidine derivatives. *FEBS Lett.* **1999**, 450, (3), 273-9.
 28. Moroni, M.; Zwart, R.; Sher, E.; Cassels, B. K.; Bermudez, I., Alpha4Beta2 nicotinic receptors with high and low acetylcholine sensitivity: pharmacology, stoichiometry, and sensitivity to long-term exposure to nicotine. *Mol. Pharmacol.* **2006**, 70, (2), 755-68.
 29. Koh, J. T.; Cornish, V. W.; Schultz, P. G., An experimental approach to evaluating the role of backbone interactions in proteins using unnatural amino acid mutagenesis. *Biochemistry* **1997**, 36, 11314-11322.

30. England, P. M.; Zhang, Y. N.; Dougherty, D. A.; Lester, H. A., Backbone mutations in transmembrane domains of a ligand-gated ion channel: Implications for the mechanism of gating. *Cell* **1999**, 96, (1), 89-98.
31. Deechongkit, S.; Dawson, P. E.; Kelly, J. W., Toward assessing the position-dependent contributions of backbone hydrogen bonding to beta-sheet folding thermodynamics employing amide-to-ester perturbations. *J. Am. Chem. Soc.* **2004**, 126, (51), 16762-71.
32. Deechongkit, S.; Nguyen, H.; Powers, E. T.; Dawson, P. E.; Gruebele, M.; Kelly, J. W., Context-dependent contributions of backbone hydrogen bonding to beta-sheet folding energetics. *Nature* **2004**, 430, (6995), 101-5.
33. Ma, J. C.; Dougherty, D. A., The cation- π interaction. *Chem. Rev.* **1997**, 97, (5), 1303-1324.
34. Zacharias, N.; Dougherty, D. A., Cation- π interactions in ligand recognition and catalysis. *Trends Pharmacol. Sci.* **2002**, 23, (6), 281-7.
35. Dougherty, D. A., Physical organic chemistry on the brain. *J. Org. Chem.* **2008**, 73, (10), 3667-3673.
36. Tomaselli, G. F.; McLaughlin, J. T.; Jurman, M. E.; Hawrot, E.; Yellen, G., Mutations affecting agonist sensitivity of the nicotinic acetylcholine receptor. *Biophys. J.* **1991**, 60, 721-727.
37. O'Leary, M. E.; White, M. M., Mutational analysis of ligand-induced activation of the *Torpedo* acetylcholine receptor. *J. Biol. Chem.* **1992**, 267, (12), 8360-5.
38. O'Leary, M. E.; Filatov, G. N.; White, M. M., Characterization of *d*-tubocurarine binding site of *Torpedo* acetylcholine receptor. *Am. J. Physiol.* **1994**, 266, (3Pt1), C648-C653.
39. Galzi, J. L.; Bertrand, D.; Devillers-Thiery, A.; Revah, F.; Bertrand, S.; Changeux, J. P., Functional significance of aromatic amino acids from three peptide loops of the $\alpha 7$ neuronal nicotinic receptor site investigated by site-directed mutagenesis. *FEBS Lett.* **1991**, 294, (3), 198-202.
40. Aylwin, M. L.; White, M. M., Gating properties of mutant acetylcholine-receptors. *Mol. Pharmacol.* **1994**, 46, (6), 1149-1155.
41. Spande, T. F.; Garraffo, H. M.; Edwards, M. W.; Yeh, H. J. C.; Pannell, L.; Daly, J. W., Epibatidine: a novel (chloropyridyl)azabicycloheptane with potent analgesic activity from an Ecuadoran poison frog. *J. Am. Chem. Soc.* **1992**, 114, (9), 3475-3478.
42. Horti, A. G.; Scheffel, U.; Kimes, A. S.; Musachio, J. L.; Ravert, H. T.; Mathews, W. B.; Zhan, Y.; Finley, P. A.; London, E. D.; Dannals, R. F., Synthesis and evaluation of *N*-[11C]methylated analogues of epibatidine as tracers for positron emission tomographic studies of nicotinic acetylcholine receptors. *J. Med. Chem.* **1998**, 41, (22), 4199-206.
43. London, E. D.; Scheffel, U.; Kimes, A. S.; Kellar, K. J., In vivo labeling of nicotinic acetylcholine receptors in brain with [3H]epibatidine. *Eur. J. Pharmacol.* **1995**, 278, (1), R1-2.
44. Carroll, F. I.; Liang, F.; Navarro, H. A.; Brieady, L. E.; Abraham, P.; Damaj, M. I.; Martin, B. R., Synthesis, nicotinic acetylcholine receptor binding, and antinociceptive properties of 2-exo-2-(2'-substituted 5'-pyridinyl)-7-

- azabicyclo[2.2.1]heptanes. Epibatidine analogues. *J. Med. Chem.* **2001**, 44, (13), 2229-37.
45. Nowak, M. W.; Gallivan, J. P.; Silverman, S. K.; Labarca, C. G.; Dougherty, D. A.; Lester, H. A., *In vivo* incorporation of unnatural amino acids into ion channels in a *Xenopus* oocyte expression system. *Methods Enzymol.* **1998**, 293, 504-529.
46. Fonck, C.; Cohen, B. N.; Nashmi, R.; Whiteaker, P.; Wagenaar, D. A.; Rodrigues-Pinguet, N.; Deshpande, P.; McKinney, S.; Kwoh, S.; Munoz, J.; Labarca, C.; Collins, A. C.; Marks, M. J.; Lester, H. A., Novel seizure phenotype and sleep disruptions in knock-in mice with hypersensitive alpha4 nicotinic receptors. *J. Neurosci.* **2005**, 25, (49), 11396-411.
47. Torrice, M. M., Chemical-scale studies of the nicotinic and muscarinic acetylcholine receptors. Ph.D. Thesis. California Institute of Technology, Pasadena, CA, **2009**.
48. Armstrong, A.; Bhonoah, Y.; Shanahan, S. E., Aza-Prins-pinacol approach to 7-azabicyclo[2.2.1]heptanes: syntheses of (\pm)-epibatidine and (\pm)-epiboxidine. *J. Org. Chem.* **2007**, 72, (21), 8019-24.

CHAPTER 5: Evidence for an Extended Hydrogen Bond Network in the Binding Site of the Nicotinic Receptor: Concerning the Role of the Vicinal Disulfide of the $\alpha 1$ Subunit*

5.1 ABSTRACT

The defining feature of the α subunits of the family of nicotinic acetylcholine receptors is a vicinal disulfide between C192 and C193. While this structure has played a pivotal role in a number of pioneering studies of nicotinic receptors, its functional role in native receptors remains uncertain. Using mutant cycle analysis and unnatural residue mutagenesis, including backbone mutagenesis of the peptide bond of the vicinal disulfide, we have established the presence of a network of hydrogen bonds that extends from that peptide NH, across a β turn to another backbone hydrogen bond, and then across the subunit interface to the side chain of a functionally important Asp residue in the non- α subunit. We propose that the role of the vicinal disulfide is to distort the β turn and thereby properly position a backbone NH for intersubunit hydrogen bonding to the key Asp.

5.2 INTRODUCTION

Nicotinic acetylcholine receptors (nAChRs) are neurotransmitter-gated ion channels that mediate rapid synaptic transmission throughout the central and peripheral nervous

* This work was done in collaboration with Kristin Rule Gleitsman and is adapted from: Blum, A. P.; Gleitsman, K. R.; Lester, H. A.; Dougherty, D. A., Evidence for an extended hydrogen bond network in the binding site of the nicotinic receptor: concerning the role of the vicinal disulfide of the $\alpha 1$ subunit. *The Journal of Biological Chemistry* **2011**, 286, (37), 32251-58. Copyright 2011 by the American Society for Biochemistry and Molecular Biology, Inc.

systems.¹⁻³ The nAChR family members are also the prototypes of a large class of channels termed Cys-loop (or pentameric) receptors, which are essential for learning, memory, and sensory perception, and are implicated in numerous neurological disorders, including Alzheimer's disease, Parkinson's disease, and schizophrenia.^{4, 5} Of the seventeen genes that code for subunits of the nAChR, ten produce α subunits. The α subunits of nAChRs typically contain the principal component of the agonist binding site and are distinguished by a unique vicinal disulfide at the agonist binding site formed by residues canonically labeled as C192 and C193. As shown in **Figure 5.1**, the vicinal disulfide produces an eight-membered ring that contains an amide and a disulfide, two functionalities with distinct conformational properties.

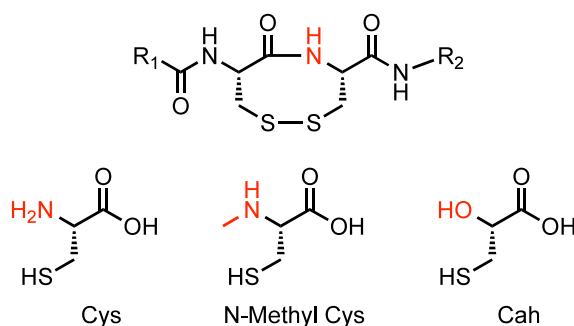


Figure 5.1. Vicinal disulfide structure. For model calculations of $\text{CH}_3\text{CO}-[\text{Cys-Cys}]-\text{NH}_2$, $\text{R}_1 = \text{CH}_3$ and $\text{R}_2 = \text{H}$. Also shown are the unnatural amino acids (*N*-Methyl Cys and α -hydroxy cysteine, Cah) used in this study.

In the 1960s, reduction of this disulfide in the *Electrophorus* electroplax led to the realization that the nAChR, long defined as controlling the membrane's ion conductance, is a protein.⁶⁻⁸ That this disulfide can be more easily reduced than a typical protein disulfide was later rationalized by the finding that the disulfide is vicinal and therefore embedded in a strained ring.^{9, 10} The vicinal disulfide has been included and discussed in

many classic studies in early nAChR research owing to its susceptibility to reduction, and proximity to the agonist binding site.^{6, 7, 11-16}

Nevertheless, the precise role of the vicinal disulfide in nAChR function is not established. Early studies¹⁷ seemed to indicate that reduction of this disulfide rendered the receptor non-functional (but see below). Computational, NMR, and crystallographic studies of model vicinal disulfides have probed the multiple conformational possibilities of this unique structural unit.¹⁸⁻²² The *trans* conformation that is overwhelmingly preferred for backbone amides is expected to be disfavored in the context of an eight-membered ring, allowing for an energetically accessible *cis* backbone conformation. Also, a *gauche* conformation is strongly preferred about the S-S disulfide bond (C-S-S-C dihedral angle $\sim 90^\circ$). In the context of the ring formed by the vicinal disulfide, the *gauche*(+) and *gauche*(-) forms produce energetically distinct (diastereomeric) structures. The combined backbone and disulfide conformational combinations give rise to four distinct conformers for the vicinal disulfide ring.

While the sulfurs of the disulfide can contact small molecules that bind to the acetylcholine binding protein (AChBP),^{23, 24} a very useful model of the nAChR binding site, any noncovalent interactions of this sort are expected to be quite weak. Instead, we and others have speculated on a role in receptor gating involving *cis-trans* isomerization of the amide and/or *gauche*(+)/*gauche*(-) interconversion of the disulfide.^{10, 18, 19, 21, 22} Conventional mutagenesis studies are expected to produce severely impaired receptors, and so it has been challenging to design unambiguous probes of disulfide function.

Here we use subtle structural variations enabled by unnatural amino acid mutagenesis to evaluate the possible functional role of the vicinal disulfide of nAChR α

subunits. We find evidence that the vicinal disulfide contributes to an interesting triad of residues that forms a network of hydrogen bonds that spans the interface between two subunits and impacts receptor function.

5.3 RESULTS

5.3.1 Conformational Analysis and Experimental Design

As noted above, both the disulfide and the amide functionalities have two distinct conformations. In the computational studies described below the *gauche*(+) and *gauche*(-) forms of the disulfide are very similar in energy, and seem unlikely to play a strong discriminating role. Our work has emphasized the *gauche*(-), as this is the conformation seen in AChBP crystal structures.

For the amide unit, the issue is *cis-trans* isomerization. In a typical protein a backbone amide shows a strong preference for the *trans* conformation (if proline is not involved). However, incorporation into an eight-membered ring is expected to favor the *cis* form. This expectation derives from studies of the conformational preferences of small molecules. For example, in cyclooctene the *trans* form is substantially strained, and the *cis* form is preferred. *Ab initio* calculations we have performed show that an amide in an eight-membered alkane ring also shows a preference for *cis*; at the HF-6-31G** level of theory, *N*-methylacetamide shows a 2.5 kcal/mol preference for *trans*, while the cyclic amide shows a 5.4 kcal/mol preference for *cis*.

More sophisticated calculations at the B3LYP/6-311++G(d,p) level of theory on a model tripeptide ($\text{CH}_3\text{CO}-[\text{Cys-Cys}]-\text{NH}_2$, **Figure 5.1**) for the nAChR vicinal disulfide likewise show an energetic preference for the *cis* amide, by 3.4 kcal/mol. This is not a large energy difference, and, indeed, both *cis* and *trans* forms have been seen in crystal

structures of molecules that contain a vicinal disulfide.^{25, 26} We and others have for some time speculated that perhaps *cis-trans* isomerization of the C192-C193 backbone may play a role in gating of nAChRs. This structural change could then easily be imagined to propagate along the protein backbone and perhaps initiate the “conformational wave”²⁷ that leads to gating.

To test this model, we sought modifications to the vicinal disulfide that would alter the innate *cis-trans* bias of the system. For example, it is well known²⁸ that esters have a stronger *trans* preference than amides; methyl acetate prefers *trans* by 8.0 kcal/mol compared to the 2.5 kcal/mol noted for *N*-methylacetamide above. It is also well established that *N*-methylation reduces the innate *trans* preference of a backbone amide in peptides and proteins.^{29, 30} Thus, we considered the strategy of modifying the amide linkage of the vicinal disulfide. If *cis-trans* isomerization of this unit plays a role in receptor function, then the ester and *N*-methyl modifications should have opposite effects.

To test this prediction *in silico*, we performed comparable B3LYP/6-311++G(d,p) calculations on the ester and *N*-methyl amide analogs of the vicinal disulfide model discussed above. The results are consistent with expectation based on the conformational preferences of small molecules discussed above. Compared to the natural backbone (an amide), which favors the *cis* by 3.4 kcal/mol, the ester favors the *trans* by 1.4 kcal/mol. *N*-methylation increases the *cis* preference of the parent (the amide backbone) to 9.3 kcal/mol, consistent with experimental studies on a similar system reported by Hondal.²²

It is difficult to apply these data to nAChR function in a quantitative way; calculations were performed on model tripeptides and depsipeptides in the gas phase, not

on a ~2.5MDa pentameric, polytropic receptor protein in a cell membrane. However, the predictions of the calculations are clear. If *cis-trans* isomerization of the vicinal disulfide amide is functionally important, the two modifications considered – backbone ester incorporation and amide *N*-methylation – should have opposite effects on receptor function.

Both modifications can be site-specifically introduced into the nAChR using the *in vivo* nonsense suppression methodology that has been developed in our labs over the past 20 years.^{31, 32} We thus set out to prepare and characterize the appropriate mutant receptors as a test of the computational modeling.

5.3.2 Mutagenesis Studies

Initial control experiments involving the vicinal disulfide clarified the effect of eliminating this structure. We found that we could introduce Ala or Ser at C192 or C193 of the wild-type muscle subtype receptor and obtain functional receptors. The EC₅₀ value shifts ~8–40 fold (**Table 5.1**), and current sizes comparable to those for the wild-type receptor are seen. We repeated these studies in three other subtypes of the nAChR – the neuronal receptors $\alpha 4\beta 2$, $\alpha 4\beta 4$ and $\alpha 7$ – and saw similar effects, but with generally larger shifts in EC₅₀ (~20 to 200-fold, **Table 5.2**).

Table 5.1. EC₅₀, Hill coefficient (\pm standard error of the mean) and ΔG° values for mutations made to $\alpha 1_2\beta 1\gamma\delta$.

Mutation	EC ₅₀ (μ M)	Hill	ΔG° (kcal/mol)
$\alpha 1\beta 1\gamma\delta$	18 \pm 0.2	1.4 \pm 0.01	-
$\alpha 1(\text{C192A})\beta 1\gamma\delta$	660 \pm 20	1.3 \pm 0.05	2.1
$\alpha 1(\text{C192S})\beta 1\gamma\delta$	520 \pm 20	1.5 \pm 0.08	2.0
$\alpha 1(\text{C193A})\beta 1\gamma\delta$	140 \pm 3	1.2 \pm 0.02	1.2
$\alpha 1(\text{C193S})\beta 1\gamma\delta$	150 \pm 7	1.4 \pm 0.07	1.3
$\alpha 1\beta 1(\text{L9'S})\gamma\delta$	0.61 \pm 0.04	1.4 \pm 0.1	-
$\alpha 1(\text{S191A})\beta 1(\text{L9'S})\gamma\delta$	0.31 \pm 0.02	1.1 \pm 0.05	-
$\alpha 1(\text{S191A/C193A})\beta 1(\text{L9'S})\gamma\delta$	5.2 \pm 0.4	1.0 \pm 0.07	1.7
$\alpha 1(\text{S191A/C193S})\beta 1(\text{L9'S})\gamma\delta$	9.5 \pm 0.7	0.96 \pm 0.06	2.0
$\alpha 1(\text{S191A/C193Cah})\beta 1(\text{L9'S})\gamma\delta$	49 \pm 4	0.80 \pm 0.03	3.0
$\alpha 1(\text{S191A/C193N-Me-Cys})\beta 1(\text{L9'S})\gamma\delta$	39 \pm 2	0.88 \pm 0.04	2.9
$\alpha 1(\text{S191Aah})\beta 1(\text{L9'S})\gamma\delta$	31 \pm 3	1.1 \pm 0.09	2.7
$\alpha 1(\text{S191A})\beta 1(\text{L9'S})\gamma(\text{D174N})\delta(\text{D180N})$	160 \pm 7	1.3 \pm 0.06	3.7

Table 5.2. EC₅₀, Hill coefficient (\pm standard error of the mean) and ΔG° values for each mutation made to the vicinal disulfide in neuronal receptors, $\alpha 4\beta 4$, $\alpha 7$ and $\alpha 4\beta 2$. n.d. = value not determined due to low current sizes for the indicated mutations. The stoichiometry of the $\alpha 4\beta 2$ ($\alpha 4_2\beta 2_3$) protein was verified as described previously.³³ The stoichiometry of $\alpha 4\beta 4$ is assumed to be $\alpha 4_2\beta 4_3$ based on injection ratios of each subunit as discussed elsewhere.³⁴

Mutation	EC ₅₀ (μ M)	Hill	ΔG° (kcal/mol)
human $\alpha 4\beta 4$			
$\alpha 4\beta 4$	15 \pm 2	1.2 \pm 0.1	-
$\alpha 4(\text{C197A})\beta 4$	180 \pm 6	1.5 \pm 0.05	1.5
$\alpha 4(\text{C197S})\beta 4$	n.d.	-	-
$\alpha 4(\text{C198A})\beta 4$	160 \pm 10	1.3 \pm 0.1	1.4
$\alpha 4(\text{C198S})\beta 4$	280 \pm 10	1.7 \pm 0.1	1.7
rat $\alpha 7(\text{T6'S})$			
$\alpha 7(\text{T6'S})$	94 \pm 2	2.2 \pm 0.1	-
$\alpha 7(\text{T6'S/C189A})$	7300 \pm 600	2.1 \pm 0.3	2.6
$\alpha 7(\text{T6'S/C189S})$	n.d.	-	-
$\alpha 7(\text{T6'S/C190A})$	4100 \pm 300	2.3 \pm 0.3	2.2
$\alpha 7(\text{T6'S/C190S})$	n.d.	-	-
rat $\alpha 4(\text{L9'A})_2\beta 2_3$			
$\alpha 4(\text{L9'A})\beta 2$	0.36 \pm 0.02	1.3 \pm 0.07	-
$\alpha 4(\text{L9'A/C197A})\beta 2$	80 \pm 10	0.87 \pm 0.07	3.2
$\alpha 4(\text{L9'A/C197S})\beta 2$	69 \pm 10	0.91 \pm 0.1	3.1
$\alpha 4(\text{L9'A/C198A})\beta 2$	47 \pm 4	1.1 \pm 0.09	2.9
$\alpha 4(\text{L9'A/C198S})\beta 2$	84 \pm 10	1.1 \pm 0.1	3.2

In 1985, Mishina *et al.* reported that C192S and C193S mutants of *Torpedo* nAChR, a close paralog of the muscle nAChR, were unresponsive to high concentrations of ACh, but did bind α -bungarotoxin.¹⁷ These findings suggested that mutation of either residue results in a receptor that is properly folded, but does not function. However, our

present finding that the nAChR can be activated even in the presence of mutated 192 and 193 side chains indicates that the vicinal disulfide linkage increases the efficiency of receptor function, but is not absolutely required.

In these studies we are reporting EC_{50} values, a functional measure that includes contributions from both ligand binding and receptor gating. For the residues emphasized here, there is no evidence that C192 and C193 interact strongly and directly with agonists, and so we anticipate that mutations primarily impact receptor gating, although we cannot prove that unambiguously. In upcoming discussion, we will be describing the results of mutant cycle analysis studies. It is standard practice in that field to convert coupling interactions (nonadditivity) to free energies ($\Delta\Delta G^\circ$).^{35, 36} In view of this, and solely for the purpose of discussion, we will put all changes in EC_{50} values on a similar energy scale: $\Delta G^\circ = RT\ln[EC_{50}(\text{mutant})/EC_{50}(\text{wild type})]$.

Before launching detailed nonsense suppression experiments with *N*-methyl Cys and Cah (cysteine, α -hydroxy), we considered several conditions and nAChR subtypes, including the muscle receptor $\alpha 1_2\beta 1\gamma\delta$ and the neuronal subtypes $\alpha 4\beta 2$, $\alpha 4\beta 4$ and $\alpha 7$. We chose to focus on the muscle subtype for the following reasons. The muscle subtype is, in general, the most studied nAChR, and it is also the receptor that gave the highest currents for nonsense suppression experiments with *N*-methyl Cys and Cah. In addition, it has a defined stoichiometry, a substantial advantage over the $\alpha 4\beta 2$ and $\alpha 4\beta 4$ receptors (which each have two possible subunit stoichiometries). It also required considerably lower agonist concentrations than those needed for experiments with $\alpha 7$.

For our nonsense suppression experiments in $\alpha 1_2\beta 1\gamma\delta$, we used the well-documented leucine to serine mutation at the 9' position in the M2 region of nAChR.

This mutation renders the nAChR ~40-times more sensitive to agonists, as judged by the decrease in EC_{50} .^{37, 38} The 9' position lies some 60 Å from the agonist binding site and from the vicinal disulfide studied here, and therefore it does not directly affect the C192-C193 region, but instead affects receptor gating. This change favors the open state of the channel once an agonist molecule has bound, also increasing the efficacy of some agonists.

We also introduced a mutation in the $\alpha 1$ subunit, S191A, of all mutant proteins used in double mutant cycle analyses as this mutant promoted more reliable current sizes for nonsense suppression experiments with α -hydroxy acids at position 191, experiments that will be discussed in greater detail below. We showed previously³⁹ that the S191A mutation has a minor effect on receptor function (see also **Table 5.1**) and that the incorporation of Aah (alanine, α -hydroxy) or Sah (serine, α -hydroxy) at S191 results in the same EC_{50} shift.

In the crucial experiments involving alteration of the backbone of the C192-C192 unit, we find that replacement of C193, whose backbone is within the eight-membered ring formed by the vicinal disulfide, with either *N*-methyl Cys or Cah produces *similar* results. Both mutations are loss-of-function, and their impacts are comparable in magnitude, with a ΔG° value of ~3 kcal/mol. These are relatively large effects for such subtle mutations (larger than the Cys-to-Ala mutations), suggesting an important functional role for the backbone of C193. These results are not consistent with a functional role for *cis-trans* isomerization, which predicts opposite effects for the two modifications.

While differing in their anticipated impact on *cis-trans* isomerization, the two backbone mutations are similar in another regard: both ablate the hydrogen bond-donating ability associated with the NH of the parent amide. An inspection of AChBP structures reveals a potential acceptor for such a hydrogen bond donor: the carbonyl of residue Y190, a conserved member of the agonist binding site. This hydrogen bond is generally present in AChBP structures, and it defines a distorted Type I β turn, with Y190, S191, C192, and C193 being residues i to $i+3$, respectively (**Figure 5.2**).

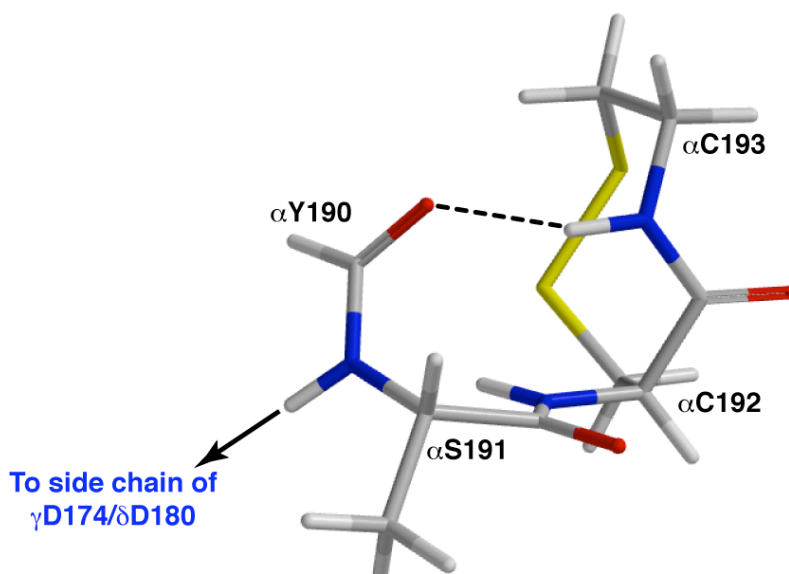


Figure 5.2. The β turn found in AChBP structures. Structure is from pdb file 1UV6²⁴ and was modified to contain an Ala at S191.²⁴ The side chain of Tyr190 is truncated (replaced with a hydrogen) for simplicity.

The inclusion of S191 in the β turn suggested a more complex interaction than just a simple hydrogen bond. Previous work from our labs³⁹ strongly supported a model in which the backbone NH of S191 makes an *intersubunit* hydrogen bond to the side chain of a critical Asp in the γ/δ subunits (γ D174/ δ D180; δ D174 is in the δ sequence WIIIDPEGF and γ D180 is in the γ sequence WIFIDPEAF). This hydrogen bond contributes to ion channel gating. In that study, we removed the critical NH by preparing

the mutant S191Sah or S191Aah, producing one of the largest perturbations ever observed in our labs for the introduction of a backbone ester. A double mutant cycle analysis combining S191Sah and γ D174N/ δ D180N provided strong functional evidence for an interaction, with a coupling energy $\Delta\Delta G^\circ = 2.7$ kcal/mol. However, many studies have shown that a backbone ester mutation not only removes a backbone NH that can donate a hydrogen bond, it also weakens the hydrogen bond-accepting ability of the associated *i-1* carbonyl.⁴⁰⁻⁴⁵ For S191 the *i-1* carbonyl comes from Y190, the carbonyl implicated in the hydrogen bond of the β turn discussed above. Could the S191Sah effect be so large because it both deletes the hydrogen bond to γ D174/ δ D180 and weakens an important β turn hydrogen bond?

We have now found support for the β turn hydrogen bond. A mutant cycle analysis (**Figure 5.3A**) combining S191Aah and C193(*N*-methyl Cys) shows a strong coupling energy, with $\Delta\Delta G^\circ = 2.7$ kcal/mol (**Table 5.3**). This finding supports the existence of a novel, 3-residue, hydrogen bond network, in which the NH of C193 hydrogen bonds to the carbonyl of the peptide bond between Y190 and S191. In addition, the NH of the Y190-S191 peptide bond hydrogen bonds to the side chain of γ D174/ δ D180 (**Figure 5.3**).

Table 5.3. EC₅₀, Hill coefficient (\pm standard error of the mean) and $\Delta\Delta G^\circ$ values for double mutations made to $\alpha 1_2\beta 1\gamma\delta$.

Double Mutation	EC ₅₀ (μ M)	Hill	$\Delta\Delta G^\circ$ (kcal/mol)
$\alpha 1$ (S191Aah/C193A) $\beta 1$ (L9'S) $\gamma\delta$	97 \pm 10	0.76 \pm 0.04	0.99
$\alpha 1$ (S191Aah/C193S) $\beta 1$ (L9'S) $\gamma\delta$	100 \pm 7	0.93 \pm 0.05	1.3
$\alpha 1$ (S191Aah/C193 <i>N</i> -Me-Cys) $\beta 1$ (L9'S) $\gamma\delta$	39 \pm 4	0.70 \pm 0.03	2.7
$\alpha 1$ (S191Aah) $\beta 1$ (L9'S) γ (D174N) δ (D180N)	140 \pm 10	1.7 \pm 0.2	2.8
$\alpha 1$ (S191A/C193A) $\beta 1$ (L9'S) γ (D174N) δ (D180N)	600 \pm 20	1.5 \pm 0.07	0.8
$\alpha 1$ (S191A/C193S) $\beta 1$ (L9'S) γ (D174N) δ (D180N)	780 \pm 20	1.6 \pm 0.06	1.1
$\alpha 1$ (S191A/C193Cah) $\beta 1$ (L9'S) γ (D174N) δ (D180N)	800 \pm 40	1.5 \pm 0.05	2
$\alpha 1$ (S191A/C193 <i>N</i> -Me-Cys) $\beta 1$ (L9'S) γ (D174N) δ (D180N)	500 \pm 20	1.5 \pm 0.07	2.2

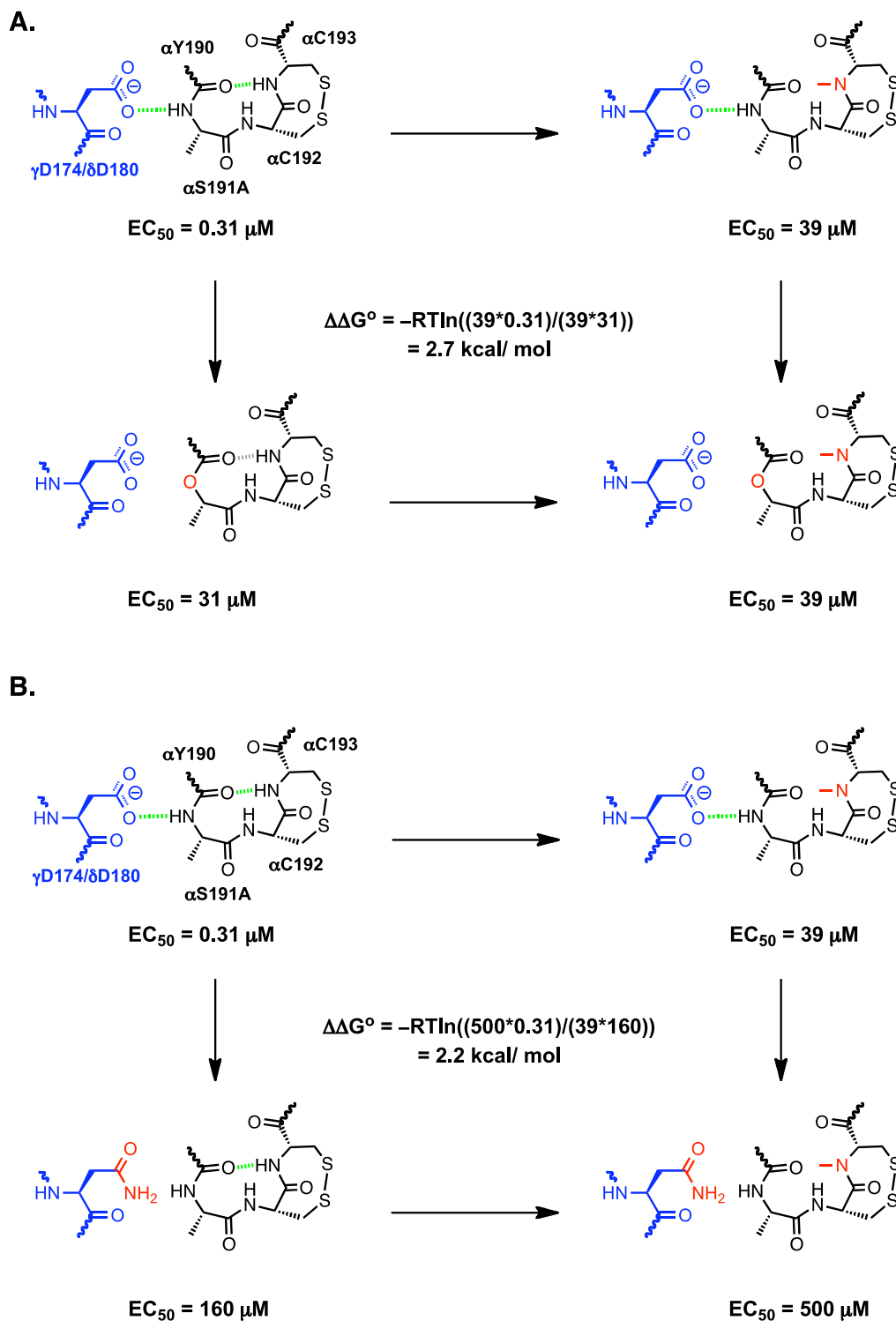


Figure 5.3. Double mutant cycle analyses. (A) Coupling between backbone mutations at $\alpha S191$ and $\alpha C193$. Note that introduction of the α -hydroxy acid at S191 attenuates the hydrogen bond acceptor for the hydrogen bond with C193 and removes the hydrogen bond donor for the hydrogen bond to $\gamma D174/\delta D180$. (B) Long-range coupling between a backbone mutation at $\alpha S191$ and a side chain mutation at $\gamma D174/\delta D180$.

If this hydrogen bonding network exists, energetic coupling between the NH of C193 and the side chain of γ D174/ δ D180 is expected. Indeed, we find strong coupling energies between the γ D174N/ δ D180N mutation and either C193(N-methyl Cys) or C193Cah, with $\Delta\Delta G^\circ$ values of 2.0 and 2.2 kcal/mol (**Table 5.3**, **Figure 5.3B**). The magnitude of this interaction is quite significant when one considers the linkage is from a residue in the α subunit, through a second residue in the α subunit, and then across the subunit interface to a residue in the γ/δ subunit.

These results suggest a key role for the peptide bond of the C192-C193 unit. In support of this view, mutations that remove the disulfide but keep the peptide bond are much less impactful. Mutant cycles that link C193A to the backbone NH of S191 or to γ D174N/ δ D180N produce $\Delta\Delta G^\circ$ coupling energies of 0.99 and 0.80 kcal/mol, respectively, clearly smaller than what is seen with backbone mutations.

A three-dimensional mutant cycle analysis (**Figure 5.4**) was also performed using the triple mutant α 1C193A/ α 1S191Aah/(γ D174N/ δ D180N) in which each member of the triad is mutated. This triple mutation gave an EC_{50} of 480 μ M, smaller than what was seen for the double mutant α 1C193A/(γ D174N/ δ D180N). Note that we were unable to obtain a dose-response relation for a triple mutant involving a backbone mutation at C193 due to small current sizes.

Figure 5.4. Three-dimensional mutant cycle analysis with the triple mutant, $\alpha 1C193A/\alpha 1S191Aah/(\gamma D174N/\delta D180N)$.

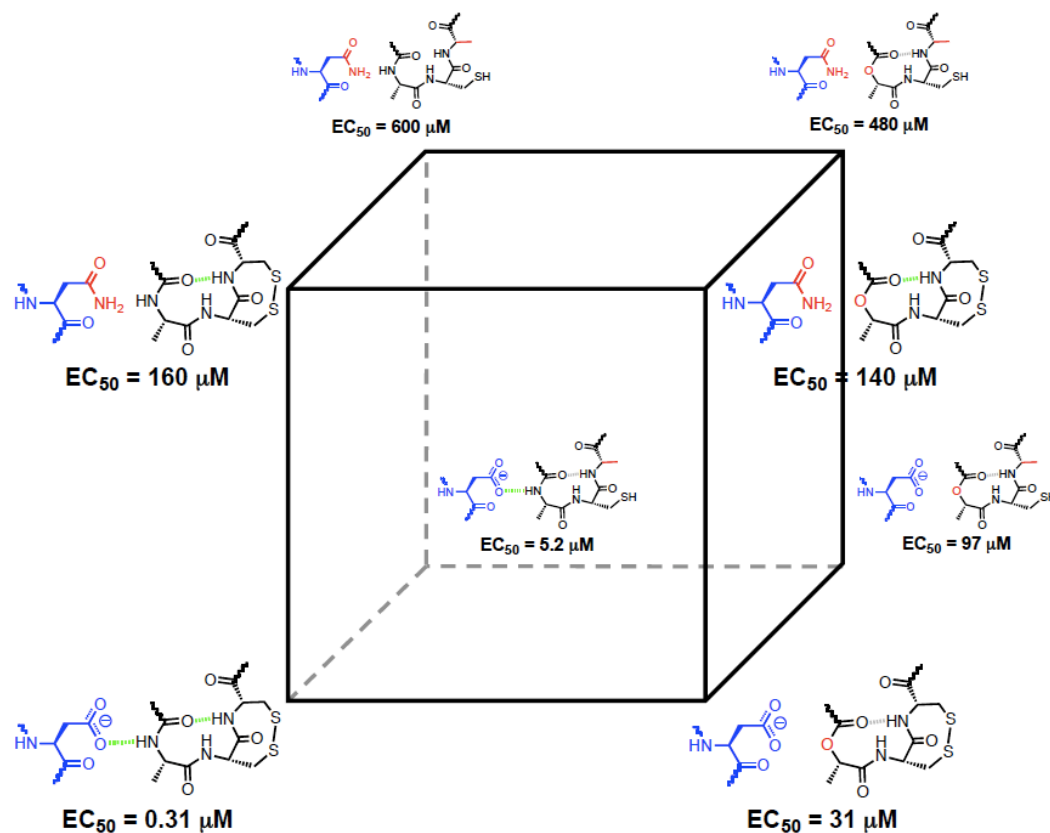


Table 5.4. Coupling energies for each face of the three-dimensional mutant cycle. $\Delta\Delta\Delta G^\circ = \Delta\Delta G^\circ$ front face – $\Delta\Delta G^\circ$ back face = $\Delta\Delta G^\circ$ left face – $\Delta\Delta G^\circ$ right face = $\Delta\Delta G^\circ$ bottom face – $\Delta\Delta G^\circ$ top face.

Face	$\Delta\Delta G^\circ$ (kcal/mol)
Front	2.8
Back	1.9
Left	0.89
Right	-0.054
Bottom	0.99
Top	0.053
$\Delta\Delta\Delta G^\circ$	~ 0.9

Multidimensional mutant cycle analysis is used to measure higher-order cooperativity between intramolecular or intermolecular interactions in proteins.^{35, 46-48}

Subtraction of the coupling energies ($\Delta\Delta G^\circ$ values) from parallel faces of the three-

dimensional mutant cycle (**Table 5.4**) gives the $\Delta\Delta\Delta G^\circ$ of the system, which is essentially an approximation of the extent that one interaction activates the other interaction³⁵ (*e.g.*, how much the hydrogen bond between of the β turn activates the intersubunit hydrogen bond). The $\Delta\Delta\Delta G^\circ$ of this system is relatively large, ~ 0.9 kcal/mol, suggesting that each interaction in the hydrogen bond network is strengthened when the other interaction is present. This is consistent with our model, given that the two hydrogen bonds should reinforce one another – the β turn hydrogen bond should make the S191 backbone NH a better hydrogen bond donor, and the intersubunit hydrogen bond should make the Y190 CO a better hydrogen bond acceptor by withdrawing or adding electron density through the amide bond, respectively.

5.4 DISCUSSION

The present work began as an effort to evaluate a possible role for *cis-trans* isomerization of the C192-C193 peptide bond embedded in the unusual vicinal disulfide of the α subunits of nAChRs. Our data do not support such a transition, but instead reveal an extended network of hydrogen bonds that appears to play a significant role in receptor function. In this network, the backbone NH of C193 hydrogen bonds to the backbone carbonyl of Y190. The Y190 carbonyl is, in turn, connected to the NH of S191, which hydrogen bonds across the subunit interface to the side chain of γ D174/ δ D180. The model is strongly supported by long-range double mutant cycle analysis that links the γ D174N/ δ D180N mutation to C193 backbone mutations. Removing the NH of C193 either by ester incorporation or *N*-methylation produces the same effect: a coupling energy $\Delta\Delta G^\circ$ of 2.0-2.2 kcal/mol to the D-to-N mutations.

The β turn hydrogen bond between the carbonyl of Y190 and the NH of C193 was suggested by AChBP structures.^{23, 24} Note, however, that the second hydrogen bond of the triad – that between the NH of S191 and the side chain of γ D174/ δ D180 – is not present in AChBPs and represents a significant difference between the actual nAChRs and the model AChBP systems. In fact, in crystal structures of AChBP, the loop F residue that corresponds to γ D174/ δ D180 is far from the adjacent subunit's C loop, and in the cryoelectron microscopy structures of *Torpedo* nAChR, the residue is over 15 Å from the C loop.^{49, 50}

Given these data, what then is the functional role of the C192-C193 vicinal disulfide of nAChR α subunits? Here we present a speculative model. An early mutagenesis study of the *Torpedo* nAChR indicated that both the C192S and C193S mutants were unresponsive to high concentrations of ACh.¹⁷ However DTT reduction of the vicinal disulfide produced only partial diminution of receptor function,⁶ and alkylation of one of these cysteines by bromo-acetylcholine⁸ or QBr¹⁶ reinstates partial function despite the absence of the vicinal disulfide. Here we also find that in mouse muscle and several neuronal nAChRs, conventional mutations at C192/C193, while certainly loss-of-function, do produce functional receptors. In the present case, C192A and C193A are both loss-of-function, but the magnitudes of the effects (2.0 and 1.7 kcal/mol with the α 1S191A background mutation) are *less* than what is seen with the backbone mutations (2.9 and 3.0 kcal/mol), for which the disulfide linkage is intact.

We propose that the role of the vicinal disulfide is to shape the structure of the β turn between Y190 and C193. The resultant distorted β turn may then help position the backbone NH of S191 for formation of the second hydrogen bond. Such a model is

supported by the observation that backbone mutations at C193 are strongly loss-of-function, suggesting that backbone positioning in this β turn is critical for receptor function.

We noted above that the β turn seen in AChBP structures is substantially distorted from idealized dihedral angle values for a Type I β turn. Quantum mechanical calculations (details available in the Supplemental Material of Blum *et al.*⁵¹) establish that reducing the disulfide does indeed allow the β turn to relax toward a more typical geometry. This structural change impacts the energetic strength of the β turn hydrogen bond only modestly (0.3 to 0.4 kcal/mol), but it does alter the positioning of the peptide linkage between Y190 and S191. Thus, we propose that the essential consequence of the distortion of the β turn induced by the disulfide is not the energetic weakening of the β turn hydrogen bond, but rather the positioning of S191 in an orientation that is favorable for interaction with γ D174/ δ D180.

Our gating model is thus as follows. In the closed state of the receptor, the β turn hydrogen bond is formed, but the intersubunit hydrogen bond (S191 to γ D174/ δ D180) is not (consistent with the AChBP crystal structures). The β turn hydrogen bond is essential to proper formation of the agonist binding site (recall that Y190 is residue C1 of the highly conserved cluster of aromatic amino acids that delineate the agonist binding site). Activation involves formation of the intersubunit hydrogen bond, an event that is facilitated by proper positioning of the backbone NH of S191 by the vicinal disulfide and the β turn hydrogen bond. The two hydrogen bonds should be mutually reinforcing, making the amide a stronger hydrogen bond acceptor and donor, which is reflected in the three-dimensional mutant cycle analysis done with the α 1C193A/ α 1S191Aah/

(γ D174N/ δ D180N) triple mutant where it was found that each interaction was strengthened by 0.9 kcal/mol when the other interaction is present. Thus, in our model the driving force for movement of the F loop (containing γ D174/ δ D180) is the formation of a network of hydrogen bonds. As discussed elsewhere,³⁹ this structural change at the subunit interface then contributes to an early phase of the conformational wave of receptor gating.

Note that our conventional mutations of C192 and C193, both of which are loss-of-function, are consistent with this model. The C192A and C193A mutants remove the disulfide and allow the β turn to relax to a more typical conformation (mirrored in the calculations). With the β turn relaxed, the backbone NH of S191 is not positioned optimally to form a hydrogen bond with γ D174/ δ D180, resulting in a loss of receptor function. The critical role of the peptide bond is further supported by our observation that disruption of the vicinal disulfide (C193A) perturbs the hydrogen bond network in a much more subtle manner than removal of the hydrogen bond donor of C193. Other Cys-loop receptors lack the vicinal disulfide of the nAChR α subunit, and it will be interesting to see if the β turn and intersubunit hydrogen bond survive in a different environment.

The vicinal disulfide has a unique historical connection to γ D174/ δ D180. Czajkowski and Karlin linked the reduced cysteine side chain at position α 193 to γ D174/ δ D180 with a 9 Å cross-linker.^{11, 12, 14, 52} Mutation of the aspartate resulted in a large loss of receptor function, leading to the suggestion that the negative charge of the aspartate side chain interacts directly with the positive charge of the agonist. Subsequent mutagenesis studies showed that the positive charge of agonists makes a cation- π interaction to a conserved tryptophan^{33, 53} and not a direct interaction with the aspartate.

Crystallographic studies of AChBP supported the cation- π interaction and revealed that γ D174/ δ D180 is positioned far from the agonist binding site.²⁴ Single channel studies from the early 2000s suggested that the residue was important for channel gating (and not binding),^{54, 55} however a role for the aspartate was only recently discovered. In 2008 we reported that γ D174/ δ D180 is a member of an important intersubunit hydrogen bond linking the F and C loops and contributing to channel gating.³⁹ We now report an additional, larger group of hydrogen bonds once again linking the vicinal disulfide to this important residue.

In summary, our mutagenesis studies unambiguously establish, through mutant cycle analysis, a hydrogen bonding network, beginning at the backbone NH of the C192-C193 disulfide, through the backbone amide linkage between Y190-S191, and across the subunit interface to the side chain of γ D174/ δ D180. Based on this, we present a speculative model in which the transition of the receptor from the closed to the open state involves formation of a network of tandem hydrogen bonds. In this model, the vicinal disulfide of the α subunit distorts the C loop β -turn in order to better position the backbone NH of S191 for optimal formation of an intersubunit hydrogen bond.

5.5 EXPERIMENTAL SECTION

Chemical synthesis. Cysteine analogs were prepared as 2-nitrobenzyl (NB) protected thiols. The 2-nitrobenzyl group was removed via irradiation with \sim 350 nm UV light prior to injection into *Xenopus* oocytes. A synthesis of nitroveratryl-protected cysteine, needed for control experiments, was described previously.⁵⁶ Cyanomethyl esters of *N*-Me-Cys and Cah were appended to the dinucleotide dCA and ligated to tRNA and

introduced to the nAChRs via unnatural amino acid mutagenesis as described previously.⁵⁷

Synthesis of *N*-Me-*N*-NVOC-Cys(SNB)-OCH₂CN. A 20 mL scintillation vial was loaded with 4 mL of methanol and placed over an ice water bath. To this was added 130 mg (5.7 mmol) of Na. The mixture was stirred until the metal dissolved (~20 min). *N*-Me-Cysteine (370 mg, 2.7 mmol), prepared as described previously,⁵⁸ was added to the vial and the mixture stirred for 10 minutes. 2-Nitrobenzyl bromide (520 mg, 2.6 mmol) was added in three portions to the stirring solution, turning a clear solution into a cloudy mixture containing a pale yellow precipitate. An hour after the last addition, 20 mL of chilled ether was added. The precipitate was filtered, washed with 10 mL of chilled ether and dried to afford *N*-Me-Cys(S-NB)-OH as a crude, pale yellow solid. 100 mg (0.37 mmol) of this powder was used directly in the next step without further purification. The powder was suspended in 3 mL of water and then an additional 1 mL of dioxane. Na₂CO₃ (59 mg, 0.56 mmol) was added and the mixture was allowed to stir for five minutes prior to the addition of 6-nitroveratryloxycarbonyl chloride (NVOC-chloride) (92 mg, 0.33 mmol) in 4 mL of dioxane. After stirring at room temperature for 48 hours, the solution was diluted with 10 mL of CH₂Cl₂ and 10 mL of water. The organic layer was discarded and the pH of the aqueous layer was decreased to 1 via the addition of 6M HCl. Following extraction with CH₂Cl₂, the new organic layer was dried over Na₂SO₄ and poured over a silica plug. The plug was rinsed with 25 mL of EtOAc and then eluted with 2% AcOH in EtOAc. The yellow eluent was concentrated to reveal *N*-Me-*N*-NVOC-Cys(S-NB)-OH as a pale yellow solid in 84% yield (158 mg, 0.310 mmol). $R_f = 0.34$ (2% AcOH in EtOAc); ¹H NMR (300 MHz, CDCl₃, 298 K) δ 7.89 (1H, m), 7.63 (1H,

m), 7.47 (1H, t, $J = 7.5$ Hz), 7.36 (2H, m), 6.89 (1H, d, $J = 14.1$ Hz), 5.50 (2H, m), 4.68 (1H, m), 4.04 (2H, s), 3.86 (6H, s), 2.81 – 3.04 (5H, m); ^{13}C NMR (75 MHz, CDCl_3 , 298K) δ 177.7, 174.9, 156.4, 153.7, 147.9, 139.3, 133.4, 133.2, 132.1, 128.6, 128.3, 125.6, 109.1, 108.1, 64.7, 58.9, 56.4, 56.4, 33.5, 32.3, 30.9; High-resolution MS analysis (FAB+) m/z : calc'd 510.1182, found 510.1180.

N-Me-*N*-NVOC-Cys(S-NB)-OH (58 mg, 0.11 mmol) was added to a 2 mL scintillation vial and suspended in 0.35 mL of chloroacetonitrile (5.5 mmol). Triethylamine (50 mL, 0.33 mmol) was added to the mixture and the resulting solution stirred for 4 hours. The solution was diluted with 15 mL of water and the organic layer was extracted with CH_2Cl_2 ($\times 3$), dried over Na_2SO_4 and concentrated to yield a yellow oil. The oil was purified by flash column chromatography on silica gel (50% EtOAc in hexanes) to afford *N*-Me, *N*-NVOC-Cys-(S-NB)- OCH_2CN as a yellow oil in 62% yield (37 mg, 0.067 mmol). $R_f = 0.25$ (50% EtOAc in hexanes); ^1H NMR (300 MHz, CDCl_3 , 298 K) δ 7.98 (1H, m), 7.70 (1H, m), 7.54 (1H, m), 7.43 (2H, m), 6.95 (1H, d, $J = 14.1$ Hz), 5.55 (2H, m), 4.72 (3H, m), 4.08 (2H, s), 4.00 (3H, s), 3.95 (3H, s), 2.89–3.10 (5H, m); ^{13}C NMR (75 MHz, CDCl_3 , 298K) δ 168.5, 156.1, 153.7, 148.1, 133.3, 133.3, 133.2, 132.1, 128.7, 128.7, 127.9, 125.6, 109.5, 108.2, 64.9, 59.0, 56.4, 56.4, 49.1, 33.6, 32.7, 31.0; High-resolution MS analysis (FAB+) m/z : calc'd 549.1291, found 549.1302.

Synthesis of HO-Cys(SNB)- OCH_2CN . The synthesis of 2-nitrobenzyl protected α -hydroxy cysteine was based on a protocol reported by Kelly and co-workers.⁵⁹ (2-nitrophenyl)methanethiol (400 mg, 3.9 mmol) was prepared as previously described⁶⁰ and added to a flame-dried 50 mL, 2-neck, round-bottom flask equipped with a reflux

condenser and under Ar (g). To this was added methyl-(2S)-glycidate (660 mg, 3.9 mmol), triethylamine (0.54 mL, 3.9 mmol) and 20 mL of MeOH. The mixture was stirred for 5 hours at reflux until completion of the reaction as determined by TLC. After cooling to room temperature, the mixture was concentrated *in vacuo*, and the resulting yellow oil was purified by flash column chromatography on silica gel (25% EtOAc in hexanes) to afford HO-Cys(SNB)-OMe in 35% yield (370 mg, 1.4 mmol). $R_f = 0.44$ (50% EtOAc in hexanes); ^1H NMR (300 MHz, CDCl_3 , 298 K) δ 7.98 (1H, d, $J = 8.2$ Hz), 7.39–7.59 (3H, m), 4.44 (1H, b), 4.19 (2H, s), 3.79 (3H, s), 3.15 (1H, b), 2.89 (1H, dd, $J = 14.4, 4.7$ Hz), 2.75 (1H, dd, $J = 14.4, 6.4$ Hz); ^{13}C NMR (75 MHz, CDCl_3 , 298K) δ 173.5, 148.6, 133.8, 133.0, 132.2, 128.3, 125.5, 71.2, 52.9, 35.3, 34.1; High-resolution MS analysis (FAB+) m/z : calc'd 272.0593, found 272.0591.

HO-Cys(SNB)-OMe (44 mg, 1.6 mmol) was added to a 20 mL scintillation vial and dissolved in 10 mL of 1M LiOH in 3:1:1 tetrahydrofuran: methanol: water. The mixture was stirred for 12 hours at room temperature. The pH of the solution was adjusted to pH 12 via the addition of 2 M NaOH. The aqueous layer was washed with 30 mL of ether and the organic layer was discarded. The pH of the aqueous layer was decreased to 1 via the addition of 6 M HCl, and extracted with EtOAc. The new organic layer was washed with brine, dried over Na_2SO_4 and concentrated to yield HO-Cys(SNB)-OH as a yellow oil in 85% crude yield (350 mg, 1.4 mmol). Cyanomethyl esterification began with the addition of HO-Cys(SNB)-OH (250 mg, 0.97 mmol) to a 4 mL scintillation vial. Chloroacetonitrile (0.5 mL, 7.9 mmol) and triethylamine (0.40 mL, 2.9 mmol) were added to the vial and the mixture stirred for 12 hours. The solution was diluted with 15 mL of water, and the organic layer was extracted with CH_2Cl_2 ($\times 3$), dried over Na_2SO_4

and concentrated to a yellow oil. The oil was purified by flash column chromatography on silica gel (50% EtOAc in hexanes) to afford HO-Cys(SNB)-OCH₂CN as a yellow oil in 55% yield (160 mg, 0.53 mmol). $R_f = 0.35$ (50% EtOAc in hexanes); ¹H NMR (400 MHz, CDCl₃, 298 K) δ 7.95 (1H, d), 7.39–7.57 (3H, m), 4.78 (2H, m), 4.52 (1H, m), 4.16 (2H, dd, $J = 19.2, 13.3$ Hz), 3.26 (1H, d, $J = 5.5$ Hz), 2.91 (1H, dd, $J = 14.5, 3.9$ Hz), 2.78 (1H, dd, $J = 14.6, 5.9$ Hz); ¹³C NMR (100 MHz, CDCl₃, 298K) δ 171.4, 148.6, 133.4, 133.2, 132.2, 128.5, 125.5, 113.8, 71.0, 49.3, 35.1, 34.2; High-resolution MS analysis (FAB+) m/z : calc'd 297.0545, found 297.0546.

Nonsense suppression experiments. Conventional and unnatural mutagenesis were performed on mouse muscle embryonic nAChR ($\alpha_1\beta_1\gamma\delta$) cDNA in the pAMV vector using the standard Stratagene QuickChange protocol. For unnatural mutagenesis, a stop codon, TAG or TGA, was made at the site of interest and verified through sequencing. The β_1 subunit contained a background mutation in the M2 transmembrane helix ($\beta_1L9'S$) that is known to lower whole-cell EC₅₀ values.^{37, 38} The α_1 subunit also contains a hemagglutinin epitope in the M3-M4 cytoplasmic loop. This epitope does not alter EC₅₀ values in control experiments. cDNA was linearized with the restriction enzyme NotI. mRNA was prepared by *in vitro* transcription using the mMessage Machine T7 kit (Ambion).

Stage V-VI *Xenopus laevis* oocytes were injected with mRNA in a 2:1:1:1 or 10:1:1:1 ratio of α_1 : β_1 : γ : δ for conventional or unnatural amino acid mutagenesis experiments, respectively. Hydroxy or amino acids were appended to the dinucleotide dCA and enzymatically ligated to the truncated 74-nucleotide THG73 or TQOpS' tRNA as

previously described.⁵⁷ NVOC and 2-nitrobenzyl protecting groups on the appended amino or α -hydroxy acids were removed by irradiation with UV light filtered to ~ 350 nm. For conventional experiments, 1-2 ng of mRNA was injected per oocyte in a single 75 nL injection. For unnatural amino acid experiments, each cell was injected with 75 nL of a 1:1 mixture of mRNA (20-25 ng of total mRNA) and tRNA (20-30 ng). Oocytes were incubated at 18 °C for 24 to 48 hours after injection. Wild-type recovery experiments (injection of tRNA appended to the natural amino acid) were performed to evaluate the fidelity of the unnatural suppression experiments. Additional controls, injections of mRNA only and mRNA with 76-mer THG73 or TQOpS', were also performed. While currents were seen for 76-mer control experiments, EC₅₀ and Hill values were distinct from the values obtained for 74-mer ligated to an α -hydroxy or amino acid. Conventional experiments with $\alpha 4\beta 2$,³³ $\alpha 4\beta 4$ and $\alpha 7$ ³⁴ were performed as described previously.

Electrophysiology. The functional effects of mutation were evaluated using two-electrode voltage clamp electrophysiology. Electrophysiology experiments were performed 24-48 hrs after injection using the OpusXpress 6000A instrument (Axon Instruments) at a holding potential of -60 mV. A Ca²⁺ free ND96 solution was used as the running buffer (96 mM NaCl, 2 mM KCl, 1 mM MgCl₂, and 5 mM HEPES, pH 7.5). Acetylcholine doses in Ca²⁺-free ND96 were applied for 15 s followed by a 116 s wash with the running buffer. Dose-response data were obtained for ≥ 8 agonist concentrations on ≥ 7 cells. All EC₅₀ and Hill coefficient values were obtained by fitting dose-response relations to the Hill equation and are reported as averages \pm standard error of the fit. A detailed error analysis of nonsense suppression experiments shows that data are reproducible to $\pm 50\%$ in EC₅₀.⁶¹

***Ab initio* calculations.** Structure building and subsequent *ab initio* calculations on CH₃CO-[Cys-Cys]-NH₂ were carried out using the Gaussian 03 software package⁶² by Kristin Rule Gleitsman⁶³ at the B3LYP/6-31++G(d,p) level of theory in the gas phase. The *cis* and *trans* isomers of a model peptide of the form CH₃CO-[Cys-Cys]-NH₂ with the S-S disulfide torsional angles of $\pm 90^\circ$ were constructed using GausView molecule building tools. The geometric parameters for these starting structures were derived from the lowest energy conformers from previous *ab initio* calculations on a similar model peptide.²¹ Energy minimizations were performed on the four starting structures of the model peptide. The lowest energy structures from these model peptide calculations then served as scaffolds for constructing the initial ester and *N*-methyl structures, which were subsequently subject to energy minimization calculations. In total, the energies for twelve geometry-optimized structures were calculated, with four conformers for each model system. Further details are provided in Kristin Rule Gleitsman's thesis.⁶³ Calculations on simple cyclic amides and related structures were performed with SPARTAN.⁶⁴

5.6 ACKNOWLEDGEMENTS

This work was supported by the National Institutes of Health Grants NS 34407 and NS 11756.

5.7 REFERENCES

1. Corringer, P. J.; Le Novère, N.; Changeux, J. P., Nicotinic receptors at the amino acid level. *Annu. Rev. Pharmacol. Toxicol.* **2000**, 40, 431-58.
2. Grutter, T.; Changeux, J. P., Nicotinic receptors in wonderland. *Trends Biochem. Sci.* **2001**, 26, (8), 459-63.
3. Karlin, A., Emerging structure of the nicotinic acetylcholine receptors. *Nat. Rev. Neurosci.* **2002**, 3, (2), 102-14.
4. Jensen, A. A.; Frolund, B.; Liljefors, T.; Krosgaard-Larsen, P., Neuronal nicotinic acetylcholine receptors: structural revelations, target identifications, and therapeutic inspirations. *J. Med. Chem.* **2005**, 48, (15), 4705-45.
5. Romanelli, M. N.; Gratter, P.; Guandalini, L.; Martini, E.; Bonaccini, C.; Gualtieri, F., Central nicotinic receptors: structure, function, ligands, and therapeutic potential. *ChemMedChem* **2007**, 2, (6), 746-67.
6. Karlin, A.; Bartels, E., Effects of blocking sulfhydryl groups and of reducing disulfide bonds on the acetylcholine-activated permeability system of the electroplax. *Biochim. Biophys. Acta* **1966**, 126, (3), 525-35.
7. Karlin, A., Chemical modification of the active site of the acetylcholine receptor. *J. Gen. Physiol.* **1969**, 54, (1), 245-64.
8. Silman, I.; Karlin, A., Acetylcholine receptor: covalent attachment of depolarizing groups at the active site. *Science* **1969**, 164, (3886), 1420-1421.
9. Kao, P. N.; Dwork, A. J.; Kaldany, R. R.; Silver, M. L.; Wideman, J.; Stein, S.; Karlin, A., Identification of the alpha subunit half-cystine specifically labeled by an affinity reagent for the acetylcholine receptor binding site. *J. Biol. Chem.* **1984**, 259, (19), 11662-5.
10. Kao, P. N.; Karlin, A., Acetylcholine receptor binding site contains a disulfide cross-link between adjacent half-cystinyl residues. *J. Biol. Chem.* **1986**, 261, (18), 8085-8.
11. Czajkowski, C.; Karlin, A., Agonist binding site of *Torpedo* electric tissue nicotinic acetylcholine receptor. A negatively charged region of the delta subunit within 0.9 nm of the alpha subunit binding site disulfide. *J. Biol. Chem.* **1991**, 266, (33), 22603-22612.
12. Czajkowski, C.; Kaufmann, C.; Karlin, A., Negatively charged amino acid residues in the nicotinic receptor delta subunit that contribute to the binding of acetylcholine. *Proc. Natl. Acad. Sci. USA* **1993**, 90, (13), 6285-9.
13. Damle, V. N.; Karlin, A., Effects of agonists and antagonists on the reactivity of the binding site disulfide in acetylcholine receptor from *Torpedo californica*. *Biochemistry* **1980**, 19, (17), 3924-32.
14. Martin, M.; Czajkowski, C.; Karlin, A., The contributions of aspartyl residues in the acetylcholine receptor gamma and delta subunits to the binding of agonists and competitive antagonists. *J. Biol. Chem.* **1996**, 271, (23), 13497-503.
15. Walker, J. W.; Lukas, R. J.; McNamee, M. G., Effects of thio-group modifications on the ion permeability control and ligand binding properties of *Torpedo californica* acetylcholine receptor. *Biochemistry* **1981**, 20, (8), 2191-9.
16. Chabala, L. D.; Lester, H. A., Activation of acetylcholine receptor channels by covalently bound agonists in cultured rat myoballs. *J. Physiol.* **1986**, 379, 83-108.

17. Mishina, M.; Tobimatsu, T.; Imoto, K.; Tanaka, K.-i.; Fujita, Y.; Fukuda, K.; Kurasaki, M.; Takahashi, H.; Morimoto, Y.; Hirose, T.; Inayama, S.; Takahashi, T.; Kuno, M.; Numa, S., Location of functional regions of acetylcholine receptor alpha-subunit by site-directed mutagenesis. *Nature* **1985**, 313, (6001), 364-369.
18. Avizonis, D. Z.; Farr-Jones, S.; Kosen, P. A.; Basus, V. J., Conformations and dynamics of the essential cysteinyl-cysteine ring derived from the acetylcholine receptor. *J. Am. Chem. Soc.* **1996**, 118, (51), 13031-13039.
19. Creighton, C. J.; Reynolds, C. H.; Lee, D. H.; Leo, G. C.; Reitz, A. B., Conformational analysis of the eight-membered ring of the oxidized cysteinyl-cysteine unit implicated in nicotinic acetylcholine receptor ligand recognition. *J. Am. Chem. Soc.* **2001**, 123, (50), 12664-9.
20. Gao, F.; Mer, G.; Tonelli, M.; Hansen, S. B.; Burghardt, T. P.; Taylor, P.; Sine, S. M., Solution NMR of acetylcholine binding protein reveals agonist-mediated conformational change of the C-loop. *Mol. Pharmacol.* **2006**, 70, (4), 1230-5.
21. Hudaky, I.; Gaspari, Z.; Carugo, O.; Cemazar, M.; Pongor, S.; Perczel, A., Vicinal disulfide bridge conformers by experimental methods and by ab initio and DFT molecular computations. *Proteins* **2004**, 55, (1), 152-68.
22. Ruggles, E. L.; Dekker, P. B.; Hondal, R. J., Synthesis, redox properties, and conformational analysis of vicinal disulfide ring mimics. *Tetrahedron* **2009**, 65, (7), 1257-1267.
23. Brejc, K.; van Dijk, W. J.; Klaassen, R. V.; Schuurmans, M.; van Der Oost, J.; Smit, A. B.; Sixma, T. K., Crystal structure of an ACh-binding protein reveals the ligand-binding domain of nicotinic receptors. *Nature* **2001**, 411, (6835), 269-76.
24. Celie, P. H.; van Rossum-Fikkert, S. E.; van Dijk, W. J.; Brejc, K.; Smit, A. B.; Sixma, T. K., Nicotine and carbamylcholine binding to nicotinic acetylcholine receptors as studied in AChBP crystal structures. *Neuron* **2004**, 41, (6), 907-914.
25. Capasso, S.; Mattia, C.; Mazzarella, L.; Puliti, R., Structure of a *cis*-peptide unit - molecular-conformation of cyclic disulfide *L*-cysteinyl-*L*-cysteine. *Acta Crystallogr. Sect. B-Struct. Commun.* **1977**, 33, 2080-2083.
26. Hata, Y.; Matsuura, Y.; Tanaka, N.; Ashida, T.; Kakudo, M., Tert-butylloxycarbonyl-*L*-cysteinyl-*L*-cysteine disulfide methyl-ester. *Acta Crystallogr. Sect. B-Struct. Commun.* **1977**, 33, 3561-3564.
27. Grosman, C.; Zhou, M.; Auerbach, A., Mapping the conformational wave of acetylcholine receptor channel gating. *Nature* **2000**, 403, (6771), 773-6.
28. Dugave, C.; Demange, L., *Cis-trans* isomerization of organic molecules and biomolecules: Implications and applications. *Chem. Rev.* **2003**, 103, (7), 2475-2532.
29. Aubry, A.; Vitoux, B.; Boussard, G.; Marraud, M., *N*-Methyl peptides. IV. Water and beta-turn in peptides. Crystal structure of *N*-pivaloyl-*L*-prolyl-*N,N'*-dimethyl-*D*-alaninamide in the anhydrous and monohydrated states. *Int. J. Pept. Protein Res.* **1981**, 18, (2), 195-202.
30. Vitoux, B.; Aubry, A.; Cung, M. T.; Boussard, G.; Marraud, M., *N*-methyl peptides. III. Solution conformational study and crystal structure of *N*-pivaloyl-*L*-prolyl-*N*-methyl-*N'*-isopropyl-*L*-alaninamide. *Int. J. Pept. Protein Res.* **1981**, 17, (4), 469-79.

31. Beene, D. L.; Dougherty, D. A.; Lester, H. A., Unnatural amino acid mutagenesis in mapping ion channel function. *Curr. Opin. Neurobiol.* **2003**, 13, (3), 264-70.
32. Nowak, M. W.; Kearney, P. C.; Sampson, J. R.; Saks, M. E.; Labarca, C. G.; Silverman, S. K.; Zhong, W.; Thorson, J.; Abelson, J. N.; Davidson, N.; Schultz, P. G.; Dougherty, D. A.; Lester, H. A., Nicotinic receptor binding site probed with unnatural amino acid incorporation in intact cells. *Science* **1995**, 268, 439-442.
33. Xiu, X.; Puskar, N. L.; Shanata, J. A.; Lester, H. A.; Dougherty, D. A., Nicotine binding to brain receptors requires a strong cation-pi interaction. *Nature* **2009**, 458, (7237), 534-7.
34. Puskar, N. L.; Xiu, X.; Lester, H. A.; Dougherty, D. A., Two neuronal nicotinic acetylcholine receptors, $\alpha 4\beta 4$ and $\alpha 7$, show differential agonist binding modes. *J. Biol. Chem.* **2011**, 286, (16), 14618-27.
35. Horovitz, A., Double-mutant cycles: a powerful tool for analyzing protein structure and function. *Fold. Des.* **1996**, 1, (6), R121-6.
36. Makhatadze, G. I.; Loladze, V. V.; Ermolenko, D. N.; Chen, X. F.; Thomas, S. T., Contribution of surface salt bridges to protein stability: Guidelines for protein engineering. *J. Mol. Biol.* **2003**, 327, (5), 1135-1148.
37. Filatov, G. N.; White, M. M., The role of conserved leucines in the M2 domain of the acetylcholine receptor in channel gating. *Mol. Pharmacol.* **1995**, 48, (3), 379-84.
38. Labarca, C.; Nowak, M. W.; Zhang, H.; Tang, L.; Deshpande, P.; Lester, H. A., Channel gating governed symmetrically by conserved leucine residues in the M2 domain of nicotinic receptors. *Nature* **1995**, 376, 514-516.
39. Gleitsman, K. R.; Kedrowski, S. M. A.; Lester, H. A.; Dougherty, D. A., An intersubunit hydrogen bond in the nicotinic acetylcholine receptor that contributes to channel gating. *J. Biol. Chem.* **2008**, 283, (51), 35638-35643.
40. Beligere, G. S.; Dawson, P. E., Design, synthesis, and characterization of 4-ester C12, a model for backbone hydrogen bonding in protein α -helices. *J. Am. Chem. Soc.* **2000**, 122, (49), 12079-12082.
41. Blankenship, J. W.; Balambika, R.; Dawson, P. E., Probing backbone hydrogen bonds in the hydrophobic core of GCN4. *Biochemistry* **2002**, 41, (52), 15676-84.
42. Deechongkit, S.; Dawson, P. E.; Kelly, J. W., Toward assessing the position-dependent contributions of backbone hydrogen bonding to beta-sheet folding thermodynamics employing amide-to-ester perturbations. *J. Am. Chem. Soc.* **2004**, 126, (51), 16762-71.
43. Deechongkit, S.; Nguyen, H.; Powers, E. T.; Dawson, P. E.; Grubele, M.; Kelly, J. W., Context-dependent contributions of backbone hydrogen bonding to beta-sheet folding energetics. *Nature* **2004**, 430, (6995), 101-5.
44. Koh, J. T.; Cornish, V. W.; Schultz, P. G., An experimental approach to evaluating the role of backbone interactions in proteins using unnatural amino acid mutagenesis. *Biochemistry* **1997**, 36, (38), 11314-22.
45. Nakhle, B. M.; Silinski, P.; Fitzgerald, M. C., Identification of an essential backbone amide bond in the folding and stability of a multimeric enzyme. *J. Am. Chem. Soc.* **2000**, 122, (34), 8105-8111.

46. Horovitz, A.; Serrano, L.; Avron, B.; Bycroft, M.; Fersht, A. R., Strength and cooperativity of contributions of surface salt bridges to protein stability. *J. Mol. Biol.* **1990**, 216, (4), 1031-44.
47. Marqusee, S.; Sauer, R. T., Contributions of a hydrogen bond/salt bridge network to the stability of secondary and tertiary structure in lambda repressor. *Protein Sci.* **1994**, 3, (12), 2217-25.
48. Waldburger, C. D.; Schildbach, J. F.; Sauer, R. T., Are buried salt bridges important for protein stability and conformational specificity? *Nat. Struct. Biol.* **1995**, 2, (2), 122-8.
49. Miyazawa, A.; Fujiyoshi, Y.; Stowell, M.; Unwin, N., Nicotinic acetylcholine receptor at 4.6 Å resolution: transverse tunnels in the channel wall. *J. Mol. Biol.* **1999**, 288, (4), 765-86.
50. Unwin, N., Refined structure of the nicotinic acetylcholine receptor at 4Å resolution. *J. Mol. Biol.* **2005**, 346, (4), 967-89.
51. Blum, A. P.; Gleitsman, K. R.; Lester, H. A.; Dougherty, D. A., Evidence for an extended hydrogen bond network in the binding site of the nicotinic receptor: concerning the role of the vicinal disulfide of the $\alpha 1$ subunit. *J. Biol. Chem.* **2011**, 286, (37), 32251-58.
52. Czajkowski, C.; Karlin, A., Structure of the nicotinic receptor acetylcholine-binding site. *J. Biol. Chem.* **1995**, 270, (7), 3160-64.
53. Zhong, W.; Gallivan, J. P.; Zhang, Y.; Li, L.; Lester, H. A.; Dougherty, D. A., From *ab initio* quantum mechanics to molecular neurobiology: a cation-pi binding site in the nicotinic receptor. *Proc. Natl. Acad. Sci. USA* **1998**, 95, (21), 12088-93.
54. Akk, G.; Zhou, M.; Auerbach, A., A mutational analysis of the acetylcholine receptor channel transmitter binding site. *Biophys J.* **1999**, 76, 207-18.
55. Sine, S. M.; Shen, X. M.; Wang, H. L.; Ohno, K.; Lee, W. Y.; Tsujino, A.; Brengmann, J.; Bren, N.; Vajsar, J.; Engel, A. G., Naturally occurring mutations at the acetylcholine receptor binding site independently alter ACh binding and channel gating. *J. Gen. Physiol.* **2002**, 120, (4), 483-96.
56. Silverman, S. K., I. Conformational and charge effects on high-spin organic polyradicals. II. Studies on the atomic-scale basis of ion selectivity in potassium channels. Ph.D. Thesis. California Institute of Technology, Pasadena, CA, 1998.
57. Nowak, M. W.; Gallivan, J. P.; Silverman, S. K.; Labarca, C. G.; Dougherty, D. A.; Lester, H. A., [28] *In vivo* incorporation of unnatural amino acids into ion channels in *Xenopus* oocyte expression system. In *Methods in Enzymology*, Conn, P. M., Ed. Academic Press: 1998; Vol. Volume 293, pp 504-529.
58. Park, J. D.; Kim, D. H., Cysteine derivatives as inhibitors for carboxypeptidase a: synthesis and structure-activity relationships. *J. Med. Chem.* **2002**, 45, (4), 911-918.
59. Deechongkit, S.; You, S.-L.; Kelly, J. W., Synthesis of all nineteen appropriately protected chiral α -hydroxy acid equivalents of the α -amino acids for boc solid-phase depsi-peptide synthesis. *Org. Lett.* **2004**, 6, (4), 497-500.
60. Sohn, C. H.; Chung, C. K.; Yin, S.; Ramachandran, P.; Loo, J. A.; Beauchamp, J. L., Probing the mechanism of electron capture and electron transfer dissociation using tags with variable electron affinity. *J. Amer. Chem. Soc.* **2009**, 131, (15), 5444-5459.

61. Torrice, M. M. Chemical-scale studies of the nicotinic and muscarinic acetylcholine receptors. Ph.D. Thesis. California Institute of Technology, Pasadena, CA, 2009.
62. Frisch, M. J.; Trucks, G. W.; Schlegel, H. B.; Scuseria, G. E.; Robb, M. A.; Cheeseman, J. R.; Montgomery, J. A.; Vreven, T.; Kudin, K. N.; Burant, J. C.; Millam, J. M.; Iyengar, S. S.; Tomasi, J.; Barone, V.; Mennucci, B.; Cossi, M.; Scalmani, G.; Rega, N.; Petersson, G. A.; Nakatsuji, H.; Hada, M.; Ehara, M.; Toyota, K.; Fukuda, R.; Hasegawa, J.; Ishida, M.; Nakajima, T.; Honda, Y.; Kitao, O.; Nakai, H.; Klene, M.; Li, X.; Knox, J. E.; Hratchian, H. P.; Cross, J. B.; Bakken, V.; Adamo, C.; Jaramillo, J.; Gomperts, R.; Stratmann, R. E.; Yazyev, O.; Austin, A. J.; Cammi, R.; Pomelli, C.; Ochterski, J. W.; Ayala, P. Y.; Morokuma, K.; Voth, G. A.; Salvador, P.; Dannenberg, J. J.; Zakrzewski, V. G.; Dapprich, S.; Daniels, A. D.; Strain, M. C.; Farkas, O.; Malick, D. K.; Rabuck, A. D.; Raghavachari, K.; Foresman, J. B.; Ortiz, J. V.; Cui, Q.; Baboul, A. G.; Clifford, S.; Cioslowski, J.; Stefanov, B. B.; Liu, G.; Liashenko, A.; Piskorz, P.; Komaromi, I.; Martin, R. L.; Fox, D. J.; Keith, T.; Laham, A.; Peng, C. Y.; Nanayakkara, A.; Challacombe, M.; Gill, P. M. W.; Johnson, B.; Chen, W.; Wong, M. W.; Gonzalez, C.; Pople, J. A., Gaussian 03, Revision C.02. In 2003.
63. Gleitsman, K. R., Chemical-scale studies of the nicotinic acetylcholine receptor: insights from amide-to-ester backbone mutagenesis. Ph.D. Thesis. California Institute of Technology, Pasadena, CA **2010**.
64. SPARTAN, *Wavefunction, Inc. Irvine, CA*.

CHAPTER 6: New Approaches to Photochemical Cleavage of Peptide and Protein Backbones*

6.1 ABSTRACT

A strategy for photochemical cleavage of peptide and protein backbones is described, which is based on a selenide-mediated cleavage of a backbone ester moiety. Studies in model systems establish the viability of the chemistry and suggest the method could be a valuable tool for chemical biology studies of proteins. Also described are two alternative strategies based on a “caged” aniline and the (2-nitrophenyl)ethyl (NPE) protecting group.

6.2 INTRODUCTION

We describe here new strategies for photochemical cleavage of peptide and protein backbones and model studies intended to evaluate the viability of the novel chemistry involved. Strategies for preparing photoresponsive biomolecules are finding increasing use in chemical biology.^{1, 2} Some time ago we introduced a strategy for photochemically initiating backbone cleavage of a protein, employing the unnatural amino acid 2-nitrophenylglycine (Npg, **Figure 6.1**).³ After incorporation of Npg into a protein or peptide, the well-known *o*-nitrobenzyl “deprotection” of the peptide bond nitrogen results in cleavage of the protein backbone, a site-specific, nitrobenzyl-induced, photochemical proteolysis (SNIPP). Other strategies for photochemical cleavage of protein and peptide

* This work was done in collaboration with Dr. Amy L. Eastwood and Dr. Niki M. Zacharias and is adapted from: Eastwood, A. L.; Blum, A. P.; Zacharias, N. M.; Dougherty, D. A., A selenide-based approach to photochemical cleavage of peptide and protein backbones at engineered backbone esters. *The Journal of Organic Chemistry* **2009**, 74, (23), 9241-44. Copyright 2009 American Chemical Society.

backbones have recently appeared. Imperiali and Kron have both employed *o*-nitro- β -phenylalanine as a linker between two protein or peptide fragments,^{4, 5} while Muir has employed an expanded nitrobenzyl linker.⁶ Otaka and co-workers introduced a novel system based on a nitrobenzyl-caged phenol and the “trimethyl lock” motif, which promoted intramolecular cleavage of the backbone amide after the phenol was decaged.⁷ Schultz and co-workers demonstrated a novel cleavage mediated by 2-nitrophenylalanine.⁸

All of these strategies have advantages and disadvantages. The Npg approach has been employed in several contexts^{3, 9, 10} and is compatible with both solid phase peptide synthesis (SPPS) and *in vivo* incorporation into full proteins via nonsense suppression. However, the photochemical efficiency of the cleavage is not high, with a ~50% cleavage yield after four hours of photolysis.³ Also, the incorporation into proteins of the relatively crowded, β -branched residue is often not efficient. Similarly low photoefficiency is seen with 2-nitrophenylalanine.⁸ The other strategies can show more efficient cleavage of peptides but are not compatible with *in vivo* incorporation into proteins.

Described herein are alternative strategies for the photochemical cleavage of peptide and protein backbones. The first strategy is based on a caged selenide. Model studies establish that this strategy is effective, with up to 72% backbone cleavage of depsipeptides. Other strategies are also described which are based on a nitroveratryloxycarbonyl (NVOC)-protected aniline and the photochemistry of (2-nitrophenyl)ethyl (NPE) derivatives.

6.3 RESULTS

6.3.1 Caged selenide strategy

In our first strategy the key cleavage reaction is based on a novel, intramolecular S_N2 reaction, shown schematically in **Figure 6.1**. Selenide is one of the most potent nucleophiles known, and at physiological pH a selenol ($pK_a \sim 5-6$) should be predominantly in the selenide form. The essential reaction, S_N2 cleavage of an ester carbon with a carboxylate as the leaving group, has ample precedent.¹¹⁻¹⁵ Formation of the ester leaving group requires incorporation of an α -hydroxy acid (rather than an α -amino acid), but such backbone esters can be efficiently incorporated into peptides by SPPS^{16, 17} and into proteins by nonsense suppression.^{10, 18-22} In addition, selenium-containing natural amino acids such as selenocysteine and selenomethionine are well-known to be efficiently incorporated into proteins. Finally, “caging” the selenide with an *o*-nitrobenzyl group allows the process to be initiated photochemically.

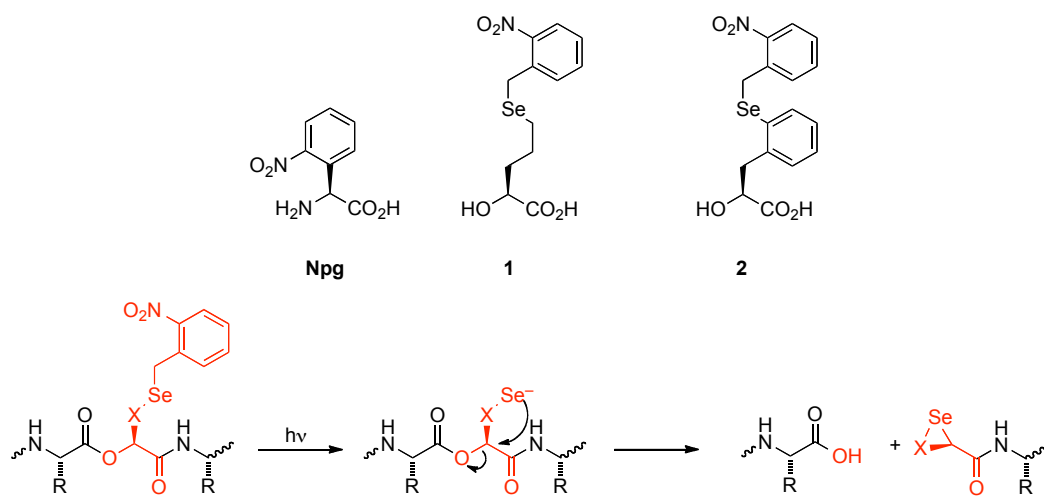


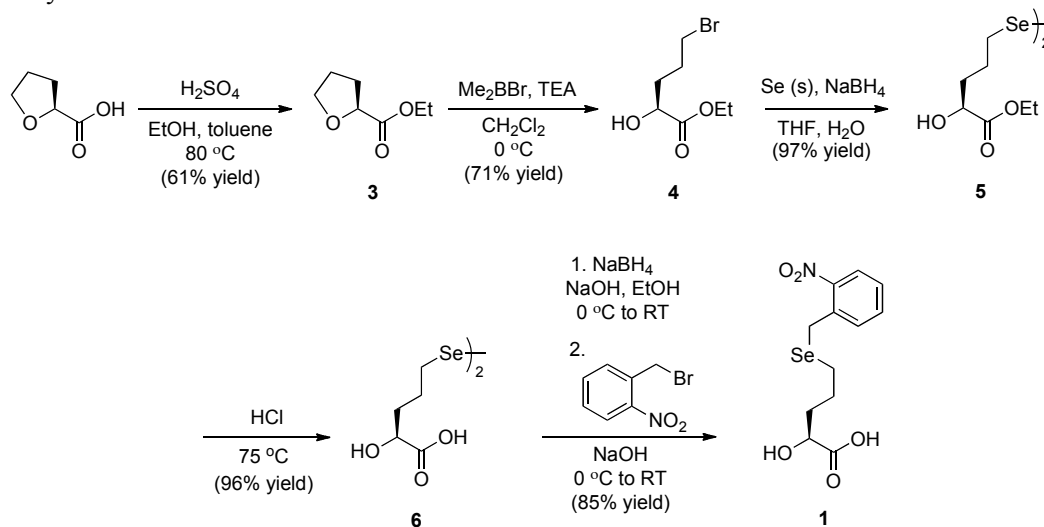
Figure 6.1. Npg and the second-generation SNIPP unnatural α -hydroxy acids, **1** and **2**.

The process proposed in **Figure 6.1**, however, raises many questions. Like all S_N2 reactions, the selenide-induced ester displacement is sensitive to steric effects. As such, the reaction is typically applied to methyl esters, although under optimal conditions and with heating, ethyl, benzyl, and even isopropyl esters along with many lactones are reactive. Certainly, the α -carbon of the α -hydroxy acid that is incorporated will be sterically crowded. The question is whether the intramolecularity of the process, perhaps aided by the inductive effect of the neighboring amide carbonyl, will overcome the steric burden. Caged selenides are not common, and so there is the question of the efficiency of the photochemical step. In addition, selenides are sensitive to oxidation, more so for aliphatic than aromatic (selenophenol) derivatives. On the other hand, an aliphatic selenide might be expected to be the stronger nucleophile, but an aryl selenide has fewer rotatable bonds that need to be restricted in the cyclization reaction.

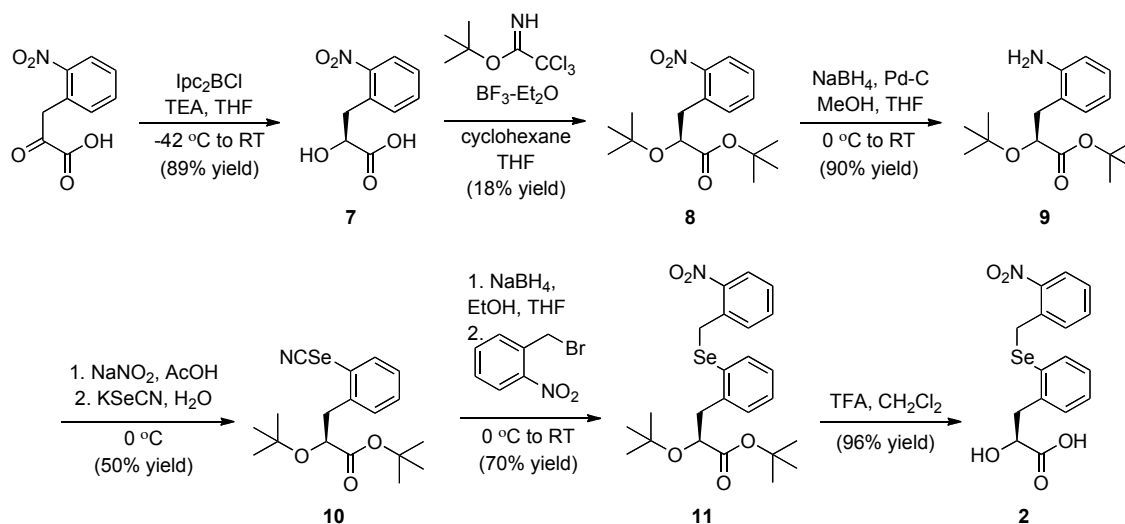
Given these chemical uncertainties, it seemed prudent to first evaluate the viability of the chemistry proposed in **Figure 6.1** before proceeding with chemical biology studies. In the present work we evaluate two structures that are meant to provide such a test. We describe the synthesis and characterization of aliphatic (**1**) and aromatic (**2**) variants of the design, along with mechanistic characterization.

Synthesis of enantiopure **1** (**Scheme 6.1**), as devised and executed by Dr. Amy L. Eastwood²³ and Dr. Niki M. Zacharias,²⁴ began with conversion of *S*-(-)-tetrahydro-2-furoic acid to the ring-opened bromide **4** as previously described.^{25, 26} Conversion to the diselenide, and ester hydrolysis then produced **6**.^{27, 28} Acid diselenide **6** was directly reduced with sodium borohydride and the product alkylated with *o*-nitrobenzyl bromide to give the target compound **1**.²⁹

Scheme 6.1. Synthesis of selenide α -hydroxy acid **1**. This route was devised and executed by Dr. Amy L. Eastwood²³ and Dr. Niki M. Zacharias.²⁴



Scheme 6.2. Synthesis of selenide α -hydroxy acid **2**.

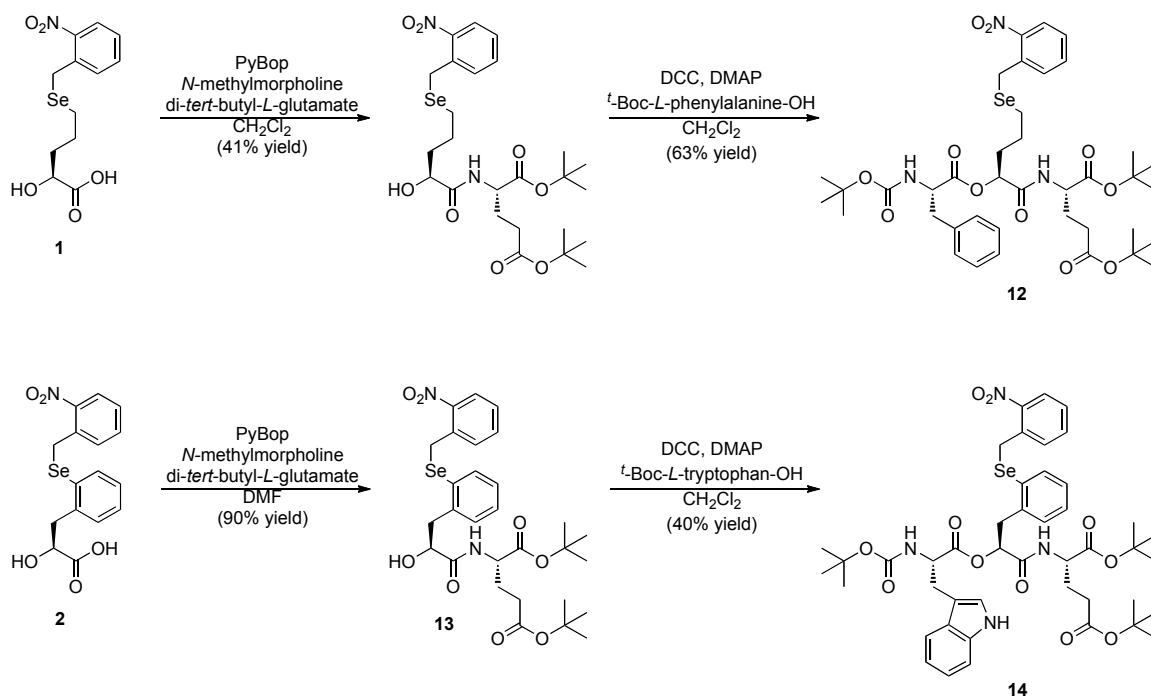


The synthesis of **2** (Scheme 6.2) began with the known reduction of 2-nitrophenylpyruvic acid by (+)- β -chlorodiisopinocampheylborane (“Ipc₂BCl”) to yield **7** in 94% ee.³⁰ The selenocyanate was prepared by a modification of the standard sequence, and the nitrobenzyl group was introduced by reductive alkylation. The bulky *t*-butyl protecting groups were installed to discourage intramolecular cyclization, which was seen when **7** was subjected to reducing conditions, as well as to improve the

solubility and ease of purification of subsequent compounds in the sequence. Alternative synthetic routes were also attempted and are described in Appendix 3.

To evaluate whether the proposed cleavage mechanism was viable, studies in model systems were performed. Depsipeptides **12** and **14** were chosen for synthetic accessibility and because they introduce a UV chromophore into the carboxylate cleavage product. They were prepared through standard solution-phase coupling procedures, employing PyBop/*N*-methylmorpholine and DCC/DMAP for the hydroxy-peptide- and depsipeptide-forming reactions, respectively (**Scheme 6.3**).

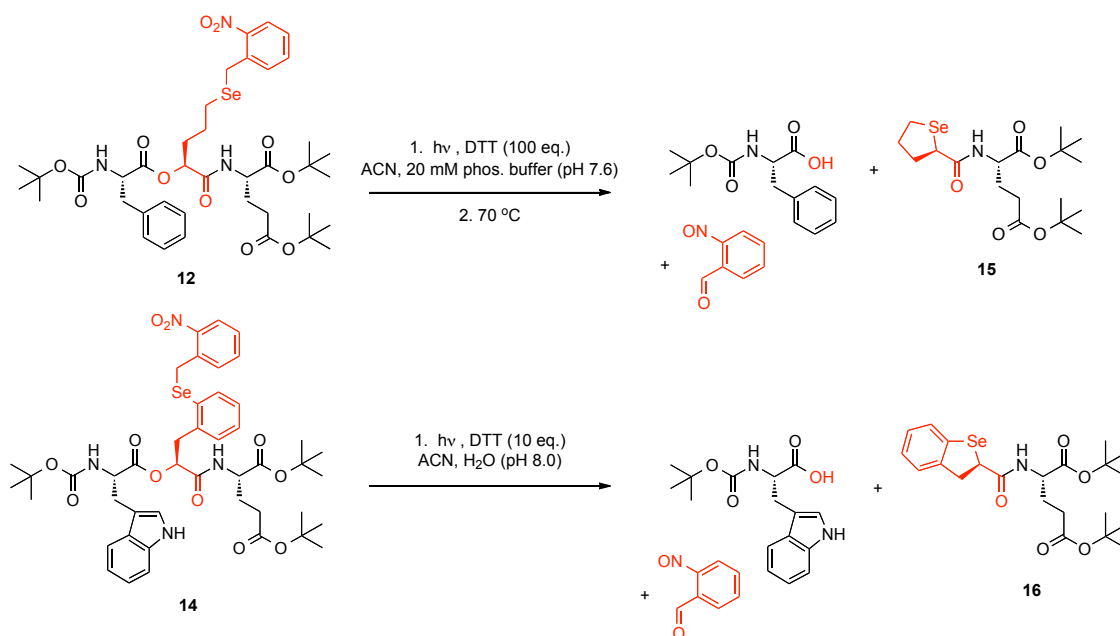
Scheme 6.3. Synthesis of depsipeptides **12** and **14**. Depsipeptide **12** was prepared by Dr. Amy L. Eastwood.²³



Mass spectrometric analysis of initial photolysis studies indicated the formation of the mechanistically revealing selenacyclopentane (**15**, **16**) and the appropriate carboxylic acid, but also suggested several complicating side reactions. Both **12** and **14** produced product *m/z* ratios consistent with the dimer of the deprotected selenide, including the

characteristic isotope pattern for a structure with two selenium atoms. In addition, the aliphatic variant **12** showed m/z ratios consistent with a depsipeptide containing dehydronorvaline (*i.e.*, an allyl side chain), presumably formed by elimination of the selenoxide produced by air oxidation. These undesirable reactions could be suppressed by running the photolyses in the presence of excess dithiothreitol (DTT),³¹ which was expected to discourage both dimerization and oxidation.

Scheme 6.4. Depsipeptide cleavage reactions.



For aryl selenide **14** an unanticipated side product, identified by mass spectrometry, was the depsipeptide in which the original nitrobenzylselenenyl group had been replaced by a hydrogen atom. While this work was in progress, Kitahara and co-workers reported that short wavelength photolysis of arylalkyl selenides can lead to C-Se bond cleavage.³² As suggested by that study, we found that changing the photolysis wavelength from >300 nm (pyrex filter) to >330 nm (uranium glass filter) eliminated this side reaction.

Of course, the novel process of **Figure 6.1** cannot be considered validated without unambiguous confirmation that the selenacyclopentanes **15** and **16** were formed. Using the knowledge gained from the preliminary studies, preparative-scale photolyses were performed (**Scheme 6.4**). For both depsipeptides the selenacyclopentane product could be isolated after irradiation, providing clear support for the proposed scheme; mass spectrometry and NMR spectroscopy confirm product identities. We find that cleavage is more efficient with the aryl selenide (**14**) than the alkyl (**12**), in that isolated yields of the selenacyclopentane are consistently higher (72% vs. 29%). In addition, obtaining significant yields of the selenacyclopentane from the aliphatic system (**12**) required heating the photolysis mixture to ~70 °C, which was not necessary in the case of aryl selenide **14** under optimal photolysis conditions. These observations, coupled with the lack of complications due to olefin formation, suggest that aryl selenide **2** may be the better system to incorporate for subsequent protein and peptide studies.

6.3.1.1 Chemical biology studies of proteolysis by 1 and 2

In preparation for nonsense suppression experiments, the key α -hydroxy acids **1** and **2** were each activated as a cyanomethyl ester and subsequently transesterified by published protocols³³ to yield acylated suppressor tRNA as needed for the following experiments.

6.3.1.2 In vitro studies of proteolysis by 1 and 2

Studies were conducted to determine whether **1** or **2** could promote proteolysis of a full-length protein *in vitro*. These studies used *in vitro* nonsense suppression methodology to incorporate **1** and **2** into the $\alpha 1$ subunit of the muscle-type nicotinic acetylcholine receptor (nAChR) at residue Met243 (located in the M2 transmembrane helix). In these

studies, the $\alpha 1$ subunit of the nAChR contains a hemmagglutinin epitope (in the M3-M4 cytoplasmic loop) to facilitate Western blotting. It was envisioned that cleavage of the nAChR protein backbone at Met243 would yield cleavage fragments that are sufficiently different in molecular weight from the full-length protein to be easily separated by polyacrylamide gel electrophoresis (PAGE) and subsequently visualized by Western blotting. We chose rabbit reticulocyte and wheat germ lysate as our *in vitro* translation systems. Rabbit reticulocyte is generally the preferred system for *in vitro* nonsense suppression, because it tends to yield higher quantities of protein than other systems, but the deep red color of this lysate (owing to its high heme content) was anticipated to complicate experiments requiring irradiation with UV light. Wheat germ lysate generally gives lower protein yields, but it is translucent and therefore more amenable to our experiments. Both systems successfully incorporated **1**, but not **2** into the nAChR. While it is unclear why proteins containing **2** did not express, it is likely that the side chain of this unnatural amino acid was too large or otherwise incompatible with the ribosomes of these translation systems. Proteins containing **1** were susceptible to base (concentrated NH_4OH) cleavage of the backbone ester, but irradiation of the samples never resulted in the appearance of cleavage products when visualized by Western blotting. Attempts to optimize photolysis conditions (including heating the solutions before or after irradiation and increasing the pH of the media) were unsuccessful. Additional *in vitro* studies (also unsuccessful) are described in the theses of Dr. Amy L Eastwood²³ and Dr. Niki M. Zacharias.²⁴

6.3.1.3 Nonsense suppression experiments with **1** and **2** in *Xenopus* oocytes

Nonsense suppression experiments were also conducted in *Xenopus* oocytes. These studies were based on experiments designed to evaluate the effectiveness of Npg, the original unnatural amino acid shown to promote photochemical cleavage of protein backbones. In these experiments, Npg was expressed in the N-terminal domain of the *Drosophila* Shaker B K⁺ channel at residues Leu47 and Pro64.³

The Shaker B (ShB) channel is a voltage-gated ion channel that is comprised of four identical subunits. Each subunit consists of six transmembrane regions, a short intracellular C-terminus and a long intracellular N-terminus (**Figure 6.2**). The pore loop resides between the fifth and sixth transmembrane regions. The first twenty amino acids of the N-terminus form a structural domain or “ball” that is known to inactivate the channel on a millisecond timescale by plugging the channel’s pore (through “ball and chain” or “N-type” inactivation).³⁴ The ball domain is tethered to the remainder of the protein by a “chain” sequence of ~60 amino acids. Channel inactivation occurs when any of the four balls of the homotetrameric protein plug the channel pore. Deletion of the ball and chain regions (residues 6-46) results in the well-characterized ShakerIR (ShIR; where IR stands for “inactivation domain removed”) channel that does not inactivate on a millisecond timescale.³⁵⁻³⁷

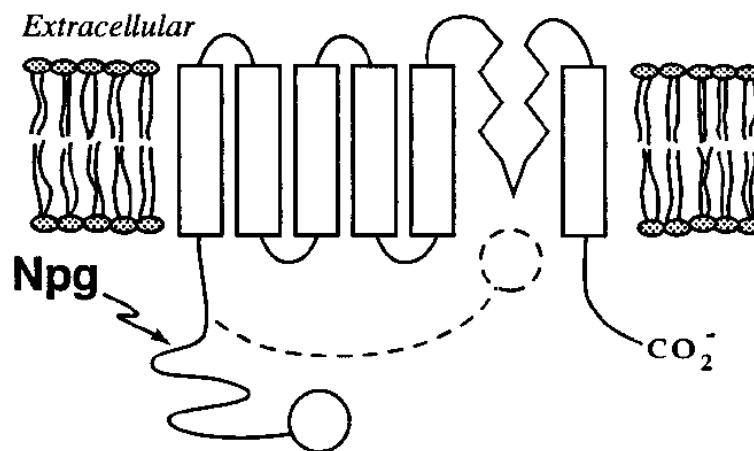


Figure 6.2. Depiction of the topology of the Shaker B K^+ channel and the location of sites used to incorporate Npg. Figure is adapted from England *et al.*³

Npg was inserted at Leu47 and Pro64 in the N-terminal ball and chain domain of ShB.³ Irradiation of the mutant channels lead to cleavage of the inactivation ball (essentially converting the ShB protein into ShIR) and a corresponding reduction in the channel inactivation as measured by two-electrode voltage-clamp electrophysiology. Thus cleavage of the inactivation ball of the ShB protein provides a convenient phenotype for evaluating the effectiveness of **1** and **2** in promoting protein backbone cleavage.

Negative control experiments led us to question the fidelity of nonsense suppression experiments at Leu47 and Pro64 using the amber THG73 suppressor tRNA. These controls included injection of THG73 without an appended amino acid to look for misacylation or “reaminoacylation” – a situation in which the suppressor tRNA is charged with a natural amino acid by an endogenous aminoacyl-tRNA synthetase, which enables incorporation of the natural amino acid at the mutation site. From these controls it was clear that misacylation was likely to be occurring, suggesting that natural amino acids might be incorporated at Leu47 and Pro64 during nonsense suppression

experiments. For this reason, we turned to frameshift nonsense suppression, because the suppressor tRNA used in this methodology is more orthogonal with the *Xenopus* oocyte translational system.^{38, 39}

Compounds **1** and **2** were successfully incorporated into the ShB protein expressed in *Xenopus* oocytes using frameshift nonsense suppression methodology as indicated by the larger currents (10-fold higher) seen for suppression with the unnatural residues relative to control (misacylation) experiments. Unfortunately, irradiation of ShB proteins expressing **1** or **2** did not give the ShIR phenotype, suggesting that, unlike Npg, α -hydroxy acids **1** and **2** could not promote backbone cleavage in these systems. Several attempts were made to optimize the conditions, including increasing the pH of the ND96 recording solution to ensure deprotonation of the selenol (to yield a the more reactive selenide), prolonged irradiation times (5 min to several hrs) with different light sources (a 1000 W Hg/Xe arc lamp and a 288 W Hg lamp), but we were never able to see evidence of backbone cleavage by either compound. Thus, despite their success in cleaving protein backbones of depsipeptide model systems, **1** and **2** have not been shown to be capable of promoting backbone cleavage *in vitro* or *in vivo*.

6.3.2 Strategies based on a photocaged aniline and the chemistry of the NPE protecting group

Two additional strategies for cleaving peptide and protein backbones were also considered. The first was based on an nitroveratryloxycarbonyl (NVOC) caged aniline (**17**) in which the key cleavage reaction is an intramolecular cyclization to afford a δ -lactam (**Figure 6.3**). Incorporation of an α -hydroxy acid at the *i+1* residue yields a strong alkoxide leaving group. The motivation for this strategy came during the synthesis of **2**

Chemical structures of compounds 7 and 17 are shown. Compound 7 is (S)-2-(2-nitrophenyl)-2-hydroxyacetic acid. Compound 17 is (S)-2-(2-((2,4-dimethoxybenzoyloxy)amino)phenyl)-2-aminopropanoic acid.

7) into a protein creates an NPE-protected backbone ester. Irradiation of the protein results in “deprotection” of the ester and cleavage of the protein backbone. This produces two protein fragments— one with a carboxy terminus and another, which is essentially an α,β - unsaturated ketone. We appreciate that the latter product could complicate our studies by serving as a cross-linking agent, but we were still interested in seeing whether this strategy could promote backbone cleavage *in vivo* especially given that we had already synthesized **7** for other purposes (**Scheme 6.2**).

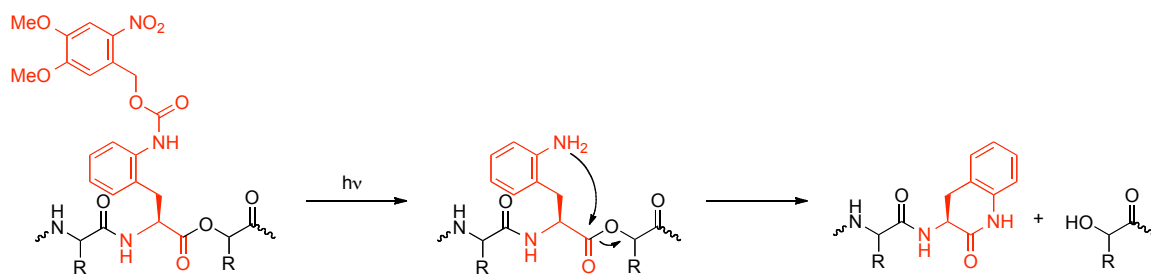


Figure 6.3. Proposed photochemical cleavage strategy using caged aniline 17.

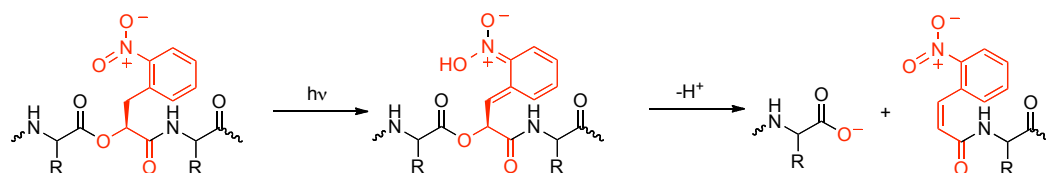
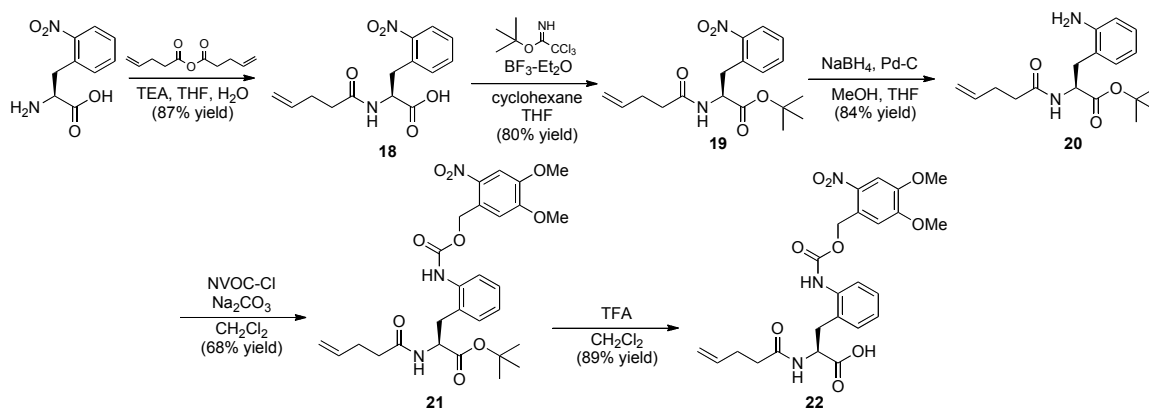


Figure 6.4. Proposed photochemical cleavage strategy using α -hydroxy acid **7**.

The synthesis of the *N*-pent-4-enoyl (4PO) derivative of **17** (**Scheme 6.5**) began with the protection of the α -amino group of *L*-2-nitrophenylalanine as the *N*-pent-4-enoyl (4PO) derivative (cleavable by treatment with I_2)^{3, 42, 43} and the carboxylic acid as the *t*-butyl ester (to prevent intramolecular cyclization) using standard protocols. Afterward, the nitro group was reduced following the protocol used in **Scheme 6.2**, and the resulting aniline was caged with a photocleavable nitroveratryloxycarbonyl (NVOC) group. Removal of the *t*-butyl protecting group gave the desired product **22**. In preparation for nonsense suppression experiments, **7** and **22** were activated as cyanomethyl esters and subsequently transesterified according to published protocols³³ to yield acylated TQOps' (opal suppressor tRNA for TGA stop codon), THG73 (amber suppressor tRNA for TAG stop codon), and YFaFs (suppressor tRNA for GGGT frameshift codon) suppressor tRNA.

Scheme 6.5. Synthesis of the *N*-pent-4-enoyl (4PO) derivative of **17**.



6.3.2.1 Nonsense suppression experiments with **7** and **17** in *Xenopus oocytes*

Given that the caged aniline-based strategy described in **Figure 6.3** requires the incorporation of two adjacent unnatural amino acids (**17** and an α -hydroxy acid in the *i*+1

position), it seemed prudent to find an appropriately tolerant site in the N-terminal region of the ShB protein (in order to make use of the ShB to ShIR cleavage phenotype).

Several combinations of stop codons and the four-base codon were used in initial screens of Pro64 (a site that Npg was incorporated at) and the *i+1* residue Lys65 (**Table 6.1**). Pro and Vah (valine, α -hydroxy) were used as indicators of the maximal current values that could be expected for nonsense suppression experiments with each codon combination. Unacylated suppressor tRNA (represented in **Table 6.1** as a dash (-)) was also used as a misacylation control. As shown in **Table 6.1**, only the Pro65TGA/Lys65TAG and Pro65GGGT/Lys65TAG combinations gave current in these experiments, and no current was seen in misacylation control experiments after a 24 hr of incubation period. To our knowledge, this is the first example of double nonsense suppression at sites that are adjacent in sequence.

Table 6.1. Current (I_{\max}) obtained for control studies of Pro64 and Lys65 in ShB using different codon combinations. “n.r.” stands for no response. A dash (-) represents a misacylation control experiment. “WT” is the wild-type ShB protein.

Mutation	Residue at Pro64	Residue at Lys65	I_{\max} (μ A)	Incubation Time (hr)
WT			42 ± 5.6	12
ShB(Pro64TGA)/(Lys65TAG)	-	Vah	n.r.	24
	Pro	-	n.r.	24
	Pro	Vah	8.3 ± 1.1	24
ShB(Pro64GGGT)/(Lys65TAG)	-	Vah	n.r.	24
	Pro	-	n.r.	24
	Pro	Vah	5.5 ± 0.91	24
ShB(Pro64GGGT)/(Lys65TGA)	-	-	n.r.	24
	Pro	Vah	n.r.	24
ShB(Pro64TAG)/(Lys65TGA)	-	-	n.r.	24
	Pro	Vah	n.r.	24

Given these results, we then incorporated **7** and **17** at Pro64 using the TAG stop codon or GGGT frameshift codon. After 48 hrs of incubation, current was seen for proteins injected with **7** and **17**, but the I_{\max} values were on the order of what was seen for misacylation control experiments (**Table 6.2**), which questioned the fidelity of these

experiments. Irradiation of oocytes injected with **7** and **17** had no effect on the inactivation of the ShB currents, suggesting that these residues cannot cleave the peptide backbone or that **7** and **17** did not actually incorporate into the protein and the currents observed are the result of misacylation of the suppressor tRNA (incorporation of a natural amino acid at the Pro64 site).

Table 6.2. Current (I_{\max}) obtained for studies with **7** and **17** at Pro64 in ShB. “n.r” stands for no response. A dash (-) represents a misacylation control experiment. Note that no current was seen after 24 hours for **7** or **17**. “WT” is the wild-type ShB protein.

Mutation	Residue at Pro64	I_{\max} (μ A)	Incubation Time (hr)
WT		52 ± 10	12
ShB(Pro64TGA)	-	8.7 ± 2	48
	7	0.99 ± 1	48
	17	n.r.	48
ShB(Pro64GGGT)	-	4.7 ± 0.7	48
	7	8.3 ± 2	48
	17	12 ± 2	48

We then repeated these experiments with **17** at Pro64 and Vah at Lys65 (to give a better leaving group for the cleavage reaction). Unfortunately, no current was seen for these experiments for reasons that we do not presently understand. Future work could revisit these studies by trying different residues in the ShB protein or a different α -hydroxy acid at the $i+1$ residue.

During the course of our studies, Schultz and co-workers reported a photochemical cleavage strategy that is nearly identical to **Figure 6.4** and is based on the amino acid derivative of **7** (2-nitrophenylalanine).⁸ They showed that 2-nitrophenylalanine could promote backbone cleavage of model peptides and also of a model protein, T4 lysozyme, expressed in *E. coli*, albeit with only 30% photochemical cleavage efficiency of the latter system. These findings are certainly encouraging (if not

overlapping) and so it would be interesting to revisit the studies of **7** to determine the origin of our photolysis problems.

6.4 DISCUSSION

In summary, we first described novel chemistry in which a photochemically-liberated selenide undergoes an intramolecular S_N2 reaction, cleaving an ester that results from the incorporation of the α -hydroxy acids **1** or **2** into a peptide. These studies suggest that for chemical biology applications, aryl selenide **2** is the preferred substrate. Two side reactions have been discovered that must be considered in possible chemical biology applications: dimerization and oxidation. For studies involving peptides prepared by SPPS, adding DTT and controlling the concentration might be appropriate. For *in vivo* nonsense suppression expression experiments, where protein concentrations are typically low, dimerization may be less likely. In addition, the reducing conditions inside cells likely will discourage dimerization and oxidation. Unfortunately, our initial efforts to see backbone cleavage by **1** or **2** *in vivo* and *in vitro* have been unsuccessful, but additional studies should be conducted to determine whether other applications of this methodology are possible.

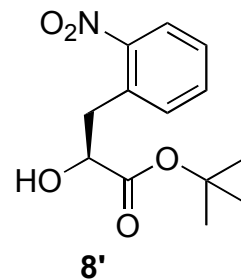
We also described two alternative strategies for photochemical protein cleavage that were inspired by chemistry we encountered during our synthesis of **2**. These strategies are based on (1) intramolecular cyclization and backbone cleavage by a photochemically-liberated aniline nucleophile and (2) the photochemistry of (2-nitrophenyl)ethyl derivatives. These new unnatural amino acids were successfully synthesized, but photolysis studies in proteins expressed in *Xenopus* oocytes have been unsuccessful thus far.

6.5 EXPERIMENTAL SECTION

Chemical synthesis. All reactions were performed at ambient temperature and pressure unless otherwise noted. All reactions involving potentially air-sensitive compounds were conducted under an inert atmosphere using Schlenk techniques. Solvents were purified by passage through alumina. Unless otherwise noted, all chemicals and reagents were used as received without further purification. Compounds **3**,²⁵ **4**,²⁶ and **7**³⁰ were prepared according to published protocols. The syntheses of **1** and **12** were performed by Dr. Amy L. Eastwood²³ and Dr. Niki M. Zacharias²⁴ and are described in their respective theses and also in Eastwood *et al.*⁴⁴ Flash chromatography was performed with EMD silica gel 60 (particle size 0.040-0.063 mm). Thin-layer chromatography (TLC) was performed using EMD silica gel 60 F₂₅₄ precoated plates (0.25 mm) and visualized by UV light, potassium permanganate, ceric ammonium molybdate, or ninhydrin. Nuclear magnetic resonance spectroscopy (NMR) was performed on either a Varian Mercury 300 or a Varian Inova 500 instrument and spectra resonances are assigned relative to Me₄Si (δ 0.0) or CD₃OD (δ 3.31 for ¹H NMR and δ 49.1 for ¹³C NMR). Data for ¹H NMR spectra are reported as follows: chemical shift (δ ppm), integration, multiplicity, and coupling constant (Hz). Data for ¹³C NMR spectra are reported as chemical shift (δ ppm). High-resolution mass spectrometry (HRMS) spectra were obtained from the Caltech Mass Spectrometry Lab. Electrospray ionization mass spectrometry (ESI-MS) used to analyze the proteolysis reactions was performed using an LCQ Classic ion trap (ThermoFinnigan) in direct infusion mode. A uranium glass absorption sleeve was prepared by the Caltech Glassblowing Shop.

Synthesis of di-*tert*-butyl-protected nitrophenylalanine derivative (8**) and *tert*-butyl-protected nitrophenylalanine derivative (where the secondary alcohol is not protected) (**8'**).**

α -Hydroxy acid **7** (0.200 g, 0.947 mmol, 1 eq) was placed in a 2-neck round-bottom flask under Ar (g) and dissolved in THF (3 mL) and cyclohexane (3.5 mL). A solution of *tert*-butyl-2,2,2-trichloroacetimidate (0.678 mL, 3.79 mmol, 4 eq) in cyclohexane (3.5 mL) was added simultaneously with boron



trifluoride diethyletherate (0.041 mL, 0.33 mmol, 0.35 eq). The reaction stirred for 45 minutes until it was quenched with saturated NaHCO₃ (aq). The organics were extracted with Et₂O (3×), washed with brine, dried over MgSO₄, and concentrated. The resulting white sludge was suspended in hexanes, filtered, and then purified by flash column chromatography (15% EtOAc in hexanes) to afford two fractions: compound **8** (0.0550 g, 0.170 mmol, 18% yield) and compound **8'** (0.101 g, 0.379 mmol, 40% yield) as clear oils. *R_f* of **8** = 0.71 (30% EtOAc in hexanes); ¹H NMR of **8** (300 MHz, CDCl₃, 298 K) δ 7.91 (1H, d, *J* = 8.0 Hz), 7.50 (1H, m), 7.37 (2H, m), 4.14 (1H, dd, *J* = 8.9, 4.9 Hz), 3.29 (1H, dd, *J* = 13.2, 4.9 Hz), 3.13 (1H, dd, *J* = 13.2, 9.1 Hz) 1.39 (9H, s), 0.95 (9H, s); ¹³C NMR of **8** (75 MHz, CDCl₃, 298 K) δ 172.9, 149.9, 134.5, 132.9, 132.6, 127.9, 124.7, 81.2, 75.2, 71.8, 37.7, 28.0, 27.6; HRMS (FAB) of **8** *m/z* calc'd for C₁₇H₂₆NO₅ [M+H]⁺: 324.1811, found 324.1820. *R_f* of **8'** = 0.44 (30% EtOAc in hexanes); ¹H NMR of **8'** (300 MHz, CDCl₃, 298 K) δ 7.90 (1H, d, *J* = 8.1 Hz), 7.51 (1H, m), 7.40 (2H, m), 4.34 (1H, dd, *J* = 8.1, 4.1 Hz), 3.48 (1H, dd, *J* = 13.8, 4.3 Hz), 3.13 (1H, dd, *J* = 13.9, 8.3 Hz), 1.42 (9H, s); ¹³C NMR of **8'** (75 MHz, CDCl₃, 298 K) δ 173.5, 150.1, 133.4, 133.0, 132.4, 128.1, 125.0, 83.3, 70.7, 37.5, 28.1; HRMS (FAB) of **8'** *m/z* calc'd for C₁₃H₁₈NO₅

[M+H]: 268.1185, found 268.1193. An enantiomeric excess of 94% was obtained for **8'** by analytical chiral HPLC analysis using a Chiralcel OD-H column (4.6 mm × 25 cm) from Daicel Chemical Industries, Ltd. with 2% isopropyl alcohol in hexanes.

Synthesis of aniline (9). Di-*tert*-butyl-protected nitrophenylalanine derivative **8** (0.606 g, 1.87 mmol, 1 eq) was placed in a 2-neck round-bottom flask under Ar (g) and dissolved in THF (30 mL) and MeOH (15 mL) at 0 °C. To this was added 10 wt % palladium on activated carbon (0.050 g) and sodium borohydride (0.141 g, 3.74 mmol, 2 eq). The reaction was followed by TLC using ninhydrin staining. The solution was stirred for 40 minutes and was then quenched with water and filtered through a pad of Celite™. The filtrate was extracted with Et₂O (3×), washed with brine, dried over MgSO₄, and concentrated to afford a pale yellow oil. The resulting liquid was purified by flash column chromatography (15% EtOAc in hexanes) to afford aniline **9** as a pale yellow oil (0.493 g, 1.68 mmol, 90% yield). *R*_f = 0.59 (30% EtOAc in hexanes); ¹H NMR (300 MHz, CDCl₃, 298 K) δ 7.27 (1H, d, *J* = 8.9 Hz), 7.17 (1H, t, *J* = 7.4 Hz), 7.04 (1H, d, *J* = 7.3 Hz), 6.83 (1H, t, *J* = 7.3 Hz), 3.99 (1H, dd, *J* = 7.8, 2.3 Hz), 2.96 (1H, dd, *J* = 13.8, 10.4 Hz), 2.68 (1H, dd, *J* = 13.8, 9.1 Hz), 1.46 (9H, s), 0.98 (9H, s); ¹³C NMR (75 MHz, CDCl₃, 298 K) δ 173.5, 149.9, 130.3, 127.8, 123.8, 121.0, 114.2, 81.6, 75.6, 74.8, 35.5, 28.0, 27.4; HRMS (ESI) *m/z* calc'd for C₁₇H₂₇NO₃ [M+H]: 294.2069, found 294.2058.

Synthesis of selenocyanate (10). Aniline **9** (0.248 g, 0.845 mmol, 1.0 eq) was placed in a round-bottom flask, dissolved by sonication in AcOH (17 mL), and cooled to 0 °C. To this solution was quickly added 3 M sodium nitrite (0.34 mL, 1.02 mmol, 1.21 eq) via syringe. The solution stirred for 1 hour and was monitored by TLC using ninhydrin

staining. The pH of the solution was then increased to ~6 by the addition of 10 wt % NaOH. To this was added potassium selenocyanate (0.366 mL, 2.54 mmol, 4.2 eq) in H₂O (36 mL) and the solution stirred for an additional 30 min. The organics were extracted with Et₂O (3×), washed with brine, filtered through a pad of Celite™, dried over MgSO₄, and concentrated. The resulting orange solid was purified by flash column chromatography (20% EtOAc in hexanes) to afford selenocyanate **10** as a yellow, non-crystalline solid (0.162 g, 0.423 mmol, 50% yield). R_f = 0.83 (40% EtOAc in hexanes); ¹H NMR (300 MHz, CDCl₃, 298 K) δ 7.82 (1H, d, J = 7.6 Hz), 7.26 (3H, m), 3.82 (1H, dd, J = 8.7, 4.7 Hz), 3.06 (2H, m, J = 9.48, 4.53 Hz), 1.46 (9H, s), 0.92 (9H, s); ¹³C NMR (75 MHz, CDCl₃, 298 K) δ 172.4, 139.2, 134.0, 131.1, 129.6, 128.7, 127.6, 105.2, 81.5, 76.2, 73.1, 40.3, 28.0, 27.4; HRMS (ESI) m/z calc'd for C₁₈H₂₅NO₃Se [M+H]: 384.1078, found 384.1073.

Synthesis of *tert*-butyl-protected arylalkyl selenide (11). Selenocyanate **10** (0.161 g, 0.421 mmol, 1 eq) was placed in a 2-neck round-bottom flask under Ar (g) and dissolved in THF (7 mL) at 0 °C. To this was added a solution of sodium borohydride (0.019 g, 0.505 mmol, 1.2 eq) in EtOH (1 mL) and the solution stirred for 1 hr. A solution of 2-nitrobenzylbromide (0.118 g, 0.547 mmol, 1.3 eq) in THF (5.5 mL) was then added. After this addition, the solution was allowed to warm to room temperature and was stirred for 3 hours until it was quenched with H₂O. The organics were extracted with Et₂O (3×), washed with brine, filtered through a pad of Celite™, dried over MgSO₄, and concentrated. The resulting solid was purified by flash column chromatography (15% EtOAc in hexanes) to afford *tert*-butyl protected arylalkyl selenide **11** as a yellow, non-crystalline solid (0.145 g, 0.295 g, 70% yield). R_f = 0.65 (30% EtOAc in hexanes); ¹H

NMR (300 MHz, CDCl₃, 298 K) δ 8.00 (1H, d, J = 7.2 Hz), 7.45 (1H, d, J = 7.1 Hz), 7.35 (2H, m), 7.21 (2H, m), 7.09 (1H, m), 6.99 (1H, m), 4.33 (2H, s), 4.15 (1H, m), 3.16 (1H, dd, J = 9.90, 4.53 Hz), 2.96 (1H, dd, J = 8.24, 5.36 Hz), 1.43 (9H, s); ¹³C NMR (75 MHz, CDCl₃, 298 K) δ 173.2, 141.2, 136.2, 135.5, 133.2, 132.1, 131.8, 130.9, 128.3, 128.0, 127.6, 125.6, 80.9, 74.9, 72.8, 40.9, 30.0, 28.0, 27.7, 22.4; HRMS (FAB) m/z calc'd for C₂₄H₃₁NO₅Se [M⁺]: 493.1367, found 493.1374.

Synthesis of arylalkyl selenide α -hydroxy acid (2). *tert*-Butyl protected arylalkyl selenide **11** (0.533 g, 1.08 mmol) was placed in a 2-neck round-bottom flask under Ar (g) and dissolved in CH₂Cl₂ (8 mL). To this was added trifluoroacetic acid (4 mL) and the solution stirred for 16 hours. The reaction mixture was concentrated to afford a yellow-orange solid, which was triturated with ether. The resulting yellow solid was dissolved in EtOAc (3 \times), rinsed with 1 N HCl, rinsed with H₂O, and then added to 5% NaHCO₃. The organic layer (colorless) was discarded, and the pH of the aqueous layer was decreased to pH 2 by the addition of 6 N HCl. The organics were extracted into EtOAc (3 \times), rinsed with brine, dried over MgSO₄, and concentrated to afford arylalkyl selenide α -hydroxy acid **2** as a yellow, non-crystalline solid (0.195 g, 0.512 mmol, 96% yield). $[\alpha]_D^{24}$ = -45.3° (c = 1, CHCl₃); ¹H NMR (300 MHz, CDCl₃, 298 K) δ 7.99 (1H, d, J = 6.6 Hz), 7.47 (1H, d, J = 7.7 Hz), 7.37 (2H, m), 7.28 (2H, m), 7.14 (1H, m), 7.01 (1H, d, J = 6.9 Hz), 4.35 (3H, m), 3.30 (1H, dd, J = 13.7, 4.40 Hz), 3.03 (1H, dd, J = 13.2, 8.5 Hz); ¹³C NMR (75 MHz, CDCl₃, 298 K) δ 178.3, 147.8, 139.9, 136.9, 135.2, 133.4, 132.2, 131.0, 130.7, 129.1, 128.2, 128.1, 125.7, 71.2, 40.4, 30.3; HRMS (FAB) m/z calc'd for C₁₆H₁₅NO₅Se [M+H]: 382.0194, found 382.0191.

Synthesis of aryl selenide-glutamate hydroxy-peptide (13). Arylalkyl selenide α -hydroxy acid **2** (0.091 g, 0.239 mmol, 1 eq), di-*tert*-butyl-L-glutamate (0.106 g, 0.359 mmol, 1.5 eq), and benzotriazol-1-yl-oxytripyrrolidinophosphonium hexafluorophosphate (0.149 g, 0.287 mmol, 1.2 eq) were placed in a round-bottom flask under Ar (g) and dissolved in CH₂Cl₂ (1.8 mL). To this was added *N*-methylmorpholine (0.09 mL, 0.790 mmol, 3.3 eq) via syringe, and the reaction stirred for 24 hours. The reaction mixture was then diluted with EtOAc, and the resulting solution was washed with 1 M KHSO₄ (2 \times), H₂O, 5% NaHCO₃ (2 \times), and brine. The organic layer was passed through a pad of Celite™, dried over MgSO₄, and concentrated. The resulting solid was purified by flash column chromatography (30% EtOAc in hexanes) to afford hydroxy-peptide **13** as a yellow oil (0.134 g, 0.215 mmol, 90% yield). *R*_f = 0.49 (50% EtOAc in hexanes); ¹H NMR (300 MHz, CDCl₃, 298 K) δ 7.98 (1H, d, *J* = 7.4 Hz), 7.45 (1H, d, *J* = 7.4 Hz), 7.36 (2H, m), 7.26 (2H, m), 7.10 (1H, m), 6.99 (1H, m), 4.46 (1H, m), 4.25 (1H, m), 3.30 (1H, dd, *J* = 14.0, 3.6 Hz), 2.96 (2H, m), 2.14 (3H, m), 1.86 (1H, m), 1.45 (18H, s); ¹³C NMR (75 MHz, CDCl₃, 298 K) δ 172.7, 172.2, 171.0, 148.0, 140.9, 136.9, 135.0, 133.4, 132.2, 131.1, 130.9, 129.2, 128.3, 128.0, 125.7, 82.6, 80.9, 72.9, 52.1, 41.1, 31.6, 30.3, 28.3, 28.2, 27.9; HRMS (FAB) *m/z* calc'd for C₂₉H₃₈N₂O₈Se [M+H]⁺: 623.1871, found 623.1881.

Synthesis of tryptophan-aryl selenide-glutamate depsipeptide (14). Hydroxy-peptide **13** (0.140 g, 0.225 mmol, 1 eq), *N* α -(*tert*-butoxycarbonyl)-*L*-tryptophan (0.137 g, 0.450 mmol, 2 eq), 4-(dimethylamino)pyridine (0.014 g, 0.113 mmol, 0.5 eq), and *N,N'*-dicyclohexylcarbodiimide (0.093g, 0.450 mmol, 2 eq) were placed in a round-bottom flask under Ar (g) and dissolved in CH₂Cl₂ (5 mL). After stirring for 48 hours, the

reaction mixture was diluted with EtOAc. The solution was washed with 1 M KHSO₄ (2×), H₂O, 5% NaHCO₃ (2×), and brine. The organic layer was filtered through a pad of Celite™, dried over MgSO₄, and concentrated. The resulting solid was purified by flash column chromatography (35% EtOAc in hexanes) to afford depsipeptide **14** as a pale yellow, non-crystalline solid (0.0817 g, 0.0900 mmol, 40% yield). R_f = 0.34 (50% EtOAc in hexanes); ¹H NMR (500 MHz, CDCl₃, 298 K) δ 8.52 (1H, b), 7.98 (1H, m), 7.57 (1H, d, J = 7.9 Hz), 7.41 (1H, d, J = 7.7 Hz), 7.34 (3H, m), 7.18 (3H, m), 7.10 (2H, m), 7.02 (1H, s), 6.91 (1H, m), 5.25 (1H, m), 4.98 (1H, d, J = 7.5 Hz), 4.57 (1H, dd, J = 12.6, 5.3 Hz), 4.41 (1H, m), 4.24 (2H, s), 3.17 (2H, m), 2.20 (1H, m), 2.08 (2H, m), 1.79 (1H, m), 1.48 (9H, s), 1.45 (9H, s), 1.31 (9H, s). ¹³C NMR (125 MHz, CDCl₃, 298 K) δ 172.4, 171.2, 169.0, 156.0, 148.0, 139.7, 136.7, 136.4, 135.1, 133.3, 132.1, 131.3, 131.0, 129.0, 128.2, 128.1, 128.0, 125.7, 123.9, 122.3, 122.3, 119.8, 118.9, 111.5, 109.6, 82.3, 80.9, 80.1, 75.1, 54.6, 52.4, 37.7, 34.2, 31.8, 30.3, 28.5, 28.4, 28.2, 27.6; HRMS (ESI) m/z calc'd for C₄₅H₅₆N₄O₁₁Se [M+H]: 909.3229, found 909.3238.

Synthesis of selenacyclopentane (15). Depsipeptide **12** (0.0722g, 0.088 mmol, 1 eq) was placed in a pyrex reaction vessel and dissolved in acetonitrile (125 mL). To this was added dithiothreitol (1.36 g, 8.8 mmol, 100 eq) and 20 mM phosphate buffer, pH 7.6 (125 mL). The resulting solution was stirred under N₂ (g), and a 450 W medium-pressure mercury-vapor UV immersion lamp (ACE Glass), filtered with a pyrex glass absorption sleeve and equipped with a water cooling jacket, was assembled and attached to the reaction vessel. The progress of the reaction was followed by ESI-MS. After 1 hour of photolysis (at which point the temperature of the reaction had increased from 25 °C to 32 °C) the two major m/z ratios seen in the mass spectrum of the reaction were the

depsipeptide **12** ($[M+Na^+] = 844\ m/z$) and the nitrobenzyl-deprotected selenol ($[M+Na^+] = 709\ m/z$). After 5 hours of photolysis, the m/z ratio attributed to **12** ($[M+Na^+] = 844\ m/z$) had diminished to a negligible level while the m/z ratios corresponding to the nitrobenzyl-deprotected selenol ($[M+Na^+] = 709\ m/z$), the nitrobenzyl-deprotected diselenide ($[M+Na^+] = 1391\ m/z$), the olefin-containing depsipeptide derived from the oxidative elimination of the selenium ($[M+Na^+] = 627\ m/z$), and the desired selenacyclopentane **15** ($[M+Na^+] = 444\ m/z$) persisted. At this time, the reaction was removed from the photoreactor, heated to 70 °C, and monitored by ESI-MS. After 3 hours of heating at this temperature, both nitrobenzyl-deprotection products (m/z ratios 709 and 1391) were no longer detectable, but the m/z ratio attributed to the desired selenacyclopentane **15** ($[M+Na^+] = 444\ m/z$) and a m/z ratio corresponding to its dimer ($[M+Na^+] = 865\ m/z$) remained. The resulting mixture was extracted with EtOAc (2×), dried over $MgSO_4$, and concentrated. The crude product was purified twice by flash column chromatography (both began with 11% EtOAc in hexanes then were changed to 33% EtOAc in hexanes after the DTT eluted, both were dry loaded in CH_2Cl_2) to afford selenacyclopentane **15** as a yellow oil (0.0107 g, 0.0255 mmol, 29% yield). $R_f = 0.28$ (33% EtOAc in hexanes); $[\alpha]^{24}_D = -16.0^\circ$ ($c = 1$, $CHCl_3$); 1H NMR (500 MHz, $CDCl_3$, 298 K) δ 7.08 (1H, d, $J = 13.5$ Hz), 4.44 (1H, dt, $J = 13.5, 8$ Hz), 4.08 (1H, m), 3.15 (1H, m), 2.97 (1H, m), 2.37 (1.5H, m), 2.26 (1.5H, m), 2.14 (4H, m), 1.92 (1H, m), 1.47 (9H, s), 1.44 (9H, s); ^{13}C NMR (125 MHz, $CDCl_3$, 298 K) δ 172.3, 172.1, 170.8, 82.3, 80.7, 52.845.4, 37.4, 32.4, 31.5, 28.1, 28.0, 27.5, 27.1. HRMS (TOF) m/z calc'd for $C_{18}H_{31}NO_5Se$ $[M+H]^+$: 422.1446, found 422.1465.

Synthesis of aryl selenacyclopentane (16). Depsipeptide **14** (0.0230 g, 0.0250 mmol, 1 eq) was placed in a pyrex reaction vessel and dissolved in acetonitrile (125 mL). To this was added dithiothreitol (0.0390 g, 0.250 mmol, 10 eq) and pH 8 H₂O (125 mL). The resulting solution was stirred under N₂ (g), and a 450 W medium-pressure mercury-vapor UV immersion lamp (ACE Glass), filtered with a uranium glass absorption sleeve and equipped with a water cooling jacket, was assembled and attached to the reaction vessel. The progress of the reaction was followed by ESI-MS. After 1 hour of photolysis, three *m/z* ratios were seen in the mass spectrum of the reaction: the depsipeptide **14** ($[M+Na^+] = 931\ m/z$), the nitrobenzyl deprotected aryl selenol ($[M+Na^+] = 796\ m/z$), and the desired aryl selenacyclopentane **16** ($[M+Na^+] = 492\ m/z$). No *m/z* ratio corresponding to the nitrobenzyl deprotected diselenide ($[M+Na^+] = 1567\ m/z$) was observed. After 2 hours, both *m/z* ratios attributed to **14** ($[M+Na^+] = 931\ m/z$) and the nitrobenzyl-deprotected aryl selenol ($[M+Na^+] = 796\ m/z$) had diminished to a negligible level while a *m/z* ratio corresponding to the desired aryl selenacyclopentane **16** ($[M+Na^+] = 492\ m/z$) persisted. At this time, the reaction was removed from the photoreactor. The acetonitrile was then removed *in vacuo*, and the resulting aqueous solution was extracted with Et₂O (3×), washed with brine, dried over MgSO₄, and concentrated. The resulting yellow oil was purified by flash column chromatography (15% EtOAc in hexanes) to afford aryl selenacyclopentane **16** as a pale yellow oil (0.00843 g, 0.0180 mmol, 72% yield). *R_f* = 0.59 (30% EtOAc in hexanes); $[\alpha]^{24}_D = -80.5^\circ$ (*c* = 1, CHCl₃); ¹H NMR (300 MHz, CDCl₃, 298 K) δ 7.30 (1H, m), 7.20 (1H, m), 7.12 (2H, m), 7.29 (2H, m), 6.92 (1H, d, *J* = 7.41 Hz), 4.50 (1H, dd, *J* = 8.2, 5.2 Hz), 4.43 (1H, dd, *J* = 7.8, 4.7 Hz), 2.25 (2H, m), 2.15 (1H, m), 1.91 (1H, m), 1.44 (9H, s), 1.41 (9H, s); ¹³C NMR (75 MHz, CDCl₃, 298

K) δ 172.4, 171.4, 170.7, 141.7, 135.3, 128.0, 125.9, 125.7, 125.5, 82.6, 81.0, 53.1, 45.9, 41.7, 31.6, 29.9, 28.3, 28.1; HRMS (ESI) m/z calc'd for $C_{22}H_{31}NO_5Se$ [M+H]: 470.1446, found 470.1469.

Synthesis of the cyanomethyl ester of 2. Compound **2** (0.12 g, 0.032 mmol, 1 eq) was added to a 20 mL scintillation vial. To this was added chloroacetonitrile (0.10 mL, 1.6 mmol, 50 eq) and triethylamine (0.013 mL, 0.095 mmol, 3 eq). The resulting mixture stirred for 6 hours. Then 10 mL of H_2O was added and the organics were extracted with CH_2Cl_2 (3 \times), washed with brine, dried over Na_2SO_4 , concentrated, and then purified by flash column chromatography (50% EtOAc in hexanes) to afford the cyanomethyl ester of **2** as a yellow oil (0.010 g, 0.024 mmol, 76% yield). R_f = 0.40 (50% EtOAc in hexanes); 1H NMR (300 MHz, $CDCl_3$, 298 K) δ 8.01 (1H, d, J = 9.5 Hz), 7.52 (1H, d, J = 7.6 Hz), 7.34 (3H, m), 7.22 (1H, m), 7.17 (1H, m), 6.97 (1H, m), 4.77 (2H, b), 4.34 (3H, b), 3.16 (1H, dd, J = 13.7, 4.5 Hz), 2.94 (1H, dd, J = 13.8, 8.5 Hz), 2.64 (1H, d, J = 5.6 Hz); ^{13}C NMR (75 MHz, $CDCl_3$, 298 K) δ 172.7, 139.6, 137.2, 135.1, 133.3, 132.0, 132.0, 130.9, 130.6, 129.2, 128.3, 128.3, 125.7, 114.0, 71.1, 49.1, 40.6, 30.5; HRMS (FAB+) m/z calc'd for $C_{18}H_{17}N_2O_5Se$ [M+H]: 421.0303, found 421.0303. A similar protocol was used to synthesize the cyanomethyl ester of **1** and is described in the theses of Dr. Amy L. Eastwood²³ and Dr. Niki M. Zacharias.²⁴

Synthesis of 4PO-protected nitrophenylalanine 18. *L*-2-nitrophenylalanine (CSPS Pharmaceuticals) (1.5 g, 7.1 mmol, 1 eq) was added to a 20 mL round-bottom flask under Ar (g) and suspended in 20 mL of THF and 10 mL of H_2O . The resulting suspension was placed in an ice bath. To this was added triethylamine (2.1 mL, 15 mmol), 2.1 eq). Pent-4-enoic anhydride (1.5 mL, 8.5 mmol, 1.2 eq) was then added dropwise. After 1 hour of

stirring, an addition 0.5 mL of triethylamine (3.6 mmol) and 0.5 mL of pent-4-enoic anhydride (2.8 mmol) was added. The solution was stirred for 1 more hour and then 50 mL of 0.2 M NaHSO₄ was added. The pH of the resulting solution was increased to pH 9 by addition of 2M NaOH. The organics were extracted with Et₂O and discarded. The pH of the aqueous layer was then decreased to pH 2 via addition of 6 M HCl. The organics were extracted with EtOAc (3×), washed with 0.2 M NaHSO₄, washed with brine, dried over Na₂SO₄, filtered, and concentrated. The resulting yellow liquid was purified by flash column chromatography (0.9% formic acid and 32% hexanes in EtOAc) to afford 4PO-protected nitrophenylalanine **18** as a yellow oil (1.8 g, 6.2 mmol, 87% yield). *R*_f = 0.46 (0.9% formic acid and 32 % hexanes in EtOAc); ¹H NMR (300 MHz, CDCl₃, 298 K) δ 9.92 (1H, b), 7.95 (1H, d, *J* = 8.2 Hz), 7.59 (1H, m), 7.46 (2H, m), 5.69 (1H, m), 4.98 (3H, m), 3.62 (1H, dd, *J* = 20, 6.8 Hz), 3.34 (1H, dd, *J* = 24, 9.4 Hz) 2.19 (2H, m); ¹³C NMR (75 MHz, CDCl₃, 298 K) δ 174.1, 173.7, 149.7, 136.4, 133.3, 132.8, 131.5, 128.3, 124.9, 115.8, 53.0, 35.3, 34.3, 29.2.

Synthesis of 4PO- *t*-butyl-protected nitrophenylalanine 19. Compound **18** (0.33 g, 1.1 mmol, 1 eq) was placed in a 2-neck round-bottom flask under Ar (g) and dissolved in THF (5 mL) and cyclohexane (5 mL). A solution of *tert*-butyl-2,2,2-trichloroacetimidate (0.82 mL, 4.6 mmol, 4 eq) in cyclohexane (5 mL) was added simultaneously with boron trifluoride diethyletherate (0.049 mL, 0.40 mmol, 0.35 eq). The reaction stirred for 1 hour until it was quenched with 20 mL of saturated NaHCO₃ (aq). The organics were extracted with Et₂O (3×), washed with brine, dried over Na₂SO₄, and concentrated. The resulting white sludge was suspended in hexanes, filtered, and then purified by flash column chromatography (30% EtOAc in hexanes) to afford 4PO- *t*-butyl-protected

nitrophenylalanine **19** as a yellow oil (0.32 g, 0.90 mmol, 80% yield). $R_f = 0.30$ (30% EtOAc in hexanes); ^1H NMR (300 MHz, CDCl_3 , 298 K) δ 7.89 (1H, d, $J = 8.4$ Hz), 7.43 (3H, m), 6.33 (1H, d, $J = 8.2$), 5.65 (1H, m), 4.89 (3H, m), 3.46 (1H, dd, $J = 13.8$, 6.1 Hz), 3.22 (1H, dd, $J = 13.8$, 8.8 Hz), 2.20 (2H, m), 1.37 (9H, m); ^{13}C NMR (75 MHz, CDCl_3 , 298 K) δ 172.0, 170.5, 149.7, 136.8, 133.0, 132.8, 132.0, 128.0, 124.8, 115.5, 82.6, 53.1, 35.4, 35.1, 29.2, 27.8; HRMS (FAB+) m/z calc'd for $\text{C}_{18}\text{H}_{25}\text{N}_2\text{O}_5$ $[\text{M}+\text{H}]$: 349.1763, found 349.1753.

Synthesis of 4PO- *t*-butyl- NVOC-protected nitrophenylalanine 20. Compound **19** (1.3 g, 3.5 mmol, 1 eq) was placed in a 2-neck round-bottom flask under Ar (g) and dissolved in THF (50 mL) and MeOH (25 mL) at 0 °C. To this was added 10 wt % palladium on activated carbon (0.060 g) and sodium borohydride (0.26 g, 7.0 mmol, 2 eq). The reaction was followed by TLC using ninhydrin staining. The solution was stirred for 40 minutes and was then quenched with water and filtered through a pad of Celite™. The filtrate was extracted with Et_2O (3×), washed with brine, dried over Na_2SO_4 , and concentrated to afford a pale yellow oil. The resulting liquid was purified by flash column chromatography (50% EtOAc in hexanes) to afford 4PO- *t*-butyl- NVOC-protected nitrophenylalanine **20** as a pale yellow oil (0.93 g, 2.9 mmol, 84% yield). $R_f = 0.40$ (50% EtOAc in hexanes); ^1H NMR (300 MHz, CDCl_3 , 298 K) δ 7.01 (1H, t, $J = 7.6$ Hz), 6.89 (1H, d, $J = 7.3$ Hz), 6.62 (2H, m), 5.76 (1H, m), 5.00 (2H, m), 4.60 (1H, m), 3.05 (1H, dd, $J = 14.1$, 4.1 Hz), 2.76 (1H, dd, $J = 14.4$, 9.0 Hz), 2.35 (2H, m), 1.34 (9H, s); ^{13}C NMR (75 MHz, CDCl_3 , 298 K) δ 172.4, 171.3, 145.3, 136.8, 131.4, 128.1, 120.7, 117.7, 115.6, 82.4, 52.4, 35.7, 29.4, 27.8. HRMS (FAB+) m/z calc'd for $\text{C}_{18}\text{H}_{25}\text{N}_2\text{O}_5$ $[\text{M}^+]$: 318.1944, found 318.1931.

Synthesis of 4PO- NVOC-protected nitrophenylalanine 21. Compound **20** (0.20 g, 0.63 mmol, 1 eq) was placed in a 20 mL scintillation vial and suspended in 10 mL of CH₂Cl₂. To this was added K₂CO₃ (0.18 g, 1.3 mmol, 2 eq) and 6-nitroveratryloxycarbonyl (NVOC) chloride (0.17 g, 0.63 mmol, 1 eq). The reaction stirred for 1 hour and then 20 mL of H₂O was added. The organics were extracted with CH₂Cl₂ (3×), washed with brine, dried over Na₂SO₄, concentrated, and then purified by flash column chromatography (40% EtOAc in hexanes) to afford 4PO- NVOC-protected nitrophenylalanine **21** as a yellow oil (0.24 g, 0.43 mmol, 68% yield). *R*_f = 0.30 (40% EtOAc in hexanes); ¹H NMR (300 MHz, CDCl₃, 298 K) δ 7.69 (1H, s), 7.33 (1H, b), 7.25 (1H, m), 7.06 (3H, m), 6.63 (1H, m), 5.68 (3H, m), 4.99 (2H, m), 4.40 (1H, m), 3.96 (3H, s), 3.90 (3H, s), 3.17 (1H, dd, *J* = 14.4, 3.6 Hz), 2.83 (1H, dd, *J* = 14.1, 9.6 Hz), 2.27 (4H, m), 1.32 (9H, s); ¹³C NMR (75 MHz, CDCl₃, 298 K) δ 172.9, 170.6, 153.8, 153.8, 147.8, 139.2, 136.7, 136.4, 131.4, 128.6, 128.0, 126.2, 123.4, 121.5, 116.0, 109.9, 108.0, 83.1, 63.7, 56.6, 56.3, 53.2, 35.5, 35.4, 29.5, 27.8.

Synthesis of 4PO- NVOC-protected aniline 22. Compound **21** (0.10 g, 0.18 mmol) was placed in a 2-neck round-bottom flask under Ar (g) and dissolved in CH₂Cl₂ (3 mL). To this was added trifluoroacetic acid (3 mL) and the solution stirred for 16 hours. The reaction mixture was concentrated to afford an orange liquid, which was triturated with ether. The resulting yellow solid was dissolved in EtOAc (3×), rinsed with 1 N HCl, rinsed with H₂O, and then added to 5% NaHCO₃. The organic layer (colorless) was discarded, and the pH of the aqueous layer was decreased to pH 2 by the addition of 6 N HCl. The organics were extracted with EtOAc (3×), rinsed with brine, dried over Na₂SO₄, and concentrated, and then purified by flash column chromatography (1%

formic acid and 15% hexanes in EtOAc) to afford 4PO, NVOC-protected aniline **22** as a yellow oil (0.80 g, 0.16 mmol, 89% yield). $R_f = 0.38$ (1% formic acid and 15% hexanes in EtOAc); ^1H NMR (300 MHz, MeOD, 298 K) δ 9.01 (1H, b), 7.75 (1H, s), 7.40 (1H, m), 7.21 (4H, m), 5.68 (1H, m), 5.56 (2H, s), 4.91 (2H, m), 4.70 (1H, m), 3.91 (6H, s), 3.29 (1H, m), 2.97 (1H, dd $J = 14.5, 9.4$ Hz), 2.18 (4H, m).

Synthesis of the cyanomethyl ester of 22. Compound **22** (0.048 g, 0.096 mmol, 1 eq) was added to a 20 mL scintillation vial. To this was added chloroacetonitrile (0.30 mL, 4.8 mmol, 50 eq) and triethylamine (0.040 mL, 0.29 mmol, 3 eq). The resulting mixture stirred for 6 hours. Then 10 mL of H_2O was added and the organics were extracted with CH_2Cl_2 (3 \times), washed with brine, dried over Na_2SO_4 , concentrated, and then purified by flash column chromatography (50% EtOAc in hexanes) to afford the cyanomethyl ester of **22** as a yellow oil (0.041 g, 0.076 mmol, 79% yield). $R_f = 0.40$ (50% EtOAc in hexanes); ^1H NMR (300 MHz, CDCl_3 , 298 K) δ 7.72 (2H, m), 7.24 (4H, m), 6.68 (1H, b), 5.66 (2H, m), 4.95 (2H, m), 4.47 (3H, m), 3.96 (6H, s), 3.19 (1H, dd $J = 14.3, 6.4$ Hz), 3.06 (1H, dd, $J = 14.5, 8.2$), 2.28 (4H, m).

Synthesis of the cyanomethyl ester of 7. Compound **7** (0.40 g, 1.9 mmol, 1 eq) was added to a 20 mL scintillation vial. To this was added chloroacetonitrile (3.0 mL, 4.8 mmol, 25 eq) and triethylamine (0.80 mL, 5.7 mmol, 3 eq). The resulting mixture stirred for 6 hours. Then 20 mL of H_2O was added and the organics were extracted with CH_2Cl_2 (3 \times), washed with brine, dried over Na_2SO_4 , concentrated, and then purified by flash column chromatography (40% EtOAc in hexanes) to afford the cyanomethyl ester of **7** as a yellow oil (0.33 g, 1.3 mmol, 70% yield). $R_f = 0.39$ (50% EtOAc in hexanes); ^1H NMR (300 MHz, CDCl_3 , 298 K) δ 7.95 (1H, d, $J = 7.4$ Hz), 7.61 (1H, dd, $J = 15.1, 7.2$), 7.48

(2H, m), 4.83 (2H, s), 4.64 (1H, m), 3.55 (1H, dd, $J = 13.9, 4.6$ Hz), 3.25 (1H, dd, $J = 14.1, 8.2$), 2.96 (1H, b); ^{13}C NMR (75 MHz, CDCl_3 , 298 K) δ 172.4, 149.6, 133.4, 133.3, 130.9, 128.4, 125.0, 113.9, 70.4, 49.2, 37.1; HRMS (FAB+) m/z calc'd for $\text{C}_{11}\text{H}_{11}\text{N}_2\text{O}_5$ [M+]: 251.0668, found 251.0677.

Nonsense Suppression *in vitro*. Rabbit Reticulocyte Lysate (Promega) and Wheat Germ Lysate (Rabbit Reticulocyte Lysate/Wheat Germ Extract Combination System from Promega) translation systems were used for *in vitro* transcription according to the manufacturer's protocol. All materials (*e.g.*, 35 μL Rabbit Reticulocyte lysate, 1.5 μL amino acid mix, 1 μL RNase inhibitor, 2.5 μL water, 6 μL mRNA at 1mg/mL and either 1 μL tRNA at 1 mg/mL or 1 μL water) were mixed and incubated at 30 °C for 3 hours. The resulting samples were stored at –80 °C until needed.

Aliquots of the *in vitro* translation reactions (5 mL) were used for photolysis and base hydrolysis experiments. For photolysis experiments, the aliquots were irradiated for 10 minutes to 1 hour using a 1000 W Hg/Xe arc lamp and UG-11 and WG-335 filters or a 288 W Hg lamp equipped with a 360 nm band-pass filter (BLAK-RAY Longwave Ultraviolet Lamp, Ultraviolet Products, Inc.) at a distance of 15-30 cm. For some experiments, the sample was heated (to various temperatures up to 90 °C) after irradiation. For base hydrolysis experiments, aliquots were treated with concentrated NH_4OH as described in England *et al.*¹⁰

Samples for SDS-polyacrylamide gel electrophoresis (PAGE) were prepared by mixing 5 μL of the *in vitro* translation mix with 5 μL of $2 \times$ SDS loading buffer (100 mM tris chloride at pH 6.8, 4% SDS, 0.2% bromophenol blue, 20% glycerol). Samples (10 μL each) were loaded onto pre-poured 7.5 or 12% tris chloride gels for SDS-PAGE. For

Western blotting, protein was transferred from the gel to nitrocellulose, which was then blotted with a mouse anti-hemagglutinin (HA) primary antibody that was in turn treated with a goat anti-mouse secondary antibody conjugated to horseradish-peroxidase for detection by chemiluminescence.

Nonsense Suppression in *Xenopus* oocytes. Nonsense suppression was performed using techniques described previously^{3, 33} on Shaker B cDNA in the pAMV vector. An appropriate codon (as described in the text) was introduced at the site of interest by the standard Stratagene QuickChange protocol and verified through sequencing. cDNA was linearized with the restriction enzyme NotI and mRNA was prepared by *in vitro* transcription using the mMessage Machine T7 kit (Ambion).

Stage V-VI *Xenopus laevis* oocytes were injected with 1 ng of mRNA per oocyte in a single 75 nL injection. For nonsense suppression experiments, each cell was injected with 75 nL of a 1:1 mixture of mRNA (20-25 ng of total mRNA) and tRNA (10-25 ng). Unnatural amino acids bearing 4PO protecting groups were deprotected prior to injection by incubating the sample with saturated I₂ (aq), which was prepared by making a saturated solution in water that was sonicated for 5 minutes and then heated at 60 °C for another 15 minutes. Oocytes were incubated at 18 °C for or 24-48 hours after injection. Wild-type recovery control experiments (injection of tRNA appended to the natural amino acid) were performed to evaluate the fidelity of the nonsense suppression experiments. Additional controls, including injections of mRNA only and mRNA with 76-mer THG73 (the misacylation control), were also performed.

Two-electrode voltage clamp electrophysiology was used to measure the functional effects of each mutation. Electrophysiology recordings were performed after

injection and incubation as described above using the OpusXpress 6000A instrument (Axon Instruments) at a holding potential of -80 mV. The running buffer was a Ca^{2+} free ND96 solution (96 mM NaCl, 2 mM KCl, 1 mM MgCl_2 , and 5 mM HEPES, pH 7.5). Currents were measured during depolarizing jumps from the holding potential to $+70$ mV in 25 mV increments.

For photolysis experiments, oocytes were irradiated for 10 minutes to 4 hours (with chilling) using a 1000 W Hg/Xe arc lamp using UG-11 and WG-335 filters or a 288 W Hg lamp equipped with a 360 nm band-pass filter (BLAK-RAY Longwave Ultraviolet Lamp, Ultraviolet Products, Inc.) at a distance of 15-30 cm.

6.6 ACKNOWLEDGEMENTS

We thank Rick Gerhart for the gift of the uranium glass filter, Mona Shahgholi for her assistance with the mass spectrometry, Michael Krout for his knowledge about the immersion lamp and Nyssa Puskar for thoughtful discussions. This work was supported by NIH (NS 34407) and an NIH training grant for Amy L. Eastwood (NRSA 5-T32-GM07616).

6.7 REFERENCES

1. Mayer, G.; Heckel, A., Biologically active molecules with a "light switch". *Angew. Chem. Int. Edit.* **2006**, 45, (30), 4900-4921.
2. Young, D. D.; Deiters, A., Photochemical control of biological processes. *Org. Biomol. Chem.* **2007**, 5, (7), 999-1005.
3. England, P. M.; Lester, H. A.; Davidson, N.; Dougherty, D. A., Site-specific, photochemical proteolysis applied to ion channels *in vivo*. *Pro. Natl. Acad. Sci. USA* **1997**, 94, (20), 11025-11030.
4. Bosques, C. J.; Imperiali, B., Photolytic control of peptide self-assembly. *J. Am. Chem. Soc.* **2003**, 125, (25), 7530-7531.
5. Parker, L. L.; Kurutz, J. W.; Kent, S. B.; Kron, S. J., Control of the yeast cell cycle with a photocleavable alpha-factor analogue. *Angew. Chem. Int. Edit.* **2006**, 45, (38), 6322-5.
6. Pellois, J. P.; Muir, T. W., A ligation and photorelease strategy for the temporal and spatial control of protein function in living cells. *Angew. Chem. Int. Edit.* **2005**, 44, (35), 5713-5717.
7. Shigenaga, A.; Tsuiji, D.; Nishioka, N.; Tsuda, S.; Itoh, K.; Otaka, A., Synthesis of a stimulus-responsive processing device and its application to a nucleocytoplasmic shuttle peptide. *ChemBioChem* **2007**, 8, (16), 1929-+.
8. Peters, F. B.; Brock, A.; Wang, J. Y.; Schultz, P. G., Photocleavage of the polypeptide backbone by 2-nitrophenylalanine. *Chem. Biol.* **2009**, 16, (2), 148-152.
9. Endo, M.; Nakayama, K.; Kaida, Y.; Majima, T., Design and synthesis of photochemically controllable caspase-3. *Angew. Chem. Int. Edit.* **2004**, 43, (42), 5643-5645.
10. England, P. M.; Lester, H. A.; Dougherty, D. A., Mapping disulfide connectivity using backbone ester hydrolysis. *Biochemistry* **1999**, 38, (43), 14409-14415.
11. Scarborough, R. M.; Smith, A. B., Efficient general synthesis of omega-olefinic methyl-esters. *Tet. Lett.* **1977**, (50), 4361-4364.
12. Liotta, D.; Markiewicz, W.; Santiesteban, H., Generation of uncomplexed phenyl selenide anion and its applicability to S_N2 - type ester cleavages. *Tet. Lett.* **1977**, (50), 4365-4368.
13. Liotta, D.; Santiesteban, H., Nucleophilic ring opening of lactones via S_N2 -type reaction with uncomplexed phenyl selenide anion. *Tet. Lett.* **1977**, 18, (50), 4369-72.
14. Liotta, D.; Sunay, U.; Santiesteban, H.; Markiewicz, W., Phenyl selenide anion, a superior reagent for the S_N2 cleavage of esters and lactones. *J. Org. Chem.* **1981**, 46, (13), 2605-2610.
15. Nazari, M.; Movassagh, B., Nucleophilic cleavage of lactones and esters with zinc selenolates prepared from diselenides in the presence of $Zn/AlCl_3$. *Tet. Lett.* **2009**, 50, (4), 438-441.
16. Blankenship, J. W.; Balambika, R.; Dawson, P. E., Probing backbone hydrogen bonds in the hydrophobic core of GCN4. *Biochemistry* **2002**, 41, (52), 15676-15684.

17. Deechongkit, S.; Nguyen, H.; Powers, E. T.; Dawson, P. E.; Gruebele, M.; Kelly, J. W., Context-dependent contributions of backbone hydrogen bonding to beta-sheet folding energetics. *Nature* **2004**, 430, (6995), 101-105.
18. Bain, J. D.; Wacker, D. A.; Kuo, E. E.; Chamberlin, A. R., Site-specific incorporation of nonnatural residues into peptides - Effect of residue structure on suppression and translation efficiencies. *Tetrahedron* **1991**, 47, (14-15), 2389-2400.
19. Ellman, J. A.; Mendel, D.; Schultz, P. G., Site-specific incorporation of novel backbone structures into proteins. *Science* **1992**, 255, (5041), 197-200.
20. Fahnestock, S.; Rich, A., Ribosome-catalyzed polyester formation. *Science* **1971**, 173, (994), 340-3.
21. Koh, J. T.; Cornish, V. W.; Schultz, P. G., An experimental approach to evaluating the role of backbone interactions in proteins using unnatural amino acid mutagenesis. *Biochemistry* **1997**, 36, (38), 11314-11322.
22. England, P. M.; Zhang, Y.; Dougherty, D. A.; Lester, H. A., Backbone mutations in transmembrane domains of a ligand-gated ion channel: implications for the mechanism of gating. *Cell* **1999**, 96, (1), 89-98.
23. Eastwood, A. E., Investigating structure-function relationships in ion channels using unnatural amino acids. Ph.D. Thesis. California Institute of Technology, Pasadena, CA, 2009.
24. Zacharias, N. M., Chemical-scale manipulation of ion channels: *in vivo* nonsense suppression and targeted disulfide crosslinking. Ph.D. Thesis. California Institute of Technology, Pasadena, CA, 2004.
25. Fujima, Y.; Hirayama, Y.; Ikunaka, M.; Nishimoto, Y., A scalable chemoenzymatic preparation of (*R*)-tetrahydrofuran-2-carboxylic acid. *Tetrahedron- Asymmet.* **2003**, 14, (10), 1385-1391.
26. Guindon, Y.; Therien, M.; Girard, Y.; Yoakim, C., Regiocontrolled opening of cyclic ethers using dimethylboron bromide. *J. Org. Chem.* **1987**, 52, (9), 1680-1686.
27. Klayman, D. L.; Griffin, T. S., Reaction of selenium with sodium borohydride in protic solvents. A facile method for the introduction of selenium into organic molecules. *J. Amer. Chem. Soc.* **1973**, 95, 197-200.
28. Stocking, E. M.; Schwarz, J. N.; Senn, H.; Salzmann, M.; Silks, L. A., Synthesis of *L*-selenocystine, *L*-Se-77 selenocystine and *L*-tellurocystine. *J. Chem. Soc.-Perkin Trans. I* **1997**, (16), 2443-2447.
29. Andreadou, I.; Menge, W.; Commandeur, J. N. M.; Worthington, E. A.; Vermeulen, N. P. E., Synthesis of novel Se-substituted selenocysteine derivatives as potential kidney selective prodrugs of biologically active selenol compounds: Evaluation of kinetics of beta-elimination reactions in rat renal cytosol. *J. Med. Chem.* **1996**, 39, (10), 2040-2046.
30. Wang, Z.; La, B.; Fortunak, J. M.; Meng, X. J.; Kabalka, G. W., Enantioselective synthesis of alpha-hydroxy carboxylic acids: Direct conversion of alpha-oxocarboxylic acids to enantiomerically enriched alpha-hydroxy carboxylic acids via neighboring group control. *Tet. Lett.* **1998**, 39, (31), 5501-5504.

31. Besse, D.; Siedler, F.; Diercks, T.; Kessler, H.; Moroder, L., The redox potential of selenocystine in unconstrained cyclic peptides. *Angew. Chem. Int. Edit.* **1997**, 36, (8), 883-885.
32. Ouchi, A.; Liu, S.; Li, Z.; Kumar, S. A.; Suzuki, T.; Hyugano, T.; Kitahara, H., Factors controlling photochemical cleavage of the energetically unfavorable Ph-Se bond of alkyl phenyl selenides. *J. Org. Chem.* **2007**, 72, (23), 8700-6.
33. Nowak, M. W.; Gallivan, J. P.; Silverman, S. K.; Labarca, C. G.; Dougherty, D. A.; Lester, H. A., *In vivo* incorporation of unnatural amino acids into ion channels in *Xenopus* oocyte expression system. In *Methods in Enzymology*, Conn, P. M., Ed. Academic Press: 1998; Vol. Volume 293, pp 504-529.
34. Demo, S. D.; Yellen, G., The inactivation gate of the Shaker K⁺ channel behaves like an open-channel blocker. *Neuron* **1991**, 7, (5), 743-753.
35. Hoshi, T.; Zagotta, W. N.; Aldrich, R. W., Biophysical and molecular mechanisms of Shaker potassium channel inactivation. *Science* **1990**, 250, (4980), 533-538.
36. Mackinnon, R.; Aldrich, R. W.; Lee, A. W., Functional stoichiometry of Shaker potassium channel inactivation. *Science* **1993**, 262, (5134), 757-759.
37. Zagotta, W. N.; Hoshi, T.; Aldrich, R. W., Restoration of inactivation in mutants of Shaker potassium channels by a peptide derived from ShB. *Science* **1990**, 250, (4980), 568-571.
38. Rodriguez, E. A.; Lester, H. A.; Dougherty, D. A., Improved amber and opal suppressor tRNAs for incorporation of unnatural amino acids *in vivo*. Part 1: minimizing misacylation. *RNA* **2007**, 13, (10), 1703-14.
39. Rodriguez, E. A.; Lester, H. A.; Dougherty, D. A., Improved amber and opal suppressor tRNAs for incorporation of unnatural amino acids *in vivo*. Part 2: evaluating suppression efficiency. *RNA* **2007**, 13, (10), 1715-22.
40. Buhler, S.; Lagoja, I.; Giegrich, H.; Stengele, K. P.; Pfeleiderer, W., New types of very efficient photolabile protecting groups based upon the [2-(2-nitrophenyl)propoxy]carbonyl (NPPOC) moiety. *Helv. Chim. Acta* **2004**, 87, (3), 620-659.
41. Walbert, S.; Pfeleiderer, W.; Steiner, U. E., Photolabile protecting groups for nucleosides: Mechanistic studies of the 2-(2-nitrophenyl)ethyl group. *Helv. Chim. Acta* **2001**, 84, (6), 1601-1611.
42. Lodder, M.; Golovine, S.; Hecht, S. M., Chemical deprotection strategy for the elaboration of misacylated transfer RNA's. *J. Org. Chem.* **1997**, 62, (4), 778-779.
43. Madsen, R.; Roberts, C.; Fraser-Reid, B., The pent-4-enoyl group: A novel amine-protecting group that is readily cleaved under mild conditions. *J. Org. Chem.* **1995**, 60, (24), 7920-7926.
44. Eastwood, A. L.; Blum, A. P.; Zacharias, N. M.; Dougherty, D. A., A selenide-based approach to photochemical cleavage of peptide and protein backbones at engineered backbone esters. *J. Org. Chem.* **2009**, 74, (23), 9241-4.

CHAPTER 7. Progress Toward Small-Molecule Activators of Voltage-Gated Ion Channels for Treatment of Visual Impairment Resulting from Photoreceptor Loss*

7.1 ABSTRACT

Vision loss in patients with age-related macular degeneration (AMD) and retinitis pigmentosa (RP) results from a loss of photoreceptors in the retina. While the photoreceptor neurons are lost, the retinal infrastructure of ganglion cells and other neurons remain intact. Previous work has shown that electrical stimulation of these remaining neurons by a microelectrode array implant can restore vision in RP patients. A collaboration was formed between laboratories at Caltech and USC to develop a small molecule alternative to the microelectrode arrays. This chapter describes our initial efforts to reach this goal by using functionalized $\text{Ru}^{2+}(\text{bpy})_3$ complexes to activate a voltage-gated ion channel in a *Xenopus* oocyte model system.

7.2 INTRODUCTION

Age-related macular degeneration (AMD) is an aging-associated disease that affects vision in the center of the visual field, leaving patients with only peripheral vision. This affects the patient's ability to see objects clearly, complicating common daily tasks such as reading and driving. AMD is the leading cause of irreversible severe vision loss in people over 50 years of age in the United States.¹ Retinitis pigmentosa (RP) refers to a

* This work was done in collaboration with the labs of Dr. Mark Humayun (USC), Prof. Robert Chow (USC), Prof. Harry Gray (Caltech), and Prof. Robert H. Grubbs (Caltech).

group of genetic eye conditions that lead to incurable blindness. AMD and RP affect millions of people worldwide and both result from loss of photoreceptors in the macula.²

The macula is located at the center of the retina, the light-sensitive tissue that lines the back of the eye.³ The retina is comprised of several layers of neurons that are interconnected by synapses. Light sensitivity in the retina is conferred by specialized neurons called photoreceptors, which are further classified as rods or cones. Rods are more sensitive than cones, responding to fewer photons of light, thereby enabling vision in dim lighting. Cones facilitate daytime vision and color perception. In humans, three types of cone cells are responsible for color vision, each responding to a different wavelength of light. In total, the human retina contains ~120 million rods and ~5 million cones. The outer segment of each photoreceptor is lined with membranes that are stacked with a light-sensitive protein called opsin (a G-protein coupled receptor) that contains the pigment molecule retinal. Upon irradiation, the retinal pigment undergoes a photoisomerization that induces a conformational change in the opsin protein, which ultimately culminates in the hyperpolarization of the photoreceptors (they are depolarized in the dark) and a halt in the release of neurotransmitter glutamate, which either activates or deactivates other neurons in the retina. These neurons process the information received and ultimately transmit it to the retinal ganglion cells whose axons form the optic nerve. The optic nerve transmits information directly to the brain for final processing.³

In AMD, photoreceptors are lost due to abnormal blood vessel growth in the macula (“wet” AMD)⁴ or atrophy of the pigment epithelial layer (“dry” AMD).⁵ Retinal degeneration in RP diseases also results in photoreceptor loss, but from genetic causes. A

loss of photoreceptors means that the affected tissue is no longer sensitive to photons, accounting for vision loss in these patients.

While the photoreceptors are lost in these diseases, the underlying bipolar and ganglion cells remain intact and capable of transmitting information to the brain. Many studies have shown that electrical stimulation of the retina can induce percepts in visually impaired animals and human subjects, presumably by activation of ganglion or other retinal neurons.⁶⁻⁹

A team led by Mark Humayun, a physician/scientist at USC, has developed a retinal prosthesis system (now in production by Second Sight Medical Products, Sylmar, CA) that is based on these findings.⁷ This prosthesis is comprised of a surgically implanted microelectrode array consisting of 60 electrodes, an inductive coil for transmitting power/data to the implant, a video processing unit (VPU) worn externally on a belt, and a small camera mounted externally on a pair of glasses. The device is designed to capture visual input from the camera, which then relays this information to the VPU that in turn digitizes and filters the signal to create a series of electrical stimulus pulses. These pulses are then delivered to the retina via the microelectrode array. In test studies, 96% (26/27) of RP patients implanted with these retinal prostheses show improvements in accuracy in spatial motor tasks and 93% (25/27) show improvements in the repeatability of these tasks, proving that electrical stimulation of the retinal neurons can restore vision.⁷ In some cases, formerly blind patients are given enough visual acuity to shoot a basketball or retrieve a cup from a table.

In recent years the Humayun and Chow labs from USC and the Gray, Grubbs and Dougherty labs from Caltech formed a collaboration to develop a small-molecule

alternative to the retinal prosthesis developed by Humayun. Our strategy is to use a light-sensitive small molecule to stimulate retinal neurons by activating the voltage-gated ion channels (VGICs) that are contained within their cellular membranes. VGICs are a class of ion channels that are activated by local changes in membrane potential. Upon opening their ion-conducting pore, VGICs allow a rapid and coordinated depolarization of the cell (or hyperpolarization depending on the specific channel and cell). In the case of a ganglion cell, this would ultimately lead to the propagation of an electrical signal to the optic nerve, much like Humayun's microelectronics-based retinal implants.

We envisioned that a membrane-imbedded small molecule capable of photo-induced electron transfer could be used to produce a small local change in membrane potential that could activate a nearby VGIC, ultimately leading to the productive cascade of electrical signaling that results in vision. In this scenario, the lost photoreceptors are essentially replaced with a light-sensitive small molecule.

We first sought to test this theory in a model system. In this chapter, the Shaker IR (ShIR) K^+ channel heterologously expressed in *Xenopus* oocytes is used as our testbed. Several $Ru^{2+}(bpy)_3$ -based small molecules were tested for their ability to activate ShIR upon irradiation. A useful assay was developed for testing the effectiveness of these compounds. Future work, conducted by Erin C. Lamb of the Dougherty lab, will use this assay to screen promising small molecule candidates.

7.3 PROGRESS

The ShIR K^+ channel is a voltage-gated potassium channel that is readily expressed in *Xenopus oocytes*. ShIR is a truncated version of the Shaker B channel discussed in

Chapter 6, where IR stands for “inactivation domain removed” because a large portion of the N-terminal tail is removed to prevent N-type inactivation.¹⁰⁻¹² Like its parent channel, ShIR is a tetramer composed of four identical subunits, each consisting of six transmembrane segments (labeled S1-S6). The fourth membrane-spanning segment (S4) of the Shaker proteins contains several Arg and Lys residues that are likely to carry a positive charge at physiological pH. The preceding segments (S1-S3) contain several negatively charged residues. Collectively, S1-S4 segments form a voltage-sensing domain that, by virtue of the location of their many charged residues, sense local changes in membrane potential. Upon sensing these changes, it is thought that the S4 domain moves, resulting in a conformational change in the Shaker protein that culminates in pore opening, allowing ions to flow across the membrane to restore the resting membrane potential.¹³

Our goal was to place a small molecule that is capable of light-induced electron-transfer in the vicinity of the voltage-sensing domain of the membrane embedded ShIR protein expressed in *Xenopus oocytes* (**Figure 7.1**). The first systems we chose to work with were based on $\text{Ru}^{2+}(\text{bpy})_3$ as shown in **Figure 7.2**. The Gray lab had previously prepared these complexes for other chemical biology applications. These systems contain long alkyl chains, which could potentially associate with cellular membrane of the oocytes, hopefully positioning the $\text{Ru}^{2+}(\text{bpy})_3$ in the vicinity of ShIR channels. We were particularly optimistic about **[Ru] 3** (**Figure 7.2**) because it contained two carboxylate groups, which should help with the water solubility of the complex, facilitate the orientation of the alkyl chains into the membrane (and the negatively charged carboxylates away from the phosphate head groups), and also give the overall complex a

net formal charge of 0. The theory is that upon irradiation, the Ru^{2+} is reduced to Ru^0 by a small molecule reductive quencher, which would create a local change in electron density of the media that could potentially be sensed by the S1-S4 voltage sensor of the ShIR protein. This process would culminate in receptor activation (ion channel opening), which we planned to measure by standard two-electrode voltage-clamp electrophysiology.

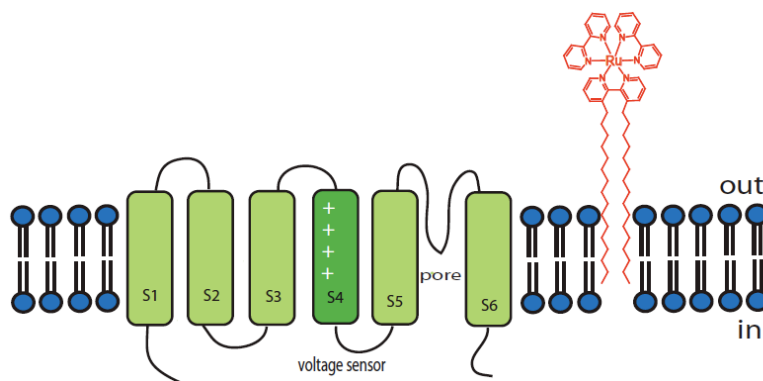


Figure 7.1. Depiction of experimental design for studies with **[Ru] 1, 2, and 3**. The alkyl chains of **[Ru]** embed into the oocyte membrane in the vicinity of the ShIR protein.

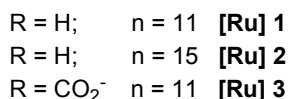
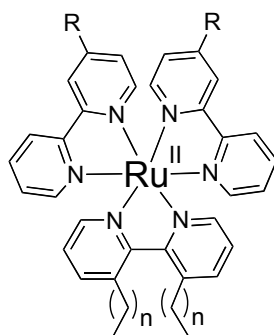


Figure 7.2. Structure of $\text{Ru}^{2+}(\text{bpy})_3$ complexes with alkyl chains (**[Ru] 1, 2, and 3**).

To test this theory, *Xenopus* oocytes expressing ShIR were incubated with micromolar concentrations of $\text{Ru}^{2+}(\text{bpy})_3$ complexes for various time periods (15 min–24 hrs). Voltage-clamp recordings were then conducted on an electrophysiology rig fitted

with an appropriately filtered Hg/Xe arc lamp. During recordings, the cells were exposed to buffered solutions containing small molecule reductive quenchers (4-methoxy-*N,N*-dimethylaniline, *N,N,N',N'*-tetramethyl-*p*-phenylenediamine, ascorbate or a combination of ascorbate with *N,N,N',N'*-tetramethyl-*p*-phenylenediamine) in the presence or absence of appropriately filtered UV light (~460 nm to excite $\text{Ru}^{2+}(\text{bpy})_3$). Importantly, the oocytes survived multiple hours of manipulation in the presence of the $\text{Ru}^{2+}(\text{bpy})_3$ complexes (they maintained their shape and healthy resting potentials). Under the conditions tested, however, no current from the ShIR channel was observed in the presence of the $\text{Ru}^{2+}(\text{bpy})_3$, quencher and filtered light, suggesting that these systems did not activate ShIR. Similar experiments were simultaneously conducted at USC in Prof. Robert Chow's lab. In these experiments, several types of mammalian cells (CHO and HEK cells) were used in place of the *Xenopus* oocytes. Unfortunately, these cells were not as tolerant to the $\text{Ru}^{2+}(\text{bpy})_3$ complexes as were our oocytes, which made voltage-clamp recordings difficult. The membranes of these cells did stain with **[Ru] 1** in confocal studies, suggesting that the alkyl chain was successfully imbedding into the cell membrane.

We then wondered whether the tethered $\text{Ru}^{2+}(\text{bpy})_3$ were being positioned in the membranes close enough to the ShIR voltage sensors. To circumvent this potential issue, we turned to a strategy that involved covalent attachment of the $\text{Ru}^{2+}(\text{bpy})_3$ complex to the voltage sensor by Cys modification (**Figures 7.3 and 7.4**). Such linkages require the presence of a free Cys residue at an appropriate position in the protein. MTS labeling experiments done by Isacoff and co-workers showed that two residues, Ala359 and Met356, in the S3-S4 linker are solvent accessible, suggesting that they would be

available for covalent modification by our $\text{Ru}^{2+}(\text{bpy})_3$ complexes.¹⁴ These sites are just 3-6 residues from the first Arg in the S4 domain (Arg362), and so it was thought that they would be at a prime location for positioning our complexes. As such, we mutated both residues to Cys. To determine whether either mutation affected the function of the channel, current-voltage (I-V) relationships were determined at several membrane potentials (**Figure 7.5**). These experiments clearly showed that at each set membrane potential, the corresponding current responses given by the mutant voltage-gated ShIR channels were equivalent to that of the wild-type receptor.

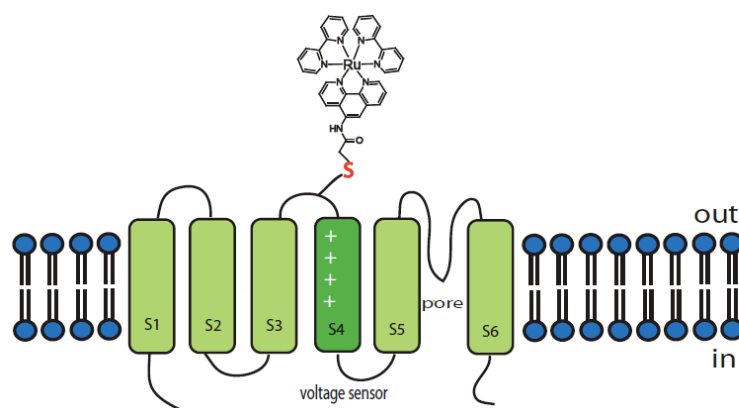


Figure 7.3. Depiction of experimental design for studies with **[Ru] 4**. The [Ru] complex covalently links to Ala359Cys or Met356Cys via an acetimide linkage.

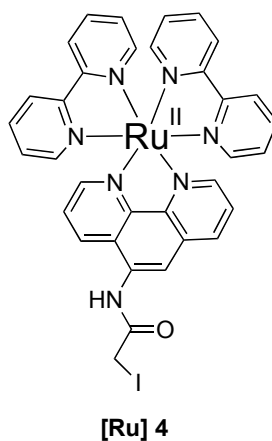


Figure 7.4. Structure of **[Ru] 4**. The iodoacetimide group reacts with free cysteines.

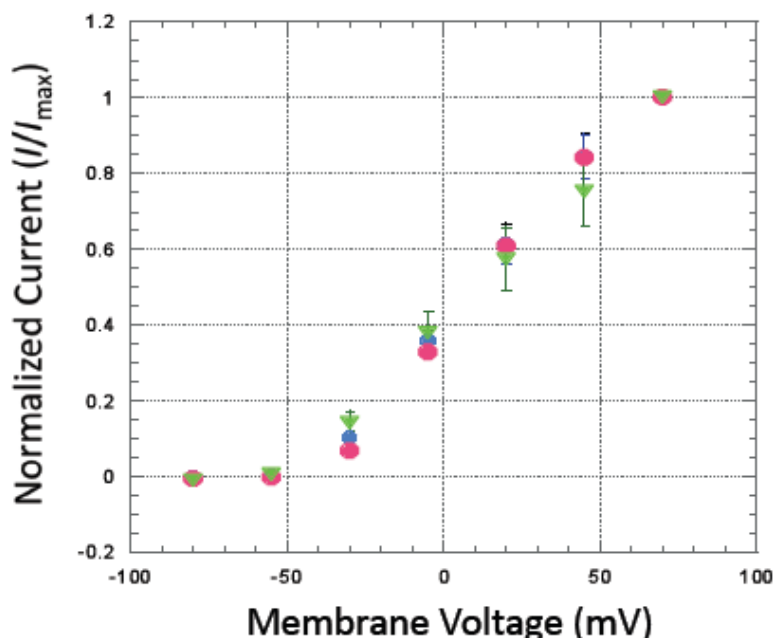


Figure 7.5. Current-voltage relationships of wild-type (WT) ShIR and ShIR mutants. Green triangles are WT ShIR; pink circles are the ShIR Met356Cys mutant; and blue circles are the ShIR Ala359Cys mutant.

At this point it was realized that this comparison could be a useful assay for measuring the impact of the $\text{Ru}^{2+}(\text{bpy})_3$ complexes. Should our experimental design make the channel gate more readily, the I-V relation should shift to the left (toward smaller membrane potentials). If on the, other hand, the channel became less sensitive to changes in membrane potential, then the I-V relation should shift right. This is a much more convenient and reliable assay than simply looking for current in voltage-clamp recordings, as a number of other factors including receptor function or cell health could affect this measurement.

We then attempted to covalently append [**Ru**] **4** to Ala359Cys or Met356Cys via the iodoacetimide. Unfortunately, these experiments never yielded any changes in the I-V relation despite the many conditions and quenchers that were tried. Similar results were seen with the mammalian cells studied in the Chow lab.

7.4 FUTURE DIRECTIONS

Given these results, it seemed prudent to confirm the hypothesis that appending a molecule bearing a negative charge to the either Ala359Cys or Met356Cys could influence activation of the receptor. To do this, we envisioned using charged MTS reagents and monitoring I-V curves. This work was taken over by the capable hands of Erin C. Lamb. She has shown that covalent appendage of charged MTS reagents at Ala359Cys and Met356Cys can influence receptor activation, but not in the direction that we had anticipated. She is now looking into repeating experiments with the **[Ru] 1-3** using the new assay and is also looking into modifying the alkyl chains to include *cis* double bonds, as recent reports^{15, 16} have suggested that *cis*-unsaturated fatty acids (but not saturated or *trans*-unsaturated fatty acids) can influence ShIR channel gating.

7.5 EXPERIMENTAL SECTION

These studies used a Shaker IR cDNA in the pBSTA vector that contains a T449V mutation (to limit C-type inactivation) and a FLAG tag. Conventional mutagenesis was performed by the standard Stratagene QuickChange protocol and verified through sequencing. cDNA was linearized with the restriction enzyme NotI and mRNA was prepared by *in vitro* transcription using the mMessage Machine T7 kit (Ambion). Stage V-VI *Xenopus laevis* oocytes were injected with 1 ng of mRNA per oocyte in a single 75 nL injection. Oocytes were incubated at 18 °C for 15-24 hours after injection. Currents from two-electrode voltage clamp electrophysiology were recorded by an OpusXpress 6000A instrument (Axon Instruments) or Geneclamp 500 amplifier (Axon Instruments) at a holding potential of -80 mV. The latter system is equipped with a 500 W Hg/Xe arc

lamp that is connected to the rig's bath by a liquid light guide. The lamp's shutter can be opened to bathe the oocyte in light. The running buffer was a Ca^{2+} free ND96 solution (96 mM NaCl, 2 mM KCl, 1 mM MgCl_2 , and 5 mM HEPES, pH 7.5). Currents were measured during depolarizing jumps from the holding potential to +70 mV in 25 mV increments.

[Ru] **1-3** were dissolved in DMSO and diluted into Ca^{+} free ND96 containing gentamycin to a total volume of <1 % DMSO and a final concentration of [Ru] ranging from 1 nM to 100 μM . Oocytes were incubated with these solutions for 15 min to 24 hrs prior to electrophysiological recordings. Small molecule quenchers (4-methoxy-*N,N*-dimethylaniline, *N,N,N',N'*-tetramethyl-*p*-phenylenediamine, and ascorbate) were dissolved in the ND96 running buffer at a concentration 10-100-fold higher than the [Ru] complexes in the original incubation media. Oocytes were irradiated during electrophysiological recordings using the 500 W Hg/Xe arc lamp system described above and appropriate wavelength cutoff filters (focused at 460 nm). Obvious controls were run (quencher only, [Ru] only, DMSO only, with and without irradiation, etc.) to ensure the fidelity of our experiments.

7.6 ACKNOWLEDGEMENTS

The ShIR construct used in these studies was a generous gift from Chris Ahern (University of British Columbia).

7.7 REFERENCES

1. Bressler, N. M.; Bressler, S. B.; Fine, S. L., Age-related macular degeneration. *Survey of Ophthalmology* **1988**, 32, (6), 375-413.
2. Humayun, M. S.; Weiland, J. D.; Fujii, G. Y.; Greenberg, R.; Williamson, R.; Little, J.; Mech, B.; Cimarusti, V.; Van Boemel, G.; Dagnelie, G.; de Juan, E., Visual perception in a blind subject with a chronic microelectronic retinal prosthesis. *Vision Res.* **2003**, 43, (24), 2573-2581.
3. Kolb, H., How the retina works - Much of the construction of an image takes place in the retina itself through the use of specialized neural circuits. *Am. Scientist* **2003**, 91, (1), 28-35.
4. Kulkarni, A. D.; Kuppermann, B. D., Wet age-related macular degeneration. *Adv. Drug Del. Rev.* **2005**, 57, (14), 1994-2009.
5. de Jong, P. T. V. M., Age-related macular degeneration. *New Eng. J. Med.* **2006**, 355, (14), 1474-1485.
6. Ahuja, A. K.; Behrend, M. R.; Kuroda, M.; Humayun, M. S.; Weiland, J. D., An *in vitro* model of a retinal prosthesis. *Biomedical Engineering, IEEE Transactions* **2008**, 55, (6), 1744-1753.
7. Ahuja, A. K.; Dorn, J. D.; Caspi, A.; McMahon, M. J.; Dagnelie, G.; daCruz, L.; Stanga, P.; Humayun, M. S.; Greenberg, R. J.; Group, A. I. S., Blind subjects implanted with the Argus II retinal prosthesis are able to improve performance in a spatial-motor task. *British Journal of Ophthalmology* **2011**, 95, (4), 539-543.
8. Crapper, D. R.; Noell, W. K., Retinal excitation and inhibition from direct electrical stimulation. *J. Neurophys.* **1963**, 26, (6), 924-947.
9. Jensen, R. J.; Ziv, O. R.; Rizzo Iii, J. F.; Scribner, D.; Johnson, L., Spatiotemporal aspects of pulsed electrical stimuli on the responses of rabbit retinal ganglion cells. *Experimental Eye Research* **2009**, 89, (6), 972-979.
10. Hoshi, T.; Zagotta, W. N.; Aldrich, R. W., Biophysical and molecular mechanisms of shaker potassium channel inactivation. *Science* **1990**, 250, (4980), 533-538.
11. Mackinnon, R.; Aldrich, R. W.; Lee, A. W., Functional stoichiometry of shaker potassium channel inactivation. *Science* **1993**, 262, (5134), 757-759.
12. Zagotta, W. N.; Hoshi, T.; Aldrich, R. W., Restoration of inactivation in mutants of shaker potassium channels by a peptide derived from ShB. *Science* **1990**, 250, (4980), 568-571.
13. Swartz, K. J., Sensing voltage across lipid membranes. *Nature* **2008**, 456, (7224), 891-897.
14. Larsson, H. P.; Baker, O. S.; Dhillon, D. S.; Isacoff, E. Y., Transmembrane movement of the Shaker K⁺ channel S4. *Neuron* **1996**, 16, (2), 387-97.
15. Borjesson, S. I.; Elinder, F., An electrostatic potassium channel opener targeting the final voltage sensor transition. *J. Gen. Physiol.* **2011**, 137, (6), 563-77.
16. Borjesson, S. I.; Hammarstrom, S.; Elinder, F., Lipoelectric modification of ion channel voltage gating by polyunsaturated fatty acids. *Biophys. J.* **2008**, 95, (5), 2242-53.

CHAPTER 8. Synthesis of *N*-Heterocyclic Carbene-Containing Metal Complexes from 2-(Pentafluorophenyl)Imidazolidines*

8.1 ABSTRACT

N-heterocyclic carbene(NHC)-containing metal complexes are prepared through a simple, base-free method involving the decomposition of 2-(pentafluorophenyl)imidazolidines under mild thermolytic conditions. Ruthenium, iridium and rhodium complexes containing NHC ligands with different electronic and steric parameters are reported.

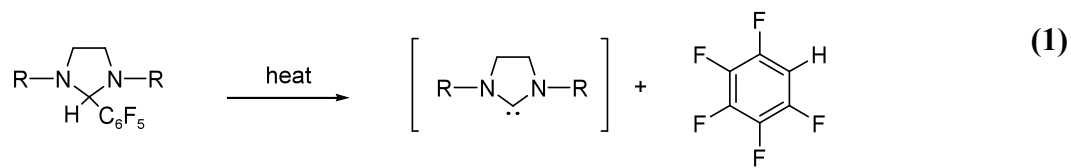
8.2 INTRODUCTION

N-heterocyclic carbene(NHC)-derived complexes have been used as powerful catalysts for effecting many transformations.¹⁻⁷ Despite their popularity, few methods are reported for their preparation. Current methods include the deprotonation⁸⁻¹⁰ or oxidative addition of imidazolium salts,^{11, 12} thermolysis of 2-(trichloromethyl)imidazolidine complexes,¹³ oxidative addition of 2-chloro-imidazolium salts,¹⁴ transmetallation of silver-NHC complexes¹⁵ and sodium reduction of imidazolidin-2-thiones.¹⁶ Recently, Crabtree and co-workers reported that *N,N'*-dialkylimidazolium-2-carboxylates can serve as precursors for the preparation of NHC-containing metal complexes with the release of CO₂.¹⁷ Many of these methods utilize imidazolium salt precursors, which are insoluble in many media

* This work was done in collaboration with Dr. Tobias Ritter in the laboratory of Prof. Robert H. Grubbs and is adapted from: Angela P. Blum, Tobias Ritter, Robert H. Grubbs, Synthesis of *N*-heterocyclic carbene-containing metal complexes from 2-(pentafluorophenyl)imidazolidines. *Organometallics* **2007**, 26, (8), 2122-24. Copyright 2007 American Chemical Society.

and difficult to further functionalize. “Protected” NHC adducts like 2-(alkoxy)imidazolidines, 2-(trichloromethyl)imidazolidines,¹³ 2-(triethylborane)imidazolidines,¹⁸ and 2-(dimethylamino)imidazolidines¹⁹ are used to prepare NHC-containing complexes and offer the advantage that they can be chemically manipulated.²⁰ However, the base that is often required to synthesize these adducts limits the scope of complexes that can be prepared.

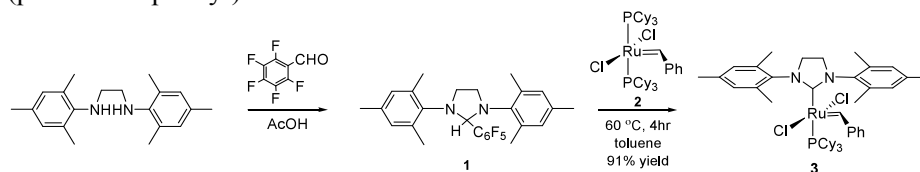
Waymouth, Hedrick and co-workers recently reported the base-free synthesis of a new set of air-stable NHC adducts that uses a pentafluorophenyl substituent as a protecting group. These adducts are formed by the condensation of diamines and pentafluorobenzaldehyde and were shown to decompose with mild heat to the corresponding carbenes (**equation 1**).²¹ The only by-product of the reaction is pentafluorobenzene (b.p. 85° C). Pentafluorophenyl adducts have been employed on three instances in the literature to prepare NHC-containing transition-metal complexes. Waymouth and Hedrick synthesized an NHC complex from allylpalladium chloride²¹ and Bedford *et al.* reported phosphite-based palladacycle NHC compounds²² as well as an iron-NHC complex that was formed *in situ*.²³ These reports illustrate the potential of utilizing pentafluorophenyl adducts for synthesizing metal-NHC complexes, and it was our goal to further explore the scope of compounds that can be prepared from these adducts. Here, we report the preparation of Ru-, Rh- and Ir-NHC complexes by the thermolysis of functionalized 2-(pentafluorophenyl)imidazolidines.



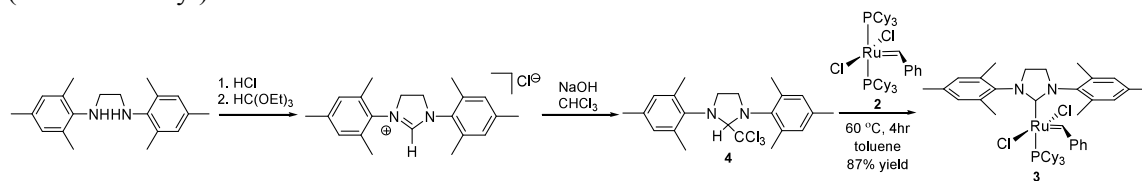
8.3 RESULTS

A direct comparison between the strategies involving the thermolysis of 1,3-bis(2,4,6-trimethylphenyl)-2-(pentafluorophenyl)imidazolidine **1** and 1,3-bis(2,4,6-trimethylphenyl)-2-(trichloromethyl)imidazolidine **4** in the synthesis of a common olefin metathesis catalyst **3** is shown in **Schemes 8.1** and **8.2**. Both methods afford **3** in comparable yield. The pentafluorophenyl adduct route offers several advantages in that it requires no base and fewer synthetic steps. In addition, **1** is stable at room temperature for greater than nine months while **4** shows signs of decomposition after a few weeks under the same conditions.

Scheme 8.1. Preparation of **3** from the thermolysis of 1,3-bis(2,4,6-trimethylphenyl)-2-(pentafluorophenyl)imidazolidine **1**.



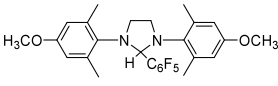
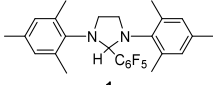
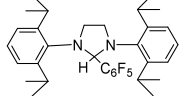
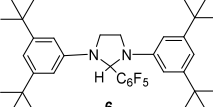
Scheme 8.2. Preparation of **3** from the thermolysis of 1,3-bis(2,4,6-trimethylphenyl)-2-(trichloromethyl)imidazolidine **4**.



The progress of the thermolysis of pentafluorophenyl adducts can be readily followed by ^{19}F NMR by monitoring the appearance of pentafluorobenzene. This fact enabled us to observe that the electron-rich adduct 1,3-bis(4-methoxy-2,6-dimethyl)-2-(pentafluorophenyl)imidazolidine (**5**) decomposes to pentafluorobenzene and the *N*-heterocyclic carbene at a faster rate (>95% conversion in 2 hours at 60 °C) than 1,3-

bis(2,4,6-trimethylphenyl)-2-(pentafluorophenyl)imidazolidine (**1**) (>95% conversion in 4 hours at 60 °C) as shown in **Table 8.1**. In addition, adducts lacking steric bulk in the *ortho* position of their phenyl rings do not form the carbene as readily. For example, the thermolysis of 1,3-bis[3,5-di(*tert*-butyl)phenyl]-2-(pentafluorophenyl)imidazolidine (**6**), an adduct with steric bulk only in the *meta* position of its phenyl groups, required 14 days and 107 °C to reach >95% conversion to pentafluorobenzene while all adducts with substituents (methyl or isopropyl groups) in the *ortho* position, required less heat (60 °C) and shorter reaction times (four or five hours for the adducts containing methyl or isopropyl groups, respectively) to reach the same conversion.

Table 8.1. Comparison of the pyrolysis of 2-(pentafluorophenyl)imidazolidines to >95% in benzene or toluene.

Adduct	Time (h)	Temp (°C)
 5	2	60
 1	4	60
	5	60
 6	336	107

A study of the thermolysis of **1** at 45 °C in varying solvents (**eq 1**, R = Mes) showed a dramatic range of rates of conversion to pentafluorobenzene as determined by percent conversions after one hour quantified by ¹⁹F NMR spectroscopy (**Table 8.2**). More polar solvents like acetone and acetonitrile were shown to yield higher conversions than less polar solvents like benzene. Although studies with acetone and acetonitrile

showed faster conversions to pentafluorobenzene, the apparent instability of some of the metal precursors prevented the preparation of NHC-containing organometallic complexes in these solvents. Studies in tetrahydrofuran and methylene chloride were also challenging because most of the reactions we attempted, which primarily involved ruthenium alkylidene species, required temperatures that exceeded the boiling points of these solvents. Despite prolonged reaction times, we found toluene to give the highest yields in our applications.

Table 8.2. Comparison of percent conversion to pentafluorobenzene in different solvents in the thermolysis of **1** after one hour at 45 °C.

solvent	%convn
C ₆ D ₆	8
toluene- <i>d</i> ₈	8
THF- <i>d</i> ₈	29
CD ₂ Cl ₂	32
acetone- <i>d</i> ₆	90
CD ₃ CN	>95

Ruthenium, rhodium and iridium-NHC complexes were easily prepared from pentafluorophenyl adducts in generally high yield under mild thermolytic conditions as shown in **Table 8.3**. We investigated substrates with different electronic and steric properties, further illustrating the effectiveness of this strategy. The preparation of a complex containing an unsymmetrically-substituted NHC ligand (1-mesityl-3-methyl-imidazol-1-ylidene) is also reported (entry 6). The synthesis of the product of entry 7 presented a particular challenge. Other methods that were attempted to prepare the complex were unsuccessful due to the apparent instability of the product. The synthesis of this complex, although in low yield, highlights the utility of this method. It is likely that the *ortho* methoxy groups of this adduct do not present the steric environment needed to convert to pentafluorobenzene and the carbene at lower temperatures. Indeed, a lack

of hindered rotation around the C-C_{aryl(C6F5)} bond is evident by the presence of only two resonances in the ¹⁹F NMR spectrum of this adduct in contrast to the five resonances seen for **1**.

Table 8.3. *N*-heterocyclic carbene complexes prepared from 2-(pentafluorophenyl)imidazolidines.

Entry	Adduct	Metal Precursor	Product	Time (hr)	Temp °C	% yield
1		2	3	4	60	91
2		[Rh(cod)Cl] ₂		2	70	90
3		[Ir(cod)Cl] ₂		2	70	89
4				5	60	80
5		2		4	60	75
6				5	60	65
7				5	100	25

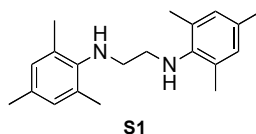
8.4 DISCUSSION

A strategy for preparing NHC-containing organometallic complexes from the thermolysis of 2-(pentafluorophenyl)imidazolidines was presented. It should be noted that this

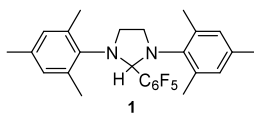
method is not meant to replace traditional strategies for preparing metal complexes containing NHC ligands. Instead it is meant to be viewed as a simple, base-free alternative that may offer access to more complicated metal-NHC complexes by eliminating possible side reactions. The reaction scope was shown to include ligands with different electronic and steric properties. This method requires no base and fewer synthetic steps than many strategies currently in use, making possible the preparation of complexes with functionality that may be incompatible with other methods.

8.5 EXPERIMENTAL SECTION

All reactions involving metal complexes were conducted under nitrogen or argon atmospheres using standard glove box or standard Schlenk techniques. Solvents were purified by passage through alumina.²⁴ Resonances for NMR spectra are reported relative to Me₄Si (δ 0.0) for ¹H and ¹³C and H₃PO₄ (δ 0.0) for ³¹P. Spectra are reported as follows: chemical shift (δ ppm), integration, multiplicity and coupling constant (Hz). (2,6-dimethoxyphenyl)imidazoline, catalyst **2** and RuCl₂(PCy₃)(=CH-*o*-iPr-Ph) were provided by Materia, Inc. 1,3-dimesitylimidazoline,²⁵ *N*-2-(mesitylimino)ethylidene-2,4,6-trimethylbenzenamine,²⁵ 1,3-bis(2,6-diisopropyl)2-pentafluorophenyl)imidazolidine,²³ and 2,4,6-trimethyl-*N*-(2-methylamino)ethyl)benzenamine²⁶ were prepared as described in the literature. All other reagents were purchased from Aldrich and used without prior purification. Crystallography data for S2 is available in Supplemental Material of Blum *et al.*²⁷

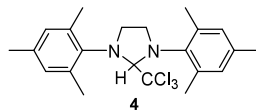


Synthesis of *N*-(2-(mesitylamino)ethyl)-2,4,6-trimethylbenzenamine (S1). A 250 mL round-bottom flask equipped with a stir bar was charged with *N*-2-(mesitylimino)ethylidene)-2,4,6-trimethylbenzenamine (2.0 g; 6.8 mmol) and sodium borohydride (1.1 g; 28 mmol), which were dissolved in 25 mL of THF at 0 °C. Concentrated HCl (1.1 mL) was added dropwise over a 30 minute period, and the solution became grey in color with the evolution of gas. The reaction stirred for an additional 20 minutes, and then 70 mL of 3 N HCl was added. The solution was allowed to warm to room temperature and was stirred for one hour. The reaction mixture was filtered through a glass frit, and the white precipitate was washed with H₂O (2 × 25 mL) and rinsed with 40 mL of a 5% acetone:hexanes mixture. The organics were extracted with CH₂Cl₂ (3 × 30 mL), washed with brine, dried over Na₂SO₄(s) and concentrated under vacuum to afford a white solid. Yield: 20%. ¹H NMR spectra match the data reported in the literature.²⁵

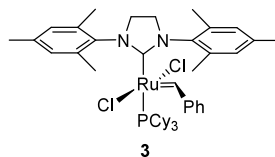


Synthesis of 1,3-dimesityl-2-(pentafluorophenyl)imidazoline (1). In a 10 mL flask equipped with a stir bar, **S1** (380 mg; 1.28 mmol) was dissolved in 0.7 mL of AcOH. Pentafluorobenzaldehyde (426 mg; 2.18 mmol) was then added and the reaction stirred overnight. The yellow precipitate was placed in a glass frit and washed with cold methanol to afford a white powder. Yield: 90%. ¹H and ¹⁹F NMR spectra match the data

reported in the literature.²¹ High-resolution MS analysis (FAB+) m/z : calcd 473.2016 [M+H], found 473.2007 [M+H].



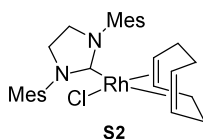
Synthesis of 1,3-dimesityl-2-(trichloromethyl)imidazolidine (4). A 10 mL round-bottom flask equipped with a stir bar was charged with sodium hydroxide (232 mg; 5.80 mmol). To this was added 1.45 mL of chloroform. The solution stirred for two minutes and then 1,3-dimesitylimidazoline (101 mg; 0.294 mmol) was added. The solution stirred for two hours and was poured into 30 mL of ice water. The organics were extracted with CH_2Cl_2 (2×20 mL), rinsed with brine, dried over $\text{MgSO}_4(\text{s})$ and concentrated under vacuum to afford a white solid. The solid was dissolved in toluene and filtered through a small silica plug with (1:20 EtOAc:hexanes) to afford a white solid. Yield: 69%. ^1H and ^{31}P NMR spectra match the data reported in the literature.²⁵



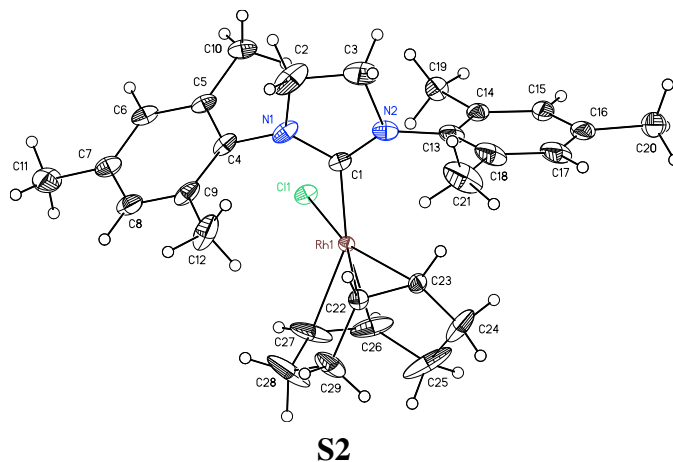
Synthesis of $(\text{H}_2\text{IMes})(\text{PCy}_3)(\text{Cl})_2\text{Ru}=\text{CHPh}$ (3) from 1. In the glove box, a 20 mL scintillation vial equipped with a stir bar was charged with **1** (100 mg; 0.211 mmol) and **2** (116 mg; 0.141 mmol). To this was added 4.2 mL of toluene. The vial was capped and removed from the glove box. It was then placed into an oil bath at 60°C and stirred for four hours. The reaction mixture was purified by flash column chromatography on TSI Scientific silica gel (8% ether:pentane) to afford a reddish-brown solid. Yield: 91%. ^1H

and ^{31}P NMR spectra match the data reported in the literature.¹³ High-resolution MS analysis (FAB+) m/z : calcd 848.3306, found 848.3322.

Synthesis of $(\text{H}_2\text{IMes})(\text{PCy}_3)(\text{Cl})_2\text{Ru}=\text{CHPh}$ (3**) from **4**.** By using the procedure described to prepare **3** from **1**, the reaction of **4** (77 mg; 0.18 mmol) and **2** (100 mg; 0.12 mmol) in 3.6 mL of toluene yielded **3** as a reddish-brown solid. Yield: 87%. ^1H and ^{31}P NMR spectra match the data reported in the literature.¹³ High-resolution MS analysis (FAB+) m/z : calcd 848.3306, found 848.3315.

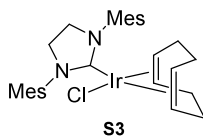


Synthesis of Chloro(h^4 -1,5-cyclooctadiene)(1,3-dimesitylimidazole-2-ylidene)rhodium(I) (S2**).** In the glove box, a 20 mL scintillation vial equipped with a stir bar was charged with $[\text{Rh}(\text{cod})\text{Cl}]_2$ (25 mg; 0.050 mmol) and **1** (0.048 mg; 0.10 mmol). To this was added 2.0 mL of toluene. The vial was capped and removed from the glove box. It was then placed into an oil bath at 70 °C and stirred for two hours.



The reaction mixture was purified by flash column chromatography on silica gel (50% ether:hexanes) to afford a yellow crystalline solid. Yield: 90%. ^1H NMR and ^{13}C NMR data (CDCl_3) are reported for **S2** in the literature,²⁸ however, in our hands we found different data. ^1H NMR (300MHz, CDCl_3 , 298 K) δ 6.98 (4H, d, J = 14.9 Hz, m -H), 4.45

(2H, s, $\text{cod}_{\text{vinyl}}$), 3.84 (4H, m, $J = 6.6, 2.0$ Hz, $\text{NCH}_2\text{CH}_2\text{N}$), 3.35 (2H, s, $\text{cod}_{\text{vinyl}}$), 2.58 (6H, s, $p\text{-CH}_3$), 2.31 (12H, d, $J = 7.15$ Hz, $o\text{-CH}_3$), 1.75 (4H, m, $J = 5.5$ Hz, $\text{cod}_{\text{alkyl}}$), 1.49 (4H, m, $J = 4.1$ Hz, $\text{cod}_{\text{alkyl}}$). ^{13}C NMR (75MHz, CDCl_3 , 298 K) δ 212.39 (d, $J = 48.7$ Hz, C-Rh), 137.9 ($p\text{-Ph}$), 136.0 ($o\text{-Ph}$), 134.9 ($m\text{-Ph}$), 129.7 ($\text{NCH}_2\text{CH}_2\text{N}$), 128.1 ($\text{NCH}_2\text{CH}_2\text{N}$), 96.9 (cod), 67.3 (cod), 51.1 (cod), 32.4 (cod), 27.9 (cod), 20.8 (cod), 19.7 ($o\text{-CH}_3$), 18.1 ($p\text{-CH}_3$). High-resolution MS analysis (FAB+) m/z : calcd 552.1778, found 552.1762. X-ray crystal structure confirms connectivity.²⁷

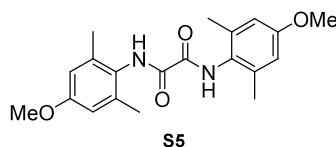


Synthesis of Chloro($\text{h}^4\text{-1,5-cyclooctadiene}$)(1,3-dimesitylimidazole-2-ylidene)iridium(I) (S3). By using the procedure described to prepare (S2), the reaction of $[\text{Ir}(\text{cod})\text{Cl}]_2$ (71 mg; 0.15 mmol) and **1** (50 mg; 0.74 mmol) in 3.0 mL of toluene yielded the product as an orange solid. The resulting reaction mixture was purified by flash column chromatography on silica gel (30% ether:hexanes) to afford an orange crystalline solid. Yield: 89%. ^1H NMR and ^{13}C NMR data (CDCl_3) are reported for **S3** in the literature,²⁸ however, in our hands we found different data. ^1H NMR (300MHz, CDCl_3 , 298 K) δ 6.94 (4H, d, $J = 10.7$ Hz, $m\text{-H}$), 4.07 (2H, m, $\text{cod}_{\text{vinyl}}$), 3.88 (4H, s, $\text{NCH}_2\text{CH}_2\text{N}$), 3.06 (2H, m, $\text{cod}_{\text{vinyl}}$), 2.53 (6H, s, $p\text{-CH}_3$), 2.31 (12H, d, $J = 9.07$ Hz, $o\text{-CH}_3$), 1.62 (4H, m, $\text{cod}_{\text{alkyl}}$), 1.26 (4H, m, $\text{cod}_{\text{alkyl}}$). ^{13}C NMR (75MHz, CDCl_3 , 298 K) δ 207.4 (C-Ir), 138.1 ($p\text{-Ph}$), 136.4 ($o\text{-Ph}$), 135.5 ($m\text{-Ph}$), 130.0 ($\text{NCH}_2\text{CH}_2\text{N}$), 128.6 ($\text{NCH}_2\text{CH}_2\text{N}$), 83.9 (cod), 51.9 (cod), 51.7 (cod), 33.6 (cod), 28.9 (cod), 21.3 (cod), 20.1

(*o*-CH₃), 18.7 (*p*-CH₃). High-resolution MS analysis (FAB⁺) *m/z*: calcd 642.2352 ([M]⁺), found 642.2347 ([M]⁺).

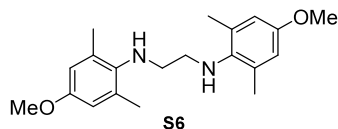


Synthesis of 4-methoxy-2,6-dimethylaniline (S4). A dry, two-neck 100 mL round-bottom flask equipped with a stir bar was charged with 4-amino-3,5-dimethylphenol (2.02 g; 14.8 mmol) and iodomethane (2.21 g; 15.6 mmol) under Ar(g). DMF (44 mL) was added and the reaction stirred at room temperature under Ar(g) for ten minutes to afford a dark solution. Potassium tertbutoxide (2.50 g; 22.3 mmol) was added, and the solution became tan and eventually dark green in color. The reaction stirred for a total of 16 hours and was then suspended in CH₂Cl₂. The organics were washed with 1 N KOH (3 × 50 mL) and brine, dried over MgSO₄(s) and concentrated under vacuum to yield a yellow solid. The crude product (with excess DMF) was used in the next reaction without characterization.

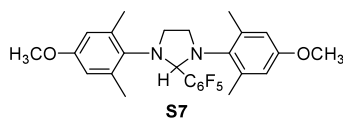


Synthesis of *N*¹,*N*²-bis(4-methoxy-2,6-dimethylphenyl)oxalamide (S5). In a 250 mL Erlenmeyer flask, sodium hydroxide (1.8 g, 45 mmol) was dissolved in 75 mL of H₂O. The solution was placed into an ice bath and **S4** (2.24 g; 14.8 mmol) was added. Oxalyl chloride (1.05 mL; 12.0 mmol) was then added slowly by syringe. Gas evolved and a

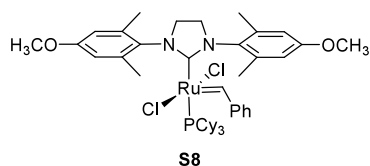
light brown precipitate formed instantaneously. The crude product was used in the next reaction without characterization. Yield: 19% over two steps.



Synthesis of *N*-(2-(4-methoxy-2,6-dimethylphenylamino)ethyl)-4-methoxy-2,6-dimethylbenzenamine(S6). A 100 mL pressure tube equipped with a stir bar was charged with **S5** (0.50 g; 1.4 mmol) under Ar(g). To this was added 12 mL of BH₃-THF (1.0 M in THF). The reaction vessel was capped and placed into an oil bath at 75 °C behind a safety shield. The solution was stirred for 16 hours at this temperature. The reaction was allowed to cool to room temperature and poured into 20 mL of MeOH in a 100 mL round-bottom flask. Then, 0.50 mL of HCl was added. A precipitate formed and the solution was concentrated under vacuum to reveal a white solid. The solid was redissolved in methanol and concentrated to dryness two more times. The white solid was suspended in CH₂Cl₂ and 2 N KOH. The organics were extracted with CH₂Cl₂ (3 × 25 mL), washed with brine, dried over MgSO₄(s) and concentrated under vacuum to afford an off-white powder. Yield: 63%. ¹H NMR (300MHz, C₆D₆, 298 K) δ 6.79 (4H, s, *m*-H), 3.54 (6H, s, OCH₃), 3.02 (4H, s, NCH₂CH₂N), 2.32 (12H, s, *o*-CH₃). ¹³C NMR (75MHz, C₆D₆, 298 K) δ 155.8 (*p*-C), 139.8 (C(Ar)-N), 132.3 (*o*-C), 114.5 (*m*-C), 55.0 (OCH₃), 49.9 (NCH₂CH₂N), 18.7 (*o*-CH₃). High-resolution MS analysis (FAB+) *m/z*: calcd 328.2151 ([M]⁺), found 328.2150 ([M]⁺).

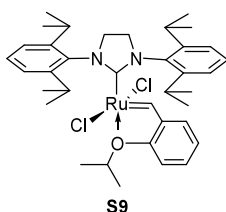


Synthesis of 1,3-Bis(4-methoxy-2,6-dimethylphenyl)-2-(pentafluorophenyl)imidazolidine (S7). In a 10 mL round-bottom flask equipped with a stir bar, **S6** (68 mg; 0.18 mmol) was suspended/dissolved in 0.7 mL of secBuOH. Pentafluorobenzaldehyde (61 mg; 0.31 mmol) was then added and the reaction stirred for two hours at room temperature. The reaction mixture was suspended in hexanes and 2 N KOH. The organics were extracted with hexanes (3 × 30 mL), washed with brine, dried over Na₂SO₄(s) and concentrated under vacuum to afford a yellow oil. The oil was purified by flash column chromatography on Brockmann IV alumina. Yield: 87%. ¹H NMR (crude) (300MHz, C₆D₆, 298 K) δ 6.54 (4H, b, *m*-H), 3.68 (2H, m, NCH₂CH₂N), 3.25 (8H, m, NCH₂CH₂N and OCH₃), 2.21 (12H, b, *o*-CH₃). ¹⁹F NMR (282MHz, C₆D₆, 298 K) δ -137.3 (1F, *J* = 14.48, 8.28 Hz), -150.3 (1F, *J* = 16.55, 6.21 Hz), -155.5 (1F, *J* = 22.8, 20.7 Hz), -162.7 (1F, *J* = 14.48, 8.28 Hz), -164.5 (1F, *J* = 14.48, 8.28 Hz). High-resolution MS analysis (FAB+) *m/z*: calcd 506.1993, found 506.2002.



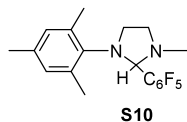
Synthesis of RuCl₂(1,3-Bis(4-methoxy-2,6-dimethylphenyl)-2-ylidene)(PCy₃)(=CHPh) (S8). In the glove box, a 20 mL scintillation vial equipped with a stir bar was charged with **S7** (35 mg; 0.068 mmol) and **2** (28 mg; 0.034 mmol). To this was added 1.4 mL of toluene. The purple solution was then transferred into a screw-top NMR tube,

removed from the glove box and then placed into an oil bath at 60 °C for 4 hours. The reaction mixture was purified by flash column chromatography on TSI Scientific silica gel (20% ether:pentane) to afford a reddish-brown solid. Yield: 75%. ^1H NMR (300MHz, CD_2Cl_2 , 298 K) δ 19.1 (1H, s), 6.8-5.4 (9H, m), 3.9-3.4 (10H, m), 1.6-1.0 (45H, m). ^{31}P NMR (121MHz, CD_2Cl_2 , 298 K) δ 29.8. High-resolution MS analysis (FAB+) m/z: calcd 880.3205, found 880.3208.

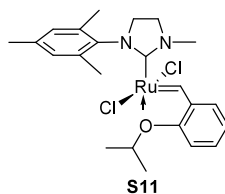


Synthesis of $\text{RuCl}_2(1,3\text{-Bis}(2,6\text{diisopropylphenyl})\text{-2-ylidene})(=\text{CH-o-iPr-Ph})$ (S9). In the glove box, a 20 mL scintillation vial equipped with a stir bar was charged with 1,3-bis(2,6-diisopropyl)-2-(pentafluorophenyl)imidazolidine (82 mg; 0.15 mmol) and $\text{RuCl}_2(\text{PCy}_3)(=\text{CH-o-iPr-Ph})$ (0.59 mg; 0.097 mmol). To this was added 3.0 mL of toluene. The vial was capped and removed from the glove box. It was then placed into an oil bath at 60 °C and stirred for five hours. The reaction mixture was purified by flash column chromatography on TSI Scientific silica gel (5% ether:hexanes) to afford a green solid. Yield: 80%. ^1H NMR and ^{13}C NMR data (C_6D_6) are reported for **S9** in the literature,²⁹ however, in our hands we found different data. ^1H NMR (300MHz, C_6D_6 , 298 K) δ 16.5 (1H, s, $\text{Ru}=\text{CHPh}$), 7.35 (2H, $J = 6.58$ Hz), 7.24 (4H, m, $J = 7.02$ Hz), 6.58 (2H, m, $J = 7.45$ Hz), 6.57 (1H, t, $J = 7.45$ Hz), 6.26 (1H, d, $J = 8.78$ Hz) 4.38 (1H, sept, $\text{OCH}(\text{CH}_3)_2$), 3.80 (8H, m, $\text{NCH}_2\text{CH}_2\text{N}$ and $\text{ArCH}(\text{CH}_3)_2$), 1.15 (6H, d, $J = 7.02$ Hz), 0.89 (24H, d, $J = 6.14$ Hz) ^{13}C NMR (75MHz, C_6D_6 , 298 K) δ 287.0 (C-Ru), 215.5,

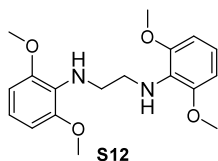
153.0, 149.6, 144.8, 137.5, 130.0, 129.1, 124.7, 122.4, 122.2, 113.2, 71.1, 54.9, 30.2, 29.2, 26.7, 23.9, 21.8. High-resolution MS analysis (FAB+) m/z : calcd 710.2344 ($[M]^+$), found 710.2371 ($[M]^+$).



Synthesis of 1-Mesityl-3-methyl-2-(pentafluorophenyl)imidzolidine (S10). In a 10 mL flask equipped with a stir bar, 2,4,6-trimethyl-*N*-(2-(methylamino)ethyl)benzenamine (207 mg; 1.08 mmol) was dissolved in 0.9 mL of AcOH. Pentafluorobenzaldehyde (359 mg; 1.82 mmol) was then added and the reaction mixture stirred for 1 hr at room temperature. The yellow solution was suspended in 50 mL of 2 N KOH and 50 mL of hexanes. The organics were extracted with hexanes (3 × 25 mL), washed with brine, dried over Na₂SO₄(s) and concentrated under vacuum to yield a yellow oil. The yellow oil was purified by flash column chromatography (5% EtOAc:hexanes) on Brockmann IV alumina and concentrated under vacuum to afford a light yellow oil. Yield: 85%. ¹H NMR (300MHz, C₆D₆, 298 K) δ 6.7 (2H, s, *m*-H), 5.4 (1H, s, NCH(C₆F₅)N), 3.5 (2H, m, *J* = 6.4 Hz, NCH₂CH₂N), 3.0 (3H, m, NCH₃), 2.7 (2H, m, NCH₂CH₂N), 2.18 (3H, s, *p*-CH₃), 2.02 (6H, d, 15.0 Hz, *o*-CH₃). ¹⁹F NMR (282MHz, C₆D₆, 298 K) δ -143.0 (2F, b), -155.8 (1F, t, *J* = 20.7 Hz), -163.3 (2F, dd, *J* = 14.5, 8.3 Hz). High-resolution MS analysis (FAB+) m/z : calcd 369.1390 ($[M]^+$), found 369.1393 ($[M]^+$).

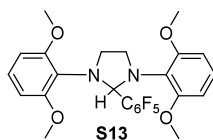


Synthesis of $\text{RuCl}_2(1\text{-mesityl-3-methyl-2-ylidene})(=\text{CH-o-iPr-Ph})$ (S11). Compound **S10** (113 mg; 0.304 mmol) was added to a 10 mL round-bottom flask and dissolved in degassed toluene (6 mL). Ar(g) was then bubbled through the solution via syringe for 20 minutes. A separate 50 mL round-bottom Schlenk flask containing $\text{RuCl}_2(\text{PCy}_3)(=\text{CH-o-}i\text{Pr-Ph})$ (122 mg; 0.203 mmol) was equipped with a stir bar and removed from the glove box. It was then placed under Ar(g) (via pump/backfill $\times 3$). To this second flask was added the solution containing 2,4,6-trimethyl-*N*-(2-(methylamino)ethyl)benzenamine via syringe. The flask was sealed and placed in an oil bath at 60 °C for 5 hours with stirring. The flask was cooled to room temperature and then placed under Ar(g) (pump/backfill $\times 3$). Copper(I) chloride (20.0 mg; 0.203 mmol) was then added and the resulting solution was allowed to stir for 1 hr at room temperature. The reaction mixture was purified by flash column chromatography (3% MeOH: CH_2Cl_2) on TSI Scientific silica gel and concentrated under vacuum to afford a green solid. Yield: 65%. ^1H and ^{13}C NMR spectra match the data reported in the literature.²⁶ High-resolution MS analysis (FAB+) m/z : calcd 522.0779, found 522.0759.



Synthesis of *N*-(2-(2,6-dimethoxyphenylamino)ethyl)-2,6-dimethoxybenzenamine

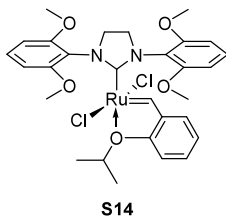
(S12). A two-neck 100 mL round-bottom flask equipped with a stir bar and condenser was charged with 1,3-(2,6-dimethoxyphenyl)imidazoline (172 mg; 0.452 mmol). To this was added 30 mL of 3 N HCl. The mixture was placed in an oil bath at 80 °C and stirred for 12 hours. The solution was then cooled to room temperature and suspended in CH₂Cl₂ and 2 N KOH. The organics were extracted with CH₂Cl₂ (3 × 25 mL), washed with brine, dried over MgSO₄(s) and concentrated under vacuum. The resulting yellow oil was then purified by flash column chromatography on Brockmann IV alumina (0.5% EtOAc: hexanes) Yield: 41%. ¹H NMR (300MHz, CDCl₃, 298 K) δ 6.82 (2H, t, *J* = 7.98 Hz, *p*-H), 6.54 (4H, d, *J* = 8.25 Hz, *m*-H), 4.24 (2H, s, NH), 3.82 (12H, s, OCH₃), 3.28 (4H, NCH₂CH₂N). ¹³C NMR (75MHz, CDCl₃, 298 K) δ 151.6 (*o*-C), 126.7 (*p*-C), 120.2 (*C*(Ar)-N), 104.6 (*m*-C), 55.9 (OCH₃), 47.0 (NCH₂CH₂N). High-resolution MS analysis (FAB+) *m/z*: calcd 333.1814 ([M+H]), found 333.1806 ([M+H]).



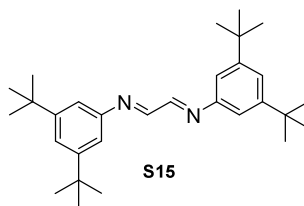
Synthesis of 1,3-Bis(2,6-dimethoxyphenyl)-2-(pentafluorophenyl)imidazolidine (S13).

In a 10 mL round-bottom flask equipped with a stir bar, **S12** (60.8 mg; 0.183 mmol) was suspended/dissolved in 0.7 mL of secBuOH. Pentafluorobenzaldehyde (61.0 mg; 0.311 mmol) was then added and the reaction stirred for 12 hours at room temperature. The

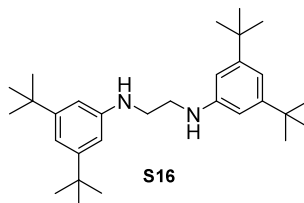
reaction mixture was suspended in hexanes and 2 N KOH. The organics were extracted with hexanes (3 × 30 mL), washed with brine, dried over Na₂SO₄(s) and concentrated under vacuum to afford a yellow oil. The oil was purified by flash column chromatography on Brockmann IV alumina (1% methanol:CH₂Cl₂) to afford a yellow solid. Yield: 70%. ¹H NMR (300MHz, C₆D₆, 298 K) δ 6.83 (2H, t, *J* = 10.1 Hz, *p*-H), 6.25 (4H, d, *J* = 8.25, *m*-H), 4.11 (2H, m, NCH₂CH₂N), 3.64 (2H, m, NCH₂CH₂N), 3.34 (12H, s, OCH₃). ¹⁹F NMR (282 MHz, C₆D₆, 298 K) δ -158.8 (2F, m, *J* = 20.69 Hz), -166.6 (3F, m, *J* = 14.48, 6.21 Hz). High-resolution MS analysis (FAB+) *m/z*: calcd 511.1656 ([M+H]), found 511.1649 ([M+H]).



Synthesis of RuCl₂[1,3-Bis(2,6-dimethoxyphenyl)-2-ylidene](=CH-o-*i*Pr-Ph) (S14). In the glove box, a 20 mL scintillation vial equipped with a stir bar was charged with **S13** (10 mg; 0.020 mmol) and RuCl₂(PCy₃)(=CH-o-*i*Pr-Ph) (7.8 mg; 0.013 mmol). To this was added 0.5 mL of toluene. The brown solution was then transferred into a screw-top NMR tube, removed from the glove box and then placed into an oil bath at 60 °C for 4 hours. The reaction mixture was purified by flash column chromatography on TSI Scientific silica gel (20% ether:pentane) to yield an olive-green solid. Yield: 25%. ¹H NMR (300MHz, CD₂Cl₂, 298 K) δ 18.4 (1H, s), 7.9-6.3 (10H), 5.0 (1H, sept, *J* = 6.4, 3.84 Hz), 4.2-3.6 (16H), 1.5 (6H). High-resolution MS analysis (FAB+) *m/z*: calcd 662.0889, found 662.0872.

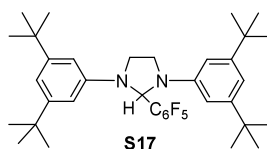


Synthesis of *N*-2-(3,5-di-*tert*-butylphenylimino)ethylidene)-3,5-di-*tert*-butylbenzenamine (S15). 3,5-di-*tert*-butylaniline (2.50g; 12.2 mmol) was added to a 100 mL round-bottom flask equipped with a stir bar and dissolved in a 1:1 mixture of isopropanol:water at 0 °C. Glyoxal (40% in H₂O) (0.7 mL; 6.1 mmol) was added. The solution was stirred vigorously for 2.5 hours and allowed to warm to room temperature. The yellow precipitate was dissolved in CH₂Cl₂ and passed through a glass frit. The yellow solution contained in the receiving flask was concentrated under vacuum to afford a yellow solid that was used in the next reaction without characterization.



Synthesis of *N*-(2-(3,5-di-*tert*-butylphenylamino)ethyl)-3,5-di-*tert*-butylbenzenamine (S16). A 10 mL round-bottom flask equipped with a stir bar was charged with **S15** (2.86 g; 6.62 mmol) and sodium borohydride (1.02 g; 27.0 mmol), which were dissolved in 24 mL of THF at 0 °C. Concentrated HCl (1.09 mL) was added dropwise over a 30 minute period, and the solution became grey in color with gas evolution. The solution stirred for an additional 20 minutes and 67 mL of 3 N HCl was added. The solution was allowed to warm to room temperature and stirred for one hour. The reaction mixture was filtered through a glass frit and the white precipitate was washed with H₂O (2 × 25 mL) and

rinsed with 40 mL of a 5% acetone:hexanes mixture. The precipitate was suspended in CH_2Cl_2 and 2 N KOH. The organics were extracted with CH_2Cl_2 (3×30 mL), washed with brine, dried over $\text{Na}_2\text{SO}_4(\text{s})$ and concentrated under vacuum to afford a white solid. Yield: 10%. ^1H NMR (300MHz, CDCl_3 , 298 K) δ 6.60 (2H, s, *p*-H), 6.39 (4H, s, *o*-H), 5.42 (2H, s, NH), 3.21 (4H, s, $\text{NCH}_2\text{CH}_2\text{N}$), 1.21 (36H, s, CH_3).



Synthesis of 1,3-Bis(3,5-di-*tert*-butylphenyl)-2-(pentafluorophenyl)imidzolidine (S17). In a 10 mL flask equipped with a stir bar, **S16** (181 mg; 0.416 mmol) was dissolved in 0.7 mL of AcOH. Pentafluorobenzaldehyde (170 mg; 0.867 mmol) was then added and a yellow precipitate began to form instantaneously. The reaction mixture stirred for 90 minutes. The precipitate was placed in a glass frit and washed with cold methanol to afford a white powder. Yield: 52%. ^1H NMR (300MHz, CDCl_3 , 298 K) δ 6.88 (2H, s, *p*-H), 6.52 (4H, s, *o*-H), 5.30 (1H, s, NH), 4.00 (2H, m, $\text{NCH}_2\text{CH}_2\text{N}$), 3.79 (2H, m, $\text{NCH}_2\text{CH}_2\text{N}$) 1.6-1.3 (36H, m, CH_3). ^{19}F NMR (282 MHz, CDCl_3 , 298 K) δ -142.0 (2F, b), -154.3 (1F, t, $J = 21.4$ Hz), -162.9 (2F, b).

Solvent dependence of the thermolysis of 1. To evaluate the dependence of the thermolysis of **1** on the solvent composition, six 5 mL scintillation vials were charged with 20 mg of **1**. A different solvent (benzene- d_6 , toluene- d_8 , CD_2Cl_2 , THF- d_8 , acetone- d_6 or acetonitrile- d_3) was added to each vial. The vials were shaken until all of **1** dissolved. The solutions were then transferred into six screw-cap NMR tubes, which

were immediately placed into an oil bath at 45 °C. After 1 hr, the NMR tubes were removed from the bath, cooled to -78 °C and ^{19}F NMR spectra were taken immediately.

^{19}F NMR data for **1**: (282 MHz, C_6D_6 , 298 K) δ -137.6 (1F, m, J = 14.5, 8.3, 6.2 Hz), -150.4 (1F, m, J = 14.5, 8.3 Hz), -155.5 (1F, m, J = 22.8, 20.2 Hz), -162.7 (1F, m), -164.5 (1F, m, J = 14.5, 8.3, 6.2 Hz). ^{19}F NMR (282 MHz, THF- d_8 , 298 K) δ -140.6 (1F, m, J = 12.4, 10.2, 8.3 Hz), -151.1 (1F, m, J = 14.5, 8.3 Hz), -158.1 (1F, m, J = 20.7 Hz), -165.4 (2F, m). ^{19}F NMR (282 MHz, CD_2Cl_2 , 298 K) δ -136.9 (1F, m, J = 14.5, 8.3 Hz), -150.1 (1F, m, J = 14.5, 8.3 Hz), -157.3 (1F, m, J = 20.7 Hz), -164.4 (2F, m). ^{19}F NMR (282 MHz, CD_3CN , 298 K) δ -135.9 (1F, m, J = 10.3, 8.3 Hz), -151.9 (1F, m, J = 14.5, 8.3 Hz), -157.5 (1F, m, J = 20.7 Hz), -164.8 (1F, m), -165.8 (1F, m, J = 15.3, 6.1 Hz). ^{19}F NMR (282 MHz, acetone- d_6 , 298 K) δ -137.4 (1F, m, J = 21.4, 9.1 Hz), -151.3 (1F, m, J = 15.3, 9.2 Hz), -157.9 (1F, m, J = 21.4, 18.3 Hz), -165.3 (1F, m, J = 21.4, 9.2 Hz), -165.7 (1F, m, J = 15.3, 6.1 Hz). ^{19}F NMR (282 MHz, toluene- d_8 , 298 K) δ -137.4 (1F, m, J = 14.5, 7.3 Hz), -150.3 (1F, m, J = 14.5, 9.7 Hz), -155.9 (1F, m, J = 21.8 Hz), -163.2 (1F, m, J = 12.1, 9.7 Hz), -164.5 (1F, m, J = 20.7 Hz).

^{19}F NMR data for pentafluorobenzene: (282 MHz, C_6D_6 , 298 K) δ -139.5 (2F, m, J = 10.3, 8.3 Hz), -154.4 (1F, t, J = 20.7 Hz), -162.7 (2F, m). ^{19}F NMR (282 MHz, THF- d_8 , 298 K) δ -137.5 (2F, m, J = 14.5, 8.3 Hz), -156.7 (1F, t, J = 20.7, 18.6 Hz), -164.5 (1F, m, J = 8.3, 6.3 Hz). ^{19}F NMR (282 MHz, CD_2Cl_2 , 298 K) δ -136.9 (1F, m, J = 14.5, 8.3 Hz), -150.1 (1F, m, J = 14.5, 8.3 Hz), -157.3 (1F, m, J = 20.7 Hz), -164.4 (1F, m). ^{19}F NMR (282 MHz, CD_3CN , 298 K) δ -141.1 (1F, m, J = 12.4, 10.3 Hz), -141.4 (1F, m, J = 12.4, 8.3 Hz), -156.7 (1F, m, J = 20.7, 18.6 Hz), -164.6 (2F, m). ^{19}F NMR (282 MHz,

acetone- d_6 , 298 K) δ -140.9 (1F, m, J = 10.3, 8.3 Hz), -141.2 (1F, m, J = 12.4, 8.3 Hz), -156.8 (1F, m, J = 20.7, 18.6 Hz), -164.7 (2F, m). ^{19}F NMR (282 MHz, toluene- d_8 , 298 K) δ -139.6 (2F, m, J = 12.1, 9.7 Hz), -154.6 (1F, m, J = 21.8, 19.3 Hz), -162.8 (2F, m, J = 14.5, 7.3 Hz).

8.6 ACKNOWLEDGEMENTS

Tobias Ritter thanks the German Academic Exchange Service (DAAD) for a postdoctoral fellowship. We thank Irina Gorodetskaya, Dr. Anna G. Wenzel and Dr. Georgios C. Vougioukalakis for starting materials. Dr. Michael W. Day and Lawrence M. Henling are thanked for crystallographic work.

8.7 REFERENCES

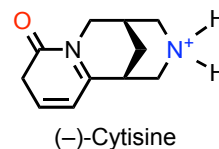
1. Bourissou, D.; Guerret, O.; Gabbai, F. P.; Bertrand, G., Stable carbenes. *Chem. Rev.* **2000**, 100, (1), 39-91.
2. Herrmann, W. A., *N*-heterocyclic carbenes: A new concept in organometallic catalysis. *Angew. Chem. Int. Edit.* **2002**, 41, (8), 1290-1309.
3. Herrmann, W. A.; Köcher, C., *N*-heterocyclic carbenes. *Angew. Chem. Int. Edit.* **1997**, 36, (20), 2162-2187.
4. Peris, E.; Crabtree, R. H., Recent homogeneous catalytic applications of chelate and pincer *N*-heterocyclic carbenes. *Coordin. Chem. Rev.* **2004**, 248, (21-24), 2239-2246.
5. Perry, M. C.; Burgess, K., Chiral *N*-heterocyclic carbene-transition metal complexes in asymmetric catalysis. *Tetrahedron-Asymmetr.* **2003**, 14, (8), 951-961.
6. Trnka, T. M.; Grubbs, R. H., The development of L(2)X(2)Ru = CHR olefin metathesis catalysts: An organometallic success story. *Accounts Chem. Res.* **2001**, 34, (1), 18-29.
7. Viciu, M. S.; Germaneau, R. F.; Nolan, S. P., Well-defined, air-stable (NHC)Pd(Allyl)Cl (NHC = *N*-heterocyclic carbene) catalysts for the arylation of ketones. *Org. Lett.* **2002**, 4, (23), 4053-4056.
8. Herrmann, W. A.; Köcher, C.; Goossen, L. J.; Artus, G. R. J., Heterocyclic carbenes: A high-yielding synthesis of novel, functionalized *N*-heterocyclic carbenes in liquid ammonia. *Chem-Eur. J.* **1996**, 2, (12), 1627-1636.
9. Méry, D.; Aranzaes, J. R.; Astruc, D., Use of an electron-reservoir complex together with air to generate *N*-heterocyclic carbenes. *J. Am. Chem. Soc.* **2006**, 128, (17), 5602-5603.
10. Öfele, K., A New Transition-Metal Carbon Complex 1,3-Dimethyl-4-Imidazolinyld-2-Ene Pentacarbonylchromium. *J. Organomet. Chem.* **1968**, 12, (3), P42-P43.
11. Gründemann, S.; Albrecht, M.; Kovacevic, A.; Faller, J. W.; Crabtree, R. H., Bis-carbene complexes from oxidative addition of imidazolium C-H bonds to palladium(0). *J. Chem. Soc. Dalton* **2002**, (10), 2163-2167.
12. McGuinness, D. S.; Cavell, K. J.; Skelton, B. W.; White, A. H., Zerovalent palladium and nickel complexes of heterocyclic carbenes: Oxidative addition of organic halides, carbon-carbon coupling processes, and the Heck reaction. *Organometallics* **1999**, 18, (9), 1596-1605.
13. Trnka, T. M.; Morgan, J. P.; Sanford, M. S.; Wilhelm, T. E.; Scholl, M.; Choi, T. L.; Ding, S.; Day, M. W.; Grubbs, R. H., Synthesis and activity of ruthenium alkylidene complexes coordinated with phosphine and *N*-heterocyclic carbene ligands. *J. Am. Chem. Soc.* **2003**, 125, (9), 2546-2558.
14. Fürstner, A.; Seidel, G.; Kremzow, D.; Lehmann, C. W., Preparation of metal-imidazolidin-2-ylidene complexes by oxidative addition. *Organometallics* **2003**, 22, (5), 907-909.
15. Garrison, J. C.; Youngs, W. J., Ag(I) *N*-heterocyclic carbene complexes: Synthesis, structure, and application. *Chem. Rev.* **2005**, 105, (11), 3978-4008.

16. Hahn, F. E.; Paas, M.; Le Van, D.; Lügger, T., Simple access to unsymmetrically substituted, saturated *N*-heterocyclic carbenes. *Angew. Chem. Int. Edit.* **2003**, 42, (42), 5243-5246.
17. Voutchkova, A. M.; Appelhans, L. N.; Chianese, A. R.; Crabtree, R. H., Disubstituted imidazolium-2-carboxylates as efficient precursors to *N*-heterocyclic carbene complexes of Rh, Ru, Ir, and Pd. *J. Am. Chem. Soc.* **2005**, 127, (50), 17624-17625.
18. Yamaguchi, Y.; Kashiwabara, T.; Ogata, K.; Miura, Y.; Nakamura, Y.; Kobayashi, K.; Ito, T., Synthesis and reactivity of triethylborane adduct of *N*-heterocyclic carbene: versatile synthons for synthesis of *N*-heterocyclic carbene complexes. *Chem. Commun.* **2004**, (19), 2160-2161.
19. Chamizo, J. A.; Morgado, J.; Bernes, S., Synthesis and structure of nickel(II) and palladium(II) carbene complexes containing the 1,3-diallylimidazolidin-2-ylidene ligand. *Transit. Metal. Chem.* **2000**, 25, (2), 161-165.
20. Waltman, A. W.; Ritter, T.; Grubbs, R. H., Rearrangement of *N*-heterocyclic carbenes involving heterocycle cleavage. *Organometallics* **2006**, 25, (18), 4238-4239.
21. Nyce, G. W.; Csihony, S.; Waymouth, R. M.; Hedrick, J. L., A general and versatile approach to thermally generated *N*-heterocyclic carbenes. *Chem-Eur. J.* **2004**, 10, (16), 4073-4079.
22. Bedford, R. B.; Betham, M.; Blake, M. E.; Frost, R. M.; Horton, P. N.; Hursthouse, M. B.; Lopez-Nicolas, R. M., *N*-Heterocyclic carbene adducts of orthopalladated triarylphosphite complexes. *Dalton T.* **2005**, (16), 2774-2779.
23. Bedford, R. B.; Betham, M.; Bruce, D. W.; Danopoulos, A. A.; Frost, R. M.; Hird, M., Iron-phosphine, -phosphite, -arsine, and -carbene catalysts for the coupling of primary and secondary 2 alkyl halides with aryl Grignard reagents. *J. Org. Chem.* **2006**, 71, (3), 1104-1110.
24. Pangborn, A. B.; Giardello, M. A.; Grubbs, R. H.; Rosen, R. K.; Timmers, F. J., Safe and convenient procedure for solvent purification. *Organometallics* **1996**, 15, (5), 1518-1520.
25. Arduengo, A. J.; Calabrese, J. C.; Davidson, F.; Dias, H. V. R.; Goerlich, J. R.; Krafczyk, R.; Marshall, W. J.; Tamm, M.; Schmutzler, R., C-H insertion reactions of nucleophilic carbenes. *Helv. Chim. Acta* **1999**, 82, (12), 2348-2364.
26. Vehlow, K.; Maechling, S.; Blechert, S., Ruthenium metathesis catalysts with saturated unsymmetrical *N*-heterocyclic carbene ligands. *Organometallics* **2006**, 25, (1), 25-28.
27. Blum, A. P.; Ritter, T.; Grubbs, R. H., Synthesis of *N*-heterocyclic carbene-containing metal complexes from 2-(pentafluorophenyl)imidazolidines. *Organometallics* **2007**, 26, (8), 2122-2124.
28. Denk, K.; Sirsch, P.; Herrmann, W. A., The first metal complexes of bis(diisopropylamino)carbene: synthesis, structure and ligand properties. *J. Organomet. Chem.* **2002**, 649, (2), 219-224.
29. Courchay, F. C.; Sworen, J. C.; Wagener, K. B., Metathesis activity and stability of new generation ruthenium polymerization catalysts. *Macromolecules* **2003**, 36, (22), 8231-8239.

APPENDIX 1: Characterizing the Pharmacophore Binding Interactions of Cytisine in the $(\alpha 4)_2(\beta 2)_3$ Receptor*

A1.1 RESULTS AND DISCUSSION

Cytisine is a natural product found in various plant species, especially *Cytisus laburnum* (the golden rain tree), and is a potent agonist of nicotinic acetylcholine receptors (nAChRs). It has been used as a smoking cessation drug for decades in Eastern Europe (marketed as Tabex®)¹ and also served as the lead compound for Pfizer's smoking cessation drug varenicline (marketed as Chantix® in the U.S.).²



We sought to characterize the nicotinic pharmacophore binding interactions of cytsine at the $\alpha 4\beta 2$ receptor. Chapter 2 describes studies that probe an important hydrogen bond between the CO of cytsine (the hydrogen bond acceptor of the nicotinic pharmacophore) and the backbone NH of $\beta 2$ L119 at both subunit stoichiometries of the pentameric $\alpha 4\beta 2$ receptor, $(\alpha 4)_2(\beta 2)_3$ (A2B3) and $(\alpha 4)_3(\beta 2)_2$ (A3B2). In these studies, cytsine was affected more than any other agonist tested by perturbations to this interaction at the A2B3 stoichiometry (giving a remarkable 62-fold increase in EC_{50} where other agonists like ACh and nicotine give only 7-fold increases³). This is an intriguing finding given the remarkably low efficacy ($\sim 3\%$ relative to ACh) of cytsine at this stoichiometry. Here we use unnatural amino acid mutagenesis to probe the remaining nicotinic pharmacophore interactions for cytsine at A2B3– a cation- π interaction to a

* This work was done in collaboration with Nyssa L. Puskar, Dr. Jai A. P. Shanata, and Ximena Da Silva Tavares Bongoll

conserved Trp in the $\alpha 4$ subunit (TrpB) and a hydrogen bond to the backbone CO of this same Trp.

We have well-established strategies for evaluating both interactions. The existence of a cation- π interaction can be established by successively fluorinating TrpB (**Figure A1.1A**).⁴⁻⁶ Fluorines diminish the cation- π binding ability of the Trp side chain, and the effect is additive. A linear correlation between the observed potency of the agonist and the cation- π binding ability of the ring is the hallmark of a cation- π interaction.

To probe hydrogen bonding interactions to the protein backbone, we replace the appropriate amino acid with its α -hydroxy analog (**Figure A1.1B**).⁵⁻⁷ This converts the backbone amide to an ester, with predictable consequences.⁸⁻¹¹ In the case of the hydrogen bonding interaction to the carbonyl of TrpB, we replace the $i+1$ residue, Thr155, with its α -hydroxy analog, Tah (threonine, α -hydroxy). This attenuates the hydrogen bond accepting ability of the backbone carbonyl, as it is an ester carbonyl rather than an amide carbonyl. We and others have seen significant impacts for mutations of this sort.⁵⁻¹¹

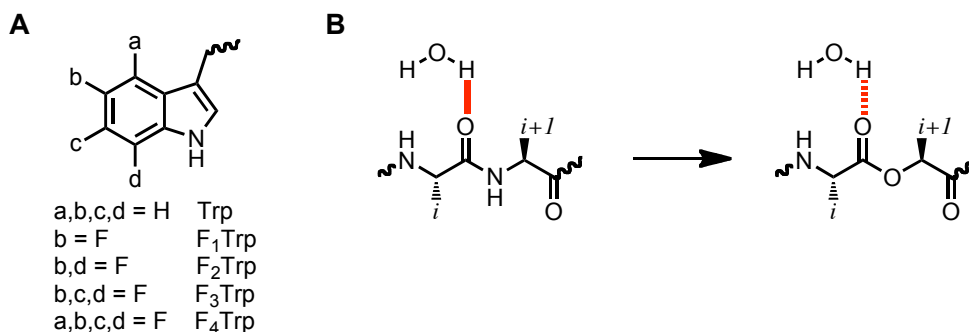


Figure A1.1. Unnatural amino acids used in this study. (A) Structures of the amino acids used to probe the cation- π interaction to TrpB and (B) the backbone ester mutation strategy for probing the hydrogen bond to the backbone CO of TrpB.

Studies of these interactions were challenging due to the very low efficacy of cytosine at the A2B3 stoichiometry. Several strategies were employed to overcome these challenges. We first injected large quantities of mRNA (~100-150 ng total per oocyte relative to the ~25 ng used in typical suppression experiments) and amino-acylated tRNA (up to 125 ng total per oocyte), and also used longer incubation times when necessary. In especially challenging cases, additional measures were taken including adding a second injection of mRNA and tRNA 24 hrs after the initial injection (with a total incubation time of 48-72 hrs), and allowing the injected oocytes to incubate at room temperature for 2-3 hrs prior to electrophysiological recordings. Even with these strategies, it was difficult to obtain adequate current sizes to construct a dose-response relation for F₄Trp (required from our studies of the cation- π interaction). In addition, the Hill coefficient obtained for this mutant is lower than what we typically see for this receptor (**Table A1.1**). Other alternative mutants were also tested, including 5-Br-Trp and 5-CN-Trp, but these mutants also gave low current sizes in electrophysiological recordings.

Despite these difficulties, a clear linear “fluorination plot” is seen for cytosine (shown in comparison to the corresponding plot for ACh⁵ in **Figure A1.2**), providing strong evidence in support of a cation- π interaction between the N⁺H of cytosine and the TrpB side chain. We have previously argued that the relative slope of a fluorination plot is an indication of the relative strength of a cation- π interaction.⁷ We also routinely use the fold-shift in EC₅₀ for the F₃Trp or F₄Trp mutants as an alternative measure of the strength of a cation- π interaction. The data in **Table A1.2** suggest mostly modest differences in the variations of fluorination plot slope values and F₃Trp/F₄Trp shifts in EC₅₀ for all agonists that have been studied at A2B3.⁵ The strongest interaction is seen

for (–)-Epi (discussed in Chapter 5 of this thesis), which gave a fluorination plot slope of 0.11 and a remarkable 180-fold increase in EC_{50} for the Trp-F₄ mutation.

Table A1.1. EC_{50} values and Hill coefficients for (–)-cytisine at the A2B3 stoichiometry. All studies gave current values at +70 mV (normalized to –110 mV) of ≤ 0.08 , confirming the A2B3 stoichiometry. Errors are standard error of the mean. Mutations identified as “Leu” and “Trp” represent recovery of the wild-type receptor by nonsense suppression.

Mutation	EC_{50} (nM)	Hill (n_H)
WT	6.9 ± 0.29	1.4 ± 0.07
$\alpha 4T155Thr$	15 ± 0.7	1.2 ± 0.05
$\alpha 4T155Tah$	130 ± 9	1.2 ± 0.08
$\alpha 4W154Trp$	11 ± 0.4	1.1 ± 0.04
$\alpha 4W154Trp-F_1$	22 ± 1	1.1 ± 0.04
$\alpha 4W154Trp-F_2$	21 ± 1	1.1 ± 0.07
$\alpha 4W154Trp-F_3$	180 ± 7	1.3 ± 0.05
$\alpha 4W154Trp-F_4$	212 ± 60	0.62 ± 0.08
$\alpha 4T155Thr$	15 ± 0.7	1.2 ± 0.05
$\alpha 4T155Tah$	130 ± 9	1.2 ± 0.08

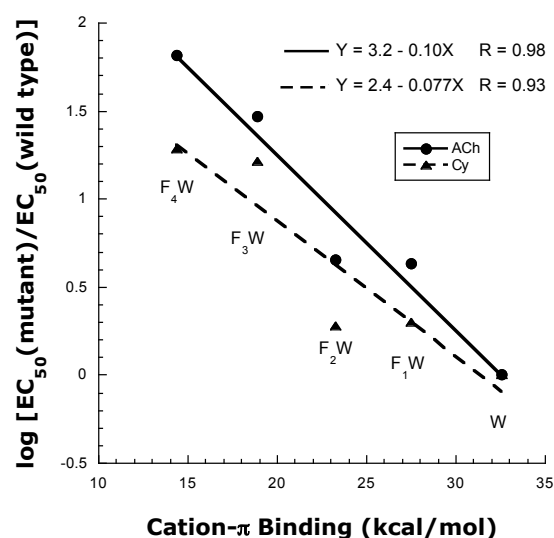


Figure A1.2. Fluorination plot for (–)-cytisine. Agonist potency is plotted against calculated gas-phase cation- π binding energies.⁴ The corresponding plot for ACh is also shown based on data from studies by Xiu *et al.*⁵

Table A1.2. EC₅₀ fold-shifts for Trp-F₃ and Trp-F₄ at TrpB, fluorination plot slopes and EC₅₀ fold-shifts for Tah at Thr155 for all agonists that have been studied at A2B3. A fold-shift is the ratio of the EC₅₀ of the mutant / EC₅₀ of the natural amino acid (obtained by nonsense suppression). Data for ACh and nicotine (*S*-Nic) is from the studies of Xiu *et al.*⁵ Varenicline (Var) data is courtesy of Nyssa L. Puskar and epibatidine (Epi) data is from Chapter 4 of this thesis.

Agonist	Trp-F ₃ Fold-Shift	Trp-F ₄ Fold-Shift	Fluorination Plot Slope	Tah Fold-Shift
ACh	30	65	0.10	1.1
S-Nic	13	47	0.089	19
Var	11	23	0.076	14
(+)-Epi	17	22	0.080	4.5
(-)-Epi	63	180	0.11	9.4
(+)-N-Methyl Epi	25	53	0.094	15
(-)-N-Methyl Epi	51	54	0.099	12
Cy	27	31	0.077	8.8

Cytisine was also impacted by the T155Tah mutation, providing compelling evidence for the hydrogen bond between cytisine's N⁺H and the backbone CO of TrpB. The 8.8-fold increase in EC₅₀ seen for cytisine is consistent with what is seen for other agonists at this stoichiometry (**Table A1.2**). Note that ACh has a quaternary N (not a protonatable amine) and therefore cannot participate in this interaction.

In summary, we have shown compelling evidence in support of a cation- π interaction and a hydrogen bond to the N⁺H of cytisine. The strength of these interactions is on par with the strengths of the analogous interactions seen for ACh, nicotine, varenicline, and the epibatidine compounds.

A1.2 EXPERIMENTAL SECTION

The molecular biology and electrophysiology protocols used in these studies can be found in Chapters 2 and 4.

A1.3 REFERENCES

1. Etter, J.-F., Cytisine for smoking cessation: a literature review and a meta-analysis. *Arch. Intern. Med.* **2006**, 166, (15), 1553-1559.
2. Coe, J. W.; Brooks, P. R.; Vetelino, M. G.; Wirtz, M. C.; Arnold, E. P.; Huang, J.; Sands, S. B.; Davis, T. I.; Lebel, L. A.; Fox, C. B.; Shrikhande, A.; Heym, J. H.; Schaeffer, E.; Rollema, H.; Lu, Y.; Mansbach, R. S.; Chambers, L. K.; Rovetti, C. C.; Schulz, D. W.; Tingley, F. D.; O'Neill, B. T., Varenicline: an $\alpha 4\beta 2$ nicotinic receptor partial agonist for smoking cessation. *J. Med. Chem.* **2005**, 48, (10), 3474-3477.
3. Blum, A. P.; Lester, H. A.; Dougherty, D. A., Nicotinic pharmacophore: the pyridine N of nicotine and carbonyl of acetylcholine hydrogen bond across a subunit interface to a backbone NH. *Proc. Natl. Acad. Sci. USA* **2010**, 107, (30), 13206-11.
4. Zhong, W.; Gallivan, J.; Zhang, Y.; Li, L.; Lester, H.; Dougherty, D., From *ab initio* quantum mechanics to molecular neurobiology: A cation- π binding site in the nicotinic receptor. *Proc. Natl. Acad. Sci. USA* **1998**, 95, 12088-12093.
5. Xiu, X.; Puskar, N. L.; Shanata, J. A.; Lester, H. A.; Dougherty, D. A., Nicotine binding to brain receptors requires a strong cation- π interaction. *Nature* **2009**, 458, (7237), 534-7.
6. Puskar, N. L.; Xiu, X.; Lester, H. A.; Dougherty, D. A., Two neuronal nicotinic acetylcholine receptors, $\alpha 4\beta 4$ and $\alpha 7$, show differential agonist binding modes. *J. Biol. Chem.* **2011**, 286, (16), 14618-27.
7. Cashin, A. L.; Petersson, E. J.; Lester, H. A.; Dougherty, D. A., Using physical chemistry to differentiate nicotinic from cholinergic agonists at the nicotinic acetylcholine receptor. *J. Am. Chem. Soc.* **2005**, 127, (1), 350-356.
8. Koh, J. T.; Cornish, V. W.; Schultz, P. G., An experimental approach to evaluating the role of backbone interactions in proteins using unnatural amino acid mutagenesis. *Biochemistry* **1997**, 36, 11314-11322.
9. England, P. M.; Zhang, Y. N.; Dougherty, D. A.; Lester, H. A., Backbone mutations in transmembrane domains of a ligand-gated ion channel: Implications for the mechanism of gating. *Cell* **1999**, 96, (1), 89-98.
10. Deechongkit, S.; Nguyen, H.; Powers, E. T.; Dawson, P. E.; Grubele, M.; Kelly, J. W., Context-dependent contributions of backbone hydrogen bonding to beta-sheet folding energetics. *Nature* **2004**, 430, (6995), 101-5.
11. Deechongkit, S.; Dawson, P. E.; Kelly, J. W., Toward assessing the position-dependent contributions of backbone hydrogen bonding to beta-sheet folding thermodynamics employing amide-to-ester perturbations. *J. Am. Chem. Soc.* **2004**, 126, (51), 16762-71.

APPENDIX 2: Full Collection of Data for the Backbone Ester Mutation at L119 in the $\alpha 4\beta 2$ and Muscle-Type Nicotinic Acetylcholine Receptors (nAChRs)

This appendix compiles all of the data from Chapters 2-4 concerning the backbone ester mutation at L119 in the complementary subunit of $\alpha 4\beta 2$ and the muscle-type nAChRs.

Key observations:

1. The largest fold shift is seen for (–)-Cytisine at the $(\alpha 4)_2(\beta 2)_3$ receptor despite its low efficacy for this receptor (~ 0.03 relative to ACh).
2. Varenicline is unaffected by this mutation at both stoichiometries of $\alpha 4\beta 2$.
3. Epibatidine is sensitive to the backbone ester mutation in $\alpha 4\beta 2$ but not in the muscle-type receptor.
4. In general, larger fold-shifts are seen in the muscle-type receptor than in $\alpha 4\beta 2$.
5. The $\alpha 1G153K$ mutation has little impact on the L119 interaction.
6. The weak agonist choline (which does not contain the hydrogen bond acceptor of the pharmacophore) is unaffected by the backbone ester mutation, but the nicotine analog *S*-MPP gives a large gain-of-function in the $\alpha 4\beta 2$ receptor.

Table A2.1. EC₅₀ values, Hill coefficients, and relative efficacies for the muscle-type receptor. Errors are standard error of the mean. Mutations identified as “Leu” represent recovery of the wild-type receptor by nonsense suppression.

Agonist	Mutation	EC ₅₀ (nM)	Fold-Shift	Hill (n _H)
α1₂β1γδ				
ACh	α1β1γδ	16000 ± 300		1.3 ± 0.1
	α1β1γ(L119Leu)δ(L121Leu)	16000 ± 500		1.5 ± 0.1
	α1β1γ(L119Lah)δ(L121Lah)	230000 ± 6000	14	1.5 ± 0.1
α1₂β1(L9'S)γδ				
ACh	α1β1(L9'S)γδ	610 ± 40		1.4 ± 0.1
	α1β1(L9'S)γ(L119Leu)δ(L121Leu)	310 ± 20		1.5 ± 0.1
	α1β1(L9'S)γ(L119Lah)δ(L121Lah)	9100 ± 700	29	1.6 ± 0.2
Ch	α1β1(L9'S)γδ	840000 ± 20000		1.6 ± 0.1
	α1β1(L9'S)γ(L119Leu)δ(L121Leu)	780000 ± 30000		1.7 ± 0.1
	α1β1(L9'S)γ(L119Lah)δ(L121Lah)	1000000 ± 50	1.3	1.8 ± 0.1
S-Nic	α1β1(L9'S)γδ	22000 ± 800		1.6 ± 0.1
	α1β1(L9'S)γ(L119Leu)δ(L121Leu)	23000 ± 700		1.7 ± 0.1
	α1β1(L9'S)γ(L119Lah)δ(L121Lah)	230000 ± 30000	10	2.2 ± 0.5
(±)-Epi	α1β1(L9'S)γδ	320 ± 20		1.5 ± 0.1
	α1β1(L9'S)γ(L119Leu)δ(L121Leu)	400 ± 20		1.5 ± 0.1
	α1β1(L9'S)γ(L119Lah)δ(L121Lah)	520 ± 30	1.3	1.6 ± 0.1
α1(G153K)₂β1(L9'S)γδ				
ACh	α1(G153K)β1(L19'S)γδ	7.2 ± 0.7		1.3 ± 0.1
	α1(G153K)β1(L9'S)γ(L119Leu)δ(L121Leu)	7.6 ± 0.7		1.8 ± 0.3
	α1(G153K)β1(L9'S)γ(L119Lah)δ(L121Lah)	180 ± 20	24	1.3 ± 0.1
Ch	α1(G153K)β1(L19'S)γδ	30000 ± 2000		1.0 ± 0.1
	α1(G153K)β1(L9'S)γ(L119Leu)δ(L121Leu)	27000 ± 2000		1.1 ± 0.1
	α1(G153K)β1(L9'S)γ(L119Lah)δ(L121Lah)	68000 ± 3000	2.5	1.3 ± 0.1
S-Nic	α1(G153K)β1(L19'S)γδ	320 ± 30		1.4 ± 0.2
	α1(G153K)β1(L9'S)γ(L119Leu)δ(L121Leu)	360 ± 40		0.95 ± 0.1
	α1(G153K)β1(L9'S)γ(L119Lah)δ(L121Lah)	6500 ± 500	18	1.3 ± 0.1
(±)-Epi	α1(G153K)β1(L19'S)γδ	4.3 ± 0.5		0.77 ± 0.5
	α1(G153K)β1(L9'S)γ(L119Leu)δ(L121Leu)	2.3 ± 0.4		0.74 ± 0.1
	α1(G153K)β1(L9'S)γ(L119Lah)δ(L121Lah)	9.6 ± 0.4	4.2	1.1 ± 0.1

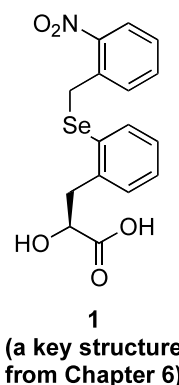
Table A2.2. EC₅₀ values, Hill coefficients, and relative efficacies for the $\alpha 4\beta 2$ receptor. All studies gave current values at +70 mV (normalized to -110 mV) of ≤ 0.08 or > 0.2 , confirming the A2B3 or A3B2 stoichiometry, respectively. Errors are standard error of the mean. Mutations identified as “Leu” represent recovery of the wild-type receptor by nonsense suppression. The relative efficacy is the ratio of the I_{\max} of a saturating concentration of agonist / I_{\max} of a saturating concentration of ACh. By definition, the relative efficacy of ACh is 1.

Agonist	Mutation	EC ₅₀ (nM)	Fold-Shift	Hill (n _H)	Relative Efficacy
$\alpha 4(L9'A)_2\beta 2_3$					
ACh	$\alpha 4(L9'A)\beta 2$	360 ± 20		1.3 ± 0.1	[1]
	$\alpha 4(L9'A)\beta 2(L119Leu)$	440 ± 20		1.3 ± 0.1	
	$\alpha 4(L9'A)\beta 2(L119Lah)$	3000 ± 100	6.8	1.2 ± 0.1	
CCh	$\alpha 4(L9'A)\beta 2$	7200 ± 80		1.3 ± 0.1	0.50 ± 0.02
	$\alpha 4(L9'A)\beta 2(L119Leu)$	7900 ± 200		1.2 ± 0.1	
	$\alpha 4(L9'A)\beta 2(L119Lah)$	29000 ± 800	3.7	1.2 ± 0.1	
Ch	$\alpha 4(L9'A)\beta 2$	140000 ± 4000		1.6 ± 0.1	0.060 ± 0.01
	$\alpha 4(L9'A)\beta 2(L119Leu)$	135000 ± 20000		1.2 ± 0.1	
	$\alpha 4(L9'A)\beta 2(L119Lah)$	150000 ± 5000	1.1	1.4 ± 0.1	
S-Nic	$\alpha 4(L9'A)\beta 2$	120 ± 5		1.3 ± 0.1	0.27 ± 0.01
	$\alpha 4(L9'A)\beta 2(L119Leu)$	120 ± 3		1.5 ± 0.1	
	$\alpha 4(L9'A)\beta 2(L119Lah)$	800 ± 30	6.7	1.3 ± 0.1	
S-MPP	$\alpha 4(L9'A)\beta 2$	11000 ± 400		1.7 ± 0.1	0.23 ± 0.01
	$\alpha 4(L9'A)\beta 2(L119Leu)$	14000 ± 900		1.5 ± 0.1	
	$\alpha 4(L9'A)\beta 2(L119Lah)$	1100 ± 40	0.1	1.5 ± 0.1	
(R/S)-MPP	$\alpha 4(L9'A)\beta 2$	19000 ± 600		1.8 ± 0.1	0.14 ± 0.02
(±)-Epi	$\alpha 4(L9'A)\beta 2$	0.79 ± 0.04		1.4 ± 0.1	0.47 ± 0.03
	$\alpha 4(L9'A)\beta 2(L119Leu)$	0.58 ± 0.05		1.5 ± 0.1	
	$\alpha 4(L9'A)\beta 2(L119Lah)$	2.9 ± 0.1	5.0	1.3 ± 0.1	
(+) -Epi	$\alpha 4(L9'A)\beta 2$	0.87 ± 0.03		1.5 ± 0.1	0.33 ± 0.01
	$\alpha 4(L9'A)\beta 2(L119Leu)$	0.58 ± 0.04		1.3 ± 0.1	
	$\alpha 4(L9'A)\beta 2(L119Lah)$	2.7 ± 0.1	4.7	1.3 ± 0.1	
(–)-Epi	$\alpha 4(L9'A)\beta 2$	1.1 ± 0.04		1.6 ± 0.1	0.74 ± 0.03
	$\alpha 4(L9'A)\beta 2(L119Leu)$	0.73 ± 0.03		1.4 ± 0.1	
	$\alpha 4(L9'A)\beta 2(L119Lah)$	3.8 ± 0.2	5.2	1.1 ± 0.1	
(+) -Epi-Me	$\alpha 4(L9'A)\beta 2$	8.6 ± 0.5		1.7 ± 0.2	0.50 ± 0.03
	$\alpha 4(L9'A)\beta 2(L119Leu)$	8.9 ± 0.7		1.3 ± 0.1	
	$\alpha 4(L9'A)\beta 2(L119Lah)$	30 ± 2	3.4	1.4 ± 0.1	
(–)-Epi-Me	$\alpha 4(L9'A)\beta 2$	0.42 ± 0.04		1.5 ± 0.1	0.55 ± 0.03
	$\alpha 4(L9'A)\beta 2(L119Leu)$	0.42 ± 0.04		1.6 ± 0.1	
	$\alpha 4(L9'A)\beta 2(L119Lah)$	0.91 ± 0.06	2.2	1.9 ± 0.2	
Cy	$\alpha 4(L9'A)\beta 2$	6.9 ± 0.3		1.4 ± 0.1	0.030 ± 0.01
	$\alpha 4(L9'A)\beta 2(L119Leu)$	8.7 ± 0.4		1.2 ± 0.1	
	$\alpha 4(L9'A)\beta 2(L119Lah)$	540 ± 30	62	0.98 ± 0.1	
Var	$\alpha 4(L9'A)\beta 2$	3.1 ± 0.1		1.4 ± 0.1	0.12 ± 0.02
	$\alpha 4(L9'A)\beta 2(L119Leu)$	2.6 ± 0.2		1.3 ± 0.1	
	$\alpha 4(L9'A)\beta 2(L119Lah)$	4.7 ± 0.2	1.8	1.3 ± 0.1	
$\alpha 4(L9'A)_3\beta 2_2$					
ACh	$\alpha 4(L9'A)\beta 2$	26 ± 0.1		1.1 ± 0.1	[1]
	$\alpha 4(L9'A)\beta 2(L119Leu)$	26 ± 0.4		1.6 ± 0.1	
	$\alpha 4(L9'A)\beta 2(L119Lah)$	220 ± 10	8.5	1.2 ± 0.1	
Ch	$\alpha 4(L9'A)\beta 2$	90000 ± 2000		1.4 ± 0.1	0.70 ± 0.06
	$\alpha 4(L9'A)\beta 2(L119Leu)$	76000 ± 200		1.4 ± 0.1	
	$\alpha 4(L9'A)\beta 2(L119Lah)$	74000 ± 2000	1.0	1.5 ± 0.1	
S-Nic	$\alpha 4(L9'A)\beta 2$	12 ± 0.1		1.6 ± 0.1	0.56 ± 0.04
	$\alpha 4(L9'A)\beta 2(L119Leu)$	12 ± 0.1		1.6 ± 0.1	
	$\alpha 4(L9'A)\beta 2(L119Lah)$	67 ± 3	5.6	1.4 ± 0.1	
S-MPP	$\alpha 4(L9'A)\beta 2$	4500 ± 100		1.1 ± 0.1	0.39 ± 0.03
	$\alpha 4(L9'A)\beta 2(L119Leu)$	4200 ± 300		1.6 ± 0.1	
	$\alpha 4(L9'A)\beta 2(L119Lah)$	130 ± 10	0.031	1.2 ± 0.1	
(R/S)-MPP	$\alpha 4(L9'A)\beta 2$	5900 ± 100		1.6 ± 0.1	0.28 ± 0.03
Cy	$\alpha 4(L9'A)\beta 2$	3.1 ± 0.1		1.9 ± 0.1	0.54 ± 0.05
	$\alpha 4(L9'A)\beta 2(L119Leu)$	3.6 ± 0.1		1.9 ± 0.1	
	$\alpha 4(L9'A)\beta 2(L119Lah)$	51 ± 2	14	1.4 ± 0.1	
Var	$\alpha 4(L9'A)\beta 2$	0.95 ± 0.02		1.7 ± 0.1	0.33 ± 0.01
	$\alpha 4(L9'A)\beta 2(L119Leu)$	1.0 ± 0.1		1.5 ± 0.1	
	$\alpha 4(L9'A)\beta 2(L119Lah)$	1.1 ± 0.1	1.1	1.2 ± 0.1	

APPENDIX 3: Synthetic Routes Considered for the Preparation of the Key Aryl Selenide α -Hydroxy Acid in Chapter 6

A3.1 RESULTS AND DISCUSSION

This appendix describes three synthetic routes for the preparation of α -hydroxy acid **1**, which was an important structure in Chapter 6. The first route was proposed by Dr. Amy L. Eastwood (Dougherty lab) and is illustrated in the retro-synthetic pathway shown in **Figure A3.1**.¹ The key step in this route is the insertion of elemental selenium into an aryl-lithium compound that is generated *in situ* by lithium-halogen exchange of a protected aryl bromide. The aryl bromide is derived from the



commercially available starting material *L*-2-bromo-Phe. There is extensive precedent for selenium insertion into aryl-lithium compounds, but a search of the literature revealed no examples of this methodology applied to highly functionalized starting materials. As such, installation of suitable protecting groups was considered a significant requirement for the success of this route. Eastwood encountered substantial difficulty when identifying a protecting group for the carboxylic acid that is compatible with *t*-butyllithium (*t*-BuLi) or alternative Grignard reagents. Eastwood's efforts to prepare an oxazolidine-protected acid were successful, but the oxazolidine ring had a tendency to open by *t*-BuLi or Grignard reagents.¹ By the time I began work on this project, there was a general consensus that the acid should be left unprotected.

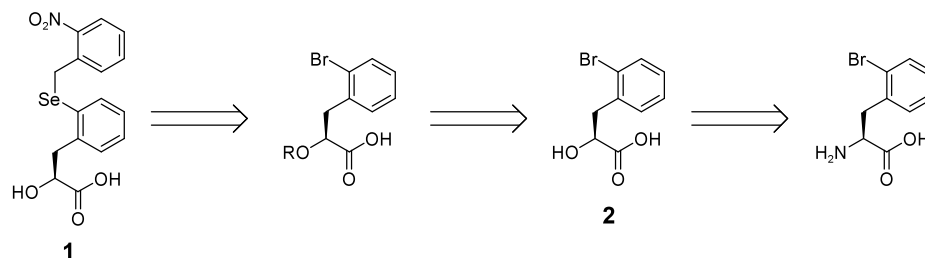
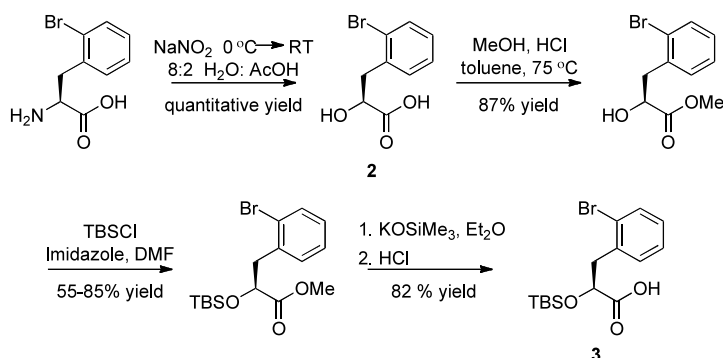
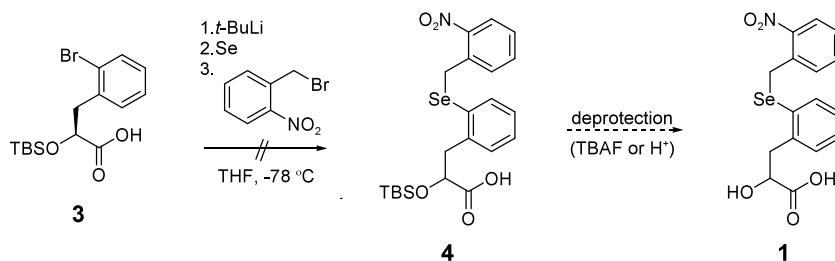


Figure A3.1. Original retro-synthetic pathway proposed by Eastwood.

The α -hydroxy acid **2** was stereo-selectivity prepared from *L*-2-bromo-Phe by Eastwood in quantitative yields via a published procedure.² I began work on this route by testing several alcohol protecting groups including *t*-butyldimethylsilyl (TBS), *t*-butyldiphenylsilyl (TBDPS) and methoxyethoxymethyl (MEM) ethers. These groups were selected for their perceived orthogonality with subsequent reaction conditions of the planned synthesis and for the ease with which they can be removed.³ Unfortunately, all protection reactions gave poor yields, which probably resulted from steric hindrance at the secondary alcohol or competing esterification reactions. To improve these yields, the free acid was esterified by Fischer esterification in methanol. This reaction gave a high yield (87%) and provided a convenient handle for flash column chromatography purification of subsequent products. A TBS group could then be readily installed by standard methods as shown in **Scheme A3.1**. The methyl group of the ester was removed by potassium trimethylsilanolate. This high-yielding reaction gave the potassium carboxylate salt, which was insoluble in organic solvents. Protonation of this salt during aqueous work-up gave TBS-protected aryl bromide **3**. Alternative methods of demethylation (including hydrolysis by 0.2 M LiOH) gave lower yields of **3**.

Scheme A3.1. Synthesis of TBS-protected aryl bromide **3**.

Compound **3** was put through several variations of the key first step shown in **Scheme A3.2**, but no conditions resulted in the desired *o*-nitrobenzyl-caged aryl selenide product **4**. Although it was apparent that all of the elemental selenium dissolved, no indication of selenium incorporation was ever observed. Many variables including temperature, reagent purities, reaction times and lithium sources (*n*-BuLi or *sec*-butyl instead of *t*-BuLi) were adjusted, but no conditions yielded the desired product or even selenium addition. These complications as well as Eastwood's inability to produce **1** through the oxazolidine-protected material inspired the design of an alternative synthetic route as depicted in the retro-synthetic pathway shown in **Figure A3.2**.

Scheme A3.2. Failed synthesis of the desired α -hydroxy acid, **1**.

It should be noted that TBS was originally chosen as the alcohol protecting group (for route 1, **Figure A3.1**) because it could be readily removed (by TBAF or acidic

media) and was noted as being compatible with Grignard and BuLi reagents.³ Contradictory reports on the compatibility of *t*-BuLi and TBS-protected alcohols were later found through subsequent literature searches. In these reports, lithiation of the TBS methyl groups was observed as a substantial side-reaction.⁴ While it is unlikely that this was the only cause of the reaction failures described above (especially given that reactions with other alcohol protecting groups by Eastwood also did not produce **1**), this side-reaction probably contributed.

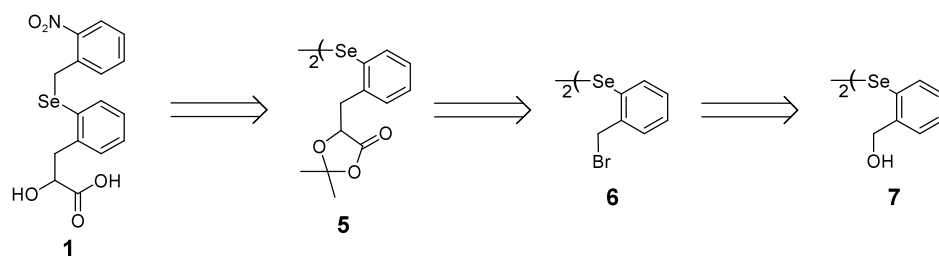


Figure A3.2. Second retro-synthetic pathway.

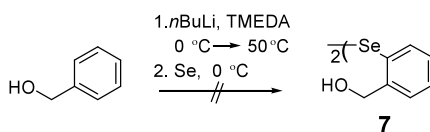
Because functional groups were suspected to be major players in the failure of the original route, selenium is introduced in the second route before the installment of the carboxylic acid and secondary alcohol (**Figure A3.2**). In this route, the desired product **1** is derived from a diselenide that was anticipated to be accessible via nucleophilic displacement of a benzyl bromide by the enolate of a Seebach-type ester.⁵⁻⁷ The conversion of aryl diselenides to phenylalkyl selenides is well-precedented and generally involves the reduction of an aryl diselenide in the presence of an alkyl halide.⁸⁻¹⁰

The nucleophilic attack of alkyl bromides by enolates of Seebach-type esters is also well-documented. Generally, chiral Seebach-type esters are employed to control the stereochemistry of the products.⁵⁻⁷ This was viewed as an advantage given that an enantio-enriched version of **1** was ultimately desired for model peptide or *in vivo* studies.

Unfortunately, no appropriate chiral Seebach-type esters are commercially available. As such, the initial goal of this route was to produce **1** racemically by the commercially available Seebach-type ester, 2,2-dimethyl-1,3-dioxolan-4-one. Had the overall route been successful, alternative chiral Seebach-type esters would have been synthesized by known methods.¹¹

Compounds **6** and **7** are both known compounds whose syntheses have been reported previously.^{12, 13} Two procedures are reported for the synthesis of the benzyl alcohol **7**. The first route is a one-step synthesis that involves the *ortho*-lithiation of benzyl alcohol as shown in **Scheme A3.3**. While the product is reported in 60% yield,¹³ all attempts to reproduce this procedure were unsuccessful. Compound **7** was never produced by this strategy despite efforts to optimize several variables including reaction temperature, reaction time, work-up procedures and reagent purities. Undissolved elemental selenium was seen throughout these reactions, and no sign of selenium incorporation was ever obtained by MS or NMR.

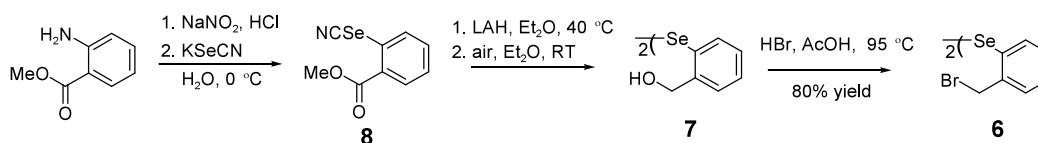
Scheme A3.3. Failed synthesis of benzyl alcohol **7** by *ortho*-lithiation of benzyl alcohol.



The second published procedure for the preparation of **7** consists of two high-yielding steps.¹² The first step in this route produces selenocyanate **8** through nucleophilic attack on a diazonium intermediate (formed *in situ* from the commercially available starting material, methyl anthranilate) by potassium selenocyanate. The methyl ester of **8** is reduced by lithium aluminum hydride, and the selenocyanate is then oxidized

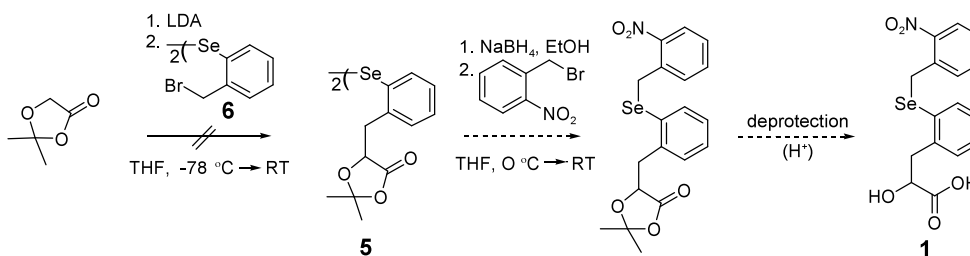
by air to yield **7**.¹² This procedure was successfully reproduced to prepare **7** in high yield as shown in **Scheme A3.4**. Compound **7** was then brominated in 80% yield by another published procedure to give benzyl bromide **6**.¹⁴

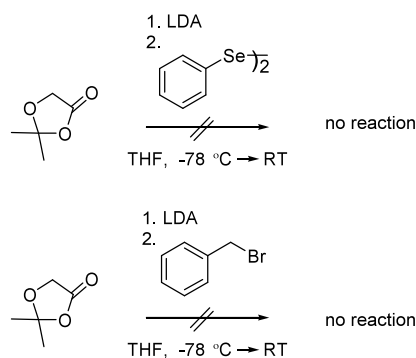
Scheme A3.4. Synthesis of benzyl bromide **6** from benzyl alcohol **7**.



With the benzyl bromide **6** in hand the key step in the synthesis, nucleophilic attack of benzyl bromide **6** by the enolate of a Seebach-type ester, could be attempted (**Scheme A3.5**). This reaction was tried many times but never yielded the desired product of this reaction (Compound **5**). The same reaction also failed with benzyl bromide and diphenyldiselenide (**Scheme A3.6**), suggesting that the presence of the diselenide functionality was not the cause for the failure of the above reaction.

Scheme A3.5. Another failed synthesis of the desired α -hydroxy acid, **1**.



Scheme A3.6. Model enolate reactions.

Several variables were also changed in this reaction including reaction time and reaction temperature. Other bases including *t*-BuLi, sodium hydride and potassium tert-butoxide were also tried, but none gave any product when tested with benzyl bromide. In fact, the starting materials were recovered quantitatively from each reaction. Lithium diisopropyl amine (LDA) was the most common base used in literature examples involving enolate chemistry with Seebach-type esters.⁵⁻⁷ It is possible that the LDA used in our reactions was of poor quality despite the fact that it was freshly prepared prior to each reaction. It is still unclear why our reactions (particularly those with benzyl bromide) failed. Had this route been pursued further, alternative Seebach-type esters would have been tested and the purity of the LDA would have been assessed.

A third synthetic route (**Figure A3.3**) was designed and tested soon after work began on the second route. This third route was inspired by the success of the selenocyanate formation reaction of the second route. All previous attempts to incorporate selenium through BuLi reactions (**Schemes A3.2, A3.3** and **A3.4**) were unsuccessful, and so it was thought that preparation of the selenocyanate would be easier.

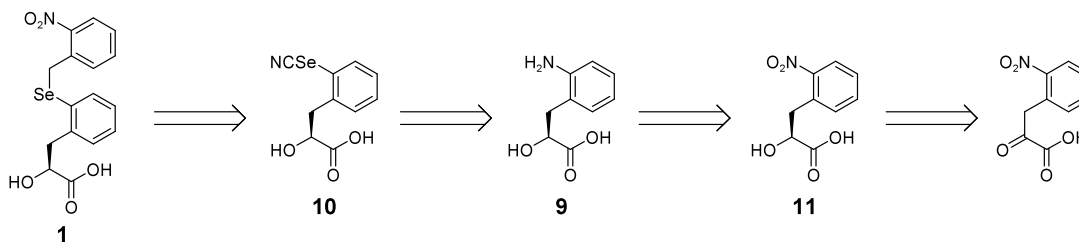
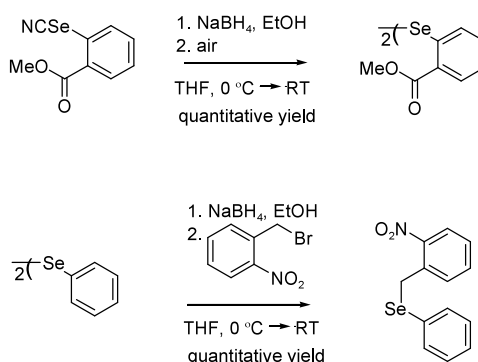


Figure A3.3. Third retro-synthetic pathway.

When this route was designed, it appeared that there were two potentially challenging steps, the conversion of the aniline **9** to the selenocyanate **10** and the transformation of this selenocyanate to the desired α -hydroxy acid, **1**. The successful conversion of methyl anthranilate to **8** (**Scheme A3.4**) provided precedent for the former transformation while the latter was preceded by the reported syntheses of other phenylalkyl selenides via reduction of aryl diselenides in the presence of alkyl halides.¹⁵⁻¹⁷ The model studies shown in **Scheme A3.7** confirm that nitrobenzyl groups can be added in this manner.

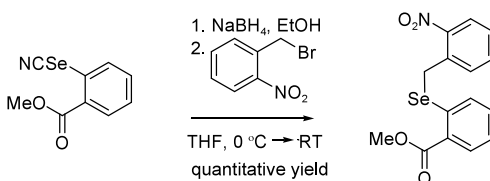
Scheme A3.7. Model reactions providing precedent for key steps in route 3.



To our knowledge, direct conversion of a selenocyanate to a disubstituted selenide has not been previously reported in the literature. All published procedures break this transformation into two steps as described above.¹⁵⁻¹⁷ Since reduction to the selenide is required for both steps, we tried to consolidate this protocol into a single step in the

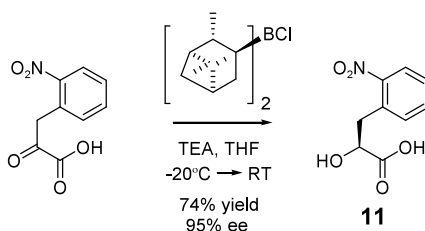
model study shown in **Scheme A3.8**. This route successfully afforded the desired model compound in quantitative yield.

Scheme A3.8. Model reaction that condense the two steps of Scheme A3.7 into one.



The remaining transformations in this retro-synthetic pathway (**Figure A3.3**) were thought to be more straightforward. The aniline could be prepared from the selective reduction of the nitro group of **11** and the asymmetric conversion of a commercially available starting material, 2-nitrophenylpyruvic acid, to **11** was previously reported by Wang *et al.*¹⁸ In this report **11** was prepared in high enantiomeric excess (95%) via reduction of 2-nitrophenylpyruvic acid by an asymmetric borane reducing agent, β -chlorodiisopinocampheylborane (DIP-Cl) as shown in **Scheme A3.9**.¹⁸

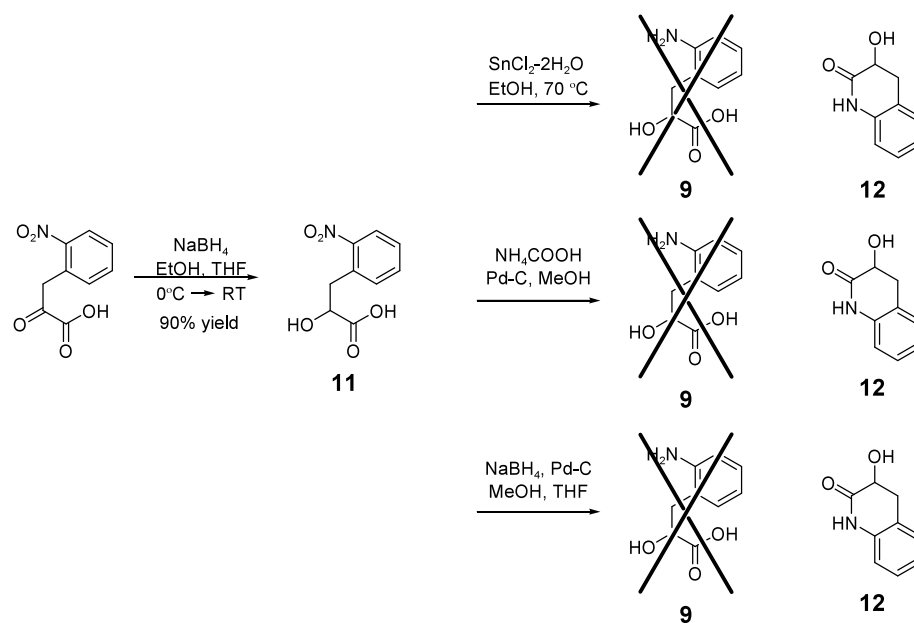
Scheme A3.9. Literature procedure for the enantio-enriched synthesis of **11** from 2-nitrophenylpyruvic acid.¹⁸



While DIP-Cl is commercially available, it was back-ordered for several weeks while the third route was first investigated. As such 2-nitrophenylpyruvic acid was reduced with sodium borohydride to yield the racemic α -hydroxy acid **11** in 90% yield. The reduction of the nitro group of **11** was expected to be facile as an assortment of

reagents are reported to selectively reduce aryl nitro groups in the presence of other reducible groups (including carboxylic acids).¹⁹⁻²¹ Several reagents were employed to reduce **11** to **9** as shown in **Scheme A3.10**. Unfortunately, none of the conditions tested resulted in the desired product **9**. Instead, each afforded the ring-closed product **12**. Analysis of the structure of this product suggests that the aniline had formed, but had immediately undergone intramolecular cyclization to afford the δ -lactam **12**.

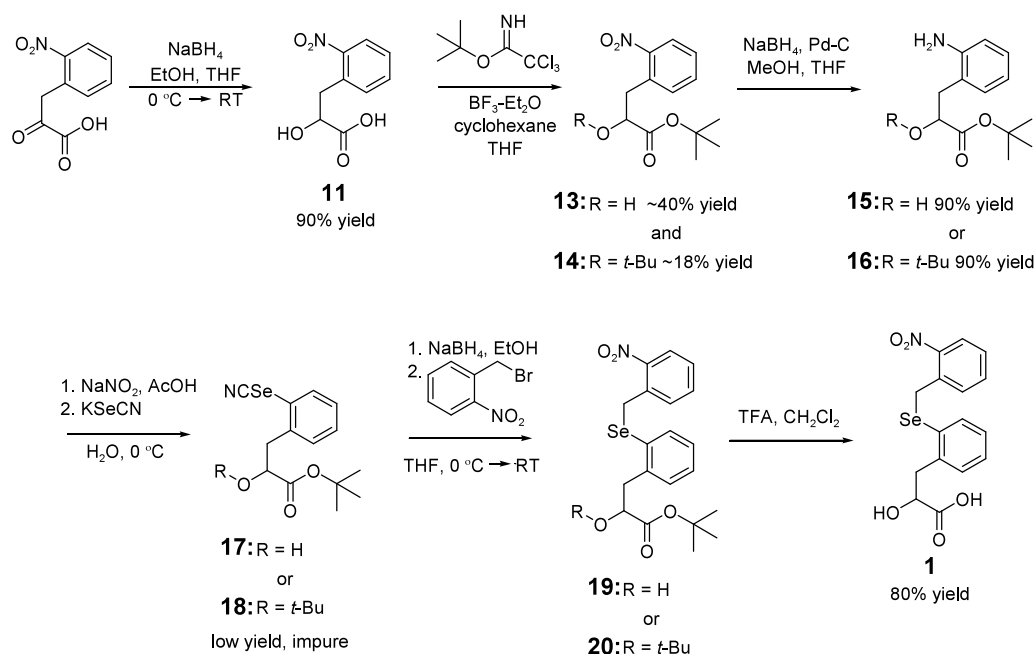
Scheme A3.10. Racemic reduction of 2-nitrophenylpyruvic acid and attempted reduction of α -hydroxy acid **11**.



At this point, a strategy was needed to prevent the formation of the δ -lactam. It was believed that the introduction of steric hindrance near the electrophilic carbon might impede cyclization. To test this theory, *t*-butyl groups were introduced by the synthetic procedure shown in **Scheme A3.11**. This reaction yielded two major products, **13** and **14**. Both products were isolated and run through subsequent reactions independently. It should be noted that the yields for this reaction are dramatically dependent upon the

reaction time. When the reaction was run for 12 hours, the total yield was <15%. A reaction time of 45 minutes, however, gave a total yield of ~60%. This yield is comparable to the yields reported for other methods of *t*-butyl esterification.³

Scheme A3.11. Successful racemic preparation of the desired α -hydroxy acid, **1**.



The sodium borohydride reduction of compounds **13** and **14** to compounds **15** and **16** was catalyzed by 10% palladium on activated carbon. No cyclization of **15** or **16** was ever observed under these conditions. It should be noted that the pH of the aqueous work-ups of the reactions was carefully monitored as acidic conditions could lead to the hydrolysis of the *t*-butyl protecting group and/or the catalysis of the intramolecular cyclization reaction. The anilines **15** and **16** were converted to their corresponding selenocyanates (**17** and **18**) by a slight modification of the standard procedure in which AcOH was used instead of a stronger acid to prevent loss of the *t*-butyl groups. These reactions gave low yields, but were optimized in the final synthetic route described in

Chapter 6. Using the protocol derived in the model studies of **Scheme A3.8**, compounds **17** and **18** were converted to the protected selenides **19** and **20**. Removal of the *t*-butyl protecting groups by TFA triumphantly afforded the α -hydroxy acid **1**.

After the racemic synthesis of **1** had been completed, DIP-Cl was no longer on back-order and an enantio-enriched version of the desired compound was prepared and optimized as described in Chapter 6.

A3.2 EXPERIMENTAL SECTION

All reactions involving potentially air-sensitive compounds were conducted under nitrogen or argon atmospheres using standard glove box or Schlenk techniques. Solvents were purified by passage through alumina.²² Resonances for NMR spectra are reported relative to Me₄Si (δ 0.0). NMR Spectra are reported as follows: chemical shift (δ ppm), integration, multiplicity and coupling constant (Hz). All reagents were purchased from Aldrich and used without prior purification.

Synthesis of α -hydroxy acid 2. The α -hydroxy acid **2** was prepared from L-2-bromo-Phe by the published procedure.² Quantitative Yield. ¹H NMR (300 MHz, CD₃OD, 298 K) δ 7.55 (1H, d, J = 6.88 Hz), 7.31 (2H, m), 7.14 (1H, m), 4.41 (1H, dd, J = 9.35, 4.40 Hz), 3.35 (1H, dd, J = 8.38, 5.50 Hz) 3.08 (1H, dd, J = 9.35, 3.85 Hz). High-resolution MS analysis (FAB+) m/z ; calcd 244.9813 ([M+H]), found 244.9818 ([M+H]) and calcd 266.9633 ([M+Na]), found 266.9750 ([M+Na]).

Synthesis of the methyl ester of 2. Compound **2** (2.00g, 8.18 mmol) was added to a 3-neck, 100 mL round-bottom flask equipped with a reflux condenser under Ar(g) and

dissolved in 66 mL of MeOH, 33 mL of toluene and 1 mL of HCl and the solution stirred for 16 hours at 75 °C. The solution was cooled to room temperature and the pH was increased to ~pH 7.0 by addition of 5% NaHCO₃ (aq). The solvent was removed by rotavap until only ~20% remained. Water was added (~50mL) and the organics were extracted with Et₂O, washed with brine, dried over Na₂SO₄ and concentrated to afford a yellow oil. Yield: 87%. ¹H NMR (300 MHz, CDCl₃, 298 K) δ 7.56 (1H, d, *J* = 7.98 Hz), 7.28 (2H, m), 7.13 (1H, dd, *J* = 7.98, 5.78 Hz), 4.52 (1H, dd, *J* = 8.53, 4.68 Hz), 3.80 (3H, s), 3.34 (1H, dd, *J* = 14.03, 4.78 Hz), 3.02 (1H, dd, *J* = 14.03, 5.50 Hz), 2.75 (1H, b). ¹³C NMR (75 MHz, CDCl₃, 298 K) δ 174.9, 136.3, 133.0, 132.0, 128.7, 127.5, 124.9, 70.1, 51.8, 41.0. MS analysis (ESI) *m/z*; calcd 281.0 ([M+Na]⁺), found 280.8 ([M+Na]⁺).

Synthesis of the TBS-protected methyl ester (of 2). The methyl ester of **2** (0.0811g, 0.313 mmol) was added to a 20 mL scintillation vial and dissolved in 1.4 mL of DMF. To this was added imidazole (0.128 g, 1.88 mmol) followed by *t*-butyldimethylsilyl chloride (0.189g, 1.25 mmol). The solution then stirred for 23 hours. The solution was suspended/diluted in brine (20 mL) and the organics were extracted with Et₂O, washed with brine, dried over Na₂SO₄ and concentrated to afford a yellow oil. This oil was purified by flash column chromatography on silica gel (3% EtOAc: Hex) to yield a clear oil. Yield: 85%. ¹H NMR (300 MHz, CDCl₃, 298 K) δ 7.53 (1H, d, *J* = 6.88 Hz), 7.23 (2H, m), 7.09 (1H, dd, *J* = 7.98, 4.68 Hz), 4.52 (1H, dd, *J* = 9.09, 5.78 Hz), 3.74 (3H, s), 3.31 (1H, dd, *J* = 9.35, 4.13 Hz), 2.96 (1H, dd, *J* = 9.63, 3.85 Hz), 0.77 (9H, s), -0.13 (3H, s), -0.27 (3H, s). ¹³C NMR (75 MHz, CDCl₃, 298 K) δ 173.7, 136.9, 133.3, 132.8, 128.7, 127.4, 124.8, 71.5, 52.2, 42.0, 25.8, 18.4, -5.4, -5.5. High-resolution MS analysis (FAB⁺) *m/z*; calcd 373.0835, found 373.0844.

Synthesis of TBS-protected acid 3. The TBS-protected methyl ester of **2** (0.128g, 0.343 mmol) was added to a 2-neck, 10 mL round-bottom flask under Ar (g) and dissolved in 3.4 mL Et₂O. To this was added potassium trimethylsilanolate (0.048g, 0.377 mmol). Within five minutes after this addition, a white precipitate appeared in the yellow solution. The solution stirred for a total of 2 hours. The yellow liquid was removed and the white solid was scintillated with cold ether (3 × 30 mL) to afford a white powder. To protonate the carboxylate, the powder was suspended/diluted in water (20 mL) and the pH was lowered to pH 4.5 by the addition of 3N HCl. The organics were extracted with CH₂Cl₂, washed with brine, dried over Na₂SO₄ and concentrated to afford a white crystalline solid. Yield: 82%. ¹H NMR (300 MHz, CDCl₃, 298 K) δ 10.94 (1H, b), 7.55 (1H, d, *J* = 7.70 Hz), 7.26 (2H, m), 7.12 (1H, dd, *J* = 7.43, 4.95 Hz), 4.59 (1H, dd, *J* = 10.18, 3.58 Hz), 3.43 (1H, dd, *J* = 13.48, 3.58 Hz), 2.99 (1H, dd, *J* = 10.18, 3.30 Hz), 0.795 (9H, s), -0.10 (3H, s), -0.28 (3H,s). ¹³C NMR (75 MHz, CDCl₃, 298 K) δ 179.3, 136.9, 133.7, 133.4, 129.3, 127.8, 125.7, 71.6, 42.3, 26.2, 18.7, -5.1, -5.2. High-resolution MS analysis (FAB+) *m/z*; calcd 359.0678 ([M+H]), found 359.0683 ([M+H]).

Synthesis of α-hydroxy acid 11. 2-nitrophenyl pyruvic acid (0.50g, 2.39 mmol) was dissolved in 20 mL of THF in a 100 mL, 3-neck round-bottom flask under Ar (g) at 0 °C. Sodium borohydride (0.181g, 4.78 mmol) in 12 mL EtOH was added to the reaction vessel dropwise via syringe. During this addition, the solution turned from yellow to orange and bubbling was observed. After fifteen minutes of stirring, the solution was slowly warmed to room temperature. Stirring was continued for a total of 3.5 hrs until the solution was quenched by the addition of 50 mL 3 N HCl. The pH of the solution was increased to pH 7 by addition of saturated NaHCO₃ (aq). After extraction with Et₂O

(2 × 30 mL), the pH of the aqueous layer was decreased to pH 1.6 by addition of 3 N HCl. The organics were extracted with Et₂O, washed with brine, dried over Na₂SO₄ and concentrated to yield a pale brown solid. Yield: 90%. ¹H NMR (300 MHz, CD₃OD, 298 K) δ 7.85 (1H, d, *J* = 6.88 Hz), 7.47 (3H, m), 4.44 (1H, b), 3.48 (1H, dd, *J* = 9.35, 3.48 Hz), 3.14 (1H, dd, *J* = 8.80, 5.23 Hz). ¹³C NMR (75 MHz, CDCl₃, 298 K) δ 175.3, 151.1, 134.4, 133.8, 132.9, 129.0, 125.5, 71.6, 38.0. High-resolution MS analysis (FAB+) *m/z*; calcd 212.0559 ([M+H]), found 212.0558 ([M+H]).

Synthesis of an enantio-enriched version of 11. The enantio-enriched version of **11** was prepared according to published procedures.¹⁹⁻²¹ The resulting solid was dry-loaded with MeOH onto a silica column in preparation for purification by flash column chromatography (1:1:0.016 ratio of EtOAc: Hex: formic acid) After purification, a yellow solid was obtained. Yield: 85%.

Synthesis of *t*-butyl-protected-nitro compounds 13 and 14. A 2-neck, 25 mL round-bottom flask under Ar(g) was charged with **11** (0.200g, 0.947 mmol), which was then dissolved in 3 mL THF. To this flask was added 3.5 mL of degassed cyclohexane. *t*-Bu-2,2,2-trichloroacetimidate(0.678 mL, 3.79 mmol) in 3.5 mL of cyclohexane was added simultaneously with 0.041 mL of boron trifluoride-diethyletherate (0.33 mmol). The reaction stirred for 45 min until it was quenched with saturated NaHCO₃ (aq). The organics were extracted with Et₂O, washed with brine, dried over MgSO₄ and concentrated. The resulting white sludge was dissolved in CH₂Cl₂ and filtered through a pad of celite to remove a majority of a white salt. The remaining liquid was purified by flash column chromatography on silica gel (10% EtOAc: Hex). Two fractions were

collected and identified as **13** ($R_f = 0.44$ in 30% EtOAc: Hex, yield = 40%) and **14** ($R_f = 0.71$ in 30% EtOAc: Hex, yield = 18%). The same procedure was used to prepare the enantio-enriched versions **13** and **14**. Analytical chiral HPLC separation of the enantio-enriched version of **13** was performed on a Chiralcel OD-H column (4.6mm \times 25 cm) from Daicel Chemical industries, Ltd with 2% isopropyl alcohol: hexanes. ^1H NMR of **13** (300 MHz, CDCl_3 , 298 K) δ 7.93 (1H, d, $J = 7.00$ Hz), 7.52 (1H, m), 7.41 (2H, m), 4.36 (1H, dd, $J = 8.38, 4.26$ Hz), 3.51 (1H, dd, $J = 13.87, 4.26$ Hz), 3.15 (1H, dd, $J = 14.01, 4.26$ Hz), 1.46 (9H, s). ^{13}C NMR of **13** (75 MHz, CDCl_3 , 298 K) δ 173.5, 150.1, 133.4, 133.0, 132.4, 128.1, 125.0, 83.4, 70.7, 37.6, 28.2. ^1H NMR of **14** (300 MHz, CDCl_3 , 298 K) δ 7.93 (1H, d, $J = 7.98$ Hz), 7.49 (1H, m, $J = 9.8$ Hz), 7.39 (2H, m), 4.15 (1H, dd, $J = 9.08, 4.76$ Hz), 3.31 (1H, dd, $J = 13.2, 4.95$ Hz), 3.14 (1H, dd, $J = 9.08, 4.13$ Hz) 1.40 (9H, s), 0.96 (9H, s). ^{13}C NMR of **14** (75 MHz, CDCl_3 , 298 K) δ 173.0, 145.0, 134.5, 132.9, 132.7, 128.0, 124.8, 81.2, 75.2, 71.9, 37.7, 28.1, 27.6. High-resolution MS analysis of **13** (FAB+) m/z ; calcd 268.1185 ($[\text{M}+\text{H}]$), found 268.1194 ($[\text{M}+\text{H}]$). High-resolution MS analysis of **14** (FAB+) m/z ; calcd 324.1811 ($[\text{M}+\text{H}]$), found 324.1827 ($[\text{M}+\text{H}]$).

Synthesis of *t*-butyl-protected-anilines 15 and 16. Compound **13** or **14** (1 eq) was placed in a 2-neck round-bottom flask and dissolved in THF (0.14 M) under Ar(g) at 0 $^\circ\text{C}$. To this was added 10 wt% palladium on carbon (0.3 eq) followed by the dropwise addition of sodium borohydride (2.5 eq) in MeOH (0.78 M). The reaction bubbled and was followed by TLC using ninhydrin as the stain. The solution was stirred for 30 min until it was quenched with water and filtered through a pad of celite. The filtrate was extracted with Et_2O , washed with brine, dried over MgSO_4 and concentrated. The resulting liquid was purified by flash column chromatography on silica gel (10–30%

EtOAc: Hex). Yield= 90% (**15**) or 90% (**16**). ^1H NMR of **15** (300 MHz, CDCl_3 , 298 K) δ 7.26 (1H, m), 7.05 (1H, m), 6.73, (1H, m), 6.69 (1H, dd, $J = 7.42, 4.49$ Hz), 4.37 (1H, dd, $J = 6.18, 3.98$ Hz), 3.10 (1H, dd, $J = 10.44, 4.12$ Hz), 2.90 (1H, dd, $J = 8.38, 6.18$ Hz), 1.48 (9H, s). ^{13}C NMR of **15** (75 MHz, CDCl_3 , 298 K) δ 173.6, 146.3, 131.7, 131.1, 128.2, 118.8, 116.7, 83.2, 72.4, 36.5, 28.3. ^1H NMR of **16** (300 MHz, CDCl_3 , 298 K) δ 7.29 (1H, d, $J = 7.70$ Hz), 7.18 (1H, m), 7.04 (1H, d, $J = 6.88$ Hz), 6.85 (1H, m), 3.99 (1H, m), 2.94 (1H, m), 2.71 (1H, m), 1.47 (9H, s), 0.98 (9H, s). ^{13}C NMR of **16** (85 MHz, CDCl_3 , 298 K) δ 173.5, 149.9, 130.5, 128.0, 124.0, 121.2, 114.4, 81.6, 75.8, 74.9, 35.7, 28.2, 27.6. MS analysis for **16** (ESI) m/z ; calcd 294.2 ($[\text{M}+\text{H}]^+$), found 294.3 ($[\text{M}+\text{H}]^+$) and calcd 332.2 ($[\text{M}+\text{K}]^+$), found 332.2 ($[\text{M}+\text{K}]^+$).

Synthesis of *t*-butyl-protected-selenocyanates **17 and **18**.** Compound **15** or **16** (1.01 eq) was added to a 10 mL round-bottom flask and dissolved in AcOH (0.05 M) at 0 °C. To this was quickly added 3 M sodium nitrite (1.21 eq) via syringe. The solution stirred for 1 hour and was monitored by TLC using ninhydrin as the stain. The pH of the solution was then increased to ~6 by the addition of saturated CH_3COONa (aq). To this was added potassium selenocyanate (1 eq) in water (0.07 M). The solution then stirred for ~30 min. The organics were extracted with Et_2O , washed with brine, dried over MgSO_4 and concentrated. The resulting brown sludge was used in the subsequent reaction without further purification. Attempts to purify **17** by flash column chromatography (10–30% EtOAc: Hex) gave ~8% yield, but it was apparent that some material was lost in the purification. In any case, the yields for this reaction are low. ^1H NMR of **17** (300 MHz, CDCl_3 , 298 K) δ 7.85 (1H, d, $J = 7.83$ Hz), 7.29 (3H, m), 4.28 (1H, dd, $J = 8.52, 4.53$ Hz), 3.31 (1H, dd, $J = 9.48, 4.53$ Hz), 3.13 (1H, dd, $J = 6.18, 3.87$ Hz), 1.49 (9H, s). ^{13}C NMR

of **17** (75 MHz, CDCl₃, 298 K) δ 172.7, 137.9, 134.8, 131.5, 129.9, 129.6, 129.2, 105.6, 84.0, 71.3, 39.9, 28.3. MS analysis of **17** (ESI) m/z ; calcd 350.0 ([M+Na]⁺), found 349.9 ([M+Na]⁺) and calcd 366.0 ([M+K]⁺), found 365.9 ([M+K]⁺).

Synthesis of *t*-butyl-protected-selenides **19 and **20**.** Compound **17** or **18** (1 eq) was added to a 2-neck round-bottom flask under Ar(g) and dissolved in THF at 0 °C. To this was added sodium borohydride (1.2 eq) in EtOH (0.5 M) and the solution stirred for 1 hr. 2-nitrobenzylbromide (1.3 eq) in THF (0.1 M) was then added to the now orange solution. After this addition, the solution was allowed to slowly warm to room temperature and was stirred for 3 hours until it was quenched with water. The organics were extracted with Et₂O, washed with brine, dried over MgSO₄ and concentrated. The resulting solid was purified by flash column chromatography on silica gel with 30% EtOAc: Hex (R_f = 0.46 for **19** using 40% EtOAc: Hex and R_f = 0.67 for **20** using 30% EtOAc: Hex) to afford a yellow solid. ¹H NMR of **19** (300 MHz, CDCl₃, 298 K) δ 8.00 (1H, d, J = 7.00 Hz), 7.48 (1H, d, J = 7.83 Hz), 7.31 (4H, m), 7.12 (1H, m), 6.99 (1H, m), 4.33 (2H, s), 4.15 (1H, m), 3.16 (1H, dd, J = 9.90, 4.53 Hz), 2.96 (1H, dd, J = 8.24, 5.36 Hz), 1.43 (9H, s). ¹H NMR of **20** (300 MHz, CDCl₃, 298 K) δ 8.01 (1H, d, J = 7.70 Hz), 7.45 (1H, d, J = 7.70 Hz), 7.37 (2H, m), 7.26 (2H, m), 7.21 (1H, m), 7.07 (1H, m), 4.35 (2H, s), 3.96 (1H, dd, J = 8.80, 5.50 Hz), 2.97 (1H, dd, J = 7.70, 5.23 Hz), 2.85 (1H, dd, J = 9.08, 4.13 Hz), 1.37 (9H, s), 0.95 (9H, s). ¹³C NMR of **20** (75 MHz, CDCl₃, 298 K) δ 173.3, 141.2, 136.2, 135.5, 133.2, 132.2, 131.8, 128.3, 128.1, 127.6, 125.7, 80.9, 74.9, 72.8, 40.9, 30.1, 28.07, 27.8. MS analysis of **20** (ESI) m/z ; calcd 516.1 ([M+Na]⁺), found 516.0 ([M+Na]⁺).

Synthesis of α -hydroxy acid 1. Compound **19** or **20** (1 eq) was added to a 2-neck round-bottom flask under Ar(g) and dissolved in CH₂Cl₂ (0.2M). To this was added trifluoroacetic acid (140 eq) and the solution stirred for 16 hours. The organics were extracted with Et₂O, washed with brine, dried over MgSO₄ and concentrated to afford a yellow solid. Yield: 80%. ¹H NMR (300 MHz, CDCl₃, 298 K) δ 7.99 (1H, d, J = 7.56 Hz), 7.45 (1H, d, J = 7.42 Hz), 7.36 (2H, m), 7.29 (2H, m), 7.13 (1H, m), 7.00 (1H, m), 4.37 (3H, m), 3.31 (1H, dd, J = 14.01, 4.40 Hz), 3.03 (1H, dd, J = 8.65, 5.22 Hz). MS analysis (ESI) m/z ; calcd 404.0 ([M+Na]⁺), found 404.1 ([M+Na]⁺) and calcd 380.0 ([M+H]⁺), found 379.9 ([M+H]⁺).

A3.3 REFERENCES

1. Eastwood, A. E., Investigating structure-function relationships in ion channels using unnatural amino acids. Ph.D. Thesis. California Institute of Technology, Pasadena, CA, 2009.
2. Deechongkit, S.; You, S.-L.; Kelly, J. W., Synthesis of all nineteen appropriately protected chiral alpha-hydroxy acid equivalents of the alpha-amino acids for boc solid-phase depsipeptide synthesis. *Org. Lett.* **2004**, 6, (4), 497-500.
3. Greene, T. W.; Wuts, P. G. M., *Protective Groups in Organic Synthesis*. 3rd edition ed.; John Wiley & Son, Inc.: New York, 1999.
4. Friesen, R. W.; Trimble, L. A., Site selectivity in the alpha-silyl lithiation of 3,4,6-tris-O-(tert-butyldimethylsilyl)-D and 3,4-bis-O-(tert-butyldimethylsilyl)-6-deoxy-L-glucal with tert-butyllithium. *J. Org. Chem.* **1996**, 61, (3), 1165-1168.
5. Seebach, D.; Naef, R., Enantioselective generation and diastereoselective reactions of chiral enolates derived from alpha-heterosubstituted carboxylic-acids - preliminary communication. *Helv. Chim. Acta* **1981**, 64, (8), 2704-2708.
6. Seebach, D.; Naef, R.; Calderari, G., Alpha-alkylation of alpha-heterosubstituted carboxylic-acids without racemization - epc-syntheses of tertiary alcohols and thiols. *Tetrahedron* **1984**, 40, (8), 1313-1324.
7. Seebach, D.; Sting, A. R.; Hoffmann, M., Self-regeneration of stereocenters (SRS) - Applications, limitations, and abandonment of a synthetic principle. *Angew. Chem. Int. Ed.* **1996**, 35, (23-24), 2708-2748.
8. Binns, M. R.; Haynes, R. K., Hexamethylphosphoramide-mediated conjugate addition of (alkylthio)allyllithium (phenylthio)allyllithium and (phenylseleno)allyllithium reagents to 2-cyclopentenone. *J. Org. Chem.* **1981**, 46, (19), 3790-3795.
9. Kundu, A.; Roy, S., Copper(II)/tin(II) reagent for allylation, propargylation, alkynylation, and benzylation of diselenides: A novel bimetallic reactivity. *Organometallics* **2000**, 19, (1), 105-107.
10. Xu, W. M.; Tang, E.; Huang, X., Preparation of isoxazol(in)yl substituted selenides and their further deselenenylation reaction to synthesize 3,5-disubstituted isoxazoles. *Tetrahedron* **2005**, 61, (2), 501-506.
11. Renaud, P.; Abazi, S., A Non-racemic equivalent of glycolic acid: preparation of both enantiomers from D-mannitol. *Helv. Chim. Acta* **1996**, 79, (6), 1696-1700.
12. Iwaoka, M.; Tomoda, S., Direct observation of intramolecular interaction between a divalent selenium and a tertiary amine by means of single-crystal X-ray-analysis and NMR-spectroscopy. *Phosphorus Sulfur* **1992**, 67, (1-4), 125-130.
13. Tripathi, S. K.; Patel, U.; Roy, D.; Sunoj, R. B.; Singh, H. B.; Wolmershauser, G.; Butcher, R. J., *o*-Hydroxymethylphenylchalcogens: Synthesis, intramolecular nonbonded chalcogen-OH interactions, and glutathione peroxidase-like activity. *J. Org. Chem.* **2005**, 70, (23), 9237-9247.
14. Iwaoka, M.; Katsuda, T.; Komatsu, H.; Tomoda, S., Experimental and theoretical studies on the nature of weak nonbonded interactions between divalent selenium and halogen atoms. *J. Org. Chem.* **2005**, 70, (1), 321-327.

15. Iwaoka, M.; Komatsu, H.; Katsuda, T.; Tomoda, S., Quantitative evaluation of weak nonbonded Se-F interactions and their remarkable nature as orbital interactions. *J. Am. Chem. Soc.* **2002**, 124, (9), 1902-1909.
16. McCulla, R. D.; Jenks, W. S., Deoxygenation and other photochemical reactions of aromatic selenoxides. *J. Am. Chem. Soc.* **2004**, 126, (49), 16058-16065.
17. Tadino, V. L. A.; Faez, J. M.; Christiaens, L. E.; Kevers, C.; Gaspar, T.; Dommes, J., Synthesis and activity of another seleniated auxin: 2,4-dichlorophenylselenoacetic acid. *Plant Growth Regul.* **2003**, 40, (3), 197-200.
18. Wang, Z.; Zhao, C. L.; Pierce, M. E.; Fortunak, J. M., Enantioselective synthesis of beta-hydroxy carboxylic acids: direct conversion of beta-oxocarboxylic acids to enantiomerically enriched beta-hydroxy carboxylic acids via neighboring group control. *Tetrahedron-Asymmetr.* **1999**, 10, (2), 225-228.
19. Chakraborty, C.; Dhavale, D. D., Short and efficient synthesis of (2*S*,3*R*,4*R*,5*R*) and (2*S*,3*R*,4*R*,5*S*)-tetrahydroxyazepanes via the Henry reaction. *Carbohydr. Res.* **2006**, 341, (7), 912-917.
20. Neilson, T.; Wood, H. C. S.; Wylie, A. G., Reduction of aromatic nitro-compounds by sodium borohydride catalysed by palladised charcoal. *J. Chem. Soc.* **1962**, (Jan), 371-372.
21. Petrini, M.; Ballini, R.; Rosini, G., Reduction of aliphatic and aromatic nitrocompounds with sodium-borohydride in tetrahydrofuran using 10-percent palladium-on-carbon as catalyst. *Synthesis* **1987**, (8), 713-714.
22. Pangborn, A. B.; Giardello, M. A.; Grubbs, R. H.; Rosen, R. K.; Timmers, F. J., Safe and convenient procedure for solvent purification. *Organometallics* **1996**, 15, (5), 1518-1520.